AFFDL-TR-68-56
VOLUME I

MAGIC: AN AUTOMATED GENERAL PURPOSE SYSTEM FOR STRUCTURAL ANALYSIS

VOLUME I: ENGINEER'S MANUAL

ROBERT H. MALLETT
STEPHEN JORDAN

Bell Aerosystems, a Textron Company

TECHNICAL REPORT AFFDL-TR-68-56

JANUARY 1969

AIR FORCE FLIGHT DYNAMICS LABORATORY
AIR FORCE SYSTEMS COMMAND
WRIGHT-PATTERSON AIR FORCE BASE, OHIO

NOTICE

When Government drawings, specifications, or other data are used for any purpose other than in connection with a definitely related Government procurement operation, the United States Government thereby incurs no responsibility nor any obligation whatsoever; and the fact that the Government may have formulated, furnished, or in any way supplied the said drawings, specifications, or other data, is not to be regarded by implication or otherwise as in any manner licensing the holder or any other person or corporation, or conveying any rights or permission to manufacture, use, or sell any patented invention that may in any way be related thereto.

This document has been approved for public release and sale; its distribution is unlimited.

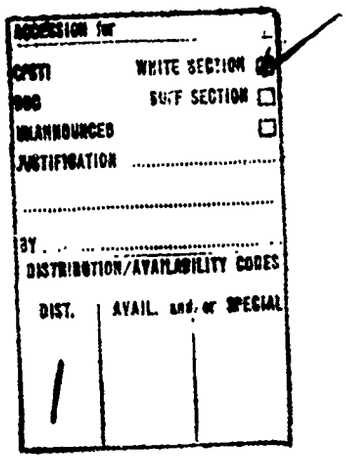

Copies of this report should not be returned unless return is required by security considerations, contractual obligations, or notice on a specific document.

500 - March 1969 - CO455 - 69-1521

MAGIC: AN AUTOMATED GENERAL PURPOSE SYSTEM FOR STRUCTURAL ANALYSIS

VOLUME I: ENGINEER'S MANUAL

ROBERT H. MALLETT

STEPHEN JORDAN

FOREWORD

This report was prepared by Textron's Bell Aerosystems, Buffalo, New York, under USAF Contract No. AF 33(615)-67-C-1505. The contract was initiated under Project No. 1467, "Structural Analysis Methods," Task No. 146702, "Thermal Elastic Analysis Methods." The program was administered by the Air Force Flight Dynamics Laboratory (AFFDL), Air Force Systems Command, Wright-Patterson Air Force Base, Ohio, 45433, under the cognizance of Mr. G. E. Maddux, AFFDL Program Manager. The program was carried out by the Structural Systems Department, Bell Aerosystems, during the period 15 March 1967 to 15 March 1968 under the direction of Dr. Robert H. Mallett, Bell Program Manager.

This report, "MAGIC: An Automated General Purpose System for Structural Analysis," is published in three volumes; "Volume I: Engineer's Manual," Volume II: User's Manual," and "Volume III: Programmer's Manual." The manuscript for Volume I was released by the authors in March 1968 for publication.

The numerical results presented in this report were obtained at the Wright-Patterson Air Force Base Electronic Data Processing Center. The utilization of this equipment and the helpful assistance of AFFDL personnel is acknowledged.

The authors wish to express appreciation to colleagues in the Advanced Structural Design Technology Section of the Structural Systems Department for their individually significant, and collectively indispensible, contributions to this effort. Special acknowledgement is given to Mr. Donald Dupree who coordinated the final documentation effort.

The authors wish to express appreciation also to Miss Beverly J. Dale and Daniel DeSantis, for the expert computer programming that transformed the analytical development into a practical working tool.

This technical report has been reviewed and is approved.

FRANCIS J. JANIK, JR.
Chief, Theoretical Mechanics Branch
Structures Division

ABSTRACT

An automated general purpose system for analysis is presented. This system, identified by the acronym "MAGIC" for "Matrix Analysis via Generative and Interpretive Computations," provides a flexible framework for implementation of the finite element analysis technology. Powerful capabilities for displacement, stress and stability analyses are included in the subject MAGIC System for structural analysis. The matrix displacement method of analysis based upon finite element idealization is employed throughout. Six versatile finite elements are incorporated in the finite element library. These are: frame, shear panel, triangular cross section ring, toroidal thin shell ring, quadrilateral thin shell and triangular thin shell elements. These finite element representations include matrices for stiffness, incremental stiffness, prestrain load, thermal load, distributed mechanical load and stress. The MAGIC System for structural analysis is presented as an integral part of the overall design cycle. Considerations in this regard include, among other things, preprinted input data forms, automated data generation, data confirmation features, restart options, automated output data reduction and readable output displays. Documentation of the MAGIC System is presented in three parts: namely, Volume I: Engineer's Manual; Volume II: User's Manual; and Volume III: Programmer's Manual. Volume I is the primary technical document. Included are a general technical discussion of the MAGIC System, an outline of the theoretical framework, statement of the individual finite element representations, and illustrative analyses for evaluation of each finite element representation. Volume II contains instructions for the preparation of input data and interpretation of output data with examples drawn from the illustrations presented in Volume I. Volume III is designed to facilitate implementation, operation, modification and extension of the MAGIC System.

CONTENTS

Section		Page
1.	INTRODUCTION	1
2.	TECHNICAL DISCUSSION	3
	A. Introduction	3
	B. Analysis Technology	3
	C. Finite Elements	7
	D. Programming Technology	9
	E. Program/Analyst Interfaces	17
	F. Size Characteristics	20
	G. Special Features	21
3.	THEORETICAL FRAMEWORK	23
	A. Introduction	23
	B. Discrete Element Matrices	23
	C. Linear Stress Analysis	33
	D. Stability Analysis	37
4.	FRAME ELEMENT	41
	A. Introduction	41
	B. Formulation	42
	C. Evaluation	56
5.	QUADRILATERAL SHEAR PANEL ELEMENT	59
	A. Introduction	59
	B. Formulation	59
	C. Evaluation	64
6.	TRIANGULAR CROSS SECTION RING ELEMENT	71
	A. Introduction	71
	B. Formulation	73
	C. Evaulation	84
7.	TOROIDAL THIN SHELL RING ELEMENT	89
	A. Introduction	89
	B. Formulation	91
	C. Evaluation	108
8.	MALLET QUADRILATERAL THIN SHELL ELEMENT	113
	A. Introduction	113
	B. Formulation	114
	C. Evaluation	151

CONTENTS (CONT)

Section		Page
9.	HELLE TRIANGULAR THIN SHELL ELEMENT	163
	A. Introduction	163
	B. Formulation	165
	C. Evaluation	192
10.	DISCUSSION AND CONCLUSIONS	205
	A. Discussion	205
	B. Conclusions	209
11.	REFERENCES	211

LIST OF FIGURES

Figure		Page
1.	Illustrative Structural Idealizations	4
2.	Structural Analysis Computational Flow	6
3.	MAGIC System Finite Elements	8
4.	General Purpose Program Organizational Chart	10
5.	Illustrative Abstraction Instruction Listing	18
6.	Frame Element Representation	42
7.	Displacement Function Mode Shapes	43
8.	Displacement Coordinate Transformation	44
9.	Frame Element Eccentricity	45
10.	Displacement Coordinate Transformation	46
11.	Stiffness Matrix	49
12.	Prestrain Load Vector	50
13.	Pressure Load Vector	50
14.	Incremental Stiffness Submatrices	52
15.	Incremental Stiffness Parameters	53
16.	Three Member Portal Frame Description	56
17.	Idealizations, Three Member Portal Frame	57
18.	Quadrilateral Shear Panel Representation	60
19.	Displacement Coordinate Transformation	63
20.	Displacement Coordinate Transformation	63
21.	Cantilever Beam with Uniformly Distributed Load	65
22.	Cantilever Beam Idealizations	66
23.	Tip and Center Deflections for Uniformly Loaded Cantilever Beam	67
24.	Bending Moment Distribution for Two Element Case	68
25.	Bending Moment Distribution for Four and Eight Element Cases	69
26.	Triangular Cross Section Ring Element Description	72
27.	Displacement Coordinate Transformation	74
28.	Matrix of the Elastic Constants	76
29.	Stress and Strain Transformation	77
30.	Displacement to Strain Transformation	79
31.	Stiffness Matrix	81
32.	Pressure Load Vector	82
33.	Prestrain Load Submatrix	83
34.	Stress Submatrix	85
35.	Thick Walled Disk Subjected to Radial Thermal Gradient	86
36.	Thick Disk Idealizations	87
37.	Stresses and Displacements in Thermally Loaded Disk	88

LIST OF FIGURES (cont)

Figure		Page
38.	Toroidal Thin Shell Ring Representation	90
39.	Displacement Coordinate Transformation	95
40.	Displacement Coordinate Transformation	96
41.	Displacement to Strain Transformations	99
42.	Notation	102
43.	Stiffness Matrix	103
44.	Element Prestrain Load Vector	104
45.	Pressure Load Matrix	105
46.	Stress Matrix	107
47.	Cylinder Subjected to End Loads	109
48.	End Loaded Cylinder Idealizations	110
49.	Meridional Moment Distribution	111
50.	Quadrilateral Thin Shell Element Representation	113
51.	Displacement Mode Shapes	116
52.	Displacement Mode Shapes	116
53.	Flexure Displacement Mode Shapes	116
54.	Membrane Displacement Coordinate Transformation	117
55.	Flexure Displacement Coordinate Transformation	118
56.	Membrane Displacement Transformation	120
57.	Flexure Displacement Coordinate Transformation	121
58.	Membrane Displacement Coordinate Transformation	122
59.	Flexure Displacement Coordinate Transformation	123
60.	Flexure Displacement Coordinate Transformation	125
61.	Eccentric Connection Transformation	126
62.	Membrane Coordinate Transformation	128
63.	Flexure Displacement Coordinate Transformation	129
64.	Plane Stress/Strain Option	131
65.	Strain Transformation	133
66.	Displacement Function Transformations	136
67.	Membrane Displacement Derivative Matrices	138
68.	Flexure Displacement Derivative Matrices	139
69.	Zone 1 Membrane Stiffness Parameters	139
70.	Zone 2 Membrane Stiffness Parameters	140
71.	Zone 3 Membrane Stiffness Parameters	140
72.	Zone 4 Membrane Stiffness Parameters	141
73.	Definition of Notation	141
74.	Stiffness Submatrices	143
75.	Zone 1 Flexure Stiffness Parameters	144
76.	Zone 2 Flexure Stiffness Parameters	144
77.	Zone 3 Flexure Stiffness Parameters	145
78.	Zone 4 Flexure Stiffness Parameters	145

LIST OF FIGURES (cont)

Figure		Page
79.	Pressure Load Vector	148
80.	Stress Resultants	149
81.	Parabolically Loaded Membrane	151
82.	Idealization	152
83.	Membrane Displacement at the Middle of the Plate's Edge versus Degrees-of-Freedom	153
84.	Membrane Displacement and Stress Behavior versus the Plate's Edge Span	154
85.	Shape Study Idealizations	156
86.	Membrane Displacement at the Middle of the Plate's Edge versus the Shape of Elements Used in the Idealization	157
87.	Simply Supported Square Plate with Uniform Normal Load	158
88.	Transverse Displacement at the Center of the Plate versus Degrees-of-Freedom	159
89.	Transverse Displacement and Stress Behavior versus the Plate's Center Span	160
90.	Transverse Displacement at the Center of the Plate versus the Shape of Elements used in the Idealization	162
91.	Triangular Thin Shell Element Representation	163
92.	Displacement Mode Shape Matrices	166
93.	Flexure Displacement Interzone Transformation	167
94.	Flexure Displacement Interzone Transformation	168
95.	Flexure Displacement Interzone Transformation	169
96.	Membrane Displacement Coordinate Transformation	171
97.	Flexure Displacement Coordinate Transformation	172
98.	Flexure Displacement Coordinate Transformation	173
99.	Flexure Displacement Coordinate Transformation	174
100.	Flexure Displacement Coordinate Transformation	175
101.	Eccentric Connection Transformation	176
102.	Membrane Displacement Coordinate Transformation	178
103.	Flexure Displacement Coordinate Transformation	179
104.	Displacement Coordinate Transformation	180
105.	Membrane Displacement Derivatives Matrix	183
106.	Flexure Displacement Derivatives Matrix	184
107.	Definition of Notation	184
108.	Definition of Integral Notation	185
109.	Definition of Notation	187
110.	Definition of Notation	188

LIST OF FIGURES (cont)

Figure		Page
111.	Pressure Load Vector	189
112.	Parabolically Loaded Membrane	192
113.	Idealization	193
114.	Membrane Displacement at the Middle of the Plate's Edge versus Degrees-of-Freedom	195
115.	Membrane Displacement and Stress Behavior versus the Plate's Edge Span	196
116.	Shape Study Idealization	197
117.	Membrane Displacement at the Middle of the Plate's Edge versus the Shape of Elements Used in the Idealization	198
118.	Simply Supported Square Plate with Uniform Normal Load	199
119.	Transverse Displacement at the Center of the Plate versus Degrees-of-Freedom	200
120.	Transverse Displacement and Stress Behavior versus the Plate's Center Span	201
121.	Transverse Displacement at the Center of the Plate versus the Shape of Element Used in the Idealization	202

TABLES

Number		Page
1.	Comparison Solutions for Three Member Portal Frame	58

LIST OF SYMBOLS

Φ_p	Potential Energy
$\{u()\}$	Displacement Functions
$[B()]$	Assumed Mode Shapes
$\{\beta\}$	Field Coordinate Displacement Degrees-of-Freedom
$[\Gamma_{\beta\delta}]$	Transformation from Field Coordinates to Gridpoint Displacement Coordinates
$\{\delta_g\}$	Gridpoint Displacement Coordinates Referenced to Element Axes
(x_g, y_g, z_g)	Coordinate Axes Defined on a Finite Element
$[\Gamma_{gs}]$	Transformation from Element Axes to Global Axes
(x_s, y_s, z_s)	Global Coordinate Axes
$\{\delta_q\}$	Gridpoint Displacements Referenced to Gridpoint Coordinate Axes
$[\Gamma_{sq}]$	Transformation from Global Axes to Gridpoint Axes
$[\Gamma_{\beta q}]$	Collective Transformation from Field Coordinates to Final Displacement Coordinates
$\{\sigma()\}$	Vector of Stresses
$\{\epsilon()\}$	Strain Vector
$\{\epsilon_i()\}$	Prestrain Vector
$[E]$	Matrix of Elastic Constants
$\{\alpha\}$	Coefficients of Thermal Expansion
ΔT	Difference between Element Temperature and Ambient Temperature
$[C()]$	Field Coordinate to Strain Transformation
$P()$	Pressure
$\sim$	Indicates Matrix Referenced to Field Coordinates

$\{F_\epsilon\}$	Prestrain Force
$\{F_p\}$	Pressure Load
$\{F_T\}$	Thermal Load
$\{F_c\}$	Concentrated Gridpoint Load Vector
$\{\epsilon_N\}$	Nonlinear Contributions to Total Strain
$[N]$	Incremental Stiffness
$\{\delta_q\}$	Vector of Element Degrees-of-Freedom for Assembly
$\{s\}$	Stress Correction Vector
$[S]$	Stress Matrix
U	Strain Energy
$[K]$	Stiffness Matrix
$[K_{SI}]$	Inflated Stiffness Matrix
$\{\Delta_I\}$	Inflated Displacement Vector
W	External Work
$\{P_{eI}\}$	Total Element Load Vector, System Level
$\{P_c\}$	Concentrated Load Vector, System Level
$\{\Delta_a\}$	Displacements of Assembled Structure
$[\Gamma_a]$	Assembly Transformation
$[\Gamma_r]$	Boundary Condition Transformation
$\{\Delta_s\}$	Final Displacement Vector System Level
$[\Gamma_{ar}]$	Collective Assemble and Bound Transformation
$\{P_s\}$	Total Applied Load Vector, System Level

LIST OF SYMBOLS (CONT)

$[S_s]$	Stress Matrix, System Level
$\{\Delta_s\}$	Stress Correction Vector, System Level
$\{F_{net}\}$	Element Force Vector, System Level
$\{R_s\}$	Reactions and Force Balance Vector
$[N_{SI}]$	Inflated Incremental Stiffness, System Level
$[N_s]$	Assembled and Reduced Incremental Stiffness
p_{cr}	Critical Load Intensity
$\bar{p}$	Prescribed Load Intensity
$[\Gamma_e]$	Eccentric Connection Transformation
$[T]$	Coordinate Axis Transformation
$[\ ]$	Rectangular Matrix
$\lceil \rfloor$	Diagonal Matrix
$\{\ \}$	Column Matrix
$\lfloor \rfloor$	Row Matrix
u	Displacement in the x or γ Direction
v	Displacement in the y or θ Direction
w	Displacement in the z Direction
$\{q\}$	Vector of Displacement Functions
$\theta_{n_{ij}}$	Slope of Element Side from i^{th} to j^{th} Gridpoint

1. INTRODUCTION

Bell Aerosystems has been active in the development of automated structural analysis tools based upon the finite element technology since the late 1950's. In a contractual outgrowth of this internal development activity, Bell furnished a series of computer programs to the Air Force Flight Dynamics Laboratory (AFFDL) in 1963. These programs, described in References 1 through 6, became an integral part of structural analysis practices at AFFDL and at numerous other recipient governmental and private organizations.

Advances in computer software and hardware signaled the impending obselescence of the foregoing computer programs for structural analysis in 1966. Attempts to salvage these programs by direct modifications to the coding proved discouraging. Moreover, newly established technological advances strongly recommended development of a second generation finite element capability for structural analysis.

In the light of the situation just described, Bell undertook, in March of 1967, to implement an advanced general purpose system for Matrix Analysis via Generative and Interpretive Computations (MAGIC) at AFFDL. This MAGIC System for structural analysis, described herein, was planned to provide, as a minimum, the capability of the prior set of Bell computer programs. The capability ultimately built into the MAGIC System is actually far more powerful than the former programs taken collectively. For example, structures characterized by "on the order of" 2000 degrees-of-freedom can be accommodated in contrast to the former 500 degrees-of-freedom limit.

Documentation of the MAGIC System for structural analysis is presented in three volumes. The subject volume (Volume 1) is the primary technical report. The major sections of this report are described in the following paragraphs. Separate supplementary volumes are provided to facilitate utilization of the MAGIC System. Volume II, the User's Manual[7], includes detailed specifications for the preparation of input data, along with illustrative examples. Volume III, the Programmer's Manual[8], presents information on the organization of the computer program as well as its operational characteristics.

A general description of the MAGIC System for structural analysis is included in Section 2. Particular attention is given to definition of the overall organization of the system. A key element of this organization is seen to be the versatile, AFFDL sponsored, FORTRAN Matrix Abstraction Technique (FORMAT II) described in References 9 through 12. Emphasis is also given in this section to special data management features which facilitate efficient utilization of the MAGIC System such as preprinted input data forms.

Section 3 of this primary technical report outlines the theoretical bases employed in derivation of the finite element representations and in development of the analysis procedures. A total of six finite elements are incorporated in the Element Library of

the MAGIC System; namely, frame, shear panel, triangular cross section ring, toroidal thin shell ring, quadrilateral thin shell and triangular thin shell elements. The computational procedures outlined in Section 3 include displacement, stress and stability analyses.

Sections 4 through 9 present statements of the matrices which comprise the individual finite element representations. In general; stiffness, incremental stiffness, pressure load, thermal load, and stress matrices are provided. Sections 4 through 9 also include numerical evaluations of the respective finite elements. These evaluations take the form of series of selected example problems.

The body of this technical report is concluded with a general retrospective discussion in Section 10. The MAGIC System is given critical review. Limitations are discussed and guidelines for utilization are presented.

2. TECHNICAL DISCUSSION

A. INTRODUCTION

Automated general purpose capabilities promise to revolutionize analysis and design practices. The matrix methods of analysis based upon discrete element idealization provide the suitable theoretical basis. High speed data processing devices establish the economic feasibility. Powerful automated tools for analysis and design have already been derived from these resources. Experience accumulated in the development and application of these tools has evolved a conceptual framework suitable for generalization.

Expansions which traverse traditional boundaries between the specialized disciplines of mechanics, improvements which provide firm theoretical bases for consistent mathematical models[13], and extensions which automate design iterations[14] are now well defined. New data management concepts which facilitate data handling[15], matrix abstraction instructions which simplify programming[9], and hardware devices which enable convenient display (and communication)[16] have also emerged. The implementation of all these generalizations within the framework of realistic hardware design poses a stimulating challenge.

The advanced general purpose system for Matrix Analysis via Generative and Interpretive Computations (MAGIC) which is described herein was developed in acceptance of the foregoing challenge. This MAGIC System furnishes the specific structural analyses capability sought and, at the same time, provides a versatile conceptual framework to facilitate the foregoing generalizations. Accordingly, general concepts are given consideration in the following discussion as well as specific features of the MAGIC System for structural analysis.

B. ANALYSIS TECHNOLOGY

The finite element approach to structural analysis is consistently stated in Section 3 within the framework of the variational methods of continuum mechanics. Within this framework, discretization can be referenced to zones designed to facilitate the construction of admissible displacement function mode shapes. Elementary illustrative physical models arising from such an idealization into zones are shown in Figures 1a and 1c. Admissible assumed displacement functions written individually for each zone, when taken collectively, form admissible assumed displacement functions whose field of definition is the entire structure.

These physical models, formed by subdivision into zones, may be equivalently viewed as assemblies of discrete structural elements interconnected such that appropriate interelement continuity is maintained. For example, the physical models shown in Figures 1a and 1c may be equivalently viewed as assemblies of the discrete structural elements of Figures 1b and 1d, respectively. It is this latter viewpoint, taken herein, which makes evident the generality of the finite element methods of

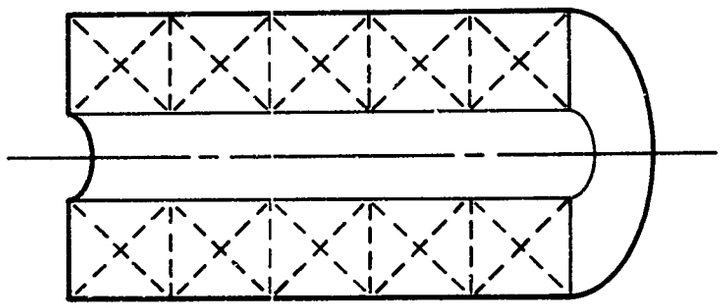

a. Structure

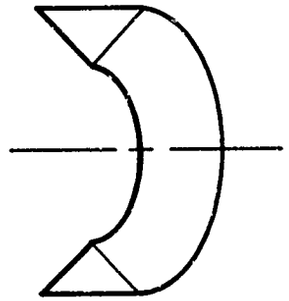

b. Element

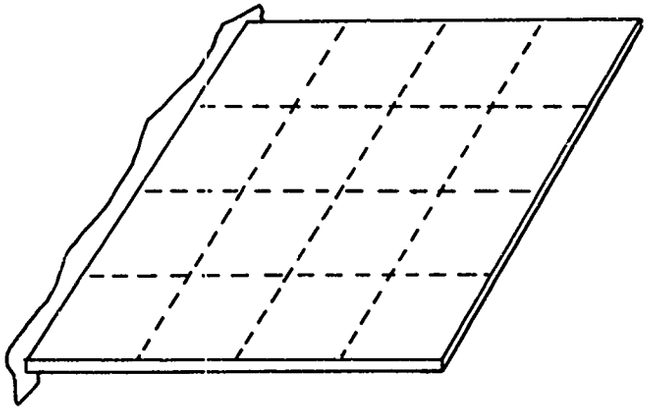

c. Structure

d. Element

Figure 1. Illustrative Structural Idealizations

analysis. Idealization into zones or structural components enables the systematic treatment of large scale complex structures as assemblages of large numbers of common elementary structural components.

Mathematical models are formulated for selected elementary structural components of parametrically specified shape. These finite element representations are then given specific dimensions to form building blocks appropriate to structures of a general problem class. Interconnection of adjacent elements is provided for by the construction of displacement function mode shapes with gridpoint displacement function quantities as undetermined coefficients. Taking these gridpoint displacement degrees-of-freedom common to adjacent elements establishes their interconnection.

The referencing of the structural idealization to elementary physical components leads naturally to specification of descriptive data with respect to these individual elements. Variations in dimensions such as thickness are accommodated by the specification of distinct values for individual elements. Material property variations arising from lamination or temperature degradation are accommodated by element related characterizations of materials.

Distributed loadings are also processed by element in order to account for variations. Elementary distributions are assumed over individual elements in much the same way that displacement function mode shapes are constructed. Intensities of distributed loadings such as pressure, temperatures and prestrain are prescribed at gridpoints. These intensities are then transformed into work equivalent forces via the assumed distributions.

The foregoing comments have indicated the facility with which finite element idealization accommodates problematical variations in geometry, material and applied loading. It is useful to emphasize this point further by examination of the overall computational process.

The basic computational flow of a finite element stress analysis is illustrated in Figure 2. The important feature to be noted in this flow chart is that the mathematical description of a structural system (Block 2) is generated independently of the construction of the objective mathematical model for the structural system (Block 3). That is, physical description (elastic constants, pressures, etc.) is referenced to the individual zones or finite elements and transformed to appropriate element mathematical representation without regard to total structure configuration and boundary conditions. It is primarily this separation which accounts for the generality of the discrete element method in regard to both complexity and broad applicability.

Regarding complexity, referencing of problem description to individual discrete elements enables convenient consideration of variations in geometry, sizing dimensions, material properties, applied loadings, and boundary conditions. Regarding applicability, this is limited only by the suitability of the discrete elements made available for idealization.

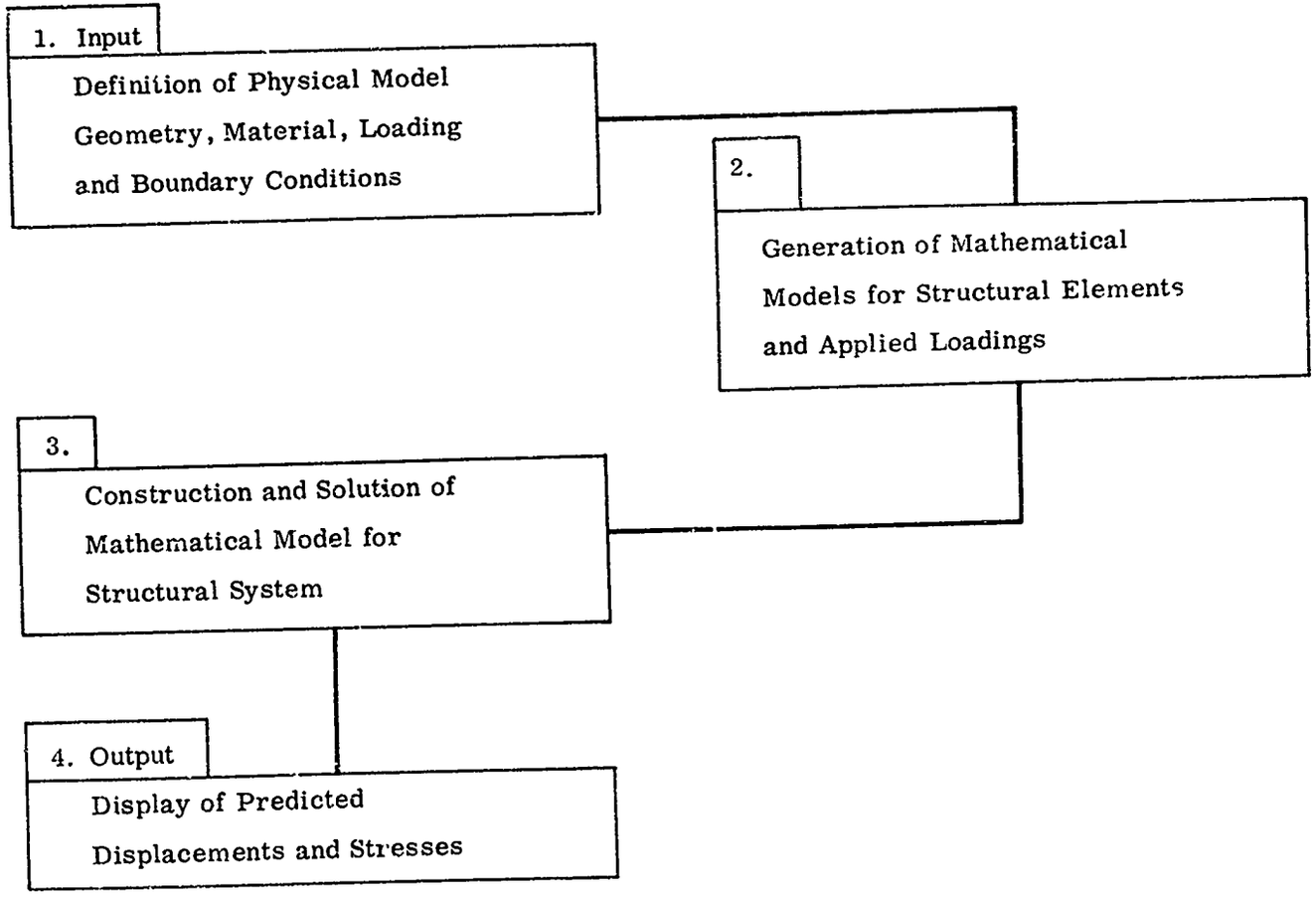

Figure 2. Structural Analysis Computational Flow

A variational point of view is maintained throughout the subject analysis process. Specifically, the principle of potential energy is employed. The well known Rayleigh-Ritz assumed mode method of analysis is invoked to generate the desired algebraic expressions for the element energy functions. Then, these are summed to obtain the energy function for the total structure. The objective governing equations follow immediately by executing the variation of the total energy. The principal advantage of maintaining the variational viewpoint throughout this process is that the matrices involved enjoy explicit and complete labeling at every step. The theoretical framework is outlined in detail in Section 3. Therein, the analysis processes are given explicit definition in terms of matrices.

C. FINITE ELEMENTS

The MAGIC System incorporates the six finite elements shown in Figure 3; namely, frame, shear panel, triangular cross section ring, toroidal thin shell ring, quadrilateral thin shell and triangular thin shell elements. These elements, taken collectively, enable the idealization of most structures.

The set of matrices embodied in each element representation determines the type of analyses which can be performed. In the MAGIC System, a complete element representation is taken to include matrices for stiffness, incremental stiffness, pressure load, prestrain load, thermal load and stress. Moreover, provision has been made for additional element matrices such as consistent mass matrices.

The frame element is a conventional "beam theory" finite element. This element is well suited to the idealization of planar and space frames. An eccentric connection feature is incorporated in this frame element representation to facilitate utilization as a shell stiffener element. The frame element is also appropriate to planar and space trusses.

The truss specialization of the frame element is particularly useful in combination with the quadrilateral shear panel element. The quadrilateral shear panel element simulates the action of a thin panel in diagonal tension. The effective extensional stiffness is allocated to truss elements. Such axial force member-shear panel idealizations have found extensive application in the analysis of airframe structures.

The triangular cross section ring element is one of the earliest and best known finite element models. This versatile element enables realistic idealization of thick-walled axisymmetric structures of arbitrary profile.

The representation of the triangular cross section ring incorporated in the MAGIC System is basically the same as the original model[17] although several useful generalizations have been introduced. One of these is the orthotropic material capability with data specified orientation of material axes.

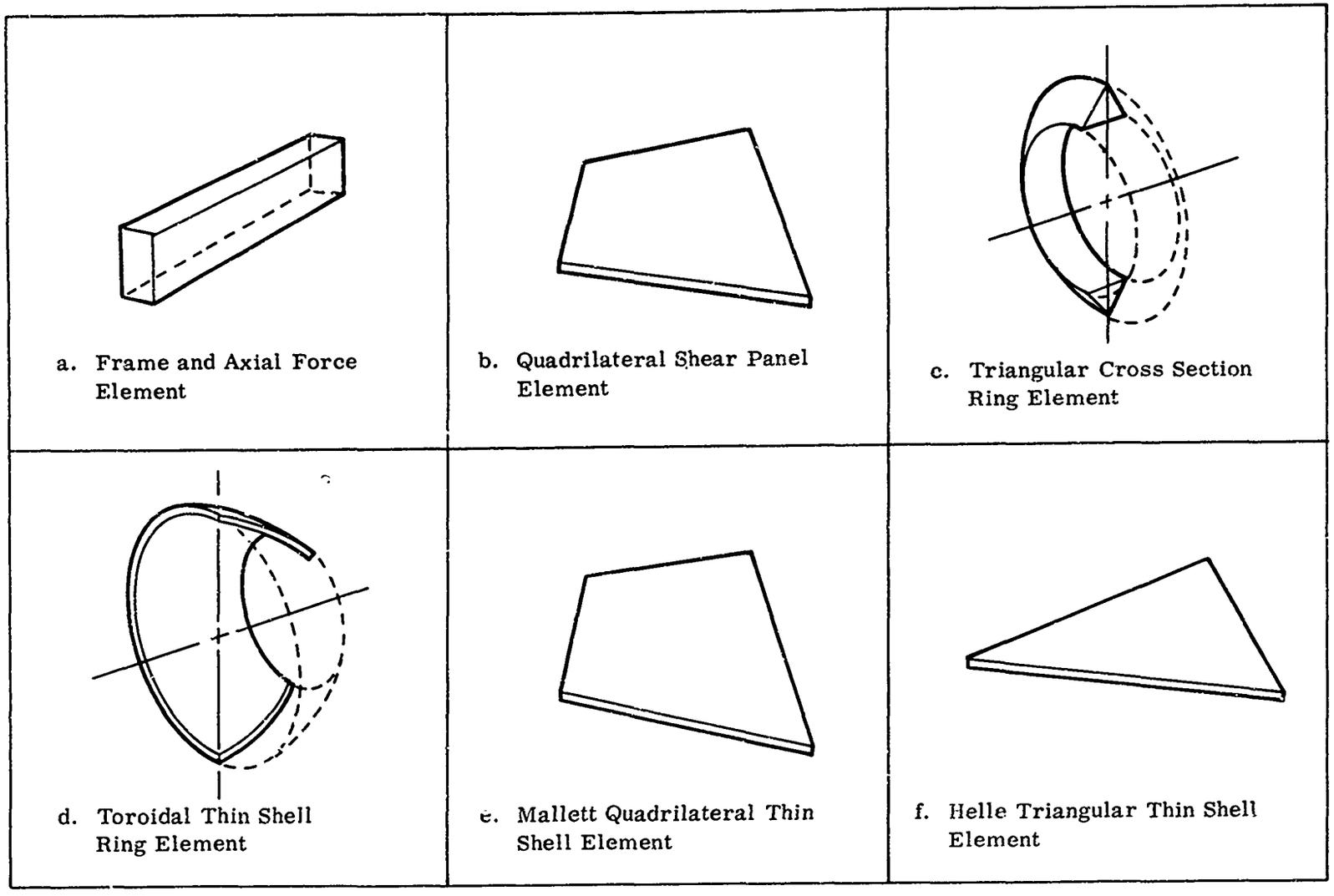

Figure 3. MAGIC System Finite Elements

The integrations conducted in formulating this element also serve to set it apart. A precise integration is carried out when the radial dimension of the cross section is not small relative to the diameter of the ring. When the radial dimension of the ring is small relative to the diameter, an approximate integration is carried out in accord with that in the conventional representation.

The MAGIC System representation of the triangular cross section ring embodies matrices for pressure and prestrain load as well as for stiffness and stress. A particularization of the prestrain load vector is included to facilitate thermal loading.

The thin shell elements incorporated in the MAGIC System are particularly noteworthy since they have not been presented previously in the open technical literature. The toroidal thin shell ring represents a substantial improvement over the predecessor conic thin shell ring[18]. In contrast to the latter, the toroidal ring yields accurate predictions of stresses for relatively coarse idealizations. In applications where the double curvature of the toroidal ring is not required, it specializes to conic and cylindrical configurations. Moreover, the toroidal ring reduces easily to a cap or end closure element.

The quadrilateral and triangular sets of thin shell elements incorporated in the MAGIC System provide an unprecedented capability for the analysis of thin membrane, plate and shell structures. The arbitrary shape of these elements enables efficient idealization of complex configurations and gridwork refinement. Supplementary mid-side gridpoints are optionally available to facilitate local gridwork refinement.

Interelement continuity is assured between elements of common and companion type. As a consequence, recourse to convergence criteria is often permitted. The variation in strains built into these elements yields accurate stress predictions relative to predecessor elements[4].

Many additional special features are included in this set of thin shell elements and in the other elements as well; for example, arbitrary material axes, arbitrary stress axes, plane strain option, etc. It is features such as these which establish the MAGIC System as a practical analysis tool as opposed to simply a large scale finite element computer program.

A separate section of this report is devoted to the presentation of each of these finite element representations. The reader is directed to the introductions within these sections for further description of the finite elements and their representations.

D. PROGRAMMING TECHNOLOGY

Useful insight into the nature of the finite element based MAGIC System for stress analysis can be gained from examination of the conceptual organizational chart shown in Figure 4. This chart illustrates the modularization which is fundamental to general purpose program organization. Overall efficiency is achieved by this modularization in much the same way that complex electronic, mechanical, and even structural systems are modularized to maximize versatility and maintainability.

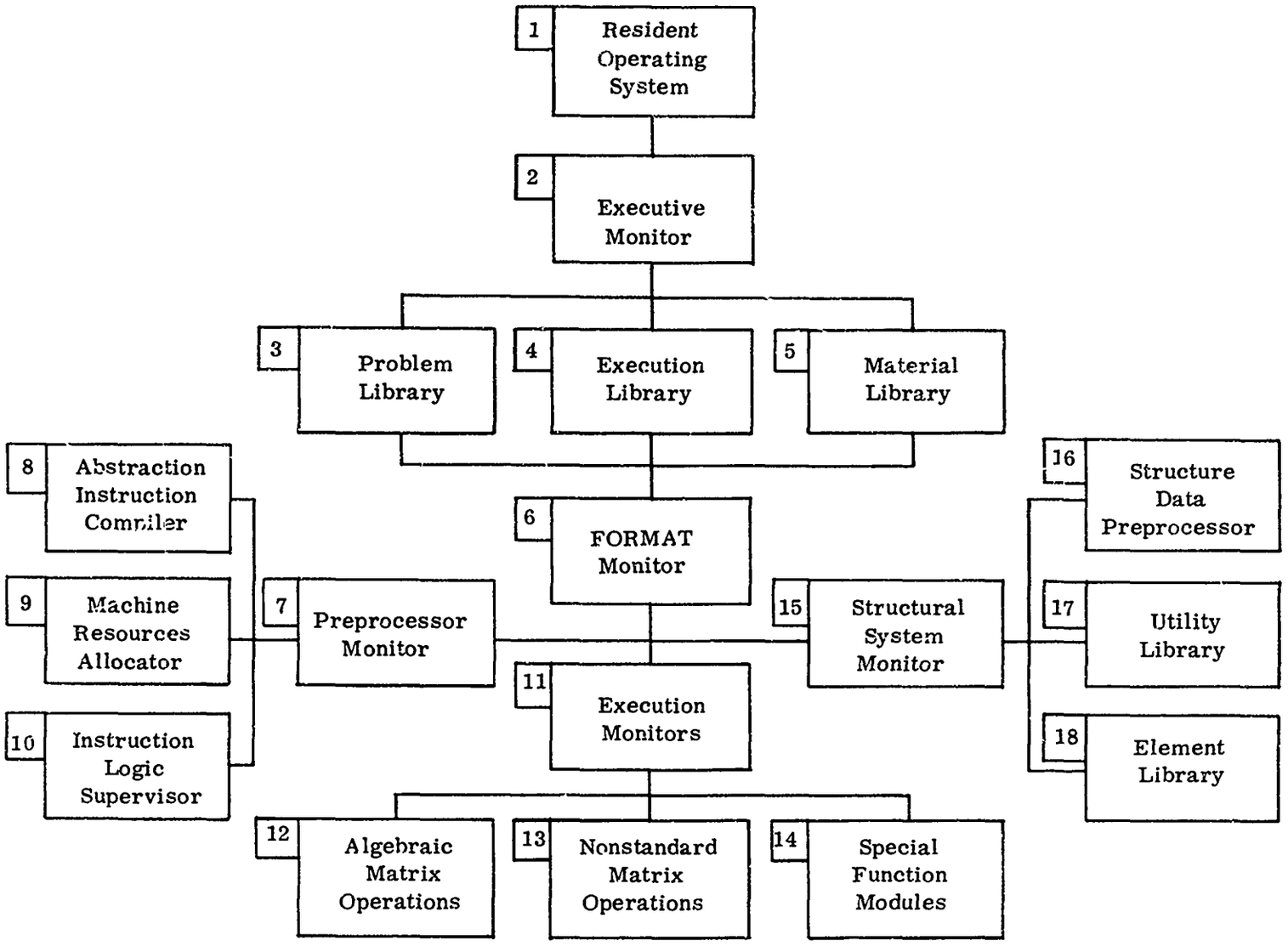

Figure 4. General Purpose Program Organizational Chart

The Libraries shown in Figure 4 are particularly noteworthy. These represent a higher level in a hierarchy of modularization in that they build in entire series of optional modules. The simultaneous availability of alternatives, achieved by standardized module interfaces, provides numerous benefits. The most obvious benefits are those derived from flexibility. Standardization also gives a repetitiveness to program developmental phases that enhances efficiency and reliability. Engineering interfaces reflect this standardization to advantage as well. These factors contribute importantly to the favorable cost effectiveness of the MAGIC System which is discussed in Section 11.

The conceptual organization shown in Figure 4 reaches slightly beyond that of the subject MAGIC System. This enables a more comprehensive discussion of the relevant programming technology and gives perspective to the actual organization of the MAGIC System. Variances between the organization of Figure 4 and that of the MAGIC System are delineated clearly.

The nature and function of the individual program modules are described in the following paragraphs. These descriptions also indicate the position of the modules in the logical flow of an analysis. As a consequence, the individual module descriptions, taken collectively, yield the objective overall picture of the programming technology intrinsic to the MAGIC System.

1. Resident Operating System

The Resident Operating System controls and coordinates job processing. It normally contains such subsystems as input/output routines, external storage supervisors, language compilers and assemblers and system accounting routines. Example Resident Operating Systems are: IBSYS for IBM 7090 and 7094, OS for the IBM System/360, EXEC for the UNIVAC 1108 and SCOPE for the CDC 6600.

Machine compatibility has been insured by the exclusive use of FORTRAN IV in the MAGIC System. The absence of machine or assembler language from every portion of the program eliminates most problems of machine dependency and implementation difficulties. Thus, even though the program is a system in itself, it is designed to function under the control of the normal operating system resident on a machine.

Avoidance of machine dependency also prevents optimum utilization of auxiliary direct access storage units. However, the overall organization of Figure 4 is designed to accommodate this generalization. The conceptual logic implied in the chart implies the addition of more modules under the Executive Monitor than just the FORMAT Monitor. In this way, direct access dependency could be incorporated into a monitor on the same level as the FORMAT Monitor. Other matrix control systems could also be placed under the Executive Monitor. Every addition would also automatically inherit the capabilities of the underlying modules.

2. Executive Monitor

The Executive Monitor is the highest level of control within the MAGIC System. This module controls location of the Problem, Execution, and Material Libraries. In addition, the Executive Monitor has sole control over maintaining and accessing the Execution Library. The primary function of the Executive Monitor is to coordinate the Libraries in conjunction with selection of the appropriate submonitor as directed by the application. Since, at the present time, the FORMAT Monitor is the only submonitor, the alternative Libraries are placed under its control and the Execution Monitor is not required.

3. Problem Library

The Problem Library takes the form of a magnetic tape prepared for the Analyst. Multiple problems are accumulated on the Problem Library tape. An entry in the Problem Library includes a complete record of the input data specification, selected intermediate results, and the output data specification. Control of the tape as regards access for subsequent additions, deletions, calculation, or displays resides with the Analyst. The Problem Library serves as a flexible interface between program and Analyst thereby providing an opportunity for effective data management.

Input data sets are made self generating insofar as is possible. This is effected in a preprocessing phase and the complete data set is recorded in the Problem Library. After approval of the input, the Analyst can invoke the Problem Library to continue the execution. Placement of intermediate results in the Problem Library provides, in the same way, for economical recovery at certain milestones in the solution process.

Localized design modifications and gridwork refinements can be accommodated without dealing with the entire structure. This is particularly important where multiple thermal loads are considered. Partitioning can sometimes be designed to circumvent ill conditioning. Very large, very sparse matrices are avoided, as are long continuous executions. Generally it can be said that the Problem Library, particularly when coupled with substructuring, allows analysis operations to be broken into manageable units.

In summary, the Problem Library (Block 3) of Figure 4, is accessible from any module below it to obtain data from previous problems and store data for the current problem. A Problem Library may be generated in the present MAGIC System to the extent provided by the availability of restart points in the analysis process as described under the FORMAT Monitor. No provision is built in to conduct analyses by substructures.

4. Execution Library

The Execution Library is designed to build in alternative abstraction instruction sequences. Entries in this module represent procedures such as displacement, stress and stability analyses. In addition to standard built-in analyses, nonstandard analyses can be conducted simply by defining an entry in the Execution Library. Revision or deletion of this module is controlled by the Executive Monitor.

The broad variety of analyses encountered in practice actually embody relatively few computations which are unique; rather, an extensive commonality exists. It is this commonality that enables the efficient development and operation of automated capabilities which are general purpose in the sense of multiple types of analyses.

This module is not built into the present MAGIC System. Abstraction instruction sequences are included in the input data deck to effect the desired type of analysis.

5. Material Library

The specification of mechanical and physical material properties can be a burdensome task. This is particularly true in the case of laminated materials or in the presence of thermal degradation of material properties. Accordingly, the Material Library is a very useful feature of the MAGIC System. This Material Library is simple in concept; yet, its availability can save time measurable in man-days against a single problem. In contending with design changes and multiple thermal load conditions, the Material Library is virtually indispensible.

The Material Library takes the form of a magnetic tape which is a permanent data set available for interrogation by the MAGIC System. The Executive Monitor is the natural control level for additions, modifications and deletions to the Material Library. In the absence of the Executive Monitor, this function is served by the Structural System Monitor in the present MAGIC System. Updating of the Material Library may be conducted as a separate execution or as an integral part of the analysis process.

A complete set of temperature referenced properties for a material constitutes an entry in the Material Library. Each entry in the Material Library is taken to include material designation, lock code, elastic constants, coefficients of thermal expansion and mass density. Provision is made for data at up to nine temperature levels. Linear interpolation is employed in interrogation of the Material Library for material property values at a specified temperature level. Material anisotropy is assumed as well as temperature dependence.

6. FORMAT Monitor

In the absence of an Executive Monitor, the control functions and responsibilities of the Executive Monitor are handled by or delegated to the FORMAT Monitor. In addition, the FORMAT Monitor carries out its normal functions.

The FORMAT Monitor controls the selection and usage of the underlying modules within the confines permitted by the Execution Monitor. At each transfer point between the underlying modules the FORMAT Monitor will make a logical decision, based upon information returned from the module, regarding the continuance or discontinuance of processing. Termination of processing is determined voluntarily by the Analyst unless unrecoverable error conditions are encountered by a module.

The FORMAT Monitor contains the correlation table between external storage devices and their respective FORMAT functions. The Analyst has at his command the option to revise the correlation table for any given application. The FORMAT Monitor has the assignment of processing any such revisions.

Restart capabilities are also controlled by the FORMAT Monitor as directed by the Analyst. By generating the desired abstraction instruction sequence and requesting pertinent information to be saved, the Analyst has at his command flexible restart capabilities. For example, in the contexts of a structral system, element matrices may be generated, saved and the problem restarted at a later level of analysis. Another example of restart would be to utilize the option of termination after the Structural System Input Data has been read and interpreted. Saving of this interpreted input would allow the Analyst to examine the input printout and restart the problem without the necessity of reinserting the original data for reading and interpretation.

Operating under the FORMAT Monitor, the basic computational flow of the program starts at the Preprocessor Monitor, passes the Execution Monitor and then to the Structural System Monitor which ends the cycle by returning control to the Execution Monitor. In this way, multiple data decks may be batched in a single MAGIC System execution.

7. Preprocessor Monitor

The Preprocessor Monitor interprets problem specification data pertinent to program setup. The processing involved includes specification of (a) master input tapes, (b) master output tapes, (c) analysis header labels, (d) problem header labels and (e) page size for printout. Matrices provided via input data cards are read and stored within the Preprocessor Monitor. Other functions of the Preprocessor Monitor are accomplished through its three underlying modules.

8. Abstraction Instruction Compiler

The Abstraction Instruction Compiler interprets the abstraction instructions and extracts matrix names, operation codes, scalars and statement numbers in the process. These quantities are stored in packed form and returned to the Preprocessor Monitor for use by the Instruction Logic Supervisor. Serious compilation errors may terminate execution at this point.

9. Machine Resources Allocator

The Machine Resources Allocator partitions the available internal storage into a program area and work area. This module also assigns program functions to the external storage facilities available. The four possible program functions for an external storage device are instruction storage, master input unit, master output unit and input/output utility unit. These allocations of storage areas are based upon program and application requirements. If no master input or master output units are needed, their function reverts to input/output utility.

10. Instruction Logic Supervisor

The Instruction Logic Supervisor scans the information assembled by the Abstraction Instruction Compiler and the Machine Resources Allocator and creates a logical path for the Execution Monitor. At the same time an optimum external storage assignment is made for each matrix named in an abstraction instruction in the knowledge of the logical path to be followed. The Instruction Logic Supervisor takes into account, in this process, such consideration as the channel addresses of external storage facilities, number of external storage facilities, capacities of external storage facilities and combinations of input and output matrices of abstraction instructions. The result is an optimum utilization of available machine resources for the sequence of operations released to the Execution Monitor from the Preprocessor Monitor.

11. Execution Monitor

The Execution Monitor follows the path specified by the Preprocessor Monitor accessing the underlying modules to perform the prescribed operations. Operations can be performed on matrices up to the order 2000. The efficient utilization of machine storage resources is assured by the setup passed from the Preprocessor Monitor.

The Execution Monitor will terminate processing if any of the rules of matrix algebra are violated. Matrices are stored by columns complete with matrix name, dimensions and sign. If a column of a matrix is less than 50% dense, it is stored in compressed format. The modular form allows ease of insertion of additional matrix manipulative or generative operations.

12. Algebraic Matrix Operation

The Algebraic Matrix Operation module is essentially a library of routines for matrix manipulation. This library includes routines for addition, subtraction, multiplication, transposed multiplication, scalar multiplication, transposition, inversion, equation solving by elimination, equation solving by iteration, and eigenvalue/eigenvector extraction.

Each of the above operations is incorporated into a separate module and all except the eigenvalue operation have out of core capability.

13. Nonstandard Matrix Operation

The Nonstandard Matrix Operation is essentially a library of routines to effect nonstandard matrix manipulation. Included in this library are routines to raise each element within a matrix to a specified power, locate maximum or minimum values in a row or column, adjoin two matrices column wise, and multiply two matrices element by element.

14. Special Function Modules

The Special Function Modules constitute a library of routines to effect non-algebraic operations. Included in this library are routines to print, skip ahead upon encountering a null matrix, select the best condition columns from a triangular matrix, and solve the selected set of simultaneous equations, form a diagonal matrix from a row or column matrix, and rename a matrix.

15. Structural System Monitor

The Structural System Monitor is the matrix generator of the structural analysis capability provided by the MAGIC System. Machine storage resources are allocated to this module by the Preprocessor Monitor. Matrices describing a structural system are released from this monitor for the conduct of the matrix manipulation phase of the structural analysis process. The Structural System Monitor together with its underlying modules comprise the major portion of the MAGIC System for structural analysis.

16. Structure Data Preprocessor

The Structure Data Preprocessor is the principal input data interface between the MAGIC System and the Structural Analyst. As such, the nature of this module is described in the subsection E, "Program/Analyst Interfaces."

The basic function of the Structure Data Preprocessor is to read and interpret all data describing the idealized structral model and to make this data available for the generation of structural matrices via the Structural System Monitor. The interpretation function carried out by the Structure Data Preprocessor is substantial since data sets are designed to be internally generated insofar as is possible.

An optional execution interruption is provided at completion of the structural data preprocessing. The completed set of structural data is printed for examination by the Analyst. Then, upon approval of the input data, the analysis process is restarted.

17. Utility Library

The Utility Library is an elementary interpretive system in the form of a collection of FORTRAN subroutines. Computational routines which are common to several element matrix generation procedures are placed in the Utility Library to avoid a duplication of programming. An extensive commonality exists among the generation procedures even for diverse types of discrete elements. Exploitation of this commonality via the Utility Library contributes measurably to the efficient development of the Element Library in the MAGIC System. Included in the Utility Library are routines for numerical integration, interpolation, specialized structural print and algebraic operations for small size matrices.

18. Element Library

The Element Library is the heart of the MAGIC System for structural analysis. Each entry in this library represents a finite element model. A call on the Element Library causes numerical generation of certain matrices of a complete element representation.

The availability in the Element Library of suitable elements for idealization determines the applicability of an analysis system to different classes of structure. Moreover, the set of matrices embodied in each element representation determines the type of analyses which can be performed. In the absence of versatile Element Libraries, even the best matrix and tape interpretive systems yield sterile analysis capabilities.

The six finite element models incorporated in the Element Library of the MAGIC System and the set of element matrices provided were described in the preceding subsection C. Experience has shown this Element Library to provide a powerful capability for structural analysis.

E. PROGRAM/ANALYST INTERFACES

Discussion of the MAGIC System for structural analysis is not complete without some comment on the program/Analyst interfaces. The acceptance of automated analysis tools by stress analysts hinges importantly on the simplicity of these interfaces. The first interface encountered by the Analyst is with the Preprocessor Monitor. The basic instruction sequence to be executed passes through this interface from the Analyst to the program. These instructions consist of a sequence of mathematical equations to be performed. An abstraction instruction sequence for linear stress analysis is illustrated in Figure 5. Such instruction sequences may be constructed at the volition of the Analyst and executed to perform a wide variety of computations.

```
*INSTRUCTION   SOURCE                                                    BELL0000
C                                                                        BELL0010
C       DISPLACEMENT AND STRESS ANALYSIS INSTRUCTION SEQUENCE            BELL0020
C                                                                        BELL0030
      MATLBA,LOADS,TR,TA,KEL,FEL,SEL,SZALEL, , , , = .USER04.            BELL0040
C                                                                        BELL0050
C       PRINT OUTPUT MATRICES                                            BELL0060
C                                                                        BELL0070
      PRINT (D.O.F.,COND. ,E6,) LOADS                                    BELL0080
      PRINT (REDDOF,C.O.F.,E6,) TR                                       BELL0090
      PRINT (NSYS  ,NORSUM,E6,) TA                                       BELL0100
      PRINT (ROW   ,COL   ,E6,) KEL                                      BELL0110
      PRINT (ROW   ,COL   ,E6,) FEL                                      BELL0120
      PRINT (ROW   ,COL   ,E6,) SEL                                      BELL0130
      PRINT (ROW   ,COL   ,E6,) SZALEL                                   BELL0140
C                                                                        BELL0150
C       FORM TAR MATRIX (ASSEMBLY AND APPLICATION OF BOUNDARY COND.)     BELL0160
C                                                                        BELL0170
      TRT = TR .TRANSP.                                                  BELL0180
      TAR = TA .TMULT. TRT                                               BELL0190
C                                                                        BELL0200
C       ASSEMBLE AND REDUCE ELEMENT STIFFNESS MATRICES                   BELL0210
C                                                                        BELL0220
      KTEMP = KEL .TMULT. TAR                                            BELL0230
      STIFF = TAR .TMULT. KTEMP                                          BELL0240
      PRINT (FORCE ,DISP. , ,) STIFF                                     BELL0250
                                                                         BELL0260
C       ASSEMBLE AND REDUCE ELEMENT APPLIED LOADS                        BELL0270
C                                                                        BELL0280
      FTELAR = TAR .TMULT. FEL                                           BELL0290
      PRINT (REDDOF,COND. , ,) FTELAR                                    BELL0300
C                                                                        BELL0310
C       APPLY BOUNDARY CONDITIONS TO SYSTEM LOADS                        BELL0320
C                                                                        BELL0330
      LOADR = TR .MULT. LOADS                                            BELL0340
      PRINT (REDDOF,COND. , ,) LOADR                                     BELL0350
C                                                                        BELL0360
C       COMBINE ELEMENT AND SYSTEM LOADS                                 BELL0370
C                                                                        BELL0380
      TLOAD = FTELAR .ADD. LOADR                                         BELL0390
      PRINT (REDDOF,COND. , ,) TLOAD                                     BELL0400
C                                                                        BELL0410
C       SOLVE FOR DISPLACEMENTS                                          BELL0420
C                                                                        BELL0430
      DISPR = STIFF .SEQEL. TLOAD                                        BELL0440
      PRINT (REDDOF,COND. , ,) DISPR                                     BELL0450
C                                                                        BELL0460
C       SOLVE FOR ELEMENT STRESSES                                       BELL0470
C                                                                        BELL0480
      STREL = SEL .MULT. TAR                                             BELL0490
      STRESF = STREL .MULT. DISPR                                        BELL0500
      STRESS = STRESF .SUBT. SZALEL                                      BELL0510
      PRINT (NRSEL ,COND. , ,) STRESS                                    BELL0520
C                                                                        BELL0530
C       SOLVE FOR ELEMENT FORCES                                         BELL0540
C                                                                        BELL0550
      FORCEL = KTEMP .MULT. DISPR                                        BELL0560
      FORCES = FORCEL .SUBT. FEL                                         BELL0570
      PRINT (D.O.F.,COND. , ,) FORCES                                    BELL0580
C                                                                        BELL0590
C       SOLVE FOR SYSTEM REACTIONS                                       BELL0600
C                                                                        BELL0610
      REACTN = TA .MULT. FORCES                                          BELL0620
      REACT = REACTN .SUBT. LOADS                                        BELL0630
      PRINT (D.O.F.,COND. , ,) REACT                                     BELL0640
```

Figure 5. Illustrative Abstraction Instruction Listing

Executions may be terminated and restarted at the corresponding exit and entry points of any abstraction instruction. Input data, intermediate results or final results can be automatically saved in this way. Then, with the retrieval of this data, computation can be resumed.

The second program/Analyst interface encountered is with the Structural System Monitor. This is the primary input data interface of the MAGIC System for structural analysis. Experience has shown that significant portions of the labor and computer costs of analyses are occasioned by incomplete or improper specification of problem input data. In recognition of this, special features are associated with the MAGIC System to facilitate the confirmation of problem data prior to execution. Included are annotated input forms, data consistency checks, and an option to read, complete and write the input data prior to attempting execution.

Preprinted input data forms are essential to the reliable specification of data. These forms provide a labeled entry position for all data items which gives engineering definition to the quantities requested. Control options are selected simply by a mark (X). These provisions help to minimize occurrences of incomplete specifications of problem data.

The printed input forms take advantage of a special MODAL data card feature. The MODAL card feature enables data-prescribed initialization of tables. Explicit data requirements are thereby limited to specification of exceptions to the MODAL initialization.

In addition to the MODAL card, a data Repeat option is available. When utilized, data from the previous point is retained for the indicated point. The combination of the MODAL card and the Repeat option significantly reduces the volume and complexity of input.

The input forms also embody permanent label cards which automatically precede subsets of data, thereby allowing flexibility in the arrangement of the subsets of data to form the total input data deck. Data associated with options not exercised are simply omitted. This is particularly useful when a problem is being restarted at an advanced stage of computation.

A data confirmation preprocessing phase, with problem execution suppressed, is a recommended practice in utilization of the MAGIC System. In this data processing execution, explicit data is read and implied data is generated. For example, MODAL card completions are conducted and material properties are interpolated from the Material Library. Consistency of all the data is checked and a complete record of the data is recorded for restart and printed for inspection.

There are basically two types of output provided by the MAGIC System. The first is matrix print provided from the Special Function Print Module. This encompasses all output external to the Structural System Monitor. A standard format is employed to print matrices.

The second basic type of output is that provided from within the Structural System Monitor. Output from this module includes a list of the completed input data with self-explanatory engineering labels. In addition, intermediate results employed in checkout are optionally available in the completed program.

F. SIZE CHARACTERISTICS

The size characteristics of the MAGIC System are twofold: first, there are the size characteristics of the program itself and second, those associated with the problem solving capability. Considering the former, the MAGIC System contains 212 subroutines (approximately 25,000 FORTRAN IV source cards) logically designed into 89 overlay links on an IBM 7090 with 32,000 words of storage. The overlay design reflects the optimum use of available storage yet maintains respectable execution efficiency.

The MAGIC System offers large scale capability with no penalties to small applications due to the fact that out of core operations are not utilized unless the magnitude of the application requires them. The size of the program has necessitated use of SUBSYS, a package which improves the loading capabilities of IBSYS, on the 7090/94. In addition to allowing the program to be loaded, SUBSYS allows the program overlay load tape to be saved, thereby improving execution time. Also, SUBSYS allows programs to be executed back to back without passing through the IBLDR section of IBJOB for each program. On the 7090 under SUBSYS the program is actually divided into three segments: Preprocessor, Execution and Structural System. Third generation computers, such as System/360 and UNIVAC 1108, have the capabilities of SUBSYS incorporated into their resident operating system.

The scale of the analysis capability provided via the MAGIC System can be characterized as "on the order of" 2000 displacement degrees-of-freedom. Other relevant maximum size characteristics are 1000 discrete elements, 1000 grid points and 10 applied load conditions. Matrices which are card input may be of order 2000 x 2000 and contain up to 4500 single precision real non-zero elements on a 32,000 word machine.

The MAGIC System needs a minimum of eight external storage units to operate, distributed into the following functions: one unit assigned as Instruction storage for the Execution Monitor, one unit assigned as a Master Input Unit, one unit assigned as a Master Output Unit, and five units assigned as Input/Output Utility Units. Every effort should be made to make the most external storage units possible available, since any increase in the available storage units increases execution efficiency.

The stated maximum size characteristics apply to the linear stress analysis capability of the MAGIC System. A stability analysis capability is also included in the MAGIC System, as with the linear stress analysis, and explicit matrix statement of the stability analysis procedure is given in Section 3. The number of displacement degrees-of-freedom which can be accommodated in the eigenvalue stability analysis is limited to 130. The other size characteristics stated for the stress analysis remain applicable.

G. SPECIAL FEATURES

Many features have been built into the MAGIC System which are not fundamental to a finite element computer program but which are essential to a general purpose analysis system for practical structures. Foremost among these features is a great variety of transformation matrices. Material axes transformations are provided to accommodate arbitrary axes of orthotropy. Stress axes transformations enable the referencing of output displays to convenient axis systems. Grid point axes transformations account for irregular boundary conditions and allow pseudo-curvilinear displacement variables. Eccentric connection transformations provide for realistic modeling of frame joints and shell stiffeners. Finally, grid point suppression transformations are included to eliminate unwanted element grid points prior to assembly.

A second feature of special interest is the element repeat feature. There are actually two levels of element repeat. The first is a repeat of element data. Under this option, all calculations proceed as usual, but the repeated provision of identical element extra data cards is avoided. The second level of element repeat is element matrix repeat and this is the more powerful option by far. Under this option, the element matrices of the prior element are simply carried forward as those of the present element; no calculation is carried out. Clearly under this option, a great saving in input data specification is realized and important savings in calculation can be realized as well. The extent to which the input data can be reduced by the element matrix repeat feature is made clear in the User's Manual.

A useful element load condition scalar is associated with the multiple load condition capability of the MAGIC System. Element load conditions arise in load condition number one. A multiplicative constant is then data prescribed for all subsequent load conditions. This scalar controls the participation of the element loading. With this feature, a total load system can be decomposed into several parts and behavior predictions can be obtained conveniently against these as well as against the total load system. This feature is particularly useful in separating effects of thermal and mechanical applied load combinations.

The majority of the special features embodied in the MAGIC System are explained best within a specific context. Accordingly, with the exception of the few included here for special emphasis, such features are treated as an integral part of other report sections. Many are disclosed in Volume II of this report in the process of explaining items of input data and interpreting example problem output data.

3. THEORETICAL FRAMEWORK

A. INTRODUCTION

The matrix methods of analysis based upon discrete element idealization have been the subject of an extensive body of technical literature and, more recently, entire books as well. [19, 20]. This documentation obviates the need for detailed theoretical development herein. Nevertheless, in the interest of clarity and completeness, presentation of the discrete element representations incorporated within the MAGIC System is prefaced in this Section by general symbolic statement of the analysis processes. This gives explicit definition to the methodology and notation employed.

Statement of the analysis processes is separated into three parts, Firstly, consideration is given to the discrete element representations. Then, having given definition to the discrete element matrices employed, the steps executed by the MAGIC System in the conduct of a linear stress analysis are described. Lastly, the stability analysis process, which is an extension of the linear stress analysis, is presented.

B. DISCRETE ELEMENT MATRICES

1. Fundamental Requirements

The development of a discrete element representation is essentially a problem in elasticity. Accordingly, the fundamental requirements to be satisfied are those of:

(a) Equilibrium,

(b) Material Behavior,

(c) Compatibility, and

(d) Boundary Conditions.

It is convenient to approach the satisfaction of these requirements for a discrete element variationally by way of the principle of potential energy[21] which states that:

> Of all possible displacement states within as given admissible class $\{\delta\}$, that which makes the total potential energy $\Phi_p\{\delta\}$ stationary, satisfies the equilibrium requirements and is the actual displacement state $\{\delta\}^*$, i.e.

$$\left.\frac{\partial \Phi_p \quad \{\delta\}}{\partial \delta_j}\right|_{\{\delta\}=\{\delta\}^*} = 0 \quad j = 1, 2, \ldots, n. \tag{1}$$

Furthermore, if

$$\Phi_p\left(\{\delta\}^*\right) < \Phi_p(\{\delta\}) \tag{2}$$

for all $\{\delta\}$ in some neighborhood of $\{\delta\}^*$, then associated equilibrium position is stable.

2. Discretization

The foregoing statement of the principle of potential energy is expressed in terms of a finite number of displacement variables $\{\delta\}$ implying prior discretization of the potential energy functional. Discretization of the potential energy functional is effected in accordance with the well known Rayleigh-Ritz techniques by the introduction of assumed displacement mode shapes. Admissibility conditions must be imposed on the characteristics of these displacement mode shapes to assure satisfaction of certain fundamental requirements.

The fundamental requirement of compatibility of strains is provided for subsequently in this development by expression of the strains in terms of displacements. Since the functional dependence of strains upon displacements involves differentiation, continuity requirements arise as criteria of admissibility to be satisfied in the construction of displacement mode shapes. It should be emphasized that these continuity requirements remain applicable across discrete element boundaries [22].

The foregoing interelement continuity admissibility conditions are peculiar to the discrete element method of analysis. The admissibility requirements associated with conventional applications of the Rayleigh-Ritz techniques apply as well. The definition of general systematic procedures for constructing displacement functions within the collective confines of these fundamental requirement related admissibility conditions has proved to be an elusive goal. However, significant progress in this direction has been made by the use of unconventional and curvelinear coordinate systems and interpolation formulae[23, 24, 25].

Practical considerations involved in the selection of assumed displacement functions go beyond the problem of admissibility. Of particular importance is the number of displacement degrees-of-freedom to be associated with an element. The provision of degree-of-freedom in excess of the number required to establish admissibility is attractive in that it reduces the number of elements required in idealizations in order to maintain a certain level of precision and correspondingly reduces the input data preparation.

Improvement in stress predictions is also realized as a consequence of including additional degrees-of-freedom in an element representation. Furthermore, it has been demonstrated on certain example problems that improved predictions of displacement behavior can be obtained with fewer total degrees-of-freedom if the number of degrees-of-freedom associated with an individual element are increased[26].

These attractive advantages of higher order assumed displacement functions are achieved at the expense of simplicity, which has been a primary recommendation of the discrete element methods. This characteristic has been somewhat obscured by the trend toward advanced geometrically complex discrete elements pursued in the interest of eliminating structure idealization errors. The additional increment in complexity of mode definition, formulation, checkout, specification, and numerical expression introduced by extra element degrees-of-freedom severely handicaps attempts to achieve the aforementioned advantages.

As a final comment regarding criteria for selection of assumed displacement functions it is pertinent to note that many practical structures have obvious physical definition in terms of panels and stiffners. A lesser element gridwork would require prohibitively complex, problem orientated, stiffened panel discrete elements. At the same time the increase in accuracy afforded by a higher order panel element representation is unwarranted in most problems of this type. Thus, it is concluded that the most significant advancements in element representations will continue to stem from elimination of structure idealization error rather than reduction of element discretization error.

The actual process of constructing displacement mode shapes begins with the definition of a convenient set of coordinate axes for the discrete element model. Then, the boundaries of the element are given parametric description. Polynomial mode shapes are the type customarily chosen to represent the displacement functions within the parametrically described boundaries of a discrete element. With reference to the selected element coordinate axes, such assumed displacement functions can be written symbolically as

$$\{u(\,)\} = [B(\,)]\{\beta\} \tag{3}$$

where

$\{u\}$ is the vector of displacement functions,
$[B]$ is the matrix of mode shapes, and
$\{\beta\}$ is the vector of mode shape participation coefficients.

The participation coefficients $\{\beta\}$ in the assumed displacement modes are referred to as "field coordinate" displacement degrees-of-freedom. These field coordinates are commonly retained throughout the algebraic development of a discrete element representation; however, in order to effect assembly of elements (establish interelement

continuity) it is necessary to transform to gridpoint displacement degrees-of-freedom $\{\delta_g\}$. This transformation results from a straightforward application of interpolation theory. The displacement functions are particularized to the selected gridpoint quantities $\{\delta_g\}$ thereby yielding,

$$\{\delta_g\} = [\Gamma_{\delta\beta}]\{\beta\} \tag{4}$$

The objective transformation is then obtained by the inversion of this relation, i.e.

$$\{\beta\} = [\Gamma_{\beta\delta}]\{\delta_g\} \tag{5}$$

The gridpoint displacement degrees-of-freedom $\{\delta\}$ are generally defined with respect to coordinate systems on the individual discrete elements. Frequently, a number of further displacement coordinate transformations are then necessary to obtain degrees-of-freedom which are suitable for assembly and convenient for interpretation. All such transformations are given explicit definition within the individual discrete element representations; however, two are common to most elements and are described here.

Generally, it is necessary to transform to a global Cartesian set of coordinate axes. This system, common to all discrete elements of an idealized structure, is suitable for interconnection of the elements. The transformation relation to obtain gridpoint displacement degrees-of-freedom $\{\delta_s\}$ referenced to global axes takes the form

$$\{\delta_g\} = [\Gamma_{gs}]\{\delta_s\} \tag{6}$$

in which the transformation matrix $[\Gamma_{gs}]$ consists of submatrices of direction cosines.

Boundary conditions on displacement quantities not aligned with the global axes require special point-related coordinate axes for these gridpoints. Taking the associated coordinate axes transformation for a gridpoint as,

$$\{x_s\} = [T_{sq}]_j \{x_q\}_j \tag{7}$$

the transformation to gridpoint axis displacement degrees-of-freedom is given by

$$\{\delta_s\} = [\Gamma_{sq}]\{\delta_q\} \tag{8}$$

Transformations of this type are employed simply to facilitate interpretation of the results in many cases.

It is useful to conclude comment on the construction of displacement function mode shapes by collecting the foregoing transformations. The result is

$$\{\beta\} = \left[\Gamma_{\beta q}\right]\{\delta_q\} \tag{9}$$

where

$$\left[\Gamma_{\beta q}\right] = \left[\Gamma_{\beta\delta}\right]\left[\Gamma_{gs}\right]\left[\Gamma_{sq}\right] \tag{10}$$

Customarily, the formulative process is carried forward using the field coordinate displacement degrees-of-freedom $\{\beta\}$ and then Equation 9 is invoked to obtain the discrete element matrices with respect to the gridpoint displacement degrees-of-freedom $\{\delta_q\}$. The matrices which actually participate in this collective transformation $\left[\Gamma_{\beta q}\right]$ vary from element to element.

3. Equilibrium

The principle of potential energy was introduced to facilitate satisfaction of the fundamental requirements for a discrete element. Having examined the nature of the discretization implied in the statement of the energy principle, attention is returned to assuring satisfaction of these fundamental requirements.

It is clear from the statement of the principle of potential energy that this variational approach circumvents explicit consideration of equilibrium requirements. The equilibrium requirements arise naturally in the Euler equations of the variation process. This is an important advantage of the method.

4. Material Behavior

Preceeding in the order listed at the outset, the second fundamental requirement to be satisfied in the elasticity problem posed by a discrete element is that of material behavior. Linear elastic behavior, governed by a generalized Hooke's law, is assumed, i.e.

$$\{\sigma()\} = \left[E\right]\left\{\{\epsilon()\} - \{\epsilon_i()\}\right\} \tag{11}$$

where

$\{\sigma\}$ is the stress state,
$\{\epsilon\}$ is the state of strain
$\left[E\right]$ is the elastic property characterization, and
$\{\epsilon_i\}$ is the prestrain state.

In recognition of the increasing utilization of high performance particulate and fibrous composite materials, material anisotropy is provided for in defining this stress-strain relation. The availability of material property data generally limits material specifications to orthotropic, at most. However, the application of a rotational transformation in order to reference the material characterization to the geometric coordinate axes of a discrete element tends to fill the material property matrices. For this reason, no terms in elastic $[E]$ and thermal $\{\alpha\}$ property characterization matrices are assumed zero.

5. Compatibility

Satisfaction of the third fundamental requirement, compatibility, is provided for by expressing strains in terms of the displacements. Interpretation of this requirement in terms of admissibility conditions on displacement mode shapes was discussed previously and appropriate functions are assumed available at this point. The introduction of these displacement mode shapes (Equation 3) into the relevant strain-displacement equations enables expression of the strains in terms of the discrete element field coordinate displacement degrees-of-freedom, i.e.

$$\{\epsilon(\,)\} = [C(\,)]\{\beta\} \tag{12}$$

Nonlinear terms have been omitted in this set of strain-displacement relations. These will be given special consideration subsequently.

6. Boundary Conditions

The final fundamental requirements which must be established are the boundary conditions. Force boundaries need not be given explicit consideration since these are accommodated implicitly by the variational process. Displacement boundary conditions, on the other hand, must be imposed. Expression of the element displacement mode shapes in terms of boundary displacement provides for the simple imposition of these boundary conditions.

7. Potential Energy

Proceeding toward algebraic expression of a discrete element representation, it remains to give definition to the potential energy function. The strain energy density, dU, which is basic to the potential energy, is defined as

$$dU = \int_{\{0\}}^{\{\epsilon\}} [\, d\epsilon \,]\{\sigma\} \tag{13}$$

Invoking the relation governing material behavior obtain expression of the total strain energy as,

$$U = \int_V \left(\frac{1}{2} \left[\epsilon \right] \left[E \right] \left\{ \epsilon \right\} - \left[\epsilon \right] \left[E \right] \left\{ \epsilon_i \right\} \right) dV \tag{14}$$

Substituting the relation governing compatibility (Equation 12) obtain, in the presence of distributed mechanical loading, $\{ p \}$ the total potential energy function in the form

$$\begin{aligned} \Phi_p = \int_V \frac{1}{2} \left[\beta \right] \left[C( ) \right]^T \left[E \right] \left[C( ) \right] \left\{ \beta \right\} \\ - \left[\beta \right] \left[C( ) \right]^T \left[E \right] \left\{ \epsilon_i \right\} \\ - \left[\beta \right] \left[B( ) \right]^T \left\{ p \right\} \end{aligned} \tag{15}$$

This substitution of the assumed displacement functions into the element total potential energy functional and the subsequent integration over the volume comprise a major part of the effort associated with the derivation of a discrete element representation. The procedure is conceptually simple though algebraically complex. Indicating the integration symbolically, obtain an algebriac expression for the element total potential energy as

$$\Phi_p = \frac{1}{2} \left[\beta \right] \left[\tilde{K} \right] \left\{ \beta \right\} - \left[\beta \right] \left\{ \tilde{F}_\epsilon \right\} - \left[\beta \right] \left\{ \tilde{F}_p \right\} \tag{16}$$

where

$$\left[\tilde{K} \right] = \int_V \left[C( ) \right]^T \left[E \right] \left[C( ) \right] dV \tag{17}$$

$$\left\{ \tilde{F} \right\} = \int_V \left[C( ) \right]^T \left[E \right] \left\{ \epsilon_i \ ( ) \right\} dV \tag{18}$$

$$\left\{ \tilde{F}_p \right\} = \int_V \left[B( ) \right]^T \left\{ p( ) \right\} \tag{19}$$

These element matrices in the potential energy expression are referenced to the field coordinate displacement degrees-of-freedom. The previously defined transformation (Equation 9) is introduced to obtain the element matrices in the potential energy expression with reference to selected gridpoint displacement degrees-of-freedom, i.e.

$$\Phi_p = \frac{1}{2} \left[\delta_q \right] \left[K \right] \left\{ \delta_q \right\} - \left[\delta_q \right] \left\{ F_\epsilon \right\} - \left[\delta_q \right] \left\{ F_p \right\} \tag{20}$$

where

$$[K] = [\Gamma_{\beta_q}]^T [\tilde{K}][\Gamma_{\beta_q}] \tag{21}$$

$$\{F_\epsilon\} = [\Gamma_{\beta_q}]^T \{\tilde{F}_\epsilon\} \tag{22}$$

$$\{F_p\} = [\Gamma_{\beta_q}]^T \{\tilde{F}_p\} \tag{23}$$

At this point the objective matrices governing behavior of a discrete element follow immediately by executing the variation of the potential energy function, i.e.

$$[K]\{\delta_q\} - \{F_\epsilon\} - \{F_p\} = \{F_c\} \tag{24}$$

where

$[K]$ is the element stiffness matrix,
$\{F_\epsilon\}$ is the element prestrain load vector,
$\{F_p\}$ is the element distributed load vector, and
$\{F_c\}$ is the concentrated gridpoint load vector.

8. Incremental Stiffness Matrix

The representation for the frame element incorporated in the MAGIC System is written to include an incremental stiffness matrix. These matrices stem from avoiding a complete linearization of the mathematical models for the discrete elements. The formulative process is outlined below. Conceptual examination of this process is deferred to the presentation of the stability analysis procedure.

As a first step, the total strain induced at a point is decomposed into a contribution linearly related to displacement quantities $\{\epsilon\}$ and one which is second order in the displacement quantities $\{\epsilon_N\}$, i.e.

$$\{\epsilon_T(\ )\} = \{\epsilon(\ )\} + \{\epsilon_N(\ )\} \tag{25}$$

Using this notation, the potential energy contribution which leads to the objective incremental stiffness matrix takes the form,

$$\Phi_c = \int_V \{\epsilon(\ )\} [E] \{\epsilon_N(\ )\} dV \tag{26}$$

All other energy terms associated with the nonlinear contribution to the total strain are assumed to be negligible in comparison.

The knowledge that each term of $\{\epsilon(\ )\}$ has a linear dependence on the displacement functions and that the dependence of each term in $\{\epsilon_N(\ )\}$ is quadratic allows alternative expression of Equation 26 as

$$\Phi_c = \Sigma_i \Sigma_j \int_v \lambda_{ij} \ f_i(\ )\, g_j(\ )\, h_j(\ )\, dV \tag{27}$$

The term λ_{ij} is simply a multiplicative constant and the f_j, g_j and h_j are displacement function forms. These displacement quantities are expressible in terms of the assumed displacement functions thereby accomplishing the discretization of the energy functional. Symbolically, this expansion in terms of the assumed displacement function mode shapes can be written

$$f_i = \left[B_f(\ ) \right] \{ a \}_i \tag{28}$$

$$g_j = \left[B_g(\ ) \right] \{ b \}_j \tag{29}$$

$$h_j = \left[B_h(\ ) \right] \{ c \}_j \tag{30}$$

The $\{B\}$ matrices contain the independent variables of the mode shapes which are common to each term of a given element respresentation and the $\{a\}_i$, $\{b\}_j$, and $\{c\}_j$ are the coefficient matrices. The discretized potential energy function which results from the introduction of these assumed mode shapes is cast into matrix form

$$\Phi_{cij} = \frac{1}{6} \lambda_{ij} \left[[a]_i, [b]_j, [c]_j \right] \begin{bmatrix} , & [C_N], & [B_N] \\ [C_N]^T, & , & [A_N] \\ [B_N]^T, & [A_N]^T, & \end{bmatrix}_{ij} \begin{Bmatrix} \{a\}_i \\ \{b\}_j \\ \{c\}_j \end{Bmatrix} \tag{31}$$

where

$$[A_N]_{ij} = \int_v f_i(\ ) \{B_g\}_j \ [B_h]_j \ dV \tag{32}$$

$$[B_N]_{ij} = \int_v g_i(\ ) \{B_f\}_j \ [B_h]_j \ dV \tag{33}$$

$$[C_N]_{ij} = \int_v h_i(\ ) \{B_f\}_j \ [B_g]_j \ dV \tag{34}$$

Now in any given application the vectors $\{a\}_i$, $\{b\}_j$ and $\{c\}_j$ must be specified for the contributing energy terms. This is done by listing λ_{ij} together with the following items for each term:

$$\{a\}_i = [\Lambda_a]_i \{\beta_a\}_i \tag{35}$$

$$\{b\}_j = [\Lambda_b]_j \{\beta_b\}_j \tag{36}$$

$$\{c\}_j = [\Lambda_c]_j \{\beta_c\}_j \tag{37}$$

The knowledge of these terms yields each typical energy contribution as a function of the field coordinate displacement degrees-of-freedom and the sum of the typical energy terms can be carried out to obtain

$$\Phi_c = \frac{1}{6} \{\beta\} [\tilde{N}] \{\beta\} \tag{38}$$

The matrix $[\tilde{N}]$ is the element incremental stiffness matrix referenced to the field coordinate displacement degrees-of-freedom. The previously defined transformation (Equation 9) is introduced to obtain the element incremental stiffness matrix with reference to selected gridpoint displacement degrees-of-freedom, i.e.

$$\Phi_c = \frac{1}{6} \{\delta_q\} [N] \{\delta_q\} \tag{39}$$

where

$$[N] = [\Gamma_{\beta q}]^T [\tilde{N}] [\Gamma_{\beta q}] \tag{40}$$

The matrix $[N]$ is the objective incremental stiffness matrix. It is clear from the foregoing development that the elements in this matrix are functions of the unknown displacement quantities $\{\beta\}$. It follows that this matrix serves to introduce the effects of finite displacements. The utilization of this nonlinear matrix is discussed as an integral part of the stability analysis procedure.

It is recognized by the authors that the foregoing outline of the development of an element incremental stiffness matrix is lacking in clarity. Matrix notation is not well suited to expression of nonlinear relations. Recourse to the explicit statement of the incremental stiffness matrix for the frame element in Section 4 is suggested for clarification of this general symbolic statement of an element incremental stiffness matrix.

9. Stress Matrices

Having completed expression of the total potential energy based element matrices, it is appropriate to define the element stress matrices. The element stress matrices stem directly from the governing equations. The stress-displacement relation is obtained upon substitution of the strain-displacement equation (Equation 12) into the stress-strain equation (Equation 11), i.e.

$$\{\sigma\} = [E][C(\ )]\{\beta\} - [E]\{\epsilon_i\} \tag{41}$$

Transformation to gridpoint coordinates and particularization to specific points within the element yields

$$\{\sigma\} = [S]\{\delta_q\} - \{\mathcal{A}\} \tag{42}$$

where the element stress matrices are given by

$$[S] = [E][C][\Gamma_{\beta q}] \tag{43}$$

$$\{\mathcal{A}\} = [E]\{\epsilon_i\} \tag{44}$$

Stress resultants rather than point stresses are sought in the thin shell and slender prismatic elements. Resultants corresponding to deformations not considered may be obtained directly from the governing differential equations of equilibrium. In general, a rotational transformation is applied in order to exhibit stress values with reference to coordinate axes which simplify interpretation.

This completes statement of the method employed in deriving the discrete element representations incorporated in the MAGIC System. The matrices of the individual discrete elements are recorded in Sections 4 through 9.

C. LINEAR STRESS ANALYSIS

1. Stiffness Equation

The mathematical model for the total structure is traditionally constructed by forming equilibrium equations corresponding to the gridpoint displacement degrees-of-freedom. A more general systematic approach to constructing the mathematical model for the total structure is realized by carrying forward the variational viewpoint. Specifically, the energy functions for the total structure can be constructed by effecting a nonconformable sum of the individual element matrix energy forms. This nonconformable sum, in which common gridpoint degrees-of-freedom are employed for adjoining elements, imposes continuity over the entire structure. Application of the Euler equation (Equation 1) then yields the objective governing equations for the structure. This variational approach to the assembly of elements to form a total structure representation is particularly attractive when generalized nonphysical displacements degrees-of-freedom such as "w_{xxy}" are retained [26].

The element matrices for a structural system are generated from the input data to the MAGIC System without regard to their interconnection as indicated in Block 2 of Figure 2. Since knowledge of these individual element matrices is required during subsequent analysis phases, they are released from the generation of the MAGIC System as distinct submatrices of system level matrices. For example, the linear strain energy stored in all the elements is written as

$$U = \tfrac{1}{2} \left[\Delta_I \right] \left[K_{SI} \right] \left\{ \Delta_I \right\} \tag{45}$$

where

$$\left\{ \Delta_I \right\}^T = \left[\left\{ \delta_q \right\}_1^T, \left\{ \delta_q \right\}_2^T, \cdots, \left\{ \delta_q \right\}_j^T, \cdots, \left\{ \delta_q \right\}_n^T \right] \tag{46}$$

$$\left[K_{SI} \right] = \begin{bmatrix} \left[K \right]_1 & & & & & \\ & \left[K \right]_2 & & & & \\ & & \ddots & & & \\ & & & \left[K \right]_j & & \\ & & & & \ddots & \\ & & & & & \left[K \right]_n \end{bmatrix} \tag{47}$$

The element column matrices are also stacked individually in system level vectors. For example, the external work of all the element loads applied to all elements takes the form,

$$W = \left[\Delta_I \right] \left\{ P_{eI} \right\} \tag{48}$$

where

$$\left\{ P_{eI} \right\}^T = \left[\left\{ F_\epsilon + F_p \right\}_1^T, \left\{ F_\epsilon + F_p \right\}_2^T \cdots, \left\{ F_\epsilon + F_p \right\}_n^T \right] \tag{49}$$

Several additional system level matrices are generated from the input data. Firstly, the matrix of the gridpoint loading at every degree-of-freedom in all loading conditions is provided, i.e.

$$\left\{ P_c \right\}^T = \left[\left\{ P_c \right\}_1^T, \left\{ P_c \right\}_2^T, \cdots, \left\{ P_c \right\}_j^T, \cdots, \left\{ P_c \right\}_m^T \right] \tag{50}$$

The input data describing the interconnection of elements is processed to obtain a system level assembly matrix. This assembly matrix takes the form of a transformation matrix between all possible gridpoint degrees-of-freedom $\left\{ \Delta_I \right\}$ and those gridpoint degrees-of-freedom which remain after interconnection of the elements to form the objective structural system $\left\{ \Delta_a \right\}$, i.e.

$$\left\{ \Delta_a \right\} = \left[\Gamma_a \right] \left\{ \Delta_I \right\} \tag{51}$$

$$\{\Delta_a\}^T = \left[\{\Delta_a\}_1^T \cdot \{\Delta_a\}_2^T, \cdots, \{\Delta_a\}_j^T, \cdots, \{\Delta_a\}_m^T\right] \quad (52)$$

A further system level matrix is generated to extract the degrees-of-freedom which actually exist from all those associated with the gridpoints of the assembled structure. This matrix takes the form of a transformation between the complete set of degrees-of-freedom $\{\Delta_a\}$ and the actual or reduced set $\{\Delta_s\}$, i.e.

where
$$\{\Delta_a\} = [\Gamma_r]\{\Delta_s\} \quad (53)$$

$$\{\Delta_s\}^T = [\Delta_{s1}, \Delta_{s2}, \cdots, \Delta_{sm}] \quad (54)$$

Provision of the foregoing system level matrices enables execution of a linear stress analysis. The first step taken is to combine the assembly and reduction transformations of Equations 51 and 53 to obtain

where
$$\{\Delta_I\} = [\Gamma_{ar}]\{\Delta_s\} \quad (55)$$

$$[\Gamma_{ar}] = [\Gamma_a][\Gamma_r] \quad (56)$$

This combined transformation is introduced into the energy expressions of Equations 45 and 48 to obtain the desired system matrices, i.e.

where
$$\Phi_p = \frac{1}{2}[\Delta_s][K_s]\{\Delta_s\} - [\Delta_s]\{P_s\} \quad (57)$$

$$[K_s] = [\Gamma_{ar}]^T[K_{sI}][\Gamma_{ar}] \quad (58)$$

$$\{P_s\} = [\Gamma_{ar}]^T\{P_{eI}\} + [\Gamma_r]^T\{P_c\} \quad (59)$$

The variation of this potential energy function now yields a governing stiffness equation which takes the form

$$[K_s]\{\Delta_s\} = \{P_s\} \quad (60)$$

This equation is presently solved by inversion. In general, multiple load conditions exist and a corresponding multiplicity of solutions is obtained.

2. Element Stresses

As in the case of stiffness and load matrices, the element stress matrices are stacked individually in system level matrices, i.e.

$$\{\sigma_s\} = [S_s]\{\Delta_I\} - \{\mathcal{A}_s\} \tag{61}$$

where

$$\{\sigma_s\}^T = \left[\{\sigma\}_1^T, \{\sigma\}_2^T, \cdots, \{\sigma\}_j^T, \cdots, \{\sigma\}_n^T\right] \tag{62}$$

$$\{\mathcal{A}_s\}^T = \left[\{\mathcal{A}\}_1^T \{\mathcal{A}\}_2^T, \cdots, \{\mathcal{A}\}_j^T, \cdots, \{\mathcal{A}\}_n^T\right] \tag{63}$$

$$[S_s] = \begin{bmatrix} [S]_1 & & & & \\ & [S]_2 & & & \\ & & \ddots & & \\ & & & [S]_j & \\ & & & & \ddots \\ & & & & & [S]_n \end{bmatrix} \tag{64}$$

Stresses are secondary variables obtained subsequent to the solution for the primary variables $\{\Delta_s\}$. Equation 55 enables direct expression of the desired stress quantities in terms of the primary displacement variables, i.e.

$$\{\sigma_s\} = [S][\Gamma_{ar}]\{\Delta_s\} - \{\mathcal{A}_s\} \tag{65}$$

3. Element Forces

Element forces are useful results in many applications. This is particularly true when the element employed is a simulation of the actual component. The back substitution for element forces takes the form

$$\{F_{net}\} = [K_{sI}][\Gamma_{ar}]\{\Delta_s\} - \{P_{eI}\} \tag{66}$$

where

$$\{F_{net}\}^T = \left[\{F_{net}\}_1^T, \{F_{net}\}_2^T, \cdots, \{F_{net}\}_j^T, \cdots, \{F_{net}\}_n^T\right] \tag{67}$$

4. Reactions

The final step is to calculate the force balances and the reactions. These are readily available from the element forces, i.e.,

$$\{R_s\} = [\Gamma_a]^T \{F_{net}\} - \{P_c\} \tag{68}$$

D. STABILITY ANALYSIS

An analysis procedure is incorporated in the MAGIC System to examine the stability of flexible lightweight structures. The structural stability phenomena associated with structures of this type inevitably involve geometrically nonlinear behavior, while, in contrast, material behavior remains linearly elastic. Thus, it is somewhat fortuitous that geometric nonlinearities are most readily incorporated in the subject, displacement methods of analysis.

There exists a hierachy of geometric nonlinearities which may be incorporated. Associated with each level of nonlinearity is a degree of complexity and a range of applicability. The stability analysis provided in the MAGIC System is restricted to the prediction of critical load values and buckling mode shapes. The prediction of nonlinear pre- and post-buckling behavior is not attempted.

The "classical" approach to buckling analysis is based upon the assumption that the membrane force distribution induced in a structure is known ab initio as a linear function of the applied loading. The intensity of the given membrane force distribution that causes the effective flexure stiffness to vanish implies a critical applied load intensity or buckling load.

The behavior of thin-shell and slender prismatic structural components of zero curvature is, within the scope of linear mechanics, naturally completely uncoupled into membrane and flexure behavior. A similar uncoupling of membrane and flexure behavior can be obtained for components of non-zero curvature subjected to certain types of boundary and applied load conditions. This uncoupling of membrane and flexure behavior is employed to advantage in the subject general instability analysis. However, the nature of the instability phenomena associated with practical built-up structures of complex configuration and applied loading transcends the scope of the preceding classical buckling analysis assumption. In general, membrane and flexure behavior can only be uncoupled within certain components or zones of the total structure. Linear coupling, which occurs at the junctures, cannot be avoided and is accounted for in the subject general stability analysis.

Geometric nonlinearities are introduced into the analytical model for stability analysis via the previously defined element incremental stiffness matrix. In the presence of the incremental stiffness matrix, the potential energy for a discrete element takes the form

$$\Phi_p = \frac{1}{2} \left[\delta_q\right]\left[K\right]\left\{\delta_q\right\} + \frac{1}{6} \left[\delta_q\right]\left[N\right]\left\{\delta_q\right\} - \left[\delta_q\right]\left\{P\right\} \qquad (69)$$

The element incremental stiffness matrices, like the stiffness and load matrices, are made available from the matrix generator in the form

$$\left[N_{sI}\right] = \begin{bmatrix} \left[N\right]_1 & & & & \\ & \left[N\right]_2 & & & \\ & & \ddots & & \\ & & & \left[N\right]_j & \\ & & & & \ddots \\ & & & & & \left[N\right]_n \end{bmatrix} \tag{70}$$

The total potential energy for a structural assembly of discrete elements can be indicated symbolically as

$$\Phi_{ps} = \frac{1}{2} \left|\Delta_s\right| \left[K_s\right] \left\{\Delta_s\right\} + \frac{1}{6} \left|\Delta_s\right| \left[N_s\right] \left\{\Delta_s\right\} - \left|\Delta_s\right| \left\{P_s\right\} \tag{71}$$

in which the definition of the one new symbol introduced, $\left[N_s\right]$, follows immediately from the statement of the linear stress analysis, i.e.

$$\left[N_s\right] = \left[\Gamma_{ar}\right]^T \left[N_{sI}\right] \left[\Gamma_{ar}\right] \tag{72}$$

Equation 71 represents a geometrically nonlinear mathematical model suitable for the prediction of certain types of nonlinear behavior. The stability analysis in the MAGIC System is directed toward the more modest goal of predicting critical buckling loads. Reference 27 is recommended as a useful source of information regarding the prediction of nonlinear pre- and post-buckling behavior.

The vanishing of the second variation of the total potential energy is invoked as the buckling criterion. Executing the second variation of the potential energy of Equation 71 obtain,

$$\left[K_s\right] \left\{\delta\Delta_s\right\} + \left[N_s\right] \left\{\delta\Delta_s\right\} = \left\{0\right\} \tag{73}$$

in which the vector $\left\{\delta\Delta_s\right\}$ represents an arbitary variation from the displacement state $\left\{\Delta_s\right\}$.

The computational utilization of Equation 73 for predicting critical loads is based upon the assumption that the incremental stiffness matrix appropriate to the critical load level p_{cr} can be expressed as a function of its value at any given load level $\bar{p}$ i.e.

$$\left[N\right]\Big|_{p = p_{cr}} = \left(\frac{p_{cr}}{\bar{p}}\right) \left[N\right]\Big|_{p = \bar{p}} \tag{74}$$

This is interpretable as assuming that the intensity of the internal force state changes linearly with changes in the applied load without affecting the relative distribution of the internal forces. Invoking this assumption transforms Equation 74 into the form,

$$\left[K\right]\left\{\delta\Delta_s\right\} = -\left(\frac{p_{cr}}{\bar{p}}\right)\left[N\right]\left\{\delta\Delta_s\right\} \tag{75}$$

Clearly, the availability of a linear solution at any load level enables specification of the matrices of this governing equation. The prediction of the critical load level is then reduced to the solution of an eigenvalue problem. The incorporation of this approach in the MAGIC System provides a powerful tool for stability analyses of general frame and thin shell structures.

4. FRAME ELEMENT

A. INTRODUCTION

A conventional frame discrete element is incorporated in the MAGIC System. This element, shown in Figure 6, is suitable for the idealization of structural components which are adequately characterized by "beam theory." Having established basic procedure and notation in Section 3, the mathematical model for the frame element is summarized in this section in terms of element matrices. The formulation is presented in detail in Reference 28.

The frame element is broadly applicable to space frame and stiffened shell structures. Connection eccentricities can be accounted for in shell stiffener applications of the frame element. Space trusses can be accommodated as a special case of space frames. The truss specialization is particularly useful in combination with the shear panel element of Section 5.

Geometric specification of the straight slender prismatic frame element is given, in part, by the end point coordinates. A third coordinate point in the positive quadrant of the element axis system (x_g, y_g) is required to specify the twist orientation.

The cross section of the frame element is assumed doubly symmetric with respect to the element coordinate axes. It is characterized by stiffnesses I_{xx}, I_{yy} and I_{zz} about the three element axes together with the cross sectional area.

A linear Hooke's law is assumed to govern material behavior. Cross sections initially orthogonal to the element axis are assumed to maintain orthogonality with the deformed axis. It is further assumed that deformations are sufficiently small to allow superposition of element loading.

Linear polynominal axial and torsional displacement mode shapes are constructed. A cubic polynominal displacement mode shape is constructed for flexure in each of the two principal planes of bending. These mode shapes lead to a total of 12 undetermined coefficients for the element which are chosen to correspond to three translational and three rotational displacement degrees-of-freedom at each end of the element. Description of stress behavior is accepted as the definition of the 12 forces acting at the two gridpoint connections.

Element matrices are provided for stiffness, incremental stiffness, stress, distributed loading, and axial thermal loading. Certain of these participate in the evaluative application to a portal frame structure presented in this section.

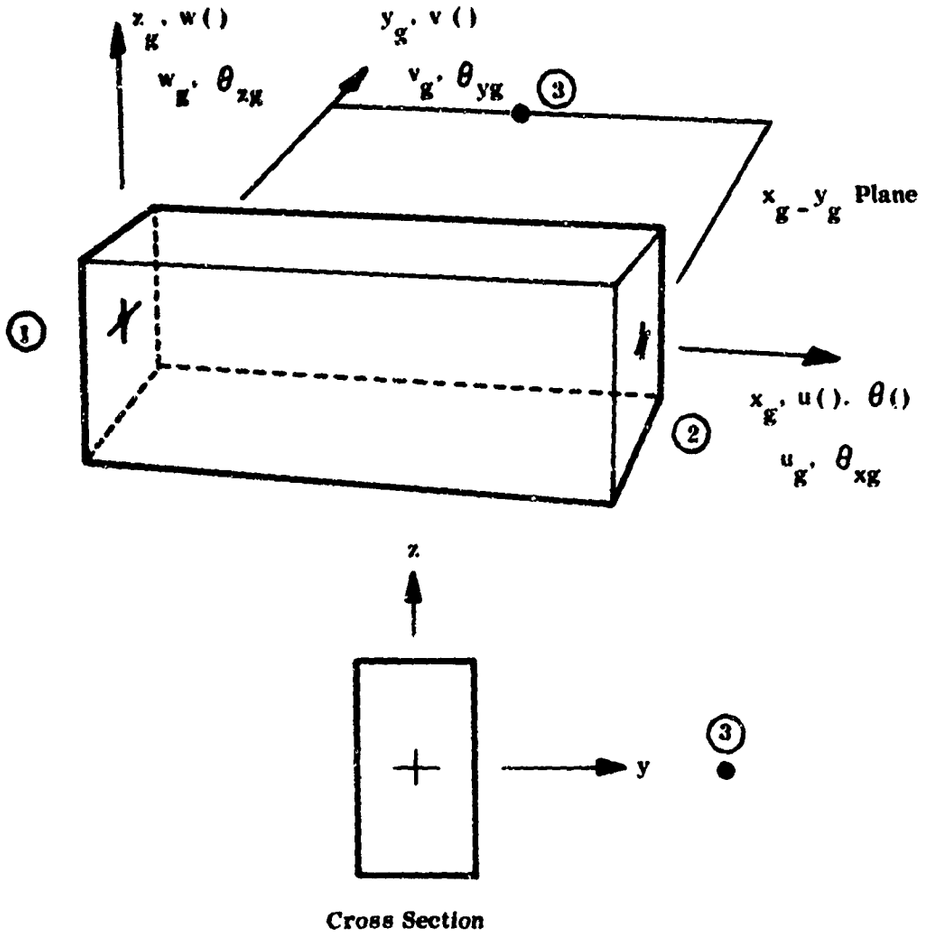

Figure 6. Frame Element Representation

B. FORMULATION

1. Displacement Functions

The polynominal mode shapes assumed for the displacement functions are written

$$\{u(\,)\} = [B(\,)]\{\beta\} \tag{76}$$

where

$$\{u(\,)\}^T = \lfloor u(\,), v(\,), w(\,), \theta(\,) \rfloor \tag{77}$$

$$\{\beta\}^T = \lfloor \beta_1, \beta_2, \cdots, \beta_{12} \rfloor \tag{78}$$

$$
\left[B(\,)\right] = \begin{matrix} u \\ v \\ w \\ \theta \end{matrix}
\begin{bmatrix}
\lfloor B_1(\,)\rfloor, & & & \\
& , \lfloor B_2(\,)\rfloor, & & \\
& & , \lfloor B_2(\,)\rfloor, & \\
& & & , \lfloor B_1(\,)\rfloor
\end{bmatrix}
$$

where

$$
\left\{B_1(\,)\right\}^T = \lfloor 1,\ x \rfloor
$$

$$
\left\{B_2(\,)\right\}^T = \lfloor 1,\ x,\ x^2,\ x^3 \rfloor
$$

Figure 7. Displacement Function Mode Shapes $\left[B(\,)\right]$

and $\left[B(\,)\right]$, the matrix of mode shapes is defined in Figure 7. Elementary interpolation theory is invoked to obtain a transformation to gridpoint displacement degrees-of-freedom, i.e.

$$
\{\beta\} = \left[\Gamma_{\beta\delta}\right]\{\delta_g\} \tag{79}
$$

where

$$
\{\delta_g\}^T = \lfloor u_{g1}, v_{g1}, w_{g1}, \theta_{xg1}, \theta_{yg1}, \theta_{zg1}, u_{g2}, v_{g2}, w_{g2}, \theta_{xg2}, \theta_{yg2}, \theta_{zg2} \rfloor \tag{80}
$$

and $\left[\Gamma_{\beta\delta}\right]$ is defined in Figure 8.

Assuming the ends of the frame element are positioned as shown in Figure 9 relative to the offset gridpoint, an eccentric connection transformation is provided via

$$
\{\delta_g\} = \left[\Gamma_e\right]\{\delta_e\} \tag{81}
$$

where

$$
\{\delta_e\}^T = \lfloor u_{e1}, v_{e1}, w_{e1}, \theta_{xe1}, \theta_{ye1}, \theta_{ze1}, u_{e2}, v_{e2}, w_{e2}, \theta_{xe2}, \theta_{ye2}, \theta_{ze2} \rfloor \tag{82}
$$

and $\left[\Gamma_e\right]$ is defined in Figure 10.

Since the eccentric connection is translational only, the subsequent transformation to system coordinates $\left\{x_s\right\}$ is based upon the original direction cosines of the element. This transformation relation takes the form

$$\left\{\delta_e\right\} = \left[\Gamma_{\delta\Delta}\right]\left\{\delta_s\right\} \tag{83}$$

	u_{g1}	u_{g1}	w_{g1}	θ_{gx1}	θ_{gy1}	θ_{gz1}	u_{g2}	v_{g2}	w_{g2}	θ_{gx2}	θ_{gy2}	θ_{gz2}
β_1	1											
β_2	$-\frac{1}{L}$						$+\frac{1}{L}$					
β_3		1										
β_4						1						
β_5		$-\frac{3}{L^2}$				$-\frac{2}{L}$		$+\frac{3}{L^2}$				$-\frac{1}{L}$
β_6			$+\frac{2}{L^2}$			$+\frac{1}{L^2}$		$+\frac{2}{L^3}$				$+\frac{1}{L^2}$
β_7			+1									
β_8				-1								
β_9			$-\frac{3}{L^2}$		$+\frac{2}{L}$				$+\frac{3}{L^2}$		$+\frac{1}{L}$	
β_{10}			$+\frac{2}{L^3}$		$-\frac{1}{L^2}$				$-\frac{2}{L^3}$		$-\frac{1}{L^2}$	
β_{11}				1								
β_{12}				$-\frac{1}{L}$						$+\frac{1}{L}$		

Figure 8. Displacement Coordinate Transformation $\left[\Gamma_{\beta\delta}\right]$

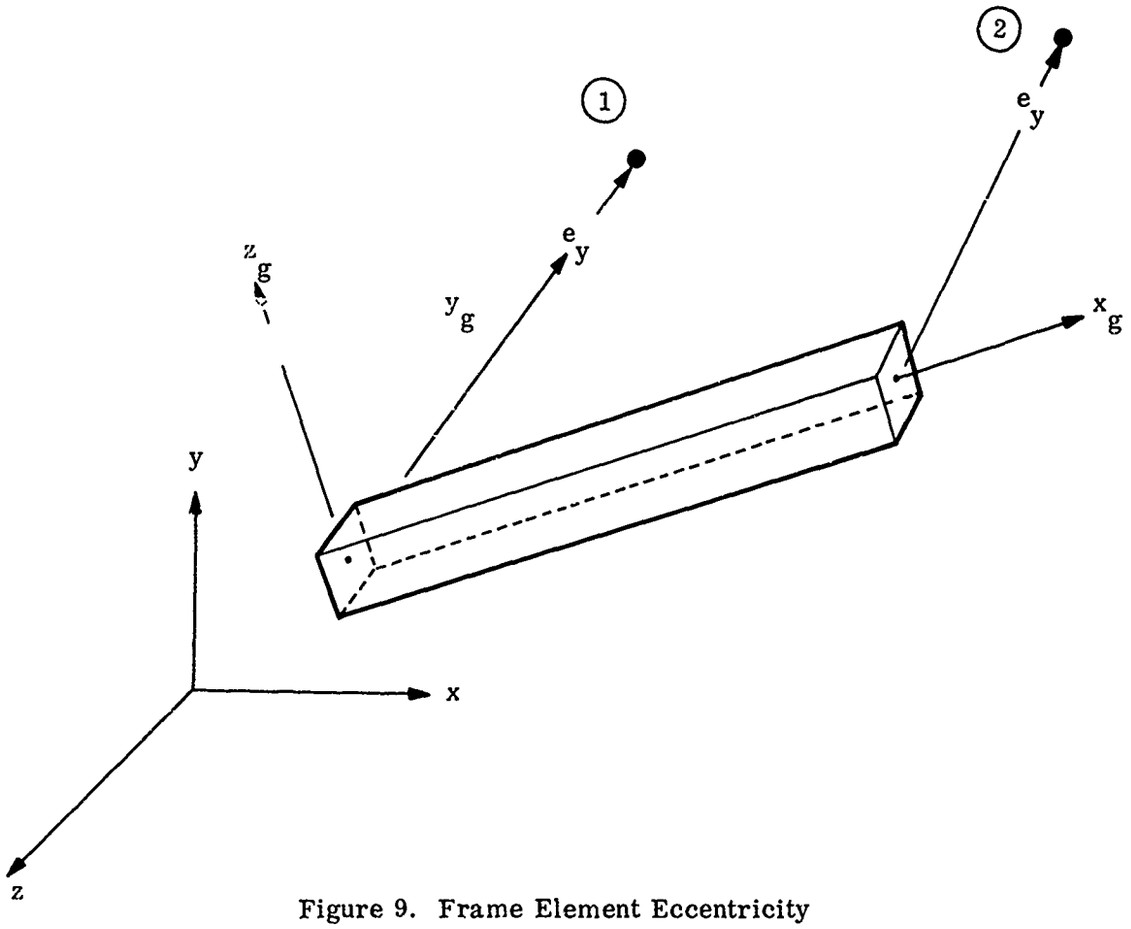

Figure 9. Frame Element Eccentricity

where

$$\left\{\delta_s\right\}^T = \left[u_{s1}, v_{s1}, w_{s1}, \theta_{xs1}, \theta_{ys1}, \theta_{zs1}, u_{s2}, v_{s2}, w_{s2}, \theta_{xs2}, \theta_{ys2}, \theta_{zs2}\right] \tag{84}$$

$$\left[\Gamma_{gs}\right] \quad \begin{bmatrix} \left[T_{gs}\right], & & & \\ & \left[T_{gs}\right], & & \\ & & \left[T_{gs}\right], & \\ & & & \left[T_{gs}\right] \end{bmatrix} \tag{85}$$

The matrix $\left[T_{gs}\right]$ is the direction cosine transformation between element $\left\{x_g\right\}$ and global $\left\{x_s\right\}$ coordinate axes, i.e.

$$\left\{x_g\right\} = \left[T_{gs}\right]\left\{x_s\right\} \tag{86}$$

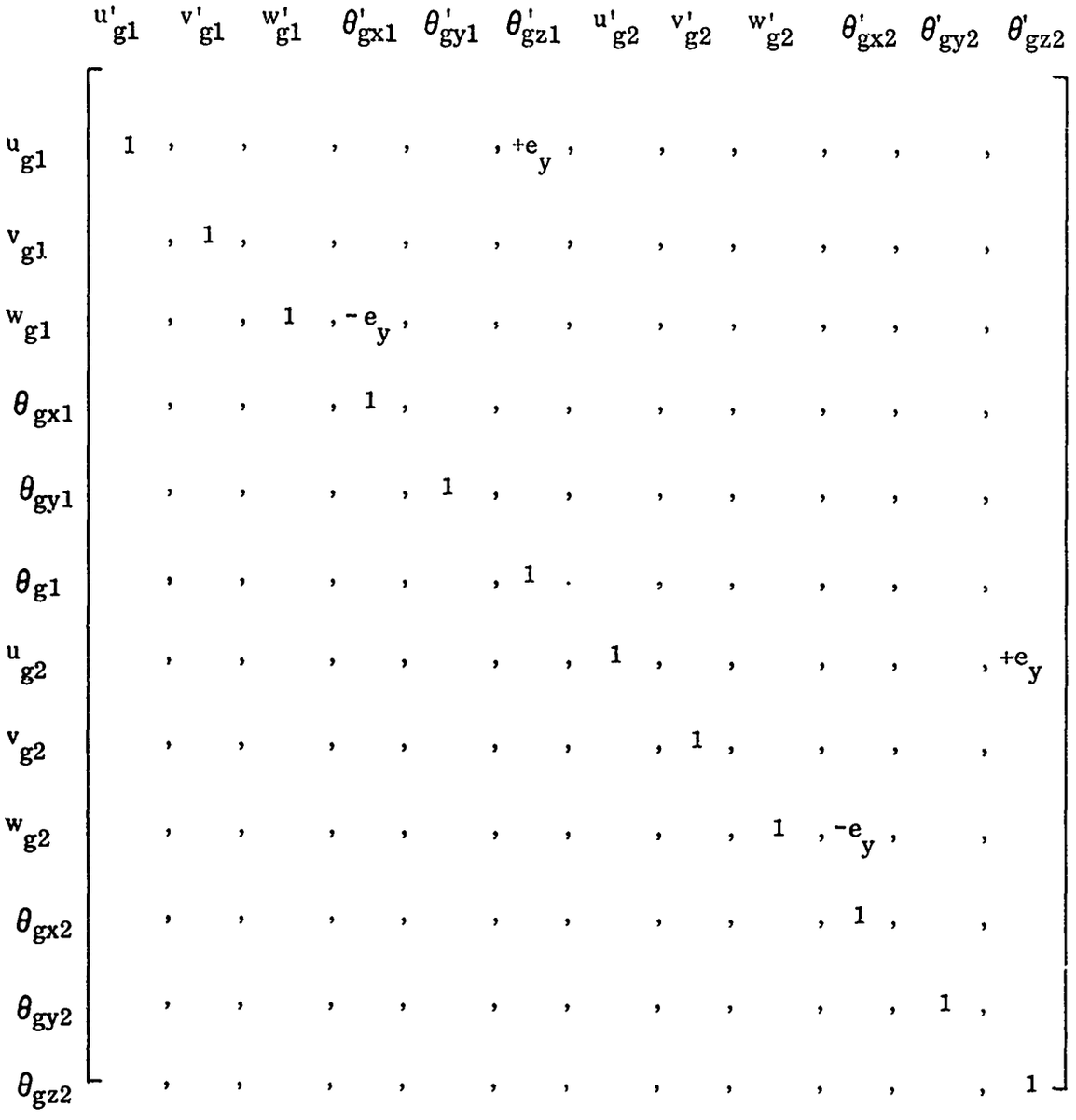

Figure 10. Displacement Coordinate Transformation $\left[\Gamma_e\right]$

The final transformation builds in the option to employ degrees-of-freedom referenced to gridpoint axes. Transformations between the gridpoint axes and system axes are known from the input to the MAGIC System. For the two gridpoints of the frame element these take the form

$$\left\{x_s\right\}_j = \left[T_{sq}\right]_j \left\{x_q\right\}_j \qquad j = 1, 2 \tag{87}$$

Given these axes transformations, the objective gridpoint displacement degrees-of-freedom are introduced via the relation

$$\{\delta_s\} = [\Gamma_{sq}]\{\delta_q\} \tag{88}$$

where (89)

$$\{\delta_q\}^T = \left\lfloor u_{q1}, v_{q1}, w_{q1}, \theta_{xq1}, \theta_{yq1}, \theta_{zq1}, u_{q2}, v_{q2}, w_{q2}, \theta_{xq2}, \theta_{yq2}, \theta_{zq2} \right\rfloor$$

$$[\Gamma_{sq}] = \begin{bmatrix} [T_{sq}]_1 & , & , \\ , & [T_{sq}]_1 & , \\ , & , & [T_{sq}]_2 \\ , & , & , [T_{sq}]_2 \end{bmatrix} \tag{90}$$

In summary, displacement functions are assumed in terms of field coordinate displacement degrees-of-freedom. These are retained for the algebraic development. Then, the foregoing sequence of transformations is invoked to yield the desired displacement degrees-of-freedom. Collectively, this set of transformations is written as

$$\{\beta\} = [\Gamma_{\beta q}]\{\delta_q\} \tag{91}$$

where

$$[\Gamma_{\beta q}] = [\Gamma_{\beta\delta}][\Gamma_e][\Gamma_{gs}][\Gamma_{sq}] \tag{92}$$

2. Linearized Potential Energy

The assumption of linear material behavior governed by

$$\sigma = E(\epsilon - \epsilon_i) \tag{93}$$

leads to a strain energy of membrane and flexure given by

$$U = \int_v \left(\frac{1}{2} E \epsilon^2 - E \epsilon_i \epsilon\right) dv \tag{94}$$

The linearized strain-displacement relation for the frame element is,

$$\epsilon = u_x - yv_{xx} - zw_{xx} \tag{95}$$

The prescribed prestrain ϵ_i is taken to be constant over the cross section and over the length.

The linear potential energy functional which arises in consequence of these strain relations is

$$\Phi_{pl} = \int_x \frac{1}{2} (EAu_x^2 + EI_z v_{xx}^2 + EI_y w_{xx}^2 + EI_x \theta_x^2 \tag{96}$$

$$-EA\epsilon_i u_x - P_y V - P_z W)\, dx$$

Note that torsion and distributed load terms have been incorporated in the above energy expression. The distributed loadings P_y and P_z are assumed to be linearly varying over the length of the element, i.e.

$$P(x) = \left[1 - \left(\frac{x}{L}\right)\right] P_1 + \left(\frac{x}{L}\right) P_2 \tag{97}$$

Substituting the displacement mode shapes into the linear potential energy functional and integrating over the cross-section obtain,

$$\Phi_{pl} = \frac{1}{2} \lfloor \beta \rfloor \left[\tilde{K}\right] \{\beta\} - \lfloor \beta \rfloor \left\{\tilde{F}_\epsilon\right\} - \lfloor \beta \rfloor \left\{\tilde{F}_p\right\} \tag{98}$$

where the matrices $\left[\tilde{K}\right]$, $\left\{\tilde{F}_\epsilon\right\}$ and $\left\{\tilde{F}_p\right\}$ are given in Figures 11, 12, and 13, respectively. In conformance with the notation of Section 3, the foregoing are the element stiffness $\left[\tilde{K}\right]$, prestrain load $\left\{\tilde{F}_\epsilon\right\}$, and pressure load $\left\{\tilde{F}_p\right\}$ matrices referenced to field coordinate displacement degrees-of-freedom.

It is convenient to define a distinct prestrain load vector for strains induced by thermal expansions. Since flexure prestrains are omitted in the absence of knowledge of the cross section geometry, specialization of the prestrain $\left\{\tilde{F}_\epsilon\right\}$ load to thermal load $\left\{\tilde{F}_{\epsilon T}\right\}$ is accomplished by the relation,

$$\epsilon_i = \alpha \Delta T \tag{99}$$

3. Incremental Stiffness

The retention of quadratic displacement terms in the strain-displacement relation for the frame element yields the strain contribution,

$$\epsilon_N(\,) = \frac{1}{2} v_x^2 + \frac{1}{2} w_x^2 \tag{100}$$

	β_1	β_2	β_3	β_4	β_5	β_6	β_7	β_8	β_9	β_{10}	β_{11}	β_{12}
β_1	,	,	,	,	,	,	,	,	,	,	,	
β_2	,	EAL	,	,	,	,	,	,	,	,	,	
β_3	,	,	,	,	,	,	,	,	,	,	,	
β_4	,	,	,	,	,	,	,	,	,	,	,	
β_5	,	,	,	,	$4EI_zL$	,	,	,	,	,	,	
β_6	,	,	,	,	$6EI_zL^2$	$12EI_zL^3$	,	,	,	,	,	
β_7	,	,	,	,	,	,	,		,	,	,	
β_8	,	,	,	,	,	,	,	,	,	,	,	
β_9	,	,	,	,	,	,	,	,	$4EI_yL$	,	,	
β_{10}	,	,	,	,	,	,	,	,	$6EI_yL^3$	$12EI_yL^3$	,	
β_{11}	,	,	,	,	,	,	,	,	,	,	,	
β_{12}	,	,	,	,	,	,	,	,	,	,	,	GJL

Figure 11. Stiffness Matrix $\left[\tilde{K}\right]$

This nonlinear strain term leads to two incremental stiffness energy contributions, i.e.

$$\Phi_c = \sum_{j=1}^{2} \Phi_{cj} \tag{101}$$

where

$$\Phi_{c1} = \int_x \frac{1}{2} EAu_x v_x^2 \, dx \tag{102}$$

$$\Phi_{c2} = \int_x \frac{1}{2} EAu_x w_x^2 \, dx \tag{103}$$

$$
\begin{matrix} \beta_1 \\ \beta_2 \\ \beta_3 \\ \beta_4 \\ \beta_5 \\ \beta_6 \\ \beta_7 \\ \beta_8 \\ \beta_9 \\ \beta_{10} \\ \beta_{11} \\ \beta_{12} \end{matrix}
\begin{Bmatrix} 0 \\ EA_{\epsilon\, i} \\ 0 \\ 0 \\ 0 \\ 0 \\ 0 \\ 0 \\ 0 \\ 0 \\ 0 \\ 0 \end{Bmatrix}
$$

Figure 12. Prestrain Load Vector $\left\{\tilde{F}_{\epsilon}\right\}$

$$
\begin{matrix} a_0 & \beta_1 \\ a_1 & \beta_2 \\ b_0 & \beta_3 \\ b_1 & \beta_4 \\ b_2 & \beta_5 \\ b_3 & \beta_6 \\ c_0 & \beta_7 \\ c_1 & \beta_8 \\ c_2 & \beta_9 \\ c_3 & \beta_{10} \\ d_0 & \beta_{11} \\ d_1 & \beta_{12} \end{matrix}
\begin{Bmatrix} 0 \\ 0 \\ \left(\frac{L}{2}\right) p_{y1} + \left(\frac{L}{2}\right) p_{y2} \\ \left(\frac{L^2}{6}\right) p_{y1} + \left(\frac{L^2}{3}\right) p_{y2} \\ \left(\frac{L^3}{12}\right) p_{y1} + \left(\frac{L^3}{4}\right) p_{y2} \\ \left(\frac{L^4}{20}\right) p_{y1} + \left(\frac{L^4}{5}\right) p_{y2} \\ \left(\frac{L}{2}\right) p_{z1} + \left(\frac{L}{2}\right) p_{z2} \\ \left(\frac{L^2}{6}\right) p_{z1} + \left(\frac{L^2}{3}\right) p_{z2} \\ \left(\frac{L^3}{12}\right) p_{z1} + \left(\frac{L^3}{4}\right) p_{z2} \\ \left(\frac{L^4}{20}\right) p_{z1} + \left(\frac{L^4}{5}\right) p_{z2} \\ 0 \\ 0 \end{Bmatrix}
$$

Figure 13. Pressure Load Vector $\left\{\tilde{F}_{p}\right\}$

Each of these terms is of the general form constructed in the symbolic development of Section 3. The general form is stated here in the context of the frame element as

$$\Phi_{cj} = \int_x \lambda f g_j h_j \, dx \tag{104}$$

where

$$f = \left[1 \right] \left\{ a \right\} \tag{105}$$

$$g_j = \left[1, x, x^2 \right] \left\{ b \right\}_j \tag{106}$$

$$h_j = \left[1, x, x^2 \right] \left\{ c \right\}_j \tag{107}$$

The matrix form of a typical contribution to the incremental stiffness energy now follows immediately in consequence of the theoretical development of Section 3, i.e.

$$\Phi_{cj} = \frac{1}{6} \lambda \left[\left\{ a \right\}^T, \left\{ b \right\}_j^T, \left\{ c \right\}_j^T \right] \begin{vmatrix} & , \left[C_N \right] & , \left[B_N \right] \\ \left[C_N \right]^T, & & , \left[A_N \right] \\ \left[B_N \right]^T, & \left[A_N \right]^T, & \end{vmatrix} \begin{Bmatrix} \left\{ a \right\} \\ \left\{ b \right\}_j \\ \left\{ c \right\}_j \end{Bmatrix} \tag{108}$$

The three matrices $\left[A_N \right]$, $\left[B_N \right]$, and $\left[C_N \right]$ are given explicit definition in Figure 14. Particularization of this general form to the individual energy contributions of Equations 102 and 103 is given in Figure 15 by specification of λ and the quantities:

$$\left\{ a \right\} = \left[\Lambda_a \right] \left\{ \beta_a \right\} \tag{109}$$

$$\left\{ b \right\}_j = \left[\Lambda_b \right] \left\{ \beta_b \right\}_j \tag{110}$$

$$\left\{ c \right\}_j = \left[\Lambda_c \right] \left\{ \beta_c \right\}_j \tag{111}$$

The knowledge of these quantities enables the execution of a nonconformable sum of the individual contributions to obtain the total incremental stiffness energy in terms of the field coordinates, i.e.

$$\Phi_c = \frac{1}{6} \left[\beta \right] \left[\tilde{N} \right] \left\{ \beta \right\} \tag{112}$$

$$\left[A_N\right]_j = \begin{bmatrix} L\,a_1 & , & \frac{L^2}{2}a_1 & , & \frac{L^3}{3}a_1 \\ \frac{L^2}{2}a_1 & , & \frac{L^3}{3}a_1 & , & \frac{L^4}{4}a_1 \\ \frac{L^3}{3}a_1 & , & \frac{L^4}{4}a_1 & , & \frac{L^5}{5}a_1 \end{bmatrix}_j$$

$$\left\{B_N\right\}_j^T = \left[\sum_{k=1}^{3}\left(\frac{L^k}{k}\right)b_k\,,\ \sum_{k=1}^{3}\left(\frac{L^{k+1}}{k+1}\right)b_k,\ \sum_{k=1}^{3}\left(\frac{L^{k+2}}{k+2}\right)b_k\right]_j$$

$$\left\{C_N\right\}_j^T = \left[\sum_{k=1}^{3}\left(\frac{L^k}{k}\right)c_k\,,\ \sum_{k=1}^{3}\left(\frac{L^{k+1}}{k+1}\right)c_k\,,\ \sum_{k=1}^{3}\left(\frac{L^{k+2}}{k+2}\right)c_k\right]_j$$

Figure 14. Incremental Stiffness Submatrices $\left[A_N\right]$, $\left\{B_N\right\}$ and $\left\{C_N\right\}$

The matrix $\left[\tilde{N}\right]$ is the objective element incremental stiffness matrix referenced to field coordinate displacement degrees-of-freedom. Transformation to the selected gridpoint displacement degrees-of-freedom is accomplished via the previously derived transformation;

$$\left\{\beta\right\} = \left[\Gamma_{\beta q}\right]\left\{\delta_q\right\} \tag{113}$$

Since the elements of the incremental stiffness are functions of subsets of the $\left\{\beta\right\}$ via the $\left\{a\right\}$, $\left\{b\right\}_j$, and $\left\{c\right\}_j$, they are indirectly functions of the independent primary displacement variables $\left\{\Delta_s\right\}$. Thus, expression of the incremental stiffness for a stability analysis required the availability of the displacement results from a prior analysis.

The incremental stiffness matrix for the frame element has been stated here in accord with the standard form outlined in Section 3. Proper interpretation is very important and, for this reason, a typical term for the frame element is resurrected here and examined in detail.

$$\Phi_{c1}: \quad \lambda_1 = \frac{EA}{2}$$

$$\left\{a\right\}_1 = \left[\ 1\ \right] \left\lfloor \beta_2 \right\rfloor^T$$

$$\left\{b\right\}_1 = \left[\ 1, 2, 3\ \right] \left\lfloor \beta_4, \beta_5, \beta_6 \right\rfloor^T$$

$$\left\{c\right\}_1 = \left\{b\right\}_1$$

$$\Phi_{c2}: \quad \lambda_2 = \frac{EA}{2}$$

$$\left\{a\right\}_2 = \left[\ 1\ \right] \left\lfloor \beta_2 \right\rfloor^T$$

$$\left\{b\right\}_2 = \left[\ 1, 2, 3\ \right] \left\lfloor \beta_8, \beta_9, \beta_{10} \right\rfloor^T$$

Figure 15. Incremental Stiffness Parameters

Beginning from Equation 102, this energy contribution is rewritten as

$$\Phi_{c1} = \int \frac{1}{2} EA\ u_x v_x v'_x\ dx \tag{114}$$

to obtain the appearance of the more general form in which all these functions are different. This form is rewritten, in turn as

$$\Phi_{c1} = \frac{1}{6} \int EA\ (\tilde{u}_x v_x v'_x + u_x \tilde{v}_x v'_x + u_x v_x \tilde{v}'_x)\, dx \tag{115}$$

The over-symbol ~ requires definition. Matrices are the natural notation of multi-dimensional linear algebra. As a consequence they have become the language of the finite element analysis technology. Recognizing this, the subject nonlinear formulation is cast into matrix form to facilitate interpretation and implementation. The over-symbol ~ serves to identify variables which will be imbedded in coefficient matrices to accommodate matrix notation. With this explanation, Equation 115 is rewritten again as

$$\Phi_{c1} = \frac{1}{6}\int \frac{EA}{2} \begin{bmatrix} u_x, & v_x, & v'_x \end{bmatrix} \begin{bmatrix} 0 & , v'_x & , v_x \\ v'_x & , 0 & , u_x \\ v_x & , u_x & , 0 \end{bmatrix} \begin{Bmatrix} u_x \\ v_x \\ v'_x \end{Bmatrix} \tag{116}$$

At this point the assumed mode shapes are introduced into the vectors in which u_x, v_x, and v'_x correspond to the f, g and h of Equations 105, 106 and 107, i.e.

$$\begin{Bmatrix} u_x \\ v_x \\ v'_x \end{Bmatrix} = \begin{vmatrix} 1 , & & \\ , 1 , x , x^2 , & & \\ & , 1 , x , x^2 & \end{vmatrix} \begin{Bmatrix} \{a\} \\ \{b\} \\ \{c\} \end{Bmatrix} \tag{117}$$

Substitution of these mode shape quantities into the energy functional yields

$$\Phi_{c1} = \frac{1}{6}\int \left[\{a\}^T, \{b\}^T, \{c\}^T \right] \begin{bmatrix} 0 & v'_x \begin{bmatrix} 1 , x , x^2 \end{bmatrix} & v_x \begin{bmatrix} 1 , x , x^2 \end{bmatrix} \\ v'_x \begin{Bmatrix} 1 \\ x \\ x^2 \end{Bmatrix} & \begin{bmatrix} 0 \end{bmatrix} & u_x \begin{bmatrix} 1 , x , x^2 \\ x , x^2 , x^3 \\ x^2 , x^3 , x^4 \end{bmatrix} \\ v_x \begin{Bmatrix} 1 \\ x \\ x^2 \end{Bmatrix} & v_x \begin{bmatrix} 1 , x , x^2 \\ x , x^2 , x^3 \\ x^2 , x^3 , x^4 \end{bmatrix} & \begin{bmatrix} 0 \end{bmatrix} \end{bmatrix} \begin{Bmatrix} \{a\} \\ \{b\} \\ \{c\} \end{Bmatrix} dx \tag{118}$$

The integrated form of this relation corresponds to the symbolic form exhibited in Equation 108. The remaining step is to bring in the field coordinate displacement degrees-of-freedom. The transformation relation required takes the form

$$\begin{Bmatrix} a_1 \\ b_1 \\ b_2 \\ b_3 \\ b_1' \\ b_2' \\ b_3' \end{Bmatrix} = \begin{bmatrix} 1 & , & , & , \\ , & 1 & , & , \\ , & , & 2 & , \\ , & , & , & 3 \\ , & 1 & , & , \\ , & , & 2 & , \\ , & , & , & 3 \end{bmatrix} \begin{Bmatrix} \beta_2 \\ \beta_4 \\ \beta_5 \\ \beta_6 \end{Bmatrix} \tag{119}$$

This relation is equivalent to the symbolic relations of Equations 109, 110 and 111 taken collectively. Introduction of this relation into Equation 118 yields the objective incremental stiffness contribution. These individual contributions are accumulated to obtain the total as expressed in Equation 112. Beyond this point, the symbolic statement of the analysis process requires no further clarification.

4. Stress Matrix

Stresses for a frame discrete element are represented by the end point forces. These "stress" quantities are exhibited with respect to element axes. Calculation is based upon the relation

$$\{\sigma\} = [S]\{q\} - \{\phi\} \tag{120}$$

where

$$\{\sigma\}^T = \left\lfloor F_{x1}, F_{y1}, F_{z1}, M_{x1}, M_{y1}, M_{z1}, F_{x2}, F_{y2}, F_{z2}, M_{x2}, M_{y2}, M_{z2} \right\rfloor \tag{121}$$

$$[S] = [\Gamma_{\beta\delta}]^T [\tilde{K}] [\Gamma_{\beta q}] \tag{122}$$

Expression of this stress matrix completes the specification of the matrices which comprise the frame discrete element representation.

C. EVALUATION

As an illustration of the use of the frame element in a structural evaluation, consider the following problem.

A three-member portal frame is shown in Figure 16, along with the loading, pertinent dimensions and material properties. The two idealizations used in this analysis are shown in Figure 17. A comparison solution is given in Reference 29 for this portal frame. Table I presents the results obtained from this analysis and the reference solution. It should be noted that the alternate finite element solution neglects axial deformation, thus producing a slightly stiffer structure.

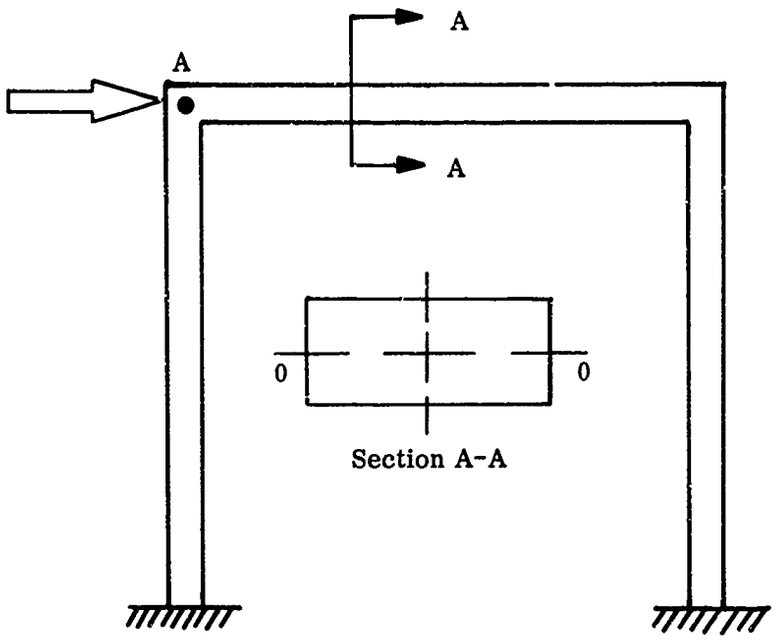

$E = 10^7$ psi

$\nu = 0.30$

$A = 18$ in.^{2}

$I_o = 13.5$ in.^{4}

$G = 3.846 \times 10^6$ psi

$P = 550$ lb

Figure 16. Three Member Portal Frame Description

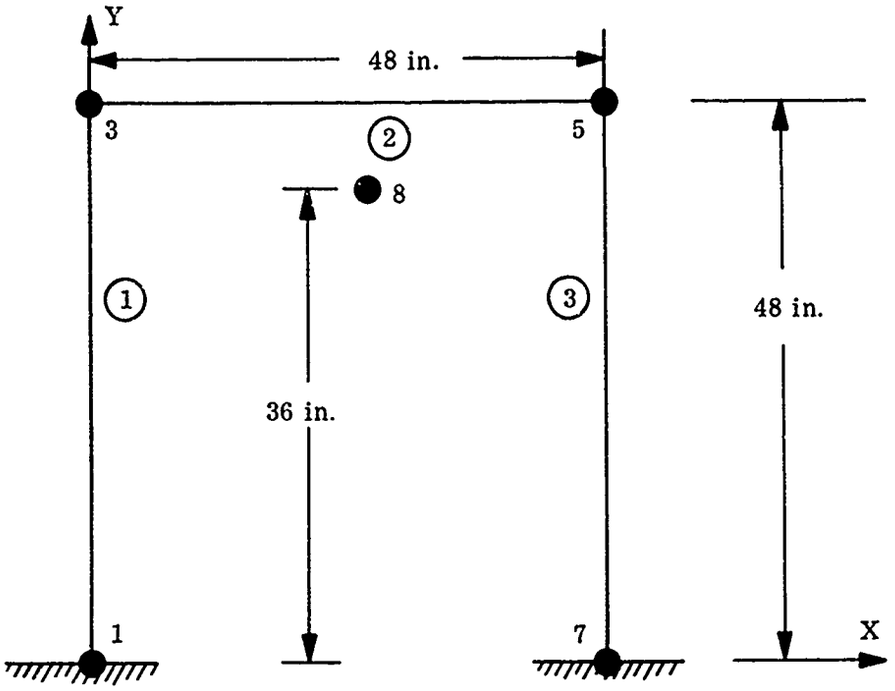

(a) Three Element Portal Frame

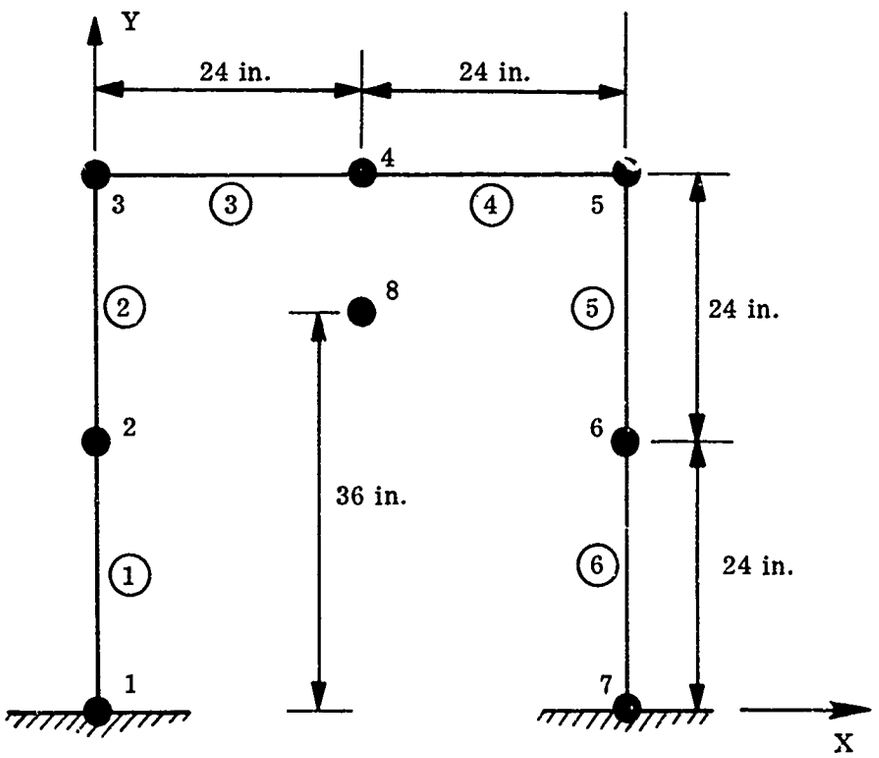

(b) Six Element Portal Frame

Figure 17. Idealizations, Three Member Portal Frame

TABLE I

COMPARISON SOLUTIONS FOR THREE MEMBER PORTAL FRAME

Node Point	Deflection, μ (inches)			Rotation, θ, x 10^{-3}		
	MAGIC (3 Elem)	MAGIC (6 Elem)	Reference	MAGIC (3 Elem)	MAGIC (6 Elem)	Reference
2		0.01143			-0.7564	
3	0.02691	0.02691	0.02682	-0.3382	-0.3382	-0.3350
4		0.02687			-0.1648	
5	0.02684	0.02684	0.02682	-0.3376	-0.3367	-0.3350
6		0.01140			-0.7544	

5. QUADRILATERAL SHEAR PANEL ELEMENT

A. INTRODUCTION

A quadrilateral shear panel is incorporated in the discrete element library of the MAGIC System. This element, shown in Figure 18, is suitable for the representation of thin membranes which carry load primarily by diagonal tension. The direct load carrying capacity of such membranes is delegated to surrounding axial force members available via the frame element of Section 4.

The general quadrilateral shape of the shear panel is defined by the coordinates of the four corner points. The geometric definition is completed by specification of an effective uniform thickness.

In contrast to the usual approach, the principle of complementary energy is employed to derive the representation for the quadrilateral shear panel. Using this approach, stress rather than displacement distributions are assumed. In particular, a constant shear stress state is employed.

Deformation behavior of the shear panel is described by the displacements of its four corner gridpoints. Description of stress behavior is accepted as the constant shear stress value.

The complete element representation for the quadrilateral shear panel is taken to consist of a stiffness matrix and a stress matrix. These matrices are employed in combination with axial force members in an evaluative application to a deep cantilevered beam in this section. Additional illustrative applications are included in Section 10.

B. FORMULATION

The element representation for the quadrilateral shear panel is derived using the principle of complementary energy. Only shearing energy is considered. The governing energy functional is given by

$$\Phi_c = \int_v \frac{1}{2G} (\tau_{xy})^2 \, dv - \left[P_g \right] \left\{ \delta_g \right\} \tag{123}$$

The matrices $\left\{ P_g \right\}$ and $\left\{ o_g \right\}$ are available from observation of Figure 18, i.e.

$$\left\{ P_g \right\}^T = \left[F_{gx1}, F_{gy1}, F_{gx2}, F_{gy2}, F_{gx3}, F_{gy3}, F_{gx4}, F_{gy4} \right] \tag{124}$$

$$\left\{ \delta_g \right\}^T = \left[u_{g1}, v_{g1}, u_{g2}, v_{g2}, u_{g3}, v_{g3}, u_{g4}, v_{g4} \right] \tag{125}$$

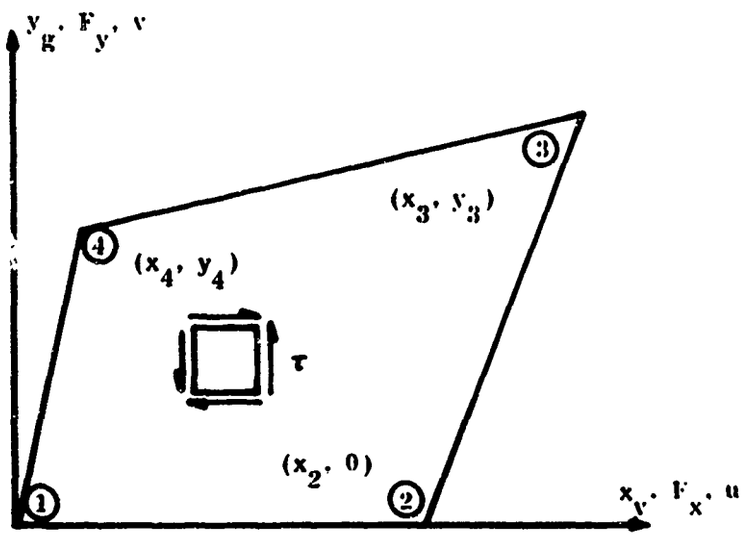

Figure 18. Quadrilateral Shear Panel Representation

The shear stress function τ_{xy} is chosen as the statically independent force quantity and is assumed constant over the element, i.e.

$$\tau_{xy}(x, y) = \tau = \text{Constant.} \tag{126}$$

Recourse is made to Figure 18 to obtain expression for the complete force set in terms of the constant shear stress. The statically equivalent corner grid-point force set is readily written as

$$\{P_g\} = \{\Gamma_\tau\}\tau \tag{127}$$

where

$$\{\Gamma_\tau\}^T = \left[+\frac{t(x_4 - x_2)}{2}, -\frac{ty_4}{2}, -\frac{tx_3}{2}, +\frac{ty_3}{2}, -\frac{t(x_4 - x_2)}{2}, +\frac{ty_4}{2}, +\frac{tx_3}{2}, -\frac{ty_3}{2}\right] \tag{128}$$

Substitution of Equations 126 and 127 into the potential energy functional yields

$$\Phi_c = \int_v \frac{1}{2G}\tau^2 \, dv - \tau\{\Gamma_\tau\}^T\{\delta_g\} \tag{129}$$

At this point an algebraic expression for the total complementary energy follows by integration, i.e.

$$\Phi_c = \frac{At}{2G}\tau^2 - \tau\{\Gamma_\tau\}^T\{\delta_g\} \tag{130}$$

The variation of Equation 129 yields the basic force-deformation relation for the shear panel in the form

$$\tau = \left(\frac{G}{At}\right)\{\Gamma_\tau\}^T\{\delta_g\} \tag{131}$$

The introduction of Equation 127 now yields the desired form of the stiffness matrix for the quadrilateral shear panel referenced to the (x_g, y_g) coordinate axis. This result is

$$\{P_g\} = [K_g]\{\delta_g\} \tag{132}$$

where

$$\left[K_g \right] = \left(\frac{G}{At} \right) \quad \left\{ \Gamma_\tau \right\} \left\{ \Gamma_\tau \right\}^T \tag{133}$$

Statement of the element matrices for the quadrilateral shear panel is completed by introduction of coordinate axis transformations. Writing the direction cosine transformation between element and global axis as

$$\left\{ x_g \right\} = \left[T_{gs} \right] \left\{ x_s \right\} \tag{134}$$

leads immediately to the force and displacement transformations, i.e.

$$\left\{ \delta_g \right\} = \left[\Gamma_{gs} \right] \left\{ \delta_s \right\} \tag{135}$$

$$\left\{ P_g \right\} = \left[\Gamma_{gs} \right] \left\{ P_s \right\} \tag{136}$$

The transformation matrix $\left[\Gamma_{gs} \right]$ is given in Figure 19. The transformation to gridpoint coordinate axes follows similarly, except that a distinct direction cosine transformation is associated with each gridpoint, i.e.

$$\left\{ x_s \right\}_j = \left[T_{sq} \right]_j \quad \left\{ x_q \right\}_j \tag{137}$$

The resultant displacement and force transformations take the form

$$\left\{ \delta_s \right\} = \left[\Gamma_{sq} \right] \left\{ \delta_q \right\} \tag{138}$$

$$\left\{ P_s \right\} = \left[\Gamma_{sq} \right] \left\{ P_q \right\} \tag{139}$$

The matrix $\left[\Gamma_{sq} \right]$ is defined in Figure 20.

The collective influence of the foregoing transformation yields

$$\left\{ P \right\} = \left[K \right] \left\{ \delta_q \right\} \tag{140}$$

where

$$\left[K \right] = \left[\Gamma_{sq} \right]^T \left[\Gamma_{gs} \right]^T \left[K_g \right] \left[\Gamma_{gs} \right] \left[\Gamma_{sq} \right] \tag{141}$$

$$\begin{bmatrix} [T_{gs}], & & & \\ & [T_{gs}], & & \\ & & [T_{gs}], & \\ & & & [T_{gs}] \end{bmatrix}$$

Figure 19. Displacement Coordinate Transformation $[\Gamma_{gs}]$

$$\begin{bmatrix} [T_{sq}]_1, & & & \\ & [T_{sq}]_2, & & \\ & & [T_{sq}]_3, & \\ & & & [T_{sq}]_4 \end{bmatrix}$$

Figure 20. Displacement Coordinate Transformation $[\Gamma_{sq}]$

Equation 139 is the objective form of the stiffness relation for the quadrilateral shear panel. Once the displacements have been calculated, the single stress quantity τ is available from a form of Equation 130 extended to accommodate the transformation relations, i.e.

$$\tau = \lfloor S \rfloor \{\delta_q\} \tag{142}$$

where

$$\lfloor S \rfloor = \left(\frac{G}{At}\right) \lfloor \Gamma_\tau \rfloor \lfloor \Gamma_{gs} \rfloor \lfloor \Gamma_{sq} \rfloor \tag{143}$$

This completes the statement of the element matrix representation for the quadrilateral shear panel.

C. EVALUATION

As an illustration of the use of the quadrilateral shear panel element in a structural evaluation consider the following problem.

A cantilever beam subjected to a uniform load of 2×10^{-2} kg per mm is shown in Figure 21 along with its pertinent dimensions and material properties. The three idealizations employed in the finite element analysis are shown in Figure 22. Axial force members are used along with the subject shear panels for idealization of this structure.

A solution to this problem was obtained in Reference 47 utilizing "equilibrium spar elements" for the web and "bar" elements for the caps. Solutions were also obtained utilizing spar elements with linear as well as quadratic displacement fields.

Figure 23 displays the tip and midpoint deflections for the three idealizations used in this analysis along with the displacements obtained in Reference 47. Figure 24 shows the bending moment distribution for the two element case and Figure 25 shows the moment distribution for the four and eight element cases. It is to be noted that the agreement of the bending moment distributions with the reference solutions are excellent.

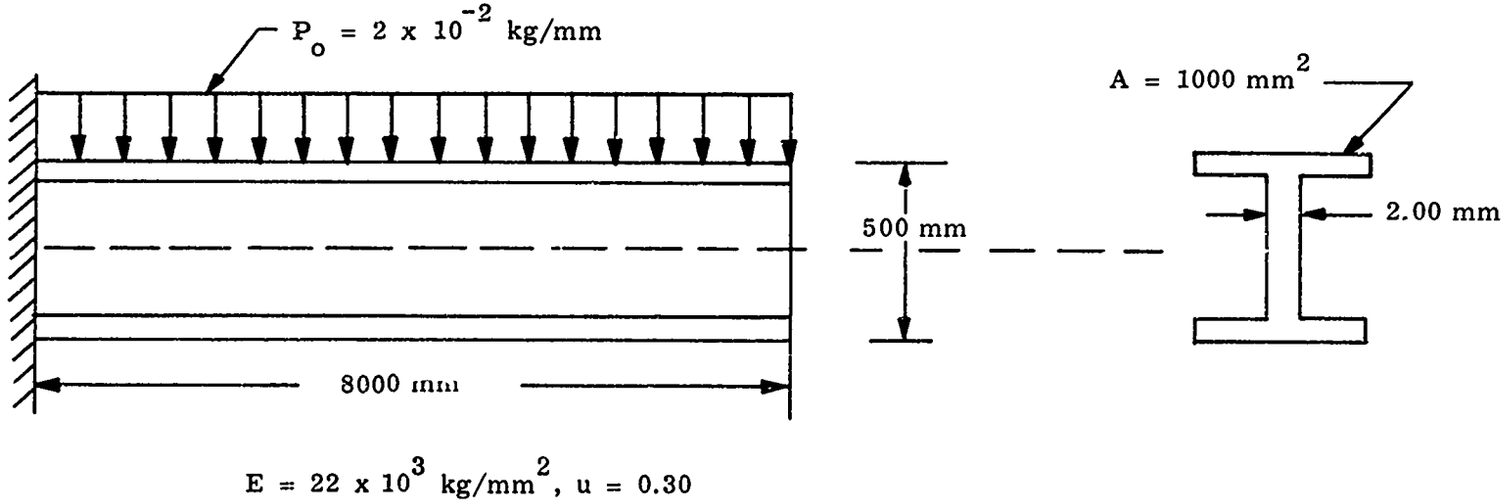

Figure 21. Cantilever Beam with Uniformly Distributed Load

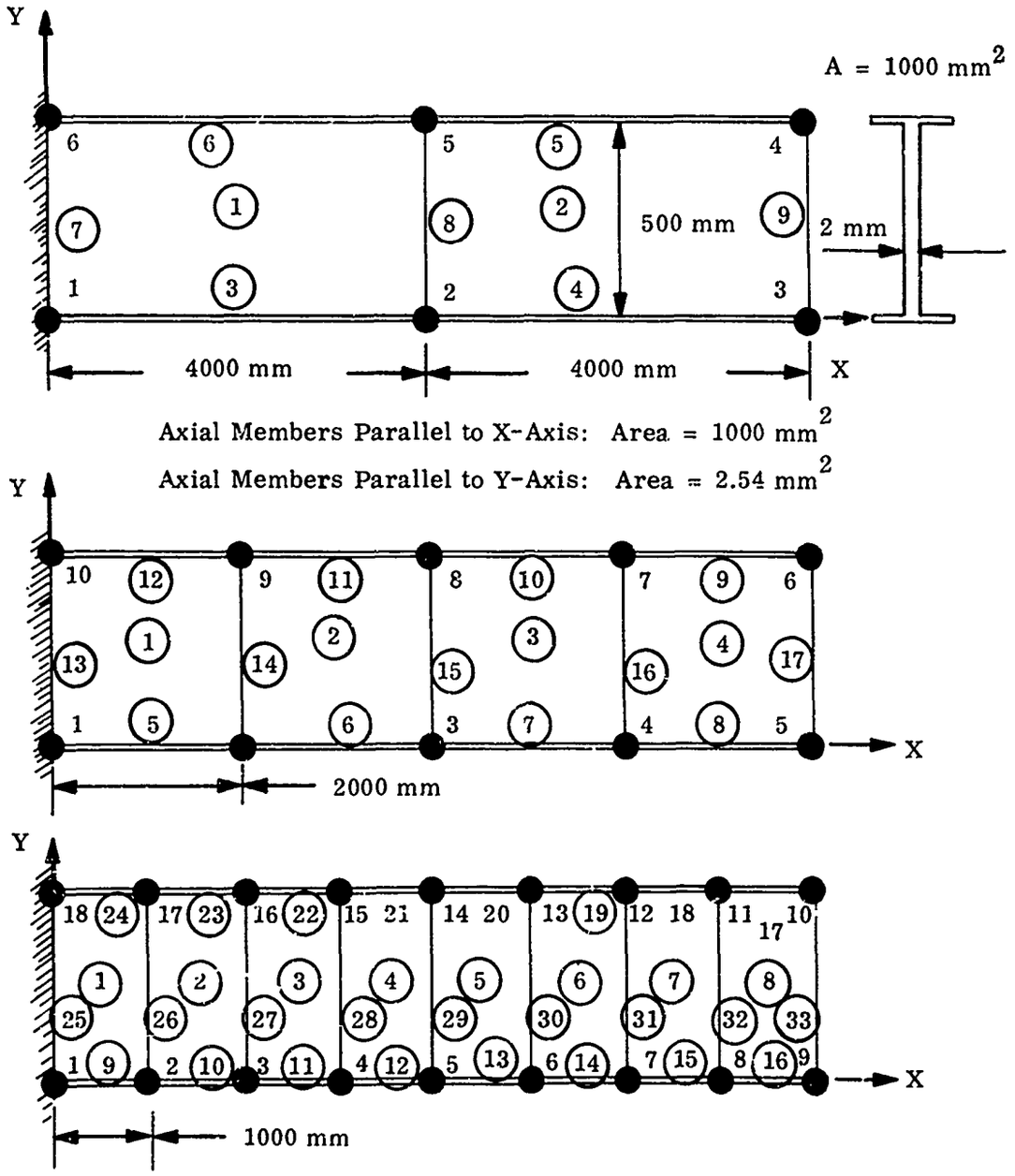

Figure 22. Cantilever Beam Idealizations

Number of Elements	Type of Analysis	Deflections in Millimeters	
		Tip	Middle
2	Linear Comp.	2.9991	0.9746
2	Quadr. Comp.	3.2648	1.171
2	Equilibrium	3.5336	1.254
-	Theory of Beams	3.2824	1.187
2	MAGIC	3.8311	1.231
4	Linear Comp.	3.1984	1.122
4	Quadr. Comp.	3.2648	1.171
4	Equilibrium	3.3341	1.204
-	Theory of Beams	3.2824	1.187
4	MAGIC	3.8311	1.348
8	Linear Comp.	3.2483	1.159
8	Quadr. Comp.	3.2648	1.171
8	Equilibrium	3.2842	1.191
-	Theory of Beams	3.2824	1.187
8	MAGIC	3.8311	1.377

Note: The Results Given for the Linear Compatible, Quadratic Compatible, Equilibrium and Theory of Beams Solutions Were Taken Directly from Reference 47.

Figure 23. Tip and Center Deflections for Uniformly Loaded Cantilever Beam

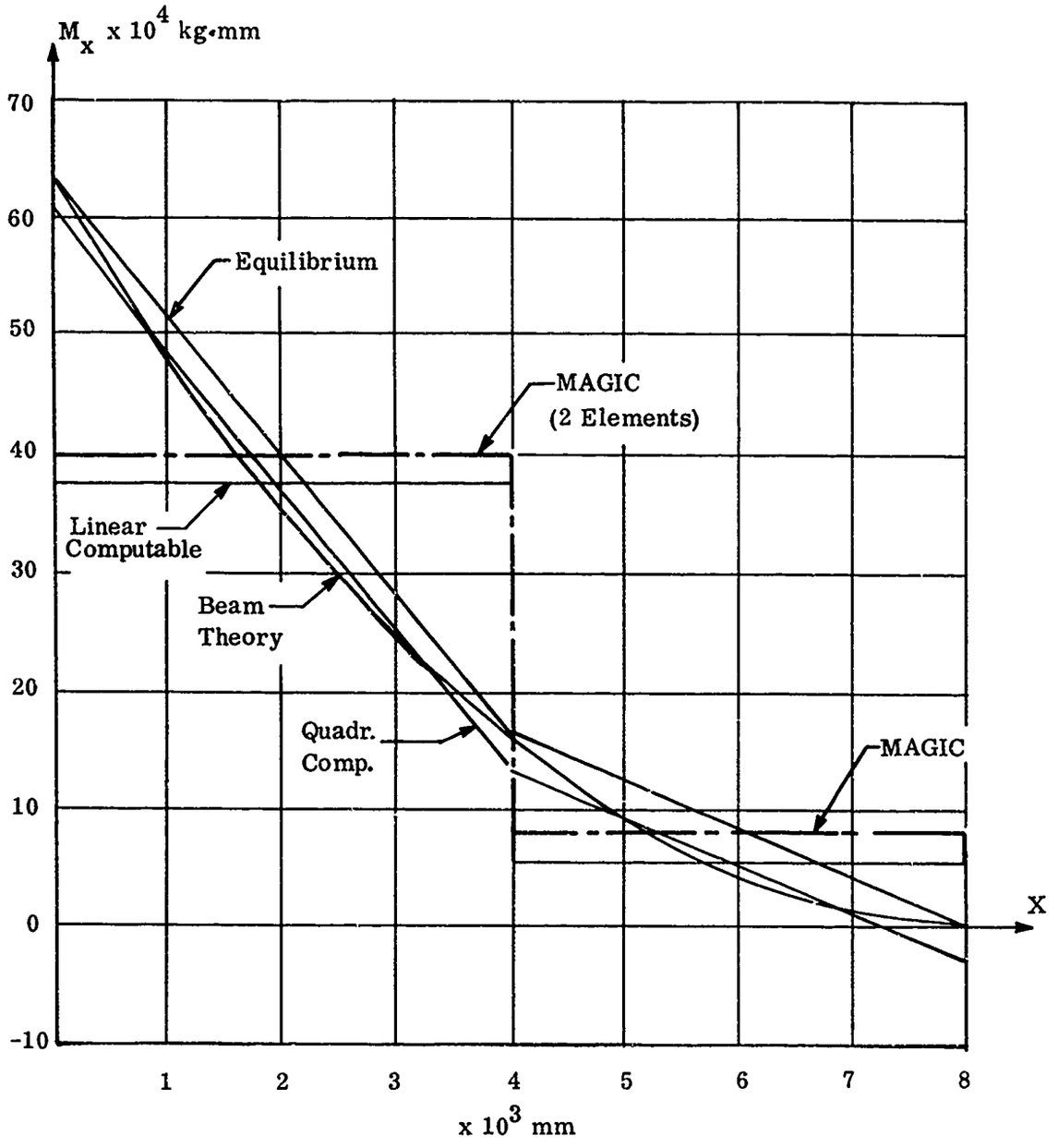

Figure 24. Bending Moment Distribution for Two Element Case

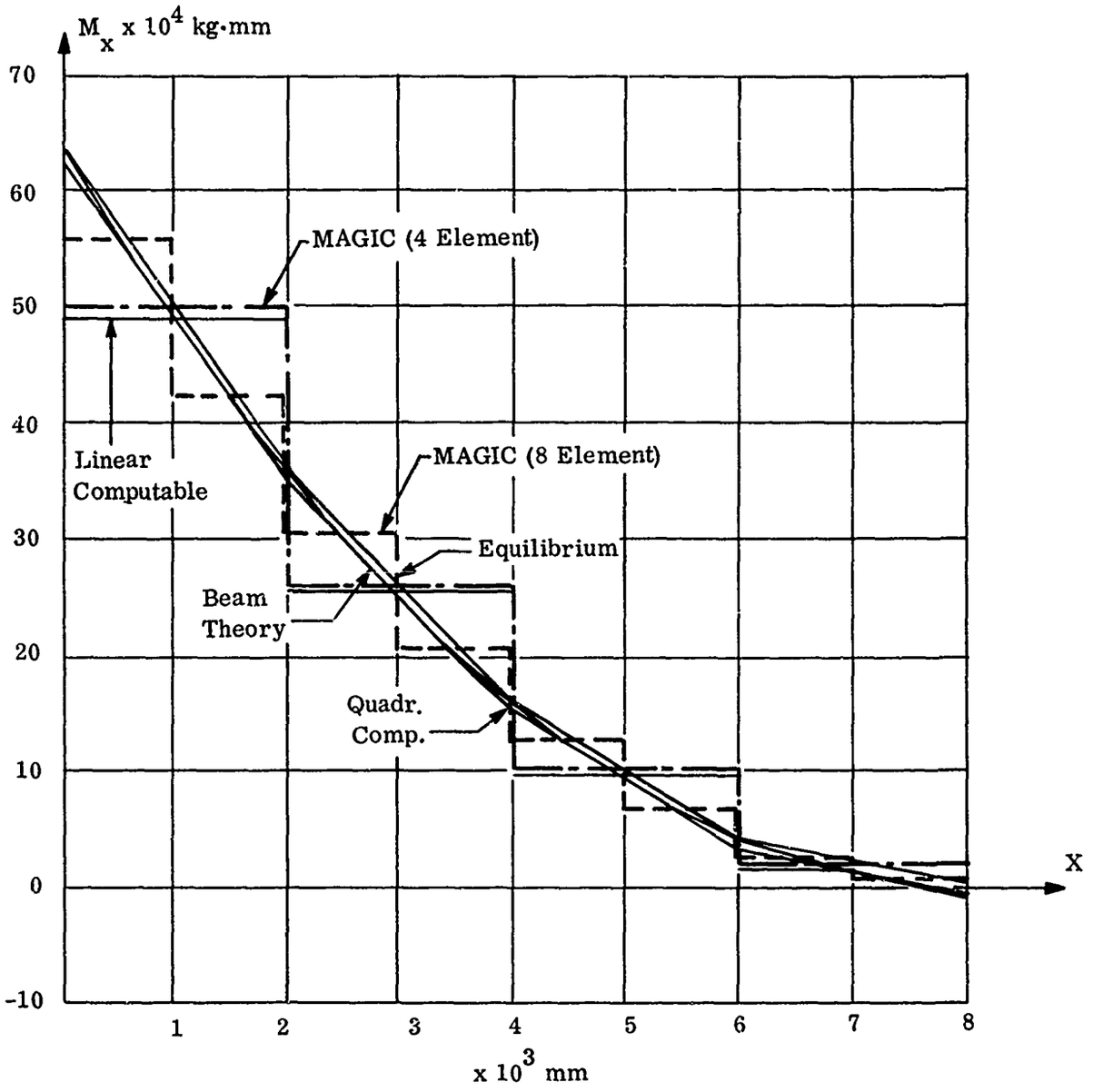

Figure 25. Bending Moment Distribution for Four and Eight Element Cases

6. TRIANGULAR CROSS SECTION RING ELEMENT

A. INTRODUCTION

A triangular cross section ring element is incorporated in the MAGIC System. This element, shown in Figure 26, is suitable for the idealization of thick walled axisymmetric structures of arbitrary shape. A detailed development of the subject element representation is presented in Reference 30.

The ring element representation is written with respect to cylindrical coordinate axes. Its configuration is completely defined by specifying the radial and axial coordinates of the three corner points. Anisotropy is provided for in the physical and mechanical properties of the ring element. Orientation of orthotropic material axes in the r, z plane is data specified.

Linear polynomial functions are employed for displacement mode shapes leading to constant element strain and stress states. Interelement continuity is maintained among triangular cross section ring elements without explicit consideration in virtue of the straight edge displacement behavior permitted by the linear polynomial mode shapes employed. The constant strain and stress states within the element lead to a requirement for relatively fine idealization gridworks when detailed stress behavior is desired. Relatively coarse idealization gridworks are suitable for the prediction of stiffness, displacement states and vibration characteristics.

Distributed loading is assumed to exist against one side of the ring element which provides for convenient consideration of pressure loading. A prestrain load vector is included in the ring element representation to accommodate directly prestrain and indirectly prestress and thermal loading as well.

Deformation behavior of the triangular cross section ring element is taken to be described by the six displacement degrees-of-freedom associated with the gridpoints which the element connects. The stress behavior induced in the element includes radial, circumferential, axial and shear stress values.

Utilization of the triangular cross section ring element is restricted to hollow structures. Generally, simulation of a solid configuration can be achieved simply by leaving a relatively small hollow cylinder.

The discrete element technique was first applied to the analysis of axisymmetrical solids by Clough and Rashid [17]. This initial formulation of the triangular cross section ring was extended by Wilson in Reference 31 to include nonaxisymmetric as well as axisymmetric loading. The subject development follows Wilson's approach, but is restricted to the axisymmetric case. The formulation is extended beyond that of Wilson, however, in several ways. One of these generalizations is

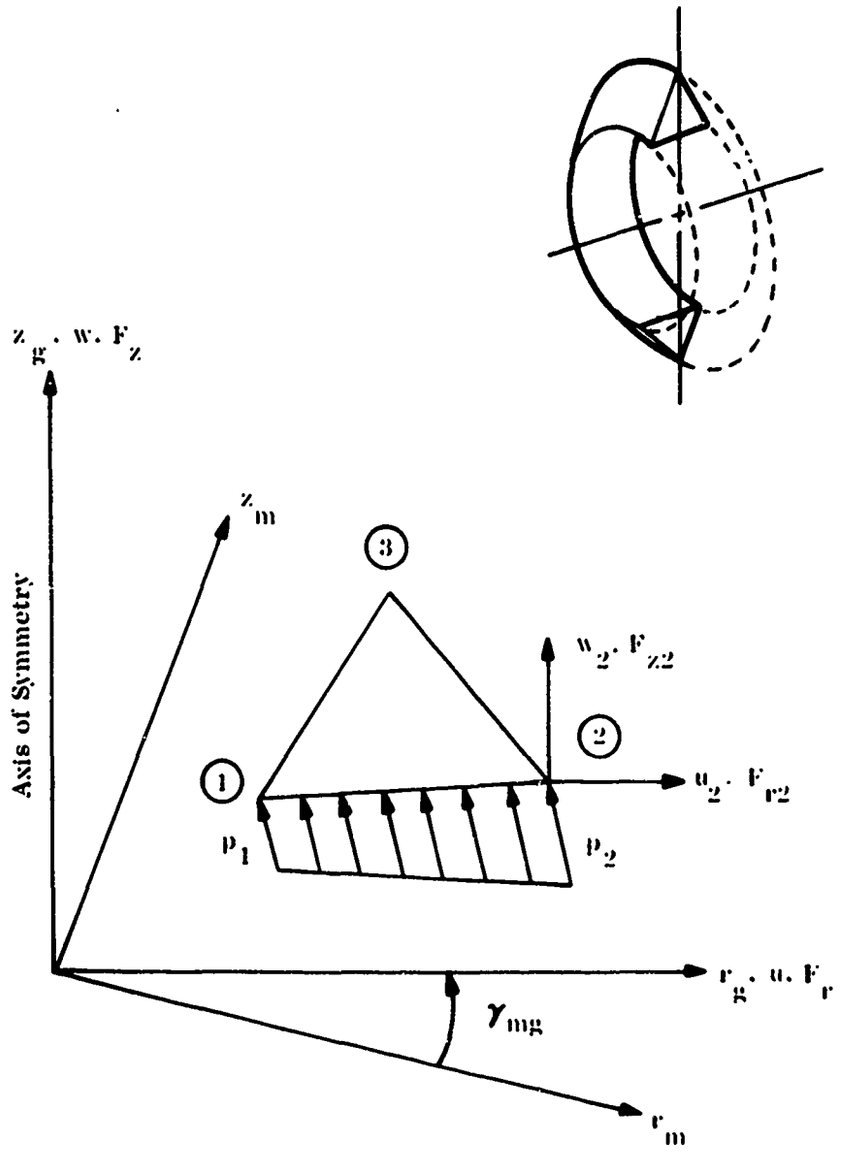

Figure 26. Triangular Cross Section Ring Element Description

that the integration over the volume of the ring is effected analytically under normal circumstances. Recourse is had to the approximate integration technique when the radial dimension of the ring is small relative to the ring diameter.

The complete representation for the triangular cross section ring is taken herein to include matrices for stiffness, pressure load, prestrain load, thermal load and stress.

B. FORMULATION

1. Displacement Functions

Linear polynomial mode shapes are taken to approximate the radial "u" and axial "w" displacement functions over the triangular cross section ring element. With respect to the global coordinate axes shown in Figure 26, these mode shapes are written as

$$\{u\,(\,)\} = [B\,(\,)]\{\beta\} \tag{144}$$

where

$$\{u\}^T = \lfloor u\,(\,), w\,(\,) \rfloor \tag{145}$$

$$[B\,(\,)] = \begin{bmatrix} 1, x, y, & , & , \\ , & , & , 1, x, y \end{bmatrix} \tag{146}$$

and the $\{\beta\}$ are simply the polynomial coefficients. These are referred to as the field coordinate displacement degrees-of-freedom. Utilization of the linear assumed modes of Equation 146 yields straight-line edge displacements and assures satisfaction of interelement continuity requirements.

The foregoing assumed displacement functions are particularized to corner point values and the resulting relationships inverted to yield a transformation between the field coordinate displacement degrees-of-freedom $\{\beta\}$ and gridpoint displacement degrees-of-freedom $\{\delta_q\}$. The results are expressed collectively as

$$\{\beta\} = [\Gamma_{\beta\delta}]\{\delta_g\} \tag{147}$$

where

$$\{\delta_g\}^T = \lfloor u_{g1}, w_{g1}, u_{g2}, w_{g2}, u_{g3}, w_{g3} \rfloor \tag{148}$$

The transformation matrix $[\Gamma_{\beta\delta}]$ is defined in Figure 27. No further displacement coordinate transformations are required since the $\{\delta_g\}$ are suitable for assembly of triangular cross section ring elements.

$$
\begin{array}{c}
 & \beta_1 & \beta_2 & \beta_3 & \beta_4 & \beta_5 & \beta_6 \\
u_{g1} & 1 & r_1 & z_1 & & & \\
w_{g1} & & & & 1 & r_1 & z_1 \\
u_{g2} & 1 & r_2 & z_2 & & & \\
w_{g2} & & & & 1 & r_2 & z_2 \\
u_{g3} & 1 & r_3 & z_3 & & & \\
w_{g3} & & & & 1 & r_3 & z_3
\end{array}
$$

Figure 27. Displacement Coordinate Transformation $\left[\Gamma_{\beta\delta}\right]^{-1}$

2. Potential Energy

Linear elastic material behavior is assumed. This behavior is taken to be governed by the relation

$$\{\sigma\} = [E]\left\{\{\epsilon\} - \{\epsilon_i\}\right\} \tag{149}$$

where

$$\{\sigma\}^T = \left\lfloor \sigma_r, \ \sigma_\theta, \ \sigma_z, \ \sigma_{rz} \right\rfloor \tag{150}$$

$$\{\epsilon\}^T = \left\lfloor \epsilon_r, \ \epsilon_\theta, \ \epsilon_z, \ \epsilon_{rz} \right\rfloor \tag{151}$$

The matrix of orthotropic elastic constants $[E]$ is specified in Figure 28. The vector $\{\epsilon_i\}$ is the initial strain state.

The element potential energy is derived as the sum of strain energy and external work contributions. Invoking the stress-strain relation of Equation 149, the strain energy is given by

$$u = \int_v \left(1/2 \lfloor \epsilon \rfloor [E] \{\epsilon\} - \lfloor \epsilon \rfloor [E] \{\epsilon_i\}\right) dV \tag{152}$$

In general, the material property characterization is known with reference to axes orientated at an angle γ_m with respect to the geometric axes. For this reason, it is necessary to introduce a matrix for the transformation of stress and strain states. The desired transformation relations are

$$\{\epsilon^{(m)}\} = [\tau_{\epsilon\sigma}] \{\epsilon^{(g)}\} \tag{153}$$

$$\{\sigma^{(m)}\} = [\tau_{\epsilon\sigma}]^T \{\sigma^{(g)}\} \tag{154}$$

These stress and strain vectors may be interpreted according to Equations 150 and 151. The transformation $[\tau_{\epsilon\sigma}]$ is given in Figure 29.

Invoking the transformation to convenient element axes, the strain energy becomes

$$U = \int_v \left(1/2 \lfloor \epsilon^{(g)} \rfloor [E^{(g)}] \{\epsilon^{(g)}\} - \lfloor \epsilon^{(g)} \rfloor \{\epsilon_i\}\right) dV \tag{155}$$

$$\frac{1}{\Delta}\begin{bmatrix} E_r(1-\nu_{\theta z}\nu_{z\theta}) & E_r(\nu_{\theta r}+\nu_{zr}\nu_{\theta z}) & E_r(\nu_{zr}+\nu_{z\theta}\nu_{\theta r}) & 0 \\ & E_\theta(1-\nu_{rz}\nu_{zr}) & E_\theta(\nu_{z\theta}+\nu_{r\theta}\nu_{zr}) & 0 \\ & & E_z(1-\nu_{r\theta}\nu_{\theta r}) & 0 \\ \text{Symmetric} & & & \Delta G_{rz} \end{bmatrix}$$

$$\Delta = (1-\nu_{r\theta}\nu_{\theta r}-\nu_{\theta z}\nu_{z\theta}-\nu_{zr}\nu_{rz}-\nu_{r\theta}\nu_{\theta z}\nu_{zr}-\nu_{rz}\nu_{\theta r}\nu_{z\theta})$$

Figure 28. Matrix of Elastic Constants $\left[E^{(m)}\right]$

$$\begin{bmatrix} \cos^2 \gamma_m & , & 0 & , & \sin^2 \gamma_m & , & \sin \gamma_m \cos \gamma_m \\ 0 & , & 1 & , & 0 & , & 0 \\ \sin^2 \gamma_m & , & 0 & , & \cos^2 \gamma_m & , & -\sin \gamma_m \cos \gamma_m \\ -2 \sin \gamma_m \cos \gamma_m & , & 0 & , & +2 \sin \gamma_m \cos \gamma_m & , & (\cos^2 \gamma_m - \sin^2 \gamma_m) \end{bmatrix}$$

Figure 29. Stress and Strain Transformation $\left[\tau_{\epsilon\sigma}\right]$

where

$$\left[E^{(g)}\right] = \left[\tau_{\epsilon\sigma}\right]^T \left[E^{(m)}\right] \left[\tau_{\epsilon\sigma}\right] \tag{156}$$

$$\left\{\bar{\epsilon}_i\right\} = \left[\tau_{\epsilon\sigma}\right]^T \left[E^{(m)}\right] \left\{\epsilon_i^{(m)}\right\} \tag{157}$$

The strain-displacement relations appropriate to the axisymmetric ring element are given by

$$\epsilon_r = u_r \tag{158}$$

$$\epsilon_\theta = u/r \tag{159}$$

$$\epsilon_z = w_z \tag{160}$$

$$\epsilon_{rz} = u_z + w_r \tag{161}$$

Introducing the assumed displacement function mode shapes, the strains are obtained in terms of the field coordinate degrees-of-freedom, i.e.

$$\left\{\epsilon^{(g)}(\,)\right\} = \left[C(\,)\right]\left\{\beta\right\} \tag{162}$$

where the matrix $\left[C\right]$ is given in Figure 30. This relation enables statement of a discretized potential energy function as

$$\Phi_p = \int_v \left(1/2 \left\lfloor\beta\right\rfloor \left[C(\,)\right]^T \left[E^{(g)}\right] \left[C(\,)\right] \left\{\beta\right\} - \left\lfloor\beta\right\rfloor \left[C(\,)\right]^T \left\{\bar{\epsilon}_i^{(g)}\right\}\right) dv$$

$$- \int_s \left[(-p \sin \alpha)u + (p \cos \alpha)w\right] \frac{2\pi r}{\cos \alpha}\, dr \tag{163}$$

The last term included in this energy function is the external work contribution. This arises in consequence of a linearly varying pressure distribution applied between element gridpoints 1 and 2 as shown in Figure 26. The functional form of this loading is

$$p(r, z) = p_1 + a_1 r + a_2 z \tag{164}$$

where

$$a_1 = -\left(\frac{z_1}{r_1 z_2 - r_2 z_1}\right) \left(P_2 - P_1\right) \tag{165}$$

$$
\begin{array}{c}
 \\
\epsilon_x \\
\epsilon_\theta \\
\epsilon_z \\
\epsilon_{rz}
\end{array}
\begin{array}{c}
\begin{array}{cccccc} \beta_1 & \beta_2 & \beta_3 & \beta_4 & \beta_5 & \beta_6 \end{array} \\
\left[\begin{array}{cccccc}
0 & 1 & 0 & 0 & 0 & 0 \\
\frac{1}{r} & 1 & \frac{z}{r} & 0 & 0 & 0 \\
0 & 0 & 0 & 0 & 0 & 1 \\
0 & 0 & 1 & 0 & 1 & 0
\end{array}\right]
\end{array}
$$

Figure 30. Displacement to Strain Transformation $\left[C()\right]$

$$a_2 = + \left(\frac{r_1}{r_1 z_2 - r_2 z_1} \right) \left(P_2 - P_1 \right) \tag{166}$$

Two algebraic forms are utlimately given for the pressure load vector to account for the special case when r_1 is equal to r_2.

The objective algebraic form of the total potential energy for the triangular cross section ring follows via integration. It is convenient to preface statement of the integrated form with the definition of additional symbolic notation. All integrals arising out of Equation 163 are of the general form

$$\delta_{ij} = \int_{(z,\, r)} r^i z^j \, dz\, dr \tag{167}$$

This symbol δ_{ij} is employed to indicate the result of the integration. With this result, the integrated form of Equation 163 is given by

$$\Phi_p = 1/2 \left[\beta\right] \left[\tilde{K}\right] \left\{\beta\right\} - \left[\beta\right] \left\{\tilde{F}_\epsilon\right\} - \left[\beta\right] \left\{\tilde{F}_p\right\} \tag{168}$$

The matrix $\left[\tilde{K}\right]$ and $\left\{\tilde{F}_p\right\}$, given in Figures 31 and 32 are the objective triangular cross section ring stiffness and pressure load matrices referenced to field coordinate displacement degrees-of-freedom. The corresponding prestrain load vector is stated under the assumption of a constant prestrain over the corss section as

$$\left\{\tilde{F}_\epsilon\right\} = \left[C'\right]^T \left[\tau_{\epsilon\sigma}\right] \left[E^{(m)}\right] \left\{\epsilon_i^{(m)}\right\} \tag{169}$$

where the single new matrix $\left[C'\right]$ is given in Figure 33. It is convenient to have a distinct load vector for prestrain due to temperature. The desired modification of Equation 166 is

$$\left\{\epsilon_i^{(m)}\right\} = \Delta T \left\{\alpha^{(m)}\right\} \tag{170}$$

where $\left\{\alpha^{(m)}\right\}$ is the vector of thermal expansion coefficients. It follows that the triangular cross section ring thermal load vector, referenced to field coordinate displacement degrees-of-freedom, is given by

$$\left\{\tilde{F}_{\epsilon T}\right\} = \Delta T \left[C'\right]^T \left[T_{\epsilon\sigma}\right] \left[E^{(m)}\right] \left\{\alpha^{(m)}\right\} \tag{171}$$

$$
2\pi \begin{bmatrix}
E_{22}\delta_{-10} & (E_{12}+E_{22})\delta_{00} & (E_{22}\delta_{-11}+E_{24}\delta_{00}) & 0 & E_{24}\delta_{00} & E_{23}\delta_{00} \\
 & & (E_{12}+E_{22})\delta_{01} & & & \\
 & (E_{11}+2E_{12}+E_{22})\delta_{10} & + & 0 & (E_{14}+E_{24})\delta_{10} & (E_{13}+E_{23})\delta_{10} \\
 & & (E_{14}+E_{24})\delta_{10} & & & \\
 & & E_{22}\delta_{-12}+2E_{24}\delta_{01} & & & \\
 & & + & 0 & E_{24}\delta_{01}+E_{44}\delta_{10} & E_{23}\delta_{01}+E_{34}\delta_{10} \\
 & & E_{44}\delta_{10} & & & \\
 & & & 0 & 0 & 0 \\
 & \text{Symmetric} & & & E_{44}\delta_{10} & E_{34}\delta_{10} \\
 & & & & & E_{33}\delta_{10}
\end{bmatrix}
$$

Figure 31. Stiffness Matrix $[\tilde{K}]$

$$\left\{\tilde{F}_p\right\} = 2\pi \begin{Bmatrix} -k_{12}\left[\left(p_1 + a_2 m_{12}\right)\delta_1 + \left(a_1 + a_2 k_{12}\right)\delta_2\right] \\ -k_{12}\left[\left(p_1 + a_2 m_{12}\right)\delta_2 + \left(a_1 + a_2 k_{12}\right)\delta_3\right] \\ -k_{12}\left[\left(p_1 + a_2 m_{12}\right)m_{12}\,\delta_1 + \left(p_1 k_{12} + m_{12}\left(a_1 + 2 a_2 k_{12}\right)\right)\delta_2 + \left(a_1 + a_2 k_{12}\right)k_{12}\,\delta_3\right] \\ \left(p_1 + a_2 m_{12}\right)\delta_1 + \left(a_1 + a_2 k_{12}\right)\delta_2 \\ \left(p_1 + a_2 m_{12}\right)\delta_2 + \left(a_1 + a_2 k_{12}\right)\delta_3 \\ \left(p_1 + a_2 m_{12}\right)m_{12}\,\delta_1 + \left(p_1 k_{12} + m_{12}\left(a_1 + 2 a_2 k_{12}\right)\right)\delta_2 + \left(a_1 + a_2 k_{12}\right)k_{12}\,\delta_3 \end{Bmatrix}$$

$$\left\{\tilde{F}_p\right\} = 2\pi r_1 \begin{Bmatrix} -\left[\left(p_1 + a_1 r_1\right)\delta_4 + a_2\,\delta_5\right] \\ -\left[\left(p_1 + a_1 r_1\right)r_1\,\delta_4 + a_2 r_1\,\delta_5\right] \\ -\left[\left(p_1 + a_1 r_1\right)\,\delta_5 + a_2\,\delta_6\right] \\ 0 \\ 0 \\ 0 \end{Bmatrix}$$

$$p(r, z) = p_1 + a_1 r + a_2 z$$

$$a_1 = -\frac{\left(p_2 - p_1\right) z_1}{r_1 z_2 - r_2 z_1}$$

$$a_2 = \frac{\left(p_2 - p_1\right) r_1}{r_1 z_2 - r_2 z_1}$$

Figure 32. Pressure Load Vector $\left\{\tilde{F}_p\right\}$

$$2\pi \begin{bmatrix} 0 & \delta_{10} & 0 & 0 & 0 & 0 \\ \delta_{00} & \delta_{10} & \delta_{01} & 0 & 0 & 0 \\ 0 & 0 & 0 & 0 & 0 & \delta_{10} \\ 0 & 0 & \delta_{10} & 0 & \delta_{10} & 0 \end{bmatrix}$$

Figure 33. Prestrain Load Submatrix $[C']$

3. Stress Matrices

The element stress matrices stem directly from the stress-strain relation of Equation 149. The strains are eliminated from this relation using Equation 162 to obtain a set of stress-displacement relations, i.e.

$$\{\sigma\} = [T_{\epsilon\sigma}]^T [E^{(m)}] \left\{ [T_{\epsilon\sigma}] [C(\,)] \{\beta\} - \{\epsilon_i^{(m)}\} \right\} \quad (172)$$

Particularization of the matrix $[C(\,)]$ to the centroidal position (x_c, y_c) on the element as shown in Figure 34 yields the objective stress matrices for the triangular cross section ring. Symbolically,

$$\{\sigma\} = [\tilde{S}] \{\beta\} - \{\Delta\} \quad (173)$$

where

$$[\tilde{S}] = [T_{\epsilon\sigma}]^T [E^{(m)}] [T_{\epsilon\sigma}] [C(x_c, y_c)] \quad (174)$$

$$\{\Delta\} = [T_{\epsilon\sigma}]^T [E^{(m)}] \{\epsilon_i^{(m)}\} \quad (175)$$

This completes specification of the element representation for the triangular cross section ring element.

C. EVALUATION

As an illustration of the use of the triangular cross section ring element in a structural evaluation, consider the following problem.

A thick walled circular disk in the plane stress subjected to a radially varying thermal load of the form $T = T_0 (1 - r^2)$ is shown in Figure 35 along with the loading, material properties and pertinent dimensions. The three idealizations used in the finite element analysis are shown in Figure 36. Reference 32 provides an alternative analytical solution for this problem which is based on the theory of elasticity. Figure 37 shows the results for radial and circumferential stresses along with radial displacements for the discrete element idealization shown in Figure 36 (c). Note that the solid lines represent the alternate analytical solution.

$$\left[D_0 \right] = \begin{bmatrix} 0 & 1 & 0 & 0 & 0 & 0 \\ \frac{1}{r_0} & 1 & \frac{z_0}{r_0} & 0 & 0 & 0 \\ 0 & 0 & 0 & 0 & 0 & 1 \\ 0 & 0 & 1 & 0 & 1 & 0 \end{bmatrix}$$

Figure 34. Stress Submatrix $\left[C\ (x_C\ ,\ y_C) \right]$

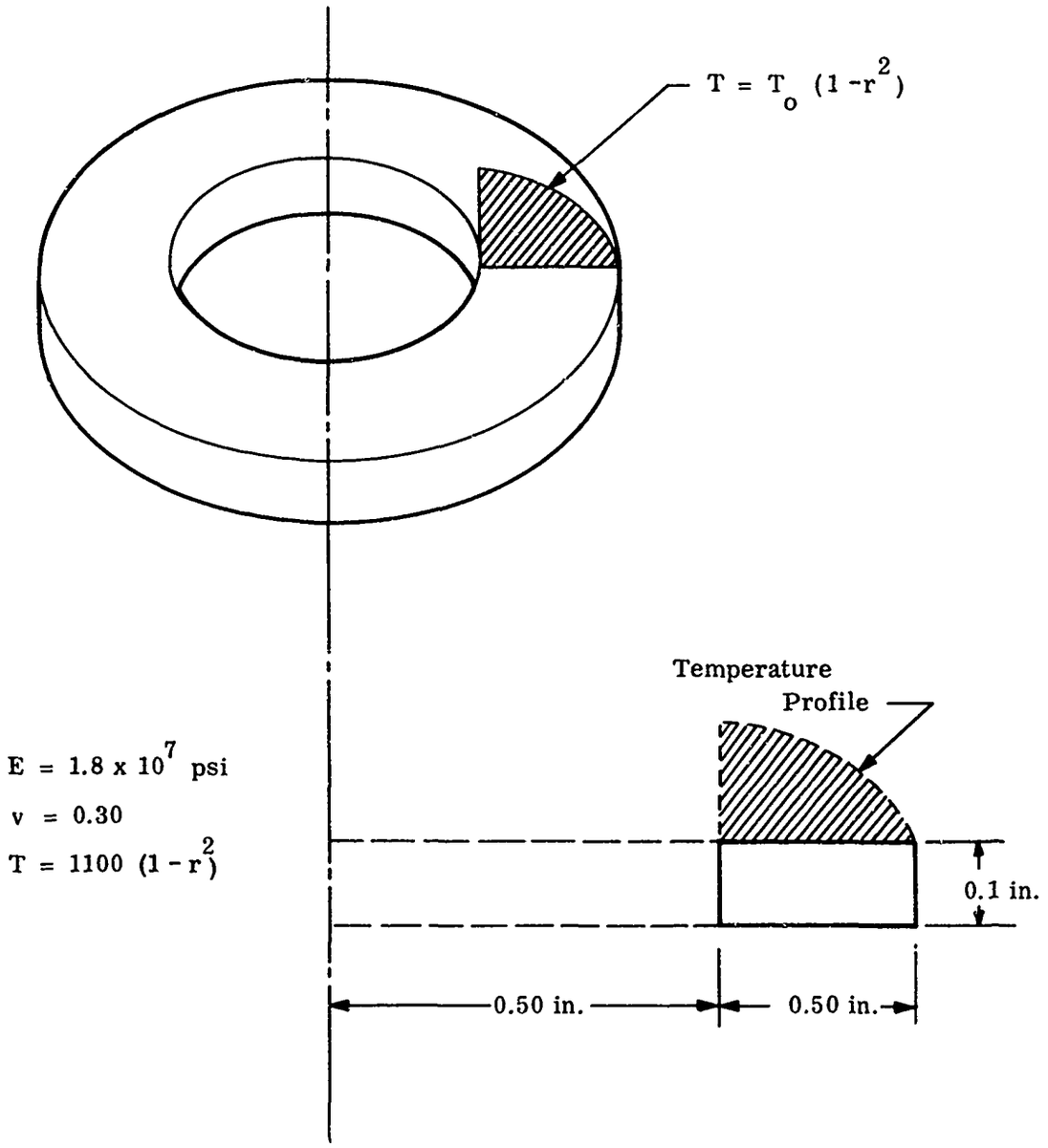

Figure 35. Thick Walled Disk Subjected to Radial Thermal Gradient

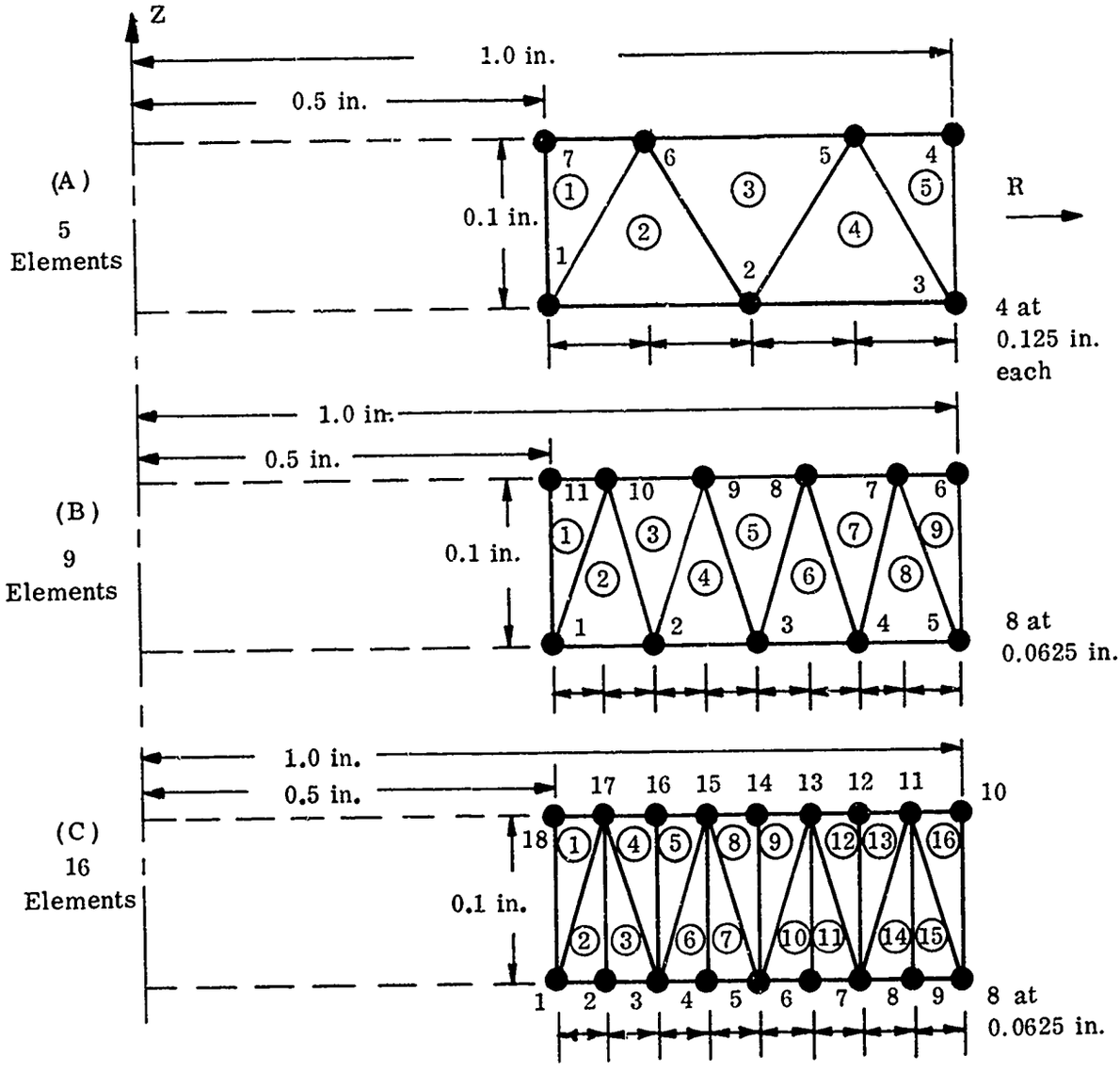

Figure 36. Thick Disk Idealizations

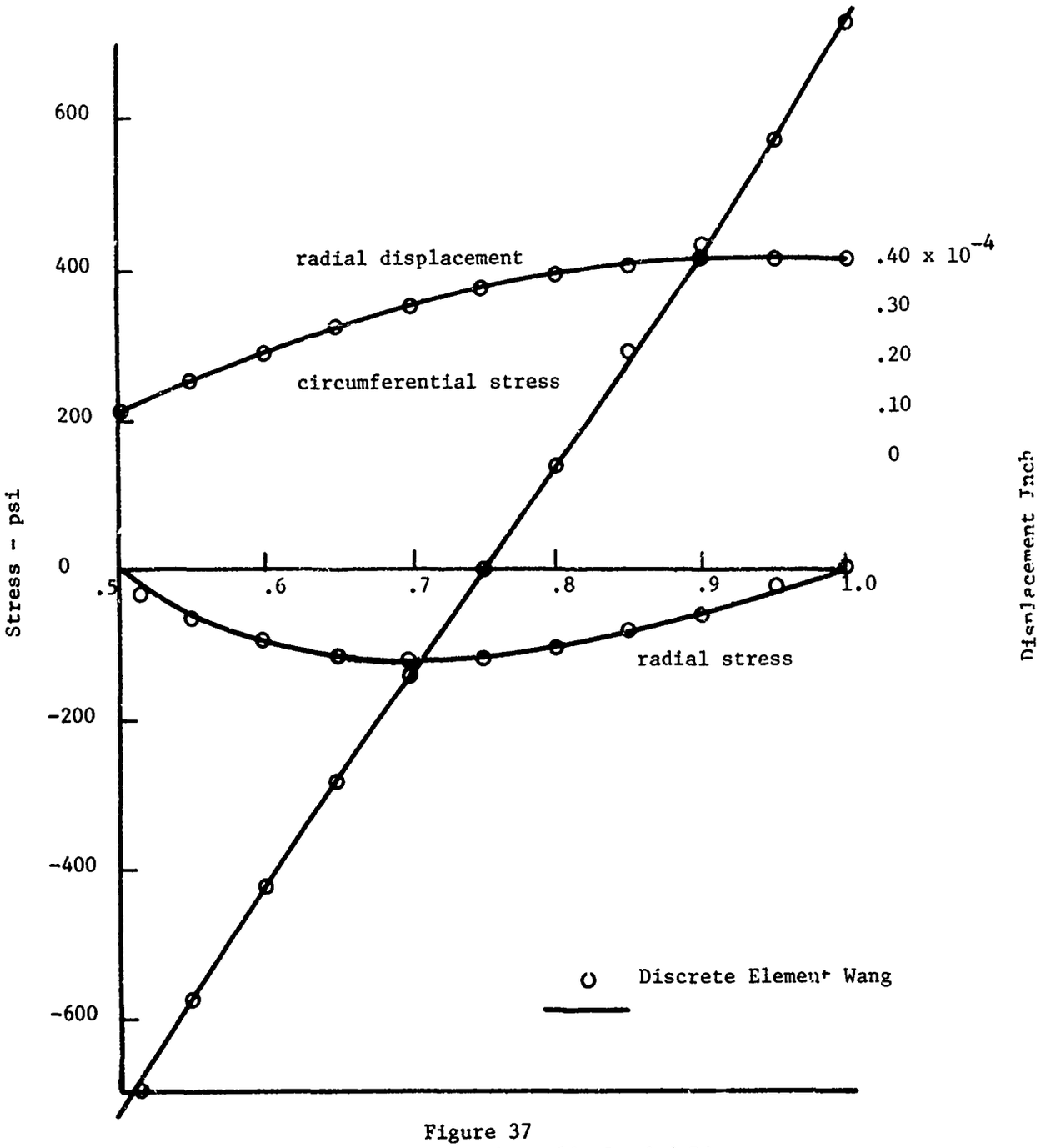

Figure 37
Stresses and Displacements in Thermally Loaded Disc

7. TOROIDAL THIN SHELL RING ELEMENT

A. INTRODUCTION

A toroidal thin shell ring element is incorporated in the MAGIC System. This element, shown in Figure 38, is suitable for the idealization of axisymmetric thin shells of arbitrary profile. The element configuration considered is that of an arbitrary section of revolution of a right circular toroidal shell. Performance of this toroidal ring element is outstanding relative to the well known conic ring element.

The first thin shell discrete element model put forward was the singly curved ring discrete element formed by a section of revolution of a thin conical shell [33]. This element has since been the subject of numerous research investigations and reports [18, 34, 35]. The reasons for this widespread attention are twofold. Firstly, there exists a broad and important class of axisymmetric thin shell structures with problematical axial variations which are amenable to formulation and solution as assemblies of ring elements. Secondly, behavior predictions based on the polygonal idealization afforded by the conic ring have proved, in some cases, to be meaningless.

Several papers have attempted to lay down guidelines for avoiding the idealization pitfalls [36, 37] and for interpreting the predicted behavior [38]. These papers identify the primary sources of difficulty in using the conic ring with the discontinuities in slope and stress which occur along element circumferential interface lines. Having made this identification, it follows that the best response is an element model which eliminates the troublesome discontinuities.

Several discrete element models have been reported which seek to eliminate idealization discontinuities by incorporating curvature of the meridian in the element model [39, 40]. These doubly curved elements have virtually eliminated the erratic stress predictions characteristic of the conic ring. The subject doubly curved ring element representation differs from these primarily in the utilization of generalized displacement functions which yield high precision stress predictions. This element representation is developed in detail in Reference 41.

The toroidal thin shell ring discrete element is formulated with respect to a toroidal coordinate system. In general, the cross section profile of the toroidal segment is circular. Specialization to conic and cylindrical shapes is automatically provided for within the MAGIC System.

The geometric shape of the element is specified by the coordinates and surface orientation at its edge grid ring. The thickness of the element is assumed constant. The subject element is written to accomodate orthotropic materials. Axes of orthotropy are assumed to coincide with the principal axes of the element.

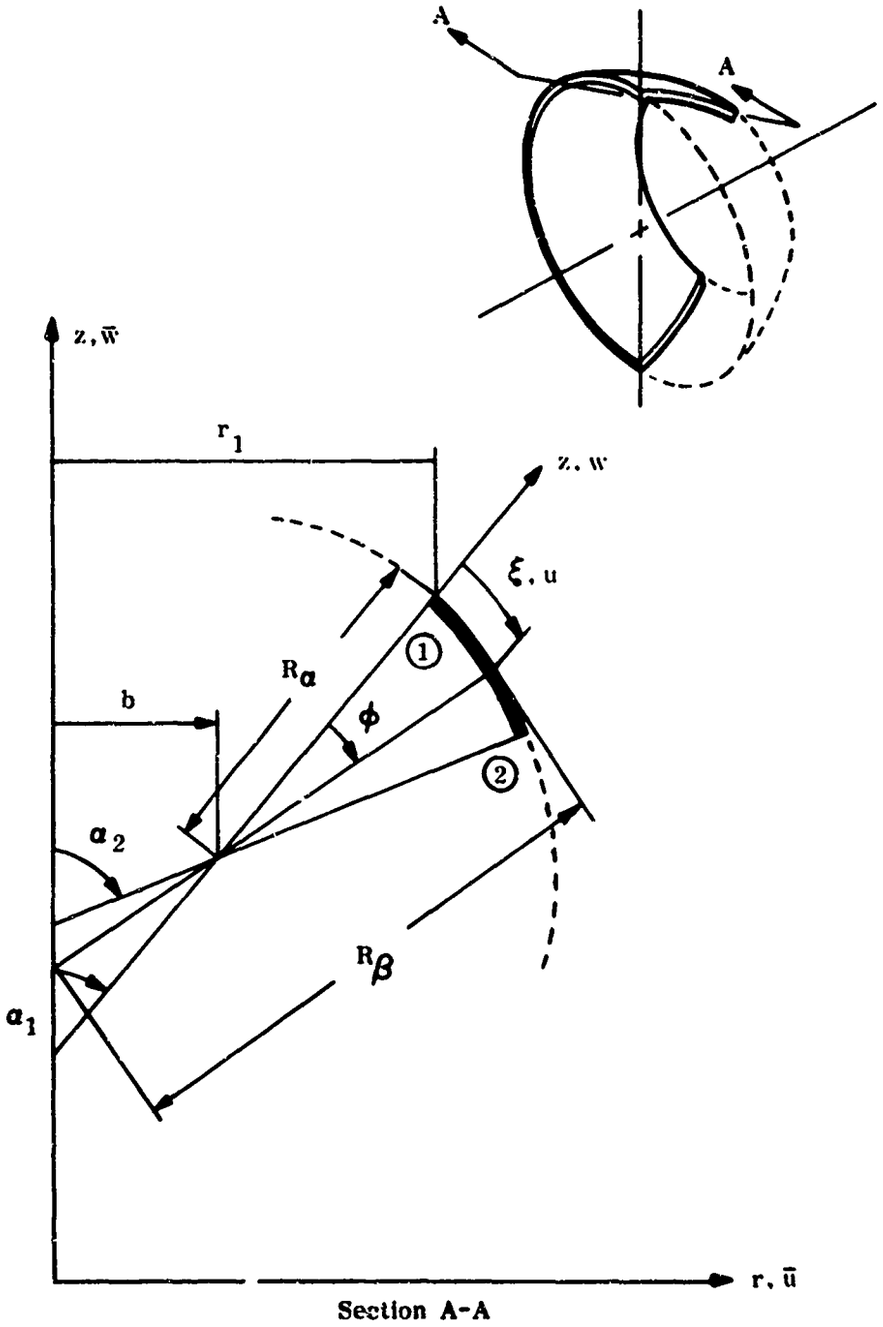

Figure 38. Toroidal Thin Shell Ring Representation

The mathematical model for the toroidal ring embodies a coupled representation of membrane and flexure behavior. A state of plane stress is assumed in formulating the element representation. Discretization is affected by the construction of polynomial displacement mode shapes. An osculatory axisymmetric polynomial interpolation function is taken to represent membrane displacement within the element. Transverse displacement is represented by a hyperosculatory interpolation function. Displacement behavior is taken to be described by the ten displacement degrees-of-freedom which are obtained from the polynomial mode shapes at the two grid rings connected by the element. These degrees-of-freedom provide a relatively high order of variation in stress and strain within the element. For this reason, stress resultants are exibited at the two boundary rings as well as at the midpoint of the element.

The toroidal axes provide a suitable set of coordinate axes for assembly of smoothly connected toroidal ring elements. If idealization discontinuities are present at element junctures, then it is necessary to reference the element representation to a set of global coordinates. Global coordinates may be used optionally when the toroidal ring elements are smoothly interconnected. The toroidal ring element is readily specialized to yield end enclosure elements. This is a particularly useful feature which was not available in the predecessor conic ring element.

The complete representation of the toroidal thin shell ring element is taken herein to include matrices for stiffness, pressure load, thermal load and stress. The toroidal ring element is somewhat more complex algebraically than the conic ring element. This increment in complexity is given justification in terms of improved accuracy with fewer elements in the set of evaluation problems included in this section.

B. FORMULATION

1. Geometric Specification

The toroidal shell parameters are obtained by reference to Figure 38. The basic coordinate system employed is toroidal. This is a right-handed orthogonal curvilinear system. The midplane of the shell is defined by the (ξ , η) coordinate surface. The principal curvatures of the shell are aligned with the coordinate axes. Complete characterization of the system is achieved by specification of the metric parameters and the principal curvatures.

The definition of an element of length (ds) is

$$(ds)^2 = (d\xi)^2 + (d\eta)^2 \tag{176}$$

where

$$d\xi - A\,d\xi \quad 0 \le \xi \le a\,(\alpha_2 - \alpha_1) \tag{177}$$

$$d\eta = B\,d\beta \tag{178}$$

This leads immediately to the metric parameters, i. e.

$$A = 1 \tag{179}$$

$$B = r_1 + \frac{\left[\sin\left(\alpha_1 + \frac{\xi}{a}\right) - \sin\alpha_1\right]}{(1/a)} \tag{180}$$

The principal curvatures are also found from Figure 38,

$$\rho_\xi = \frac{1}{R_\xi} = \frac{1}{a} \tag{181}$$

$$\rho_\beta = \frac{1}{R_\beta} = \frac{\sin(\alpha_1 + \xi/a)}{B} \tag{182}$$

These expressions for the general toroidal configuration readily degenerate to conical and cylindrical ring cases, i. e.

(a) Conical Ring

$$A = 1 \tag{183}$$

$$B = r_1 + \xi\cos\alpha_1 \tag{184}$$

$$\rho_\xi = 0 \tag{185}$$

$$\rho_\beta = \frac{\sin\alpha_1}{B} \tag{186}$$

$$0 \le \xi \le \left[(r_2 - r_1)^2 + (z_2 - z_1)^2\right]^{1/2} \tag{187}$$

(b) Cylindrical Ring

$$A = 1 \tag{188}$$

$$B = r_1 \tag{189}$$

$$\rho_\xi = 0 \tag{190}$$

$$\rho_\beta = 1/B \tag{191}$$

$$0 \le \xi \le (z_2 - z_1) \tag{192}$$

This multiplicity of parameter sets increases formulative effort since integrations must reflect the alternatives; however, an automated select feature eliminates any impact of this multiplicity in utilization of the operational capability.

The foregoing sets of parameters, taken collectively, enable exact idealization of cylindrical, conical, and piece-wise circular shells of revolution. More general shell profiles can be realistically approximated by combinations of these elements.

2. Displacement Functions

The construction of admissible displacement functions is straightforward since the functions are essentially one-dimensional. Polynominal mode shapes are assumed. The membrane displacement is taken to be cubic in the meridianal arc length. A quintic polynomial is assumed for normal displacement. These assumed modes are expressed in matrix form as

$$\{u(\,)\} = [\,B(\,)\,]\,\{\beta\} \tag{193}$$

where

$$\{u(\,)\}^T = \lfloor\, u, w \,\rfloor \tag{194}$$

$$[B(\,)] = \begin{bmatrix} 1, & \xi, \xi^2, \xi^3, & , & , & , & , & , \\ , & , & , & , & 1, \xi, \xi^2, \xi^3, \xi^4, & \xi^5 \end{bmatrix} \tag{195}$$

and the $\{\beta\}$ are simply the polynomial coefficients or, alternatively, the field coordinate displacement degrees-of-freedom. Transformation from the $\{\beta\}$ to gridpoint displacement degrees-of-freedom $\{\delta\}$ is required to enable proper interconnection with adjacent toroidal thin shell ring elements. This transformation is effected by imposing the following conditions on the assumed functions.

$$u(\xi)\Big|_{\xi=0} = u_1 \qquad u(\xi)\Big|_{\xi=s} = u_2 \tag{196}$$

$$u_\xi(\xi)\Big|_{\xi=0} = u_{\xi 1} \qquad u_\xi(\xi)\Big|_{\xi=s} = u_{\xi 2} \tag{197}$$

$$w(\xi)\Big|_{\xi=0} = w_1 \qquad w(\xi)\Big|_{\xi=s} = w_2 \tag{198}$$

$$w_\xi(\xi)\Big|_{\xi=0} = w_{\xi 1} \qquad w_\xi(\xi)\Big|_{\xi=s} = w_{\xi 2} \tag{199}$$

$$w_{\xi\xi}(\xi)\Big|_{\xi=0} = w_{\xi\xi 1} \qquad w_{\xi\xi}(\xi)\Big|_{\xi=s} = w_{\xi\xi 2} \tag{200}$$

This set of conditions can be expressed collectively in matrix form as

$$\{\delta\} = [\Gamma_{\delta\beta}]\{\beta\} \tag{201}$$

where

$$\{\delta\}^T = \left\lfloor u_1, u_{\zeta 1}, u_2, u_{\zeta 2}, w_1, w_{\zeta 1}, w_{\zeta\zeta 1}, w_2, w_{\zeta 2}, w_{\zeta\zeta 2} \right\rfloor \tag{202}$$

Specific definition of $[\Gamma_{\delta\beta}]$ is not included since it is the inversion of this relation which is desired. The inverted relation is written as

$$\{\beta\} = [\Gamma_{\beta\delta}]\{\delta\} \tag{203}$$

where the $[\Gamma_{\beta\delta}]$ is now given explicit definition in Figure 39.

The gridpoint degrees-of-freedom $\{\delta\}$ are common to adjacent toroidal thin shell ring elements and are, therefore, suitable for the assembly process. On some occasions it is convenient to use degrees-of-freedom referenced to a rectangular global set of coordinate axes. Moreover, such a system must be employed if adjacent elements do not interconnect smoothly. This further transformation relation is given by:

$$\{\delta\} = [\Gamma_{gs}]\{\delta_s\} \tag{204}$$

where

$$\{\delta_s\} = \left\lfloor u_1, 0, w_1, 0, w_{\xi 1}, 0, u_{\xi 1}, 0, w_{\zeta\zeta 1} \right. \\ \left. u_2, 0, w_2, 0, w_{\xi 2}, 0, u_{\xi 2}, 0, w_{\zeta\zeta 2} \right\rfloor \tag{205}$$

and the transformation $[\Gamma_{gs}]$ is specified in Figure 40.

The two foregoing transformations may be collected symbolically to obtain a single transformation between the field coordinate $\{\beta\}$ and gridpoint $\{\delta_s\}$ displacement degrees-of-freedom.

$$\{\beta\} = [\Gamma_{\beta\delta}]\{\delta_s\} \tag{206}$$

where

$$[\Gamma_{\beta g}] = [\Gamma_{\beta\delta}][\Gamma_{gs}] \tag{207}$$

This completes the explicit statement of the displacement functional employed for the toroidal thin shell ring discrete element.

$$
\begin{bmatrix}
\begin{bmatrix}
1 & 0 & 0 & 0 \\
0 & 1 & 0 & 0 \\
-\frac{3}{S^2} & -\frac{2}{S} & \frac{3}{S^2} & -\frac{1}{S} \\
\frac{2}{S^3} & \frac{1}{S^2} & -\frac{2}{S^3} & \frac{1}{S^2}
\end{bmatrix} & \\
 & \begin{bmatrix}
1 & 0 & 0 & 0 & 0 & 0 \\
0 & 1 & 0 & 0 & 0 & 0 \\
0 & 0 & \frac{1}{2} & 0 & 0 & 0 \\
-\frac{10}{S^3} & -\frac{6}{S^2} & -\frac{3}{2S} & \frac{10}{S^3} & -\frac{4}{S^2} & \frac{1}{2S} \\
\frac{15}{S^4} & \frac{8}{S^3} & \frac{3}{2S^2} & -\frac{15}{S^4} & \frac{7}{S^3} & -\frac{1}{S^2} \\
-\frac{6}{S^5} & -\frac{3}{S^4} & -\frac{1}{2S^3} & \frac{6}{S^5} & -\frac{3}{S^4} & \frac{1}{2S^3}
\end{bmatrix}
\end{bmatrix}
$$

Figure 39. Displacement Coordinate Transformation $\left[\Gamma_{\beta\delta}\right]$

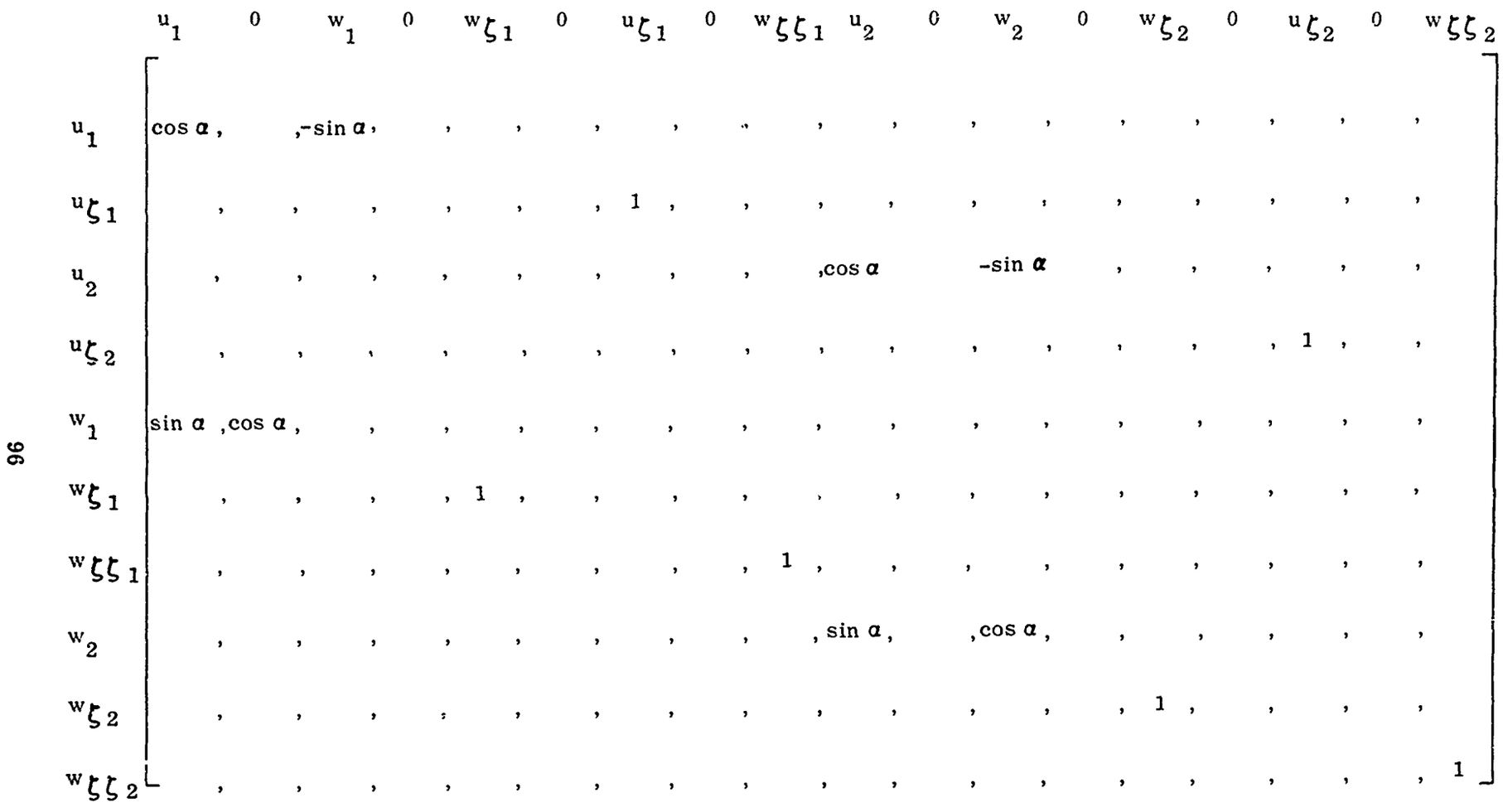

Figure 40. Displacement Coordinate Transformation $\left[\Gamma_{gs}\right]$

3. Potential Energy

Linear elastic material behavior is assumed. In accordance with this assumption, a generalized Hooke's law is employed, i.e.

$$\{\sigma(\,)\} = [E]\left\{\{\epsilon(\,)\} - \{\epsilon_i(\,)\}\right\} \tag{208}$$

where

$$\{\sigma(\,)\}^T = \lfloor \sigma_\xi, \sigma_\beta \rfloor \tag{209}$$

$$\{\epsilon\}^T = \lfloor \epsilon_\xi, \epsilon_\beta \rfloor \tag{210}$$

$$[E] = \frac{1}{(1-\nu_{\xi\beta}\nu_{\beta\xi})}\begin{bmatrix} E_\xi, & \nu_{\beta\xi} E_\xi \\ \nu_{\xi\beta} E_\beta, & E_\beta \end{bmatrix} \tag{211}$$

The term $\{\epsilon_i\}$ is prestrain state and can be interpreted in accord with Equation 210.

In virtue of the assumption of linear material behavior, the strain energy can be written as

$$U = \int_V \left(1/2 \lfloor \epsilon \rfloor [E]\{\epsilon\} - \lfloor \epsilon \rfloor [E]\{\epsilon_i\}\right) d\,V \tag{212}$$

The next step in proceeding toward the potential energy functional is to express the strains in terms of displacements. These equations, recorded from Reference 42, are written

$$\{\epsilon\} = \{\Delta_m\} + Z\{\Delta_f\} \tag{213}$$

where

$$\{\Delta_m\}^T = \lfloor u_\xi + \lambda_1 w,\ \lambda_2 u + \lambda_3 w \rfloor \tag{214}$$

$$\{\Delta_f\}^T = \lfloor w_{\xi\xi},\ -\lambda_2 w_\xi \rfloor \tag{215}$$

The quantities λ_j are defined as

$$\lambda_1 = \rho_\xi,\ \lambda_2 = 1/B \frac{\partial B}{\partial \xi},\ \lambda_3 = \rho_\beta \tag{216}$$

These are given explicit definition by the element configuration according to Equations 179 through 192.

Based on these strain-displacement relations, the total potential energy functional is given by

$$\Phi_p = \int_o^s \Big(1/2 \left[\Delta_m\right]\left[I_K\right]\left\{\Delta_m\right\} + 1/2 \left[\Delta_f\right]\left[J_K\right]\left\{\Delta_f\right\} - \left[\Delta_m\right]\left\{I_\epsilon\right\} - \left[\Delta_f\right]\left\{J_\epsilon\right\} - 2\pi P_z w \Big) B\, d\xi \tag{217}$$

where

$$\left[I_K\right] = 2\pi t \left[E\right] \tag{218}$$

$$\left[J_K\right] = \frac{2\pi t^3}{12}\left[E\right] \tag{219}$$

$$\left\{I_\epsilon\right\} = 2\pi t \left[E\right]\left\{\epsilon_i\right\} \tag{220}$$

$$\left\{J_\epsilon\right\} = \frac{2\pi t^3}{12}\left[E\right]\left\{\kappa_i\right\} \tag{221}$$

This completes the statement of the potential energy functional for the toroidal thin shell ring element. The next step in proceeding toward the objective element representation is to effect the discretization of the functional. Invoking the strain-displacement relations of Equation 214 and 215 against the assumed mode shapes of Equation 193 accomplishes the discretization of the displacement functions. The results may be written symbolically as

$$\left\{\Delta_m(\,)\right\} = \left[D_m(\,)\right]\left\{\beta\right\} \tag{222}$$

$$\left\{\Delta_f(\,)\right\} = \left[D_f(\,)\right]\left\{\beta\right\} \tag{223}$$

The displacement to strain transformation matrices $\left[D_m\right]$ and $\left[D_f\right]$ are defined in Figure 41.

The applied load functions also require discretization by the assumption of mode shapes. Considering first the pressure load, a linear variation is assumed. Translating this assumption into functional form yields

$$
\begin{array}{c}
 \\
\left[D_m\right] = \\
 \\
 \\
\left[D_f\right] = \\
 \\
 \\
\end{array}
\begin{array}{c}
\begin{array}{cccccccccc} \beta_1 & \beta_2 & \beta_3 & \beta_4 & \beta_5 & \beta_6 & \beta_7 & \beta_8 & \beta_9 & \beta_{10} \end{array} \\
\begin{array}{c} \xi_\zeta \\ \xi_\eta \end{array}
\left[\begin{array}{cccccccccc}
0 & 1 & 2\zeta & 3\zeta^2 & \lambda_1 & \lambda_1\zeta & \lambda_1\zeta^2 & \lambda_1\zeta^3 & \lambda_1\zeta^4 & \lambda_1\zeta^5 \\
\lambda_2 & \lambda_2\zeta & \lambda_2\zeta^2 & \lambda_2\zeta^3 & \lambda_3 & \lambda_3\zeta & \lambda_3\zeta^2 & \lambda_3\zeta^3 & \lambda_3\zeta^4 & \lambda_3\zeta^5
\end{array}\right] \\
\begin{array}{cccccccccc} \beta_1 & \beta_2 & \beta_3 & \beta_4 & \beta_5 & \beta_6 & \beta_7 & \beta_8 & \beta_9 & \beta_{10} \end{array} \\
\begin{array}{c} \xi_\zeta \\ \xi_\eta \end{array}
\left[\begin{array}{cccccccccc}
0 & 0 & 0 & 0 & 0 & 0 & -2 & -6\zeta & -12\zeta^2 & -20\zeta^3 \\
0 & 0 & 0 & 0 & 0 & -\lambda_2 & -2\lambda_2\zeta & -3\lambda_2\zeta^2 & -4\lambda_2\zeta^3 & -5\lambda_2\zeta^4
\end{array}\right]
\end{array}
$$

Figure 41. Displacement to Strain Transformations

$$p_z(\zeta) = p(0) + \frac{\zeta}{s}\left(p(s) - p(0)\right) \tag{224}$$

Compressing the notation, this expression is rewritten

$$p_z(\zeta) = p_z^{(0)} + \left(\frac{\zeta}{s}\right) p_z^{(0)} \tag{225}$$

A similar linear form is assumed to approximate the prestrain load distribution. The corresponding functional form is given by

$$\{\epsilon_i\} = \{\epsilon_i(0)\} + z\{\kappa_i(0)\} + \frac{\zeta}{s}\left\{\{e_i(s)\} - \{e_i(0)\}\right\} + z\left(\frac{\zeta}{s}\right)\left\{\{\kappa_i(s)\} - \{\kappa_i(0)\}\right\} \tag{226}$$

Notational convenience is realized by rewriting this relation as

$$\{\epsilon_i\} = \{e_i^{(0)}\} + z\{\kappa_i^{(0)}\} + \left(\frac{\zeta}{s}\right)\{e_i^{(10)}\} + z\left(\frac{\zeta}{s}\right)\{\kappa_i^{(10)}\} \tag{227}$$

A distinct prestrain vector is provided in the MAGIC System for prestrains due to temperature. Specification of the temperature load is accepted via for temperatures, i.e.,

T_{1i}	-	internal surface temperature at gridpoint no. 1
T_{1o}	-	external surface temperature at gridpoint no. 1
T_{2i}	-	internal surface temperature at gridpoint no. 2
T_{2o}	-	external surface temperature at gridpoint no. 2

The thermal prestrain quantities follow immediately from this data. These quantities are defined as follows:

$$\{e_i^{(0)}\} = 1/2\left(T_{1i} + T_{1o}\right)\{\alpha\} \tag{228}$$

$$\{e_i^{(10)}\} = 1/2\left(T_{2i} + T_{2o} - T_{1i} - T_{1o}\right)\{\alpha\} \tag{229}$$

$$\{K_i^{(0)}\} = 1/2\left(T_{1i} - T_{1o}\right)\{\alpha\} \tag{230}$$

$$\{K_i^{(10)}\} = 1/2\left(T_{2i} - T_{2o} - T_{1i} + T_{1o}\right)\{\alpha\} \tag{231}$$

This completes the definition of assumed functions. Invoking these, obtain the discretized potential energy functional, i. e.,

$$\Phi_p = \int_o^s \Big(1/2 \lfloor \beta \rfloor \left[D_m \right]^T \left[I_K \right] \left[D_m \right] \{\beta\}$$

$$+ \; 1/2 \lfloor \beta \rfloor \left[D_f \right]^T \left[J_K \right] \left[D_f \right] \{\beta\}$$

$$- \lfloor \beta \rfloor \left[D_m \right]^T \left[I_K \right] \{ e_i^{(0)} \} - \frac{\zeta}{s} \lfloor \beta \rfloor \left[D_m \right]^T \left[I_K \right] \{ e_i^{(10)} \} \qquad (232)$$

$$- \lfloor \beta \rfloor \left[D_f \right]^T \left[J_K \right] \{ \kappa_i^{(0)} \} - \frac{\zeta}{s} \lfloor \beta \rfloor \left[D_f \right]^T \left[J_K \right] \{ \kappa_i^{(10)} \}$$

$$- 2\pi \left(p_z^{(0)} + \frac{\zeta}{s} p_z^{(10)} \right) w \Big) \, Bd\, \zeta$$

Integration now yields the objective potential energy form of the representation for the toroidal thin shell ring element. The symbolic result is

$$\Phi_p = 1/2 \lfloor \beta \rfloor \left[\tilde{K} \right] \{\beta\} - \lfloor \beta \rfloor \{ \tilde{F}_\epsilon \} - \lfloor \beta \rfloor \{ \tilde{F}_p \} \qquad (233)$$

Presentation of these matrices is prefaced by definition of additional notation in Figure 42. Then, matrices $\left[\tilde{K} \right]$, $\{ \tilde{F}_\epsilon \}$ and $\{ \tilde{F}_p \}$ are given explicit definition in Figures 43, 44, and 45, respectively. The matrix $\left[\tilde{K} \right]$ is the element stiffness matrix referenced to field coordinate displacement degrees-of-freedom $\{\beta\}$. The matrices $\{ \tilde{F}_p \}$ and $\{ \tilde{F}_\epsilon \}$ are the corresponding element pressure and prestrain loads.

The transformation of Equation 206 is introduced to reference the element matrices to degrees-of-freedom amenable to assembly of the elements. The result is

$$\Phi_p = 1/2 \lfloor \delta_q \rfloor \left[K \right] \{ \delta_q \} - \lfloor \delta_q \rfloor \{ F_\epsilon \} - \lfloor \delta_q \rfloor \{ F_p \} \qquad (234)$$

where

$$\left[K \right] = \left[\Gamma_{\beta q} \right]^T \left[\tilde{K} \right] \left[\Gamma_{\beta q} \right] \qquad (235)$$

$$\{ F_\epsilon \} = \left[\Gamma_{\beta q} \right]^T \{ \tilde{F}_\epsilon \} \qquad (236)$$

$$\{ F_p \} = \left[\Gamma_{\beta q} \right]^T \{ \tilde{F}_p \} \qquad (237)$$

$$\delta_1^{\,j} = \int_o^s \xi^j \, B \, d\xi$$

$$\delta_2^{\,j} = \int_o^s \xi^j \lambda_2 \, B \, d\xi$$

$$\delta_3^{\,j} = \int_o^s \xi^j \lambda_3 \, B \, d\xi$$

$$\delta_4^{\,j} = \int_o^s \xi^j \lambda_2^{\,2} \, B \, d\xi$$

$$\delta_5^{\,j} = \int_o^s \xi^j \lambda_2 \lambda_3 \, B \, d\xi$$

$$\delta_6^{\,j} = \int_o^s \xi^j \lambda_3^2 \, B \, d\xi$$

Figure 42. Notation

$$\tilde{K}(1,1) \quad I_{22}\,\delta_1^{\,0}$$

$$\tilde{K}(1,2) \quad \cdot I_{12}\,\delta_2^{\,0} + I_{22}\,\delta_1^{\,1}$$

$$\tilde{K}(2,2) \quad I_{11}\,\delta_1^{\,1} + \cdot I_{12}\,\delta_2^{\,1} + I_{22}\,\delta_1^{\,2}$$

$$\tilde{K}(3,1) \quad \cdot 2\,I_{12}\,\delta_2^{\,1} + I_{22}\,\delta_1^{\,2}$$

$$\tilde{K}(3,2) \quad \cdot 2\,I_{11}\,\delta_1^{\,1} \quad 3\,I_{12}\,\delta_2^{\,2} + I_{22}\,\delta_1^{\,3}$$

$$\tilde{K}(3,3) \quad \cdot 3\,I_{11}\,\delta_1^{\,2} + 3\,I_{12}\,\delta_2^{\,2} + I_{22}\,\delta_1^{\,3}$$

$$\tilde{K}(4,1) \quad \cdot 3\,I_{12}\,\delta_2^{\,2} + I_{22}\,\delta_1^{\,3}$$

$$\tilde{K}(4,2) \quad \cdot 4\,I_{11}\,\delta_1^{\,2} \quad 4\,I_{12}\,\delta_2^{\,3} + I_{22}\,\delta_1^{\,4}$$

$$\tilde{K}(4,3) \quad \cdot 6\,I_{11}\,\delta_1^{\,3} \quad 5\,I_{12}\,\delta_2^{\,3} + I_{22}\,\delta_1^{\,4}$$

$$\tilde{K}(4,4) \quad \cdot \lambda_1\,I_{11}\,\delta_1^{\,0} + I_{12}\,\delta_1^{\,0} + \lambda_1\,I_{12}\,\delta_2^{\,1} + I_{22}\,\delta_2^{\,1}$$

$$\tilde{K}(5,1) \quad \cdot \lambda_1\,I_{11}\,\delta_1^{\,1} + 2\,\lambda_1\,I_{12}\,\delta_3^{\,1} + I_{22}\,\delta_2^{\,1}$$

$$\tilde{K}(5,2) \quad \cdot \lambda_1\,I_{11}\,\delta_1^{\,1} + I_{12}\,\delta_3^{\,1} + \lambda_1\,I_{12}\,\delta_2^{\,2} + I_{22}\,\delta_2^{\,2}$$

$$\tilde{K}(5,3) \quad \cdot 3\,\lambda_1\,I_{11}\,\delta_1^{\,2} + 3\,I_{12}\,\delta_3^{\,2} + \lambda_1\,I_{12}\,\delta_2^{\,3} + I_{22}\,\delta_2^{\,3}$$

$$\tilde{K}(5,4) \quad \cdot 3\,\lambda_1\,I_{11}\,\delta_1^{\,3} + 4\,I_{12}\,\delta_3^{\,3} + \lambda_1\,I_{12}\,\delta_2^{\,4} + I_{22}\,\delta_2^{\,4}$$

$$\tilde{K}(5,5) \quad \cdot \lambda_1^{\,2}\,I_{11}\,\delta_1^{\,0} + 2\,\lambda_1\,I_{12}\,\delta_3^{\,0} \quad I_{22}\,\delta_2^{\,0}$$

$$\tilde{K}(6,1) \quad \cdot \lambda_1\,I_{12}\,\delta_2^{\,1} + I_{22}\,\delta_1^{\,1}$$

$$\tilde{K}(6,2) \quad \cdot \lambda_1\,I_{11}\,\delta_1^{\,1} + I_{12}\,\delta_3^{\,1} + \lambda_1\,I_{12}\,\delta_2^{\,2} + I_{22}\,\delta_1^{\,2}$$

$$\tilde{K}(6,3) \quad \cdot 2\,\lambda_1\,I_{11}\,\delta_1^{\,2} + 2\,I_{12}\,\delta_3^{\,2} + \lambda_1\,I_{12}\,\delta_2^{\,3} + I_{22}\,\delta_1^{\,3}$$

$$\tilde{K}(6,4) \quad \cdot 3\,\lambda_1\,I_{11}\,\delta_1^{\,3} + 3\,I_{12}\,\delta_3^{\,3} + \lambda_1\,I_{12}\,\delta_2^{\,4} + I_{22}\,\delta_1^{\,4}$$

$$\tilde{K}(6,5) \quad \cdot \lambda_1^{\,2}\,I_{11}\,\delta_1^{\,1} + 2\,\lambda_1\,I_{12}\,\delta_3^{\,1} + I_{22}\,\delta_2^{\,1}$$

$$\tilde{K}(6,6) \quad \cdot \lambda_1^{\,2}\,I_{11}\,\delta_1^{\,2} + 2\,\lambda_1\,I_{12}\,\delta_3^{\,2} + I_{22}\,\delta_2^{\,2} \quad J_{22}\,\delta_1^{\,0}$$

$$\tilde{K}(7,1) \quad \cdot \lambda_1\,I_{12}\,\delta_2^{\,2} + I_{22}\,\delta_1^{\,2}$$

$$\tilde{K}(7,2) \quad \cdot \lambda_1\,I_{11}\,\delta_1^{\,2} + I_{12}\,\delta_3^{\,2} + \lambda_1\,I_{12}\,\delta_2^{\,3} + I_{22}\,\delta_1^{\,3}$$

$$\tilde{K}(7,3) \quad \cdot 2\,\lambda_1\,I_{11}\,\delta_1^{\,3} \quad 2\,I_{12}\,\delta_3^{\,3} + \lambda_1\,I_{12}\,\delta_2^{\,4} + I_{22}\,\delta_1^{\,4}$$

$$\tilde{K}(7,4) \quad \cdot 3\,\lambda_1\,I_{11}\,\delta_1^{\,4} + 3\,I_{12}\,\delta_3^{\,4} + \lambda_1\,I_{12}\,\delta_2^{\,5} + I_{22}\,\delta_1^{\,5}$$

$$\tilde{K}(7,5) \quad \cdot \lambda_1^{\,2}\,I_{11}\,\delta_1^{\,2} + 2\,\lambda_1\,I_{12}\,\delta_3^{\,2} + I_{22}\,\delta_2^{\,2}$$

$$\tilde{K}(7,6) \quad \cdot \lambda_1^{\,2}\,I_{11}\,\delta_1^{\,3} + 2\,\lambda_1\,I_{12}\,\delta_3^{\,3} - I_{22}\,\delta_0^{\,3} + 2\,J_{12}\,\delta_2^{\,0} + 2\,J_{22}\,\delta_1^{\,1}$$

$$\tilde{K}(7,7) \quad \cdot \lambda_1^{\,2}\,I_{11}\,\delta_1^{\,4} + 2\,\lambda_1\,I_{12}\,\delta_3^{\,4} + I_{22}\,\delta_0^{\,4} + 4\,I_{11}\,\delta_1^{\,0} + 8\,J_{12}\,\delta_2^{\,1} + 4\,J_{22}\,\delta_4^{\,2}$$

$$\tilde{K}(8,1) \quad \cdot \lambda_1\,I_{12}\,\delta_2^{\,3} + I_{22}\,\delta_1^{\,3}$$

$$\tilde{K}(8,2) \quad \cdot \lambda_1\,I_{11}\,\delta_1^{\,3} + I_{12}\,\delta_3^{\,3} + \lambda_1\,I_{12}\,\delta_2^{\,4} + I_{22}\,\delta_1^{\,4}$$

$$\tilde{K}(8,3) \quad \cdot 2\,\lambda_1\,I_{11}\,\delta_1^{\,4} + 2\,I_{12}\,\delta_3^{\,4} + \lambda_1\,I_{12}\,\delta_2^{\,5} + I_{22}\,\delta_1^{\,5}$$

$$\tilde{K}(8,4) \quad \cdot 3\,\lambda_1\,I_{11}\,\delta_1^{\,5} + 3\,I_{11}\,\delta_1^{\,3} + \lambda_1\,I_{12}\,\delta_2^{\,6} + I_{22}\,\delta_1^{\,6}$$

$$\tilde{K}(8,5) \quad \lambda_1^{\,2}\,I_{11}\,\delta_1^{\,3} + 2\,\lambda_1\,I_{12}\,\delta_3^{\,3} + I_{22}\,\delta_0^{\,3}$$

$$\tilde{K}(8,6) \quad \cdot \lambda_1^{\,2}\,I_{11}\,\delta_1^{\,4} + 2\,\lambda_1\,I_{12}\,\delta_3^{\,4} + I_{22}\,\delta_0^{\,4} + 6\,J_{12}\,\delta_2^{\,1} + 3\,J_{22}\,\delta_4^{\,2}$$

$$\tilde{K}(8,7) \quad \cdot \lambda_1^{\,2}\,I_{11}\,\delta_1^{\,5} + 2\,\lambda_1\,I_{12}\,\delta_3^{\,5} + I_{22}\,\delta_0^{\,5} + 12\,J_{11}\,\delta_1^{\,1} + 18\,J_{12}\,\delta_2^{\,2} + 6\,J_{22}\,\delta_4^{\,3}$$

$$\tilde{K}(8,8) \quad \cdot \lambda_1^{\,2}\,I_{11}\,\delta_1^{\,6} + 2\,\lambda_1\,I_{12}\,\delta_3^{\,6} + I_{22}\,\delta_0^{\,6} + 30\,I_{11}\,\delta_1^{\,2} + 36\,J_{12}\,\delta_2^{\,3} + 9\,I_{22}\,\delta_4^{\,4}$$

$$\tilde{K}(9,1) \quad \cdot \lambda_1\,I_{12}\,\delta_2^{\,4} + I_{22}\,\delta_1^{\,4}$$

$$\tilde{K}(9,2) \quad \cdot \lambda_1\,I_{11}\,\delta_1^{\,4} + I_{12}\,\delta_3^{\,4} + \lambda_1\,I_{12}\,\delta_2^{\,5} + I_{22}\,\delta_1^{\,5}$$

$$\tilde{K}(9,3) \quad \cdot 2\,\lambda_1\,I_{11}\,\delta_1^{\,5} + 2\,I_{12}\,\delta_3^{\,5} + \lambda_1\,I_{12}\,\delta_2^{\,6} + I_{22}\,\delta_1^{\,6}$$

$$\tilde{K}(9,4) \quad \cdot 3\,\lambda_1\,I_{11}\,\delta_1^{\,6} + 3\,I_{12}\,\delta_3^{\,6} + \lambda_1\,I_{12}\,\delta_2^{\,7} + I_{22}\,\delta_1^{\,7}$$

$$\tilde{K}(9,5) \quad \cdot \lambda_1^{\,2}\,I_{11}\,\delta_1^{\,4} + 2\,\lambda_1\,I_{12}\,\delta_3^{\,4} + I_{22}\,\delta_0^{\,4}$$

$$\tilde{K}(9,6) \quad \cdot \lambda_1^{\,2}\,I_{11}\,\delta_1^{\,5} + 2\,\lambda_1\,I_{12}\,\delta_3^{\,5} + I_{22}\,\delta_0^{\,5} + 12\,J_{12}\,\delta_2^{\,2} + 4\,J_{22}\,\delta_4^{\,3}$$

$$\tilde{K}(9,7) \quad \cdot \lambda_1^{\,2}\,I_{11}\,\delta_1^{\,6} + 2\,\lambda_1\,I_{12}\,\delta_3^{\,6} + I_{22}\,\delta_0^{\,6} + 24\,J_{11}\,\delta_2^{\,2} + 32\,J_{12}\,\delta_2^{\,3} + 8\,J_{22}\,\delta_4^{\,4}$$

$$\tilde{K}(9,8) \quad \cdot \lambda_1^{\,2}\,I_{11}\,\delta_1^{\,7} + 2\,\lambda_1\,I_{12}\,\delta_3^{\,7} + I_{22}\,\delta_0^{\,7} + 72\,J_{11}\,\delta_1^{\,3} + 60\,J_{12}\,\delta_2^{\,4} + 12\,J_{22}\,\delta_4^{\,5}$$

$$\tilde{K}(9,9) \quad \cdot \lambda_1^{\,2}\,I_{11}\,\delta_1^{\,8} + 2\,\lambda_1\,I_{12}\,\delta_3^{\,8} + I_{22}\,\delta_0^{\,8} + 144\,I_{11}\,\delta_1^{\,4} + 96\,J_{12}\,\delta_2^{\,5} + 16\,J_{22}\,\delta_4^{\,6}$$

$$\tilde{K}(10,1) \quad \cdot \lambda_1\,I_{12}\,\delta_2^{\,5} + I_{22}\,\delta_1^{\,5}$$

$$\tilde{K}(10,2) \quad \cdot \lambda_1\,I_{11}\,\delta_1^{\,5} + I_{12}\,\delta_3^{\,5} + \lambda_1\,I_{12}\,\delta_2^{\,6} + I_{22}\,\delta_5^{\,6}$$

$$\tilde{K}(10,3) \quad \cdot 2\,\lambda_1\,I_{11}\,\delta_1^{\,6} + 2\,I_{12}\,\delta_3^{\,6} + \lambda_1\,I_{12}\,\delta_2^{\,7} + I_{22}\,\delta_5^{\,7}$$

$$\tilde{K}(10,4) \quad \cdot 3\,\lambda_1\,I_{11}\,\delta_1^{\,7} + 3\,I_{12}\,\delta_3^{\,7} + \lambda_1\,I_{12}\,\delta_2^{\,8} \quad I_{22}\,\delta_5^{\,8}$$

$$\tilde{K}(10,5) \quad \cdot \lambda_1^{\,2}\,I_{11}\,\delta_1^{\,5} + 2\,\lambda_1\,I_{12}\,\delta_3^{\,5} + I_{22}\,\delta_0^{\,5}$$

$$\tilde{K}(10,6) \quad \cdot \lambda_1^{\,2}\,I_{11}\,\delta_1^{\,6} + 2\,\lambda_1\,I_{12}\,\delta_3^{\,6} + I_{22}\,\delta_0^{\,6} + 20\,J_{12}\,\delta_2^{\,3} + 5\,J_{22}\,\delta_4^{\,4}$$

$$\tilde{K}(10,7) \quad \cdot \lambda_1^{\,2}\,I_{11}\,\delta_1^{\,7} + 2\,\lambda_1\,I_{12}\,\delta_3^{\,7} + I_{22}\,\delta_0^{\,7} + 40\,J_{11}\,\delta_1^{\,3} + 50\,J_{12}\,\delta_2^{\,4} + 10\,J_{22}\,\delta_4^{\,5}$$

$$\tilde{K}(10,8) \quad \cdot \lambda_1^{\,2}\,I_{11}\,\delta_1^{\,8} + 2\,\lambda_1\,I_{12}\,\delta_3^{\,8} + I_{22}\,\delta_0^{\,8} + 120\,J_{11}\,\delta_1^{\,4} + 90\,J_{12}\,\delta_2^{\,5} + 15\,J_{22}\,\delta_4^{\,6}$$

$$\tilde{K}(10,9) \quad \cdot \lambda_1^{\,2}\,I_{11}\,\delta_1^{\,9} + 2\,\lambda_1\,I_{12}\,\delta_3^{\,9} + I_{22}\,\delta_0^{\,9} + 240\,J_{11}\,\delta_1^{\,5} + 140\,J_{12}\,\delta_2^{\,5} + 20\,J_{22}\,\delta_4^{\,7}$$

$$\tilde{K}(10,10) \quad \cdot \lambda_1^{\,2}\,I_{11}\,\delta_1^{\,10} + 2\,\lambda_1\,I_{12}\,\delta_3^{\,10} + I_{22}\,\delta_0^{\,10} + 400\,J_{11}\,\delta_1^{\,6} + 200\,J_{12}\,\delta_2^{\,7} + 25\,J_{22}\,\delta_4^{\,8}$$

Figure 43 Stiffness Matrix, $[\tilde{K}]$

$$
\begin{array}{c}
 & \left[I_\epsilon^{(0)}\right] & & \left[I_\epsilon^{(10)}\right] & & \left[J_\epsilon^{(0)}\right] & & \left[J_\epsilon^{(10)}\right] \\
\left\{\tilde{F}_\epsilon\right\} = \beta_1 & \left[\begin{array}{cccccccc}
0 & \delta_2^{\,0} & 0 & \frac{1}{S}\delta_2^{\,1} & 0 & 0 & 0 & 0 \\
\delta_1^{\,0} & \delta_2^{\,1} & \frac{1}{S}\delta_1^{\,1} & \frac{1}{S}\delta_2^{\,2} & 0 & 0 & 0 & 0 \\
2\delta_1^{\,1} & \delta_2^{\,2} & \frac{2}{S}\delta_1^{\,2} & \frac{1}{S}\delta_2^{\,3} & 0 & 0 & 0 & 0 \\
3\delta_1^{\,2} & \delta_2^{\,3} & \frac{3}{S}\delta_1^{\,3} & \frac{1}{S}\delta_2^{\,4} & 0 & 0 & 0 & 0 \\
\lambda_1\delta_1^{\,0} & \delta_3^{\,0} & \frac{\lambda_1}{S}\delta_1^{\,1} & \frac{1}{S}\delta_3^{\,1} & 0 & 0 & 0 & 0 \\
\lambda_1\delta_1^{\,1} & \delta_3^{\,1} & \frac{\lambda_1}{S}\delta_1^{\,2} & \frac{1}{S}\delta_3^{\,2} & 0 & -\delta_2^{\,0} & 0 & -\frac{1}{S}\delta_2^{\,1} \\
\lambda_1\delta_1^{\,2} & \delta_3^{\,2} & \frac{\lambda_1}{S}\delta_1^{\,3} & \frac{1}{S}\delta_3^{\,3} & -2\delta_1^{\,0} & -2\delta_2^{\,1} & -\frac{2}{S}\delta_1^{\,1} & -\frac{2}{S}\delta_2^{\,2} \\
\lambda_1\delta_1^{\,3} & \delta_3^{\,3} & \frac{\lambda_1}{S}\delta_1^{\,4} & \frac{1}{S}\delta_3^{\,4} & -6\delta_1^{\,1} & -3\delta_2^{\,2} & -\frac{6}{S}\delta_1^{\,2} & -\frac{3}{S}\delta_2^{\,3} \\
\lambda_1\delta_1^{\,4} & \delta_3^{\,4} & \frac{\lambda_1}{S}\delta_1^{\,5} & \frac{1}{S}\delta_3^{\,5} & -12\delta_1^{\,2} & -4\delta_2^{\,3} & -\frac{12}{S}\delta_1^{\,3} & -\frac{4}{S}\delta_2^{\,4} \\
\lambda_1\delta_1^{\,5} & \delta_3^{\,5} & \frac{\lambda_1}{S}\delta_1^{\,6} & \frac{1}{S}\delta_3^{\,6} & -20\delta_1^{\,3} & -5\delta_2^{\,4} & -\frac{20}{S}\delta_1^{\,4} & -\frac{5}{S}\delta_2^{\,5}
\end{array}\right]
\end{array}
\left\{\begin{array}{c}
\left\{I_\epsilon^{(10)}\right\} \\
\left\{I_\epsilon^{(10)}\right\} \\
\left\{J_\epsilon^{(10)}\right\} \\
\left\{J_\epsilon^{(10)}\right\}
\end{array}\right\}
$$

Figure 44. Element Prestrain Load Vector $\left\{\tilde{F}_\epsilon\right\}$

$$
2\pi \left\{ \begin{bmatrix}
0 \\
0 \\
0 \\
0 \\
P_1 d_1^{\,0} + \left(\frac{P_2 - P_1}{5}\right) d_1^{\,1} \\
P_1 d_1^{\,1} + \left(\frac{P_2 - P_1}{5}\right) d_1^{\,2} \\
P_1 d_1^{\,2} + \left(\frac{P_2 - P_1}{5}\right) d_1^{\,3} \\
P_1 d_1^{\,3} + \left(\frac{P_2 - P_1}{5}\right) d_1^{\,4} \\
P_1 d_1^{\,4} + \left(\frac{P_2 - P_1}{5}\right) d_1^{\,5} \\
P_1 d_1^{\,5} + \left(\frac{P_2 - P_1}{5}\right) d_1^{\,6}
\end{bmatrix} \right\}
$$

Figure 45. Pressure Load Matrix, $\left\{\tilde{F}_p\right\}$

This completes the statement of the stiffness and applied load matrices for the toroidal thin shell ring element.

4. Stress Matrices

An element stress matrix is required to transform the solution for the primary displacement unknowns to a solution for the secondary stress resultant unknowns as well. Stress resultants corresponding to deformations considered are available directly from integrations of Equation 208, i. e.,

$$T_\xi \approx \int_z \sigma_\xi \, dz \qquad T_\beta \approx \int \sigma_\beta \, dz \tag{238}$$

$$M_\beta \approx \int_z z\sigma_\xi \, dz \qquad M_\xi \approx -\int_z z\sigma_\beta \, dz \tag{239}$$

The calculation of shear stress resultant which is associated with deformation not considered is based upon equilibrium requirements, i. e.,

$$Q_\xi = \lambda_2 \left[M_\beta + M_\xi \right] + \frac{\partial M_\beta}{\partial \xi} \tag{240}$$

The integrated form of the discretized stress-displacement relations may be written symbolically as

$$\{\Sigma\} = [S]\{\beta\} - \{\Delta\} \tag{241}$$

where

$$\{\Sigma\}^T = \left\lfloor T_\xi, \; T_\beta, \; M_\beta, \; M_\xi, \; Q_\xi \right\rfloor \tag{242}$$

and $[\tilde{S}]$ is given explicit definition in Figure 46. The final form of the element stress matrix is obtained by transformation to boundary displacement degrees-of-freedom, i.e.,

$$[S] = [S][\Gamma_{\beta_q}] \tag{243}$$

This completes specification of the matrices which comprise the toroidal thin shell ring element representation.

$\tilde{S}(1,1) \quad +t\lambda_2 E_{12}$

$\tilde{S}(2,1) \quad +t\lambda_2 E_{22}$

$\tilde{S}(3,1) \quad 0$

$\tilde{S}(4,1) \quad 0$

$\tilde{S}(5,1) \quad 0$

$\tilde{S}(1,2) \quad +t\,(\lambda_2 E_{12}\,\xi + E_{11})$

$\tilde{S}(2,2) \quad +t\,(\lambda_2 E_{22}\,\xi + E_{12})$

$\tilde{S}(3,2) \quad 0$

$\tilde{S}(4,2) \quad 0$

$\tilde{S}(5,2) \quad 0$

$\tilde{S}(1,3) = +t\,(\lambda_2 E_{12}\,\xi^2 + 2 E_{11}\,\xi)$

$\tilde{S}(2,3) = +t\,(\lambda_2 E_{22}\,\xi^2 + 2 E_{12}\,\xi)$

$\tilde{S}(3,3) = 0$

$\tilde{S}(4,3) = 0$

$\tilde{S}(5,3) = 0$

$\tilde{S}(1,4) = +t\,(\lambda_2 E_{12}\,\xi^3 + 3 E_{11}\,\xi^2)$

$\tilde{S}(2,4) = +t\,(\lambda_2 E_{22}\,\xi^3 + 3 E_{12}\,\xi^2)$

$\tilde{S}(3,4) = 0$

$\tilde{S}(4,4) = 0$

$\tilde{S}(5,4) = 0$

$\tilde{S}(1,5) \quad +t\,(\lambda_1 E_{11} + \lambda_3 E_{12})$

$\tilde{S}(2,5) = +t\,(\lambda_1 E_{12} + \lambda_3 E_{22})$

$\tilde{S}(3,5) \quad 0$

$\tilde{S}(4,5) = 0$

$\tilde{S}(5,5) = 0$

$\tilde{S}(1,6) = +t\,(\lambda_1 E_{11} + \lambda_3 E_{12})\xi$

$\tilde{S}(2,6) = +t\,(\lambda_1 E_{12} + \lambda_3 E_{22})\xi$

$\tilde{S}(3,6) \quad -\frac{t^3}{12}(\lambda_2 E_{12})$

$\tilde{S}(4,6) = +\frac{t^3}{12}(\lambda_2 E_{22})$

$\tilde{S}(5,6) = +\frac{t^3}{12}(\lambda_2^2 E_{22} - \lambda_4 E_{12})$

$\tilde{S}(1,7) = +t\,(\lambda_1 E_{11} + \lambda_3 E_{12})\,\xi^2$

$\tilde{S}(2,7) = +t\,(\lambda_1 E_{12} + \lambda_3 E_{22})\,\xi^2$

$\tilde{S}(3,7) = -\frac{t^3}{12}(2\lambda_2 E_{12}\,\xi + 2 E_{11})$

$\tilde{S}(4,7) = +\frac{t^3}{12}(2\lambda_2 E_{22}\,\xi + 2 E_{12})$

$\tilde{S}(5,7) = +\frac{t^3}{12}\left[2\,(\lambda_2^2 E_{22} - \lambda_4 E_{12})\,\xi - 2\lambda_2 E_{11}\right]$

$\tilde{S}(1,8) = +t\,(\lambda_1 E_{11} + \lambda_3 E_{12})\,\xi^3$

$\tilde{S}(2,8) = +t\,(\lambda_1 E_{12} + \lambda_3 E_{22})\,\xi^3$

$\tilde{S}(3,8) \quad -\frac{t^3}{12}(3\lambda_2 E_{12}\,\xi^2 + 6 E_{11}\,\xi)$

$\tilde{S}(4,8) = +\frac{t^3}{12}(3\lambda_2 E_{22}\,\xi^2 + 6 E_{12}\,\xi)$

$\tilde{S}(5,8) = +\frac{t^3}{12}\left[3(\lambda_2^2 E_{22} - \lambda_4 E_{12})\,\xi^2 - 6\lambda_2 E_{11}\,\xi - 6 E_{11}\right]$

$\tilde{S}(1,9) = +t\,(\lambda_1 E_{11} + \lambda_3 E_{12})\,\xi^4$

$\tilde{S}(2,9) = +t\,(\lambda_1 E_{12} + \lambda_3 E_{22})\,\xi^4$

$\tilde{S}(3,9) = -\frac{t^3}{12}(4\lambda_2 E_{12}\,\xi^3 + 12 E_{11}\,\xi^2)$

$\tilde{S}(4,9) = +\frac{t^3}{12}(4\lambda_2 E_{22}\,\xi^3 + 12 E_{12}\,\xi^2)$

$\tilde{S}(5,9) = +\frac{t^3}{12}\left[4\,(\lambda_2^2 E_{22} - \lambda_4 E_{12})\,\xi^3 - 12\lambda_2 E_{11}\,\xi^2 - 24 E_{11}\,\xi\right]$

$\tilde{S}(1,10) = +t\,(\lambda_1 E_{11} + \lambda_3 E_{12})\,\xi^5$

$\tilde{S}(2,10) = +t\,(\lambda_1 E_{12} + \lambda_3 E_{22})\,\xi^5$

$\tilde{S}(3,10) = -\frac{t^3}{12}(5\lambda_2 E_{12}\,\xi^4 + 20 E_{11}\,\xi^3)$

$\tilde{S}(4,10) = +\frac{t^3}{12}(5\lambda_2 E_{22}\,\xi^4 + 20 E_{12}\,\xi^3)$

$\tilde{S}(5,10) = +\frac{t^3}{12}\left[5(\lambda_2^2 E_{22} - \lambda_4 E_{12})\,\xi^4 - 20\lambda_2 E_{11}\,\xi^3 - 60 E_{11}\,\xi^2\right]$

Figure 46. Stress Matrix $\left[\tilde{S}\right]$

C. EVALUATION

As an illustration of the use of the Toroidal Thin Shell Ring Element in a structural evaluation, consider the following example problem.

A thin walled circular cylinder, cantilevered at one end, is subjected to the action of bending moments, M, and shearing forces, Q, both uniformly distributed along the free edge of the cylinder. This cylinder is shown in Figure 47 along with the loading, pertinent dimensions and material properties.

Five finite element idealizations shown in Figure 48 were employed in obtaining results for distribution of meriodional moment in the cylinder. The results shown in Figure 49 were obtained from the 16 element idealization shown in Figure 48 (e). Reference 37 provides an alternate analytical solution and it is designated by the solid line in Figure 49.

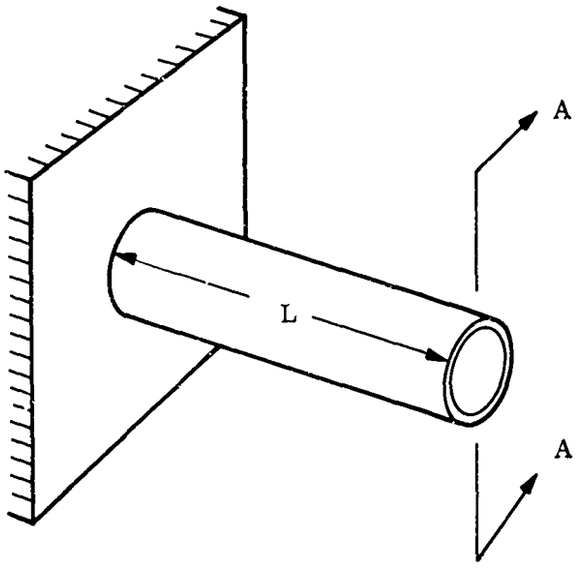

E = 3×10^6 psi

ν = 0.30

t = 3.0 in.

R = 20.0 in.

L = 35.0 in.

Q = 1500 lb/in.

M = 1000 in. - lb/in.

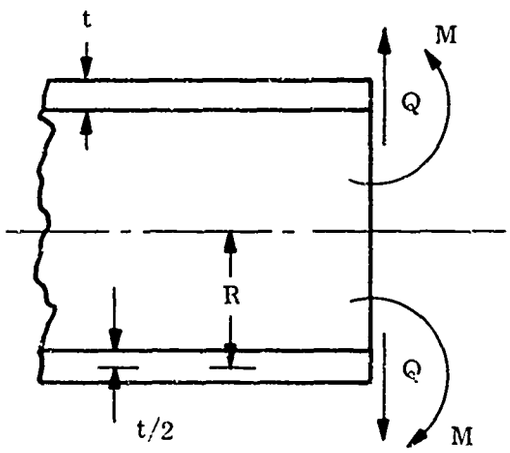

Section A-A

Figure 47. Cylinder Subjected to End Loads

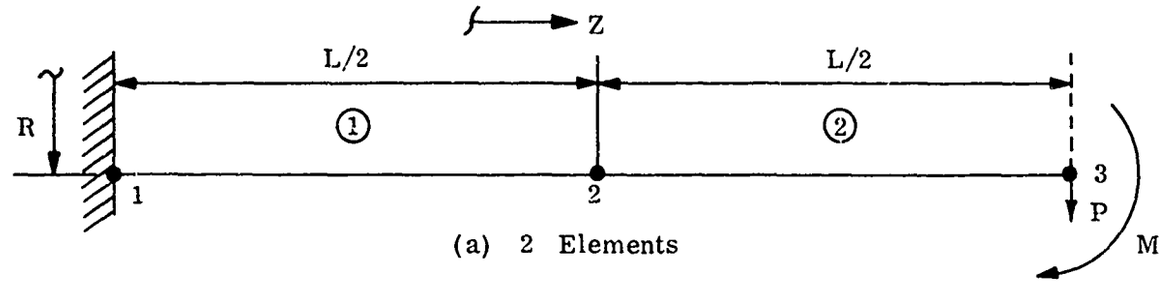

(a) 2 Elements

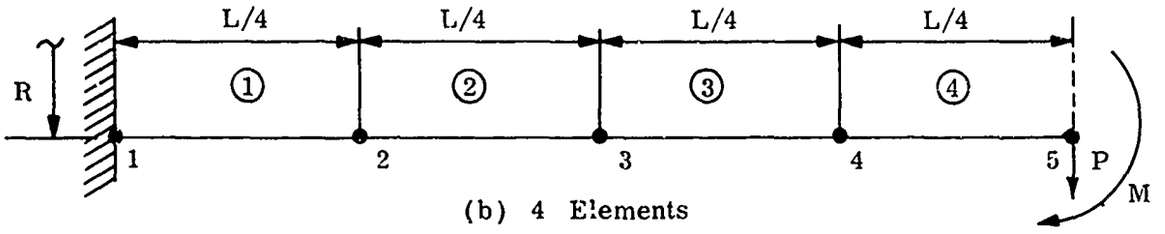

(b) 4 Elements

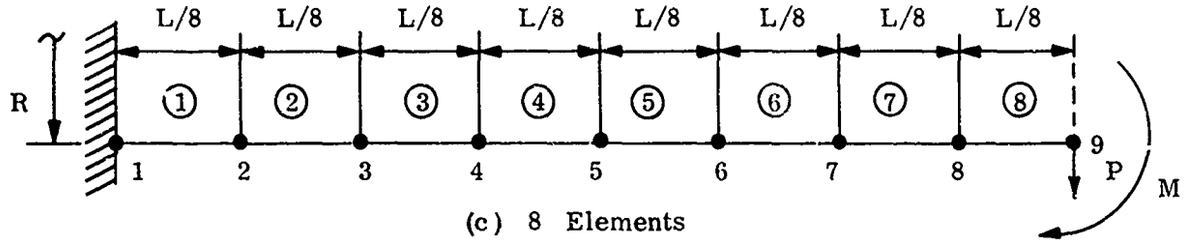

(c) 8 Elements

All Elements L/16

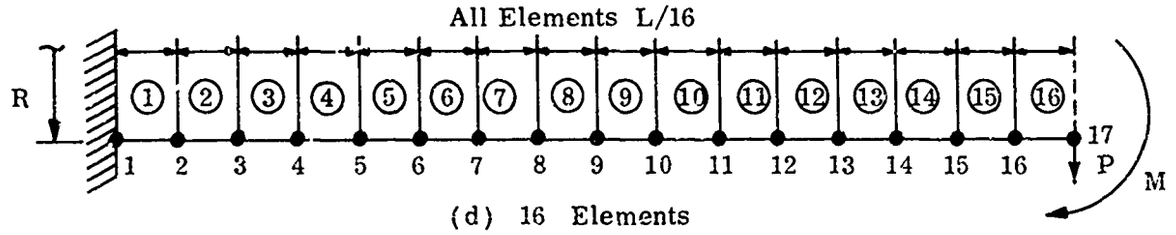

(d) 16 Elements

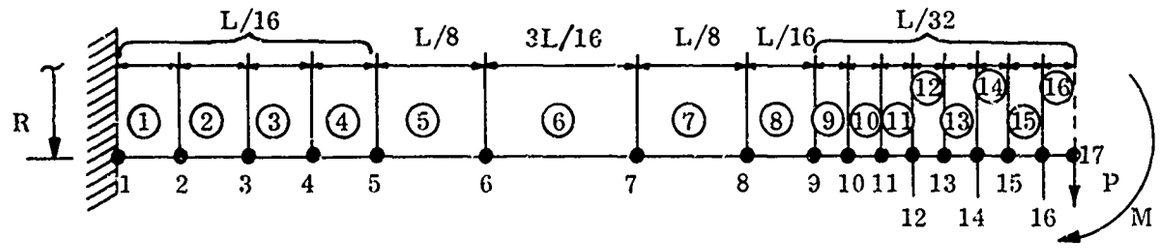

(e) 16 Elements

Figure 48. End Loaded Cylinder Idealizations

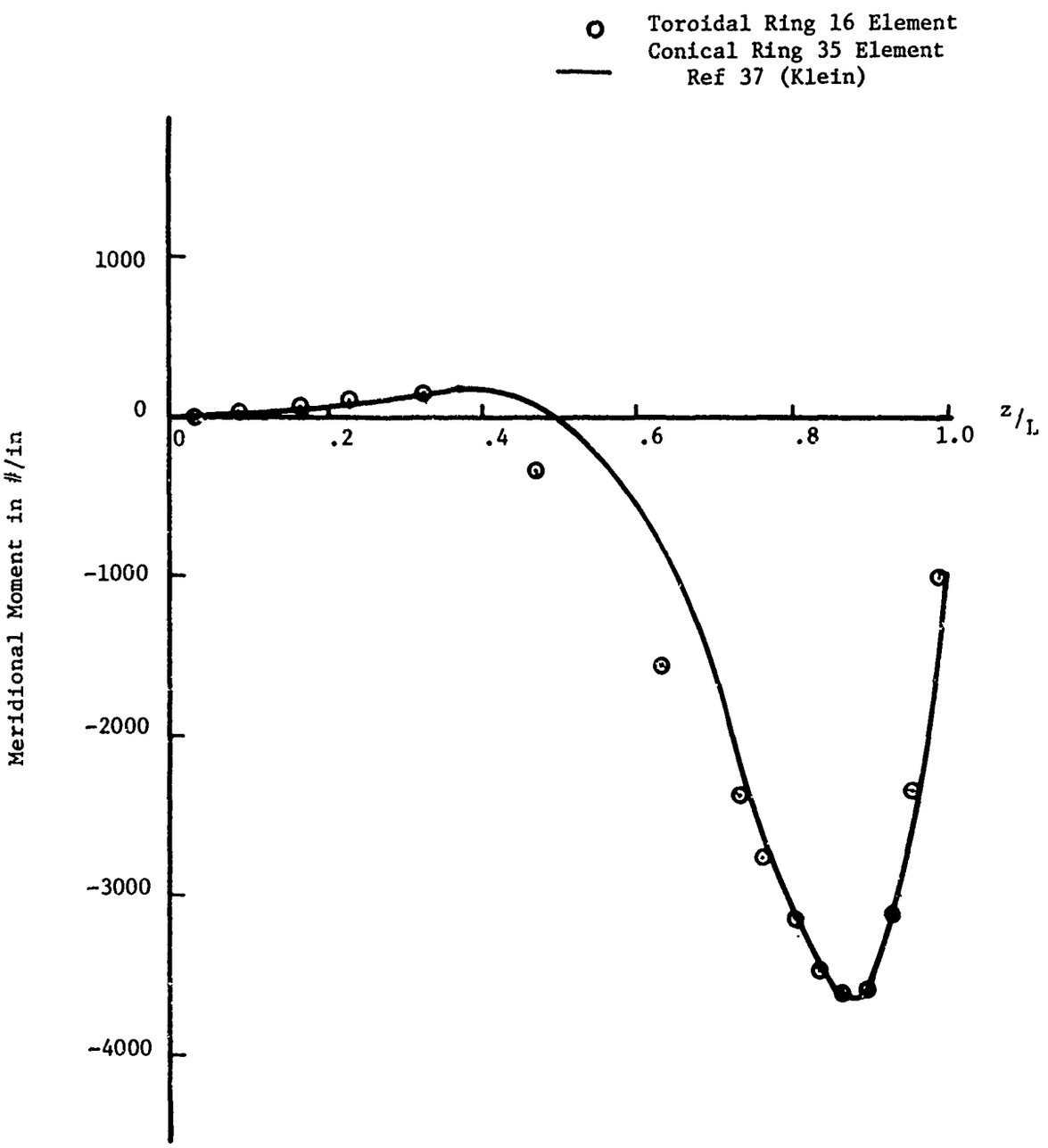

Figure 49
Meridional Moment Distribution

8. MALLET QUADRILATERAL THIN SHELL ELEMENT

A. INTRODUCTION

A quadrilateral thin shell element is incorporated in the discrete element library of the MAGIC System. This element, shown in Figure 50, is recommended for use as the basic building block for membranes, plates, and shells. The Helle triangular thin shell element is a compatible companion element useful in regions of irregularity and prominent double curvature. The Mallett quadrilateral thin shell element representation is developed in detail in Reference 43.

The shape of the general quadrilateral element is defined by the coordinates of the four corner points. It is a zero curvature element. The plane of the element is determined by its first three corner point coordinates.

The subject element is a thin shell element in that both membrane and flexure action are represented. Referenced to axes in the plane of the element, the membrane and flexure representations are uncoupled. Optional generation of either or both of the representations is controlled by the provision of associated effective thicknesses. The distinct membrane and flexure effective thicknesses are assumed constant over the plane of the element.

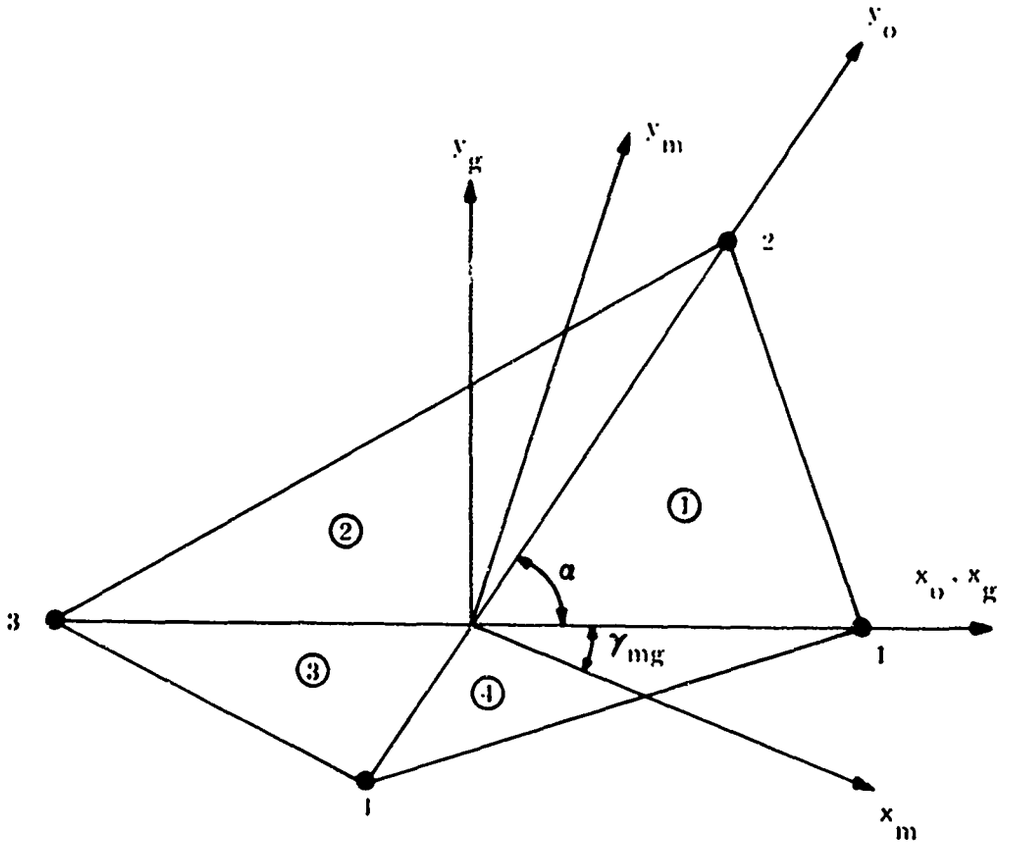

Figure 50. Quadrilateral Thin Shell Element Representation

Under normal circumstances, four corner points and four midside points participate in establishing continuous connection of the Mallett quadrilateral thin shell element with adjacent elements. Used in this way input data volume is reduced and accuracy is enhanced. An option is provided to suppress the midside nodes individually if associated complexities arise in grid refinement or nonstandard connections with adjacent elements. Invoking this suppression option causes linear variation to be imposed on the specified midside variables.

The Mallett thin shell element is written to accommodate anisotropy of mechanical and physical material properties. Orientation of material axes is data specified. Temperature referenced material properties, selected from the materials library, are assumed constant over the element.

A linear generalized Hooke's Law is employed for the equations of state. Three options are provided; conventional plane stress, generalized plane stress, and restricted plane strain.

The element formulation is discretized by the construction of mode shapes. Membrane displacements within the subject element are approximated by quadratic polynomials. Transverse displacement is represented by cubic polynomials. A linear variation is provided for midplane and gradient variations in thermal loading. Other element loadings, such as pressure, are assumed constant over the element. Deformation behavior of the Mallett quadrilateral thin shell element is taken to be described by the displacement degrees-of-freedom associated with the gridpoints which it connects.

The variation in strain within the element which is permitted by the assumed displacement functions, leads to similar stress variation. Advantage is taken of this by exhibiting predicted stress resultants at the four corners as well as at the center of the element. Inplane and normal direct, shear, and bending stress resultants are included. The display of stress implies a set of axes of reference. These axes are data specified.

B. FORMULATION

1. Displacement Functions

The displacement functions for the quadrilateral thin shell element are constructed with reference to the oblique coordinate axes (x_o, y_o) shown in Figure 50. The origin of this system is taken at the intersection of the diagonals of the quadrilateral. The orientation of these axes coincide with the diagonals. The x_o -axis goes through gridpoint number 1. The y_o -axis goes through the first gridpoint in the counterclockwise direction which is designated as number 2.

Polynominal mode shapes are assumed for each of the four zones shown in Figure 50. With respect to the oblique coordinate axes these mode shapes are written as

$$u_o^{(j)} = \left[B_u^{(j)} \right] \left\{ \beta_m \right\} \quad j = 1, 2, 3, 4. \tag{244}$$

$$v_o^{(j)} = \left[B_v^{(j)} \right] \left\{ \beta_m \right\} \quad j = 1, 2, 3, 4. \tag{245}$$

$$w_o^{(j)} = \left[B_w^{(j)} \right] \left\{ \beta_f \right\} \quad j = 1, 2, 3, 4. \tag{246}$$

where

$$\left\{ \beta_m \right\}^T = \left[\beta_{m1}, \beta_{m2}, \ldots, \beta_{m16} \right] \tag{247}$$

$$\left\{ \beta_f \right\}^T = \left[\beta_{f1}, \beta_{f2}, \ldots, \beta_{f16} \right] \tag{248}$$

and the mode shape matrices $\left\{ B_u^{(j)} \right\}$, $\left\{ B_v^{(j)} \right\}$ and $\left\{ B_w^{(j)} \right\}$ are given in Figures 51, 52, and 53, respectively. It is apparent from these matrices that the mode shapes employed for each zone are complete up to the order of truncation.

Elementary interpolation theory is invoked to obtain transformation to gridpoint displacement degrees-of-freedom, i.e.

$$\left\{ \beta_m \right\} = \left[\Gamma_{\beta o}^{(m)} \right] \left\{ \delta_{om} \right\} \tag{249}$$

$$\left\{ \beta_f \right\} = \left[\Gamma_{\beta o}^{(f)} \right] \left\{ \delta_{of} \right\} \tag{250}$$

where

$$\left\{ \delta_{om} \right\}^T = \left[u_{o1}, u_{o2}, u_{o3}, u_{o4}, u_{o5}, u_{o6}, u_{o7}, u_{o8}, \right.$$
$$\left. v_{o1}, v_{o2}, v_{o3}, v_{o4}, v_{o5}, v_{o6}, v_{o7}, v_{o8} \right] \tag{251}$$

$$\left\{ \delta_{of} \right\}^T = \left[w_{o1}, w_{o2}, w_{o3}, w_{o4}, w_{ox1}, w_{ox2}, w_{ox3}, w_{ox4}, \right.$$
$$\left. w_{oy1}, w_{oy2}, w_{oy3}, w_{oy4}, w_{on5}, w_{on6}, w_{on7}, w_{on8} \right] \tag{252}$$

and $\left[\Gamma_{\beta o}^{(m)} \right]$ and $\left[\Gamma_{\beta o}^{(c)} \right]$ are defined in Figures 54 and 55.

$$\beta_{m1}\ \beta_{m2}\ \beta_{m3}\ \beta_{m4}\ \beta_{m5}\ \beta_{m6}\ \beta_{m7}\ \beta_{m8}\ \beta_{m9}\ \beta_{m10}\ \beta_{m11}\ \beta_{m12}\ \beta_{m13}\ \beta_{m14}\ \beta_{m15}\ \beta_{m16}$$

$$\left[B_u^{(1)}\right] = u_o \left[1\ ,\ x\ ,\ y\ ,\ x^2\ ,\ xy\ ,\ y^2\ ,\ ,\ ,\ ,\ ,\ ,\ ,\ ,\ ,\ ,\ ,\ ,\ \right]$$

$$\left[B_u^{(2)}\right] = u_o \left[1\ ,\ x\ ,\ y\ ,\ ,\ xy\ ,\ y^2\ ,\ ,\ x^2\ ,\ ,\ ,\ ,\ ,\ ,\ ,\ ,\ ,\ ,\ \right]$$

$$\left[B_u^{(3)}\right] = u_o \left[1\ ,\ x\ ,\ y\ ,\ ,\ xy\ ,\ ,\ y^2\ ,\ x^2\ ,\ ,\ ,\ ,\ ,\ ,\ ,\ ,\ ,\ ,\ \right]$$

$$\left[B_u^{(4)}\right] = u_o \left[1\ ,\ x\ ,\ y\ ,\ x^2\ ,\ xy\ ,\ ,\ y^2\ ,\ ,\ ,\ ,\ ,\ ,\ ,\ ,\ ,\ ,\ ,\ \right]$$

Figure 51. Displacement Mode Shapes $u_o^{(j)}$

$$\beta_{m1}\ \beta_{m2}\ \beta_{m3}\ \beta_{m4}\ \beta_{m5}\ \beta_{m6}\ \beta_{m7}\ \beta_{m8}\ \beta_{m9}\ \beta_{m10}\ \beta_{m11}\ \beta_{m12}\ \beta_{m13}\ \beta_{m14}\ \beta_{m15}\ \beta_{m16}$$

$$\left[B_v^{(1)}\right] = v_o \left[\ ,\ ,\ ,\ ,\ ,\ ,\ ,\ ,\ ,\ 1\ ,\ x\ ,\ y\ ,\ x^2\ ,\ xy\ ,\ y^2\ ,\ ,\ \right]$$

$$\left[B_v^{(2)}\right] = v_o \left[\ ,\ ,\ ,\ ,\ ,\ ,\ ,\ ,\ ,\ 1\ ,\ x\ ,\ y\ ,\ ,\ xy\ ,\ y^2\ ,\ ,\ x^2\ \right]$$

$$\left[B_v^{(3)}\right] = v_o \left[\ ,\ ,\ ,\ ,\ ,\ ,\ ,\ ,\ ,\ 1\ ,\ x\ ,\ y\ ,\ ,\ xy\ ,\ ,\ y^2\ ,\ x^2\ \right]$$

$$\left[B_v^{(4)}\right] = v_o \left[\ ,\ ,\ ,\ ,\ ,\ ,\ ,\ ,\ ,\ 1\ ,\ x\ ,\ y\ ,\ x^2\ ,\ xy\ ,\ ,\ y^2\ ,\ \right]$$

Figure 52. Displacement Mode Shapes $v_o^{(j)}$

$$\beta_{f1}\ \beta_{f2}\ \beta_{f3}\ \beta_{f4}\ \beta_{f5}\ \beta_{f6}\ \beta_{f7}\ \beta_{f8}\ \beta_{f9}\ \beta_{f10}\ \beta_{f11}\ \beta_{f12}\ \beta_{f13}\ \beta_{f14}\ \beta_{f15}\ \beta_{f16}$$

$$\left[B_w^{(1)}\right] = w_o \left[1\ ,\ x\ ,\ y\ ,\ x^2\ ,2xy\ ,\ y^2\ ,4x^3\ ,\ 4x^2y\ ,4xy^2\ ,4y^3\ ,\ ,\ ,\ ,\ ,\ ,\ \right]$$

$$\left[B_w^{(2)}\right] = w_o \left[1\ ,\ x\ ,\ y\ ,\ ,2xy\ ,\ ,\ ,\ ,4xy^2\ ,\ 4y^3\ ,\ ,\ ,\ ,\ x^2\ ,\ 4x^3\ ,4x^2y\right]$$

$$\left[B_w^{(3)}\right] = w_o \left[1\ ,\ x\ ,\ y\ ,\ ,2xy\ ,\ ,\ ,\ ,\ ,\ ,\ y^2\ ,4xy^2\ ,\ 4y^3\ ,x^2\ ,\ 4x^3\ ,4x^2y\right]$$

$$\left[B_w^{(4)}\right] = w_o \left[1\ ,\ x\ ,\ y\ ,\ x^2\ ,2xy\ ,\ ,4x^3\ ,\ 4x^2y\ ,\ ,\ ,\ y^2\ ,4xy^2\ ,\ 4y^3\ ,\ ,\ ,\ \right]$$

Figure 53. Flexure Displacement Mode Shapes $w_o^{(j)}$

$$\left[\Gamma_{\beta_o}^{(m)}\right] = \begin{bmatrix} \left[\Gamma_m\right]^{-1} & , \\ , & \left[\Gamma_m\right]^{-1} \end{bmatrix}$$

where

$$\left[\Gamma_m\right] = \begin{array}{cc} & \begin{matrix} \beta_{m9} & \beta_{m10} & \beta_{m11} & \beta_{m12} & \beta_{m13} & \beta_{m14} & \beta_{m15} & \beta_{m16} \\ \beta_{m1} & \beta_{m2} & \beta_{m3} & \beta_{m4} & \beta_{m5} & \beta_{m6} & \beta_{m7} & \beta_{m8} \end{matrix} \\ \begin{matrix} \delta_9 \\ \delta_{16} \\ \delta_{11} \\ \delta_{12} \\ \delta_{13} \\ \delta_{14} \\ \delta_{15} \\ \delta_{16} \end{matrix} & \begin{matrix} \delta_1 \\ \delta_2 \\ \delta_3 \\ \delta_4 \\ \delta_5 \\ \delta_6 \\ \delta_7 \\ \delta_8 \end{matrix} \begin{bmatrix} 1 & x_1 & 0 & x_1^2 & 0 & 0 & 0 & 0 \\ 1 & 0 & y_2 & 0 & 0 & y_2^2 & 0 & 0 \\ 1 & x_3 & 0 & 0 & 0 & 0 & 0 & x_3^2 \\ 1 & 0 & y_4 & 0 & 0 & 0 & y_4^2 & 0 \\ 1 & \frac{1}{2}x_1 & \frac{1}{2}y_2 & \frac{1}{4}x_1^2 & \frac{1}{4}x_1y_2 & \frac{1}{4}y_2^2 & 0 & 0 \\ 1 & \frac{1}{2}x_3 & \frac{1}{2}y_2 & 0 & \frac{1}{4}x_3y_2 & \frac{1}{4}y_2^2 & 0 & \frac{1}{4}x_3^2 \\ 1 & \frac{1}{2}x_3 & \frac{1}{2}y_4 & 0 & \frac{1}{4}x_3y_4 & 0 & \frac{1}{4}y_4^2 & \frac{1}{4}x_3^2 \\ 1 & \frac{1}{2}x_1 & \frac{1}{2}y_4 & \frac{1}{4}x_1^2 & \frac{1}{4}x_1y_4 & 0 & \frac{1}{4}y_4^2 & 0 \end{bmatrix} \end{array}$$

Figure 54. Membrane Displacement Coordinate Transformation $\left[\Gamma_{\beta_o}^{(m)}\right]$

$$\left[\Gamma_{\beta o}^{(f)}\right]^{-1} =$$

	β_1	β_2	β_3	β_4	β_5	β_6	β_7	β_8	β_9	β_{10}	β_{11}	β_{12}	β_{13}	β_{14}	β_{15}	β_{16}
w_1	1	x_1	0	x_1^2	0	0	$4x_1^3$	0	0	0	0	0	0	0	0	0
w_2	1	0	y_2	0	0	y_2^2	0	0	0	$4y_2^3$	0	0	0	0	0	0
w_3	1	x_3	0	0	0	0	0	0	0	0	0	0	0	x_3^2	$4x_3^3$	0
w_4	1	0	y_4	0	0	0	0	0	0	0	y_4^2	0	$4y_4^3$	0	0	0
w_{x1}	0	1	0	$2x_1$	0	0	$12x_1^3$	0	0	0	0	0	0	0	0	0
w_{x2}	0	1	0	0	$2y_2$	0	0	0	$4y_2^2$	0	0	0	0	0	0	0
w_{x3}	0	1	0	0	0	0	0	0	0	0	0	0	0	$2x_3$	$12x_3^2$	0
w_{x4}	0	1	0	0	$2y_4$	0	0	0	0	0	0	$4y_4^2$	0	0	0	0
w_{y1}	0	0	1	0	$2x_1$	0	0	$4x_1^2$	0	0	0	0	0	0	0	0
w_{y2}	0	0	1	0	0	$2y_2$	0	0	0	$12y_2^2$	0	0	0	0	0	0
w_{y3}	0	0	1	0	$2x_3$	0	0	0	0	0	0	0	0	0	0	$4x_3^2$
w_{y4}	0	0	1	0	0	0	0	0	0	0	$2y_4$	0	$12y_4^2$	0	0	0
w_{n5}		a_1	b_1	a_1x_1	$a_1y_2 + b_1x_1$	b_1y_2	$3a_1x_1^2$	$2a_1x_1y_2 + b_1x_1^2$	$a_1y_2^2 + 2b_1x_1y_2$	$3b_1y_2^2$						
w_{n6}		a_2	$+b_2$		$a_2y_2 + b_2x_3$	a_2y_2			$a_2y_2^2 + 2b_2x_3y_2$	$3b_2y_2^2$				a_2x_3	$3a_2x_3^2$	$2a_2x_3y_2 + b_2x_3^2$
w_{n7}		a_3	$+b_3$		$a_3y_4 + b_3x_3$					$+b_3y_4$		$a_3y_4^2 + 2b_3x_3y_4$	$3b_3y_4^2$	a_3x_3	$3a_3x_3^2$	$2a_3x_3y_4 + b_3x_3^2$
w_{n8}		a_4	$+b_4$	a_4x_1	$a_4y_4 + b_4x_1$		$3a_4x_1^2$	$2a_4x_1y_4 + b_4x_1^2$		$+b_4y_4$		$a_4y_4^2 + 2b_4x_1y_4$	$3b_4y_4^2$			

Figure 55. Flexure Displacement Coordinate Transformation $\left[\Gamma_{\beta o}^{(f)}\right]$

The next step is to introduce a transformation to gridpoint degrees-of-freedom referenced to the element orthogonal axes (x_g, y_g). The transformation relations take the form

$$\{\delta_{om}\} = [\Gamma_{og}^{(m)}] \{\delta_{gm}\} \tag{253}$$

$$\{\delta_{of}\} = [\Gamma_{of}^{(f)}] \{\delta_{gf}\} \tag{254}$$

where

$$\{\delta_{gm}\}^T = \lfloor u_{g1}, u_{g2}, \ldots, u_{g8}, v_{g1}, v_{g2}, \ldots, v_{g8} \rfloor \tag{255}$$

$$\{\delta_{gf}\}^T = \lfloor w_{g1}, w_{g2}, w_{g3}, w_{g4}, w_{gx1}, w_{gx2}, w_{gx3}, w_{gx4}, w_{gy1}, w_{gy2}, w_{gy3}, w_{n5}, w_{n6}, w_{n7}, w_{n8} \rfloor \tag{256}$$

and the transformation relations $[\Gamma_{og}^{(m)}]$ and $[\Gamma_{og}^{(f)}]$ are given in Figures 56 and 57.

At this point the optional transformations for the suppression of midpoint displacement degrees-of-freedom are introduced. This feature provides flexibility in idealization and facilitates eccentric connection of elements. The transformations take the form,

$$\{\delta_{gm}\} = [\Gamma_{sup}^{(m)}] \{\delta'_{gm}\} \tag{257}$$

$$\{\delta_{gf}\} = [\Gamma_{sup}^{(f)}] \{\delta'_{gf}\} \tag{258}$$

The degrees-of-freedom $\{\delta'_{gm}\}$ and $\{\delta'_{gf}\}$ may be interpreted according to Equations 255 and 256. The suppression transformations $[\Gamma_{sup}^{(m)}]$ and $[\Gamma_{sup}^{(f)}]$ are defined in Figures 58 and 59. The effect of these transformations is to build in linear variations in place of the degrees-of-freedom suppressed.

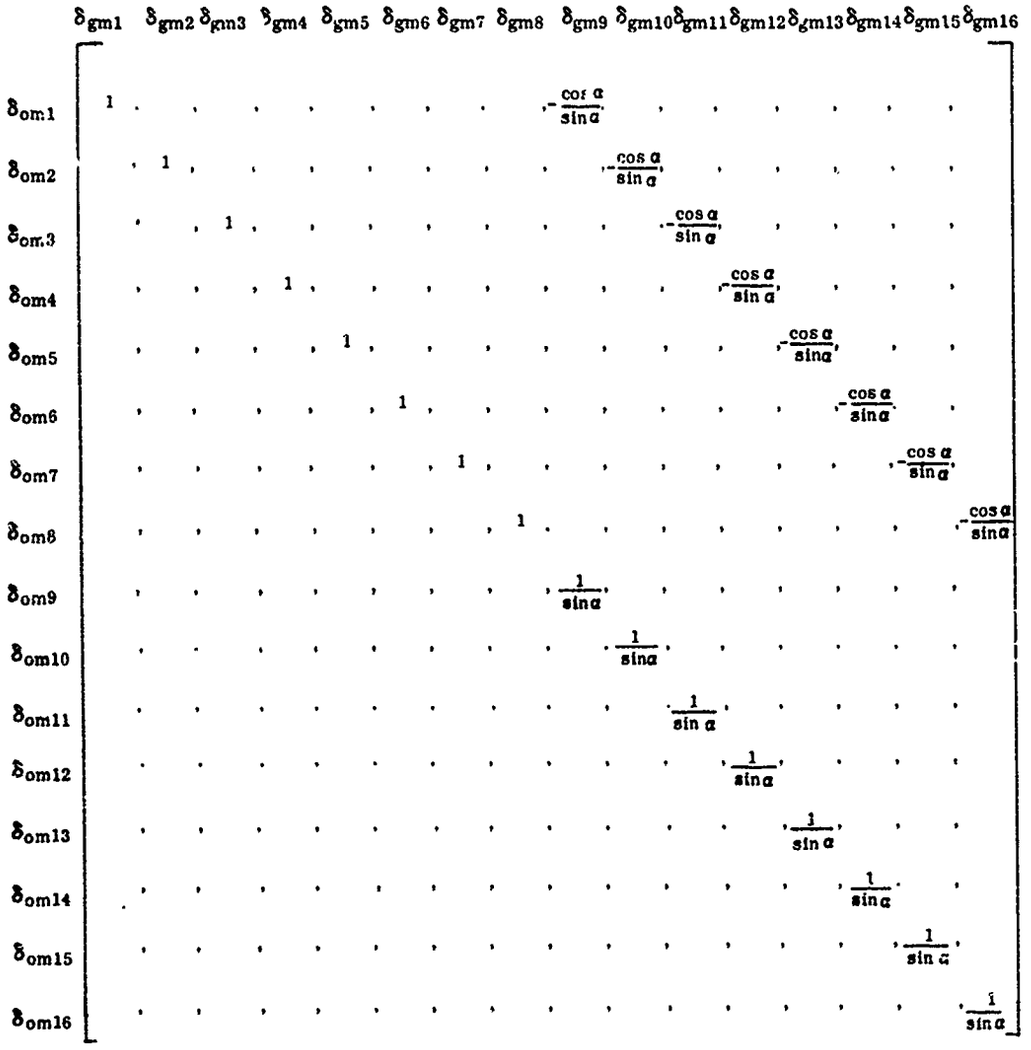

Figure 56. Membrane Displacement Transformation $\left[\Gamma_{2g}^{(cm)}\right]$

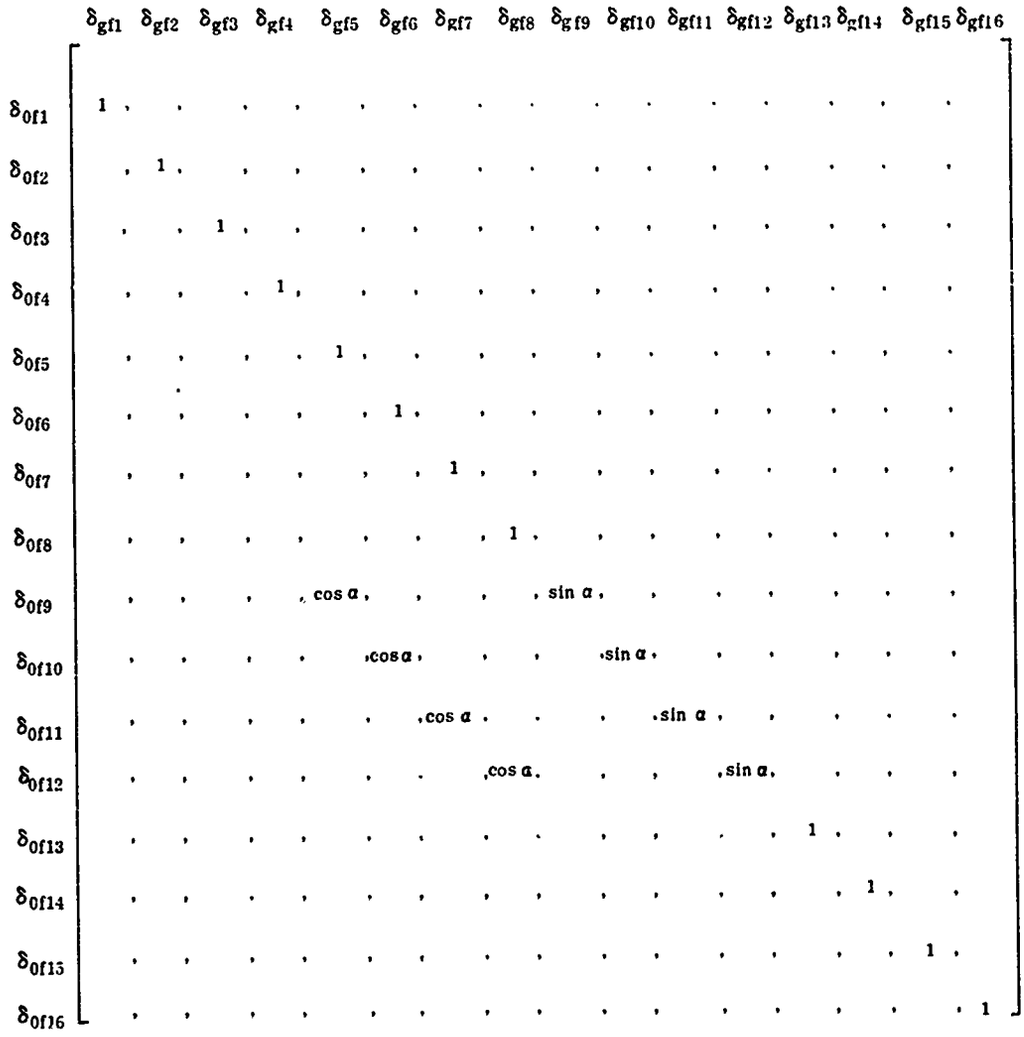

Figure 57. Flexure Displacement Coordinate Transformation $\left[\Gamma_{og}^{(f)}\right]$

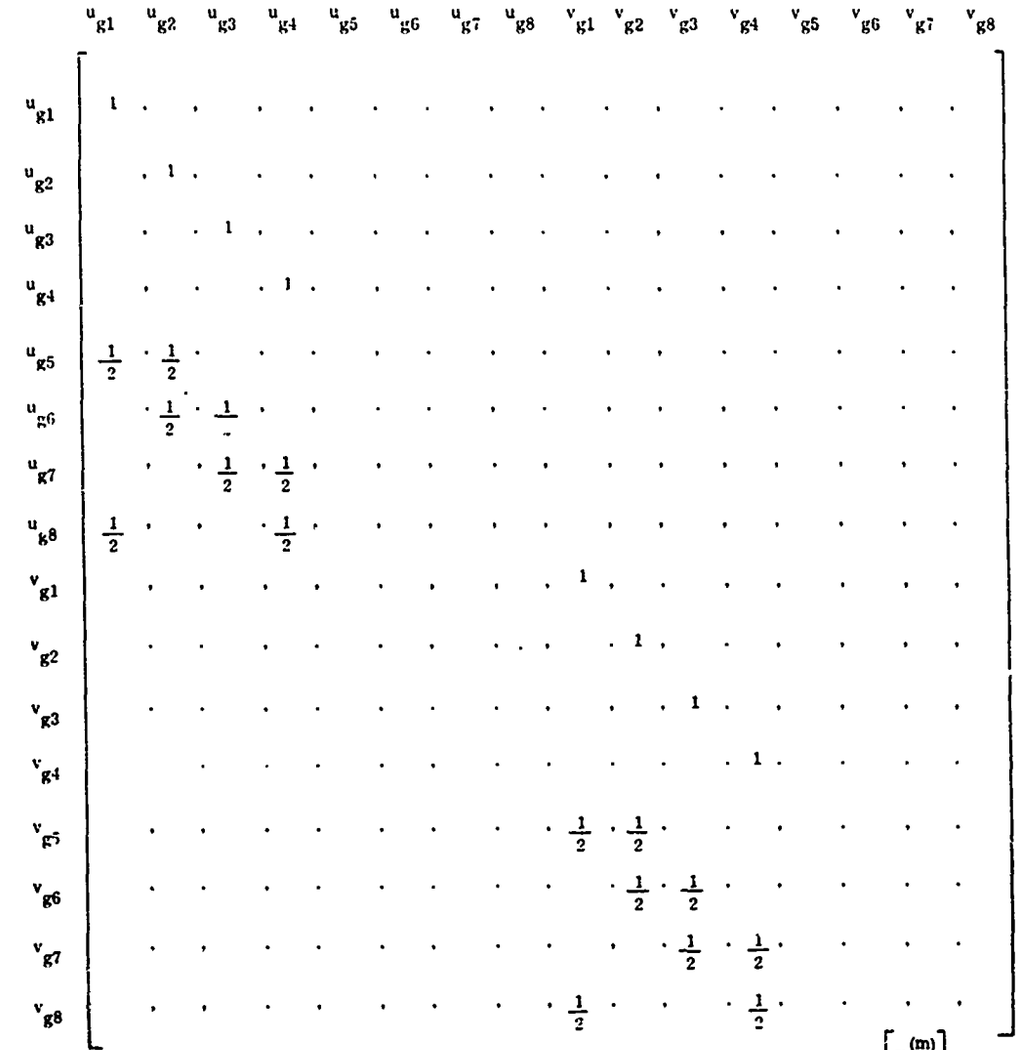

Figure 58. Membrane Displacement Coordinate Transformation

where: $a_j = \frac{1}{2} \sin \theta_j = \frac{1}{2}\left(\frac{\Delta y}{l}\right)_j$

$b_j = -\frac{1}{2} \cos \theta_j = -\frac{1}{2}\left(\frac{\Delta x}{l}\right)_j$

	w_{g1}	w_{g2}	w_{g3}	w_{g4}	w_{gx1}	w_{gx2}	w_{gx3}	w_{gx4}	w_{gy1}	w_{gy2}	w_{gy3}	w_{gy4}	w_{gn5}	w_{gn6}	w_{gn7}	w_{gn8}
w_{g1}	1															
w_{g2}		1														
w_{g3}			1													
w_{g4}				1												
w_{gx1}					1											
w_{gx2}						1										
w_{gx3}							1									
w_{gx4}								1								
w_{gy1}									1							
w_{gy2}										1						
w_{gy3}											1					
w_{gy4}												1				
w_{gn5}					a_2	a_1			b_1	b_1						
w_{gn6}						a_2	a_2			b_2	b_2					
w_{gn7}							a_3	a_3			b_3	b_3				
w_{gn8}					a_4			a_4	b_4			b_4				

Figure 59. Flexure Displacement Coordinate Transformation $\left[\Gamma_{sup}^{(e)}\right]$

At this point a transformation is defined to establish a vectorial sign convention for the rotational degrees-of-freedom associated with the four corner gridpoints. In addition, the midside rotations, if not previously suppressed, are assigned to be vectorially positive from the corner point with the smaller gridpoint number toward the corner point with the larger gridpoint number. This transformation is written symbolically as

$$\{\delta'_{gf}\} = [\Gamma_{sgn}^{(f)}]\{\delta''_{gf}\} \tag{259}$$

where

$$\{\delta''_{gf}\} = \lfloor w_{g1}, w_{g2}, w_{g3}, w_{g4}, \theta_{gx1}, \theta_{gx2}, \theta_{gx3}, \theta_{gx4}, \theta_{gy1}, \theta_{gy2}, \theta_{gy3}, \theta_{gy4}, \theta_{n5}, \theta_{n6}, \theta_{n7}, \theta_{n8} \rfloor \tag{260}$$

and the transformation matrix $[\Gamma_{sgn}^{(f)}]$ is exhibited in Figure 60.

A second set of optional transformations is introduced to enable eccentric connection of the quadrilateral thin shell element to a surface which is a distance e_z above the element. This transformation takes the form

$$\{\delta'_{gm}\} = [I, \Gamma_e]\begin{Bmatrix}\delta''_{gm}\\ \delta''_{gf}\end{Bmatrix} \tag{261}$$

The degrees-of-freedom $\{\delta''_{gm}\}$ and $\{\delta''_{gf}\}$ may be interpreted according to Equation 255, and the transformation matrix $[\Gamma_e]$ is shown in Figure 61. Note that utilization of this transformation requires the presuppression of midpoint displacement degrees-of-freedom.

Global or "system" displacement degrees-of-freedom are obtained by the introduction of further transformations of the form:

$$\{\delta''_{gm}\} = [\Gamma_{gs}^{(m)}]\{\delta_s\} \tag{262}$$

where

$$\{\delta''_{gf}\} = [\Gamma_{gs}^{(f)}]\{\delta_s\} \tag{263}$$

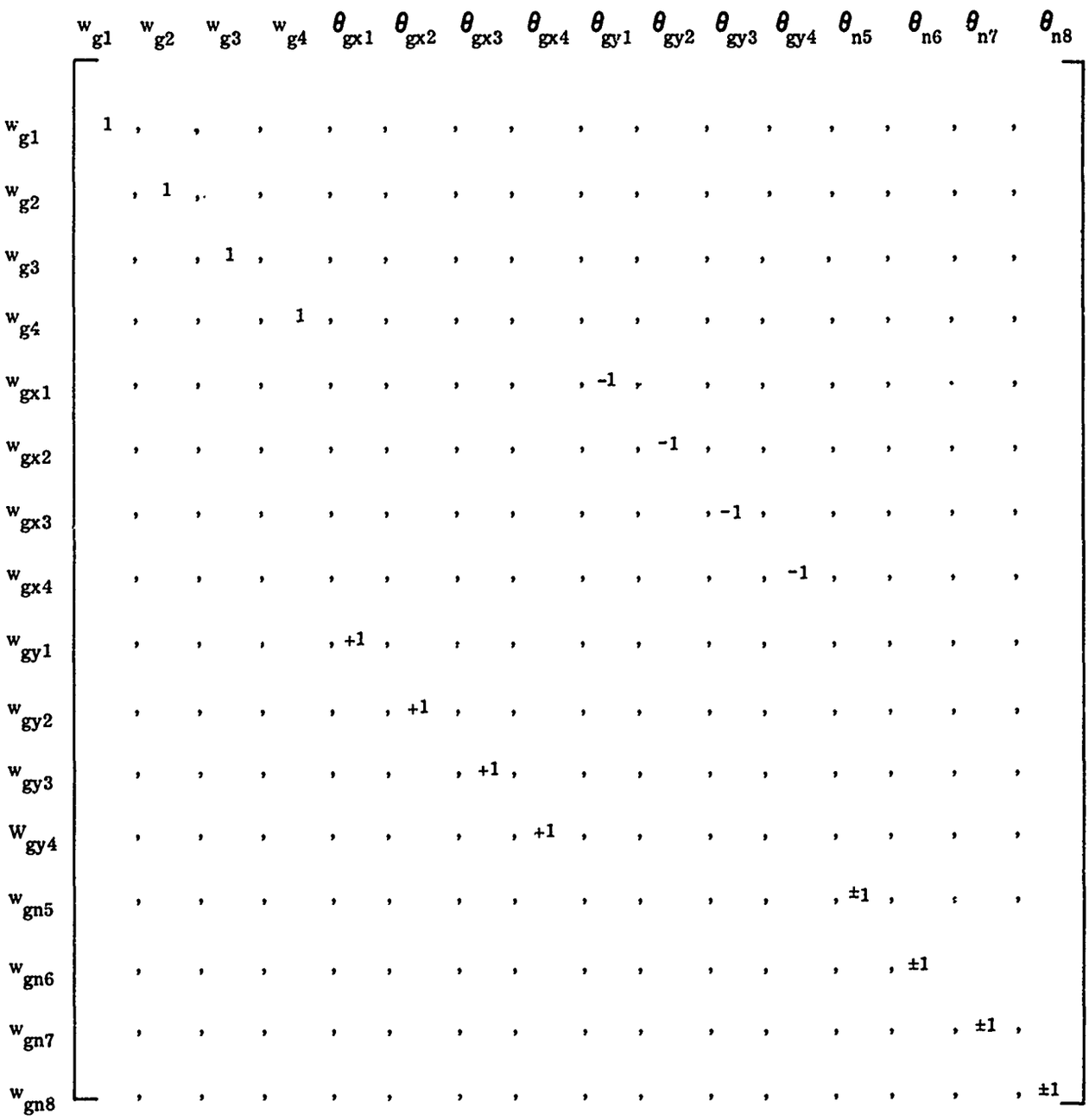

Figure 60. Flexure Displacement Coordinate Transformation $\left[\Gamma_{sgn}\right]$

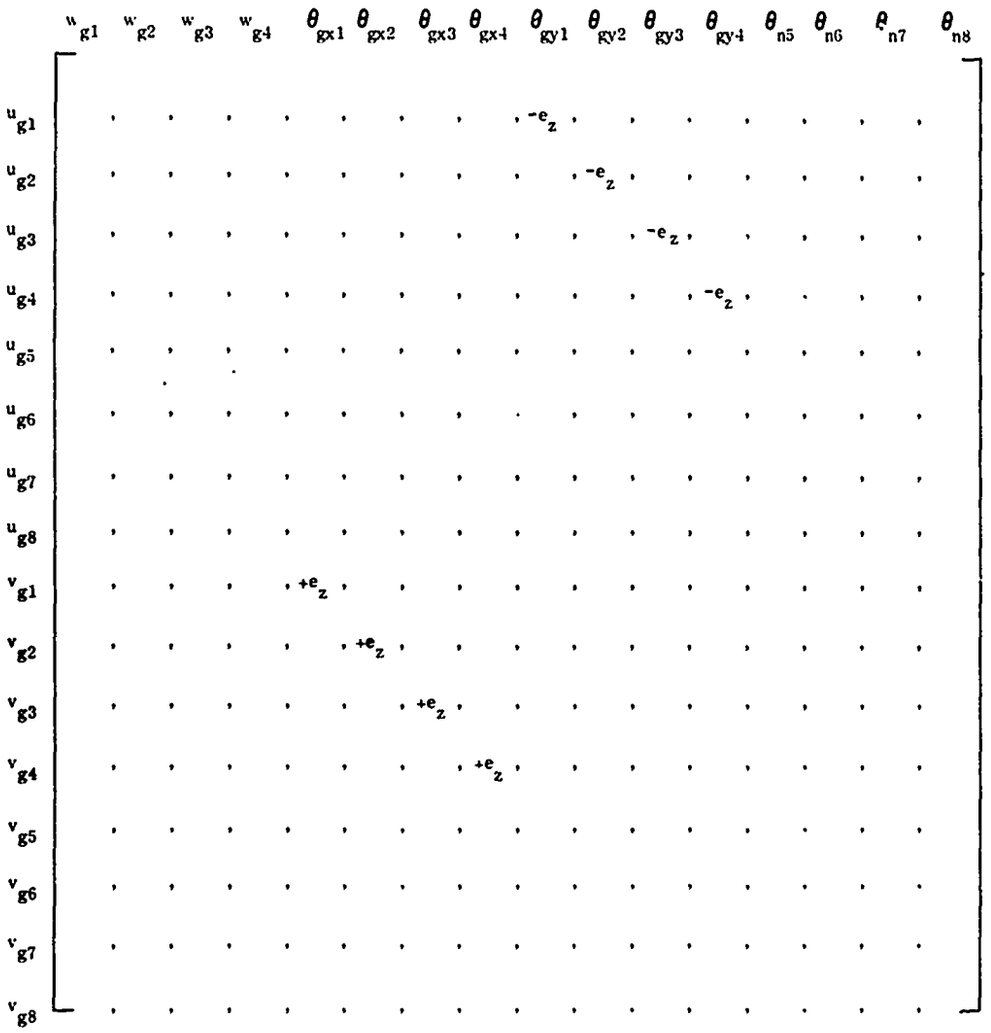

Figure 61. Eccentric Connection Transformation, $[\Gamma_e]$

$$\{\delta_s\}^T = \lfloor u_{s1}, v_{s1}, w_{sx1}, \theta_{sy1}, \theta_{sz1}, u_{s2}, v_{s2}, w_{s2}, \theta_{sx2}, \theta_{sy2}, \theta_{sz2},$$
$$u_{s3}, v_{s3}, w_{sx3}, \theta_{sz3}, u_{s4}, v_{s4}, w_{s4}, \theta_{sx4}, \theta_{sy4}, \theta_{sz4}, u_{s5},$$
$$v_{s5}, w_{s5}, \theta_{n5}, 0, 0, u_{s6}, v_{s6}, w_{s6}, \theta_{n6}, 0, 0, u_{s7},$$
$$v_{s7}, w_{s7}, \theta_{n7}, 0, 0, u_{s8}, v_{s8}, w_{s8}, \theta_{n8}, 0, 0, \rfloor \quad (264)$$

The transformation matrices $[\Gamma_{gs}^{(m)}]$ and $[\Gamma_{gs}^{(f)}]$ are given in Figures 62 and 63. Assembly of the thin shell element can be referenced to these system displacement degrees-of-freedom; however, it is convenient in many cases to employ special gridpoint coordinate axes. Accordingly, a final transformation to gridpoint displacement degrees-of-freedom is provided, i.e.

$$\{\delta_s\} = [\Gamma_{sq}]\{q\} \quad (265)$$

where

$$\{g\}^T = \lfloor u_{q1}, v_{q1}, w_{q1}, \theta_{xq1}, \theta_{yq1}, \theta_{zq1},$$
$$u_{q2}, v_{q2}, w_{q2}, \theta_{xq2}, \theta_{yq2}, \theta_{zq2},$$
$$u_{q3}, v_{q3}, w_{q3}, \theta_{xq3}, \theta_{yq3}, \theta_{zq3},$$
$$u_{q4}, v_{q4}, w_{q4}, \theta_{xq4}, \theta_{yq4}, \theta_{zq4},$$
$$u_{q5}, v_{q5}, w_{q5}, \theta_{nq5}, 0, 0,$$
$$u_{q6}, v_{q6}, w_{q6}, \theta_{nq6}, 0, 0,$$
$$u_{q7}, v_{q7}, w_{q7}, \theta_{nq7}, 0, 0,$$
$$u_{q8}, v_{q8}, w_{q8}, \theta_{nq8}, 0, 0, \rfloor \quad (266)$$

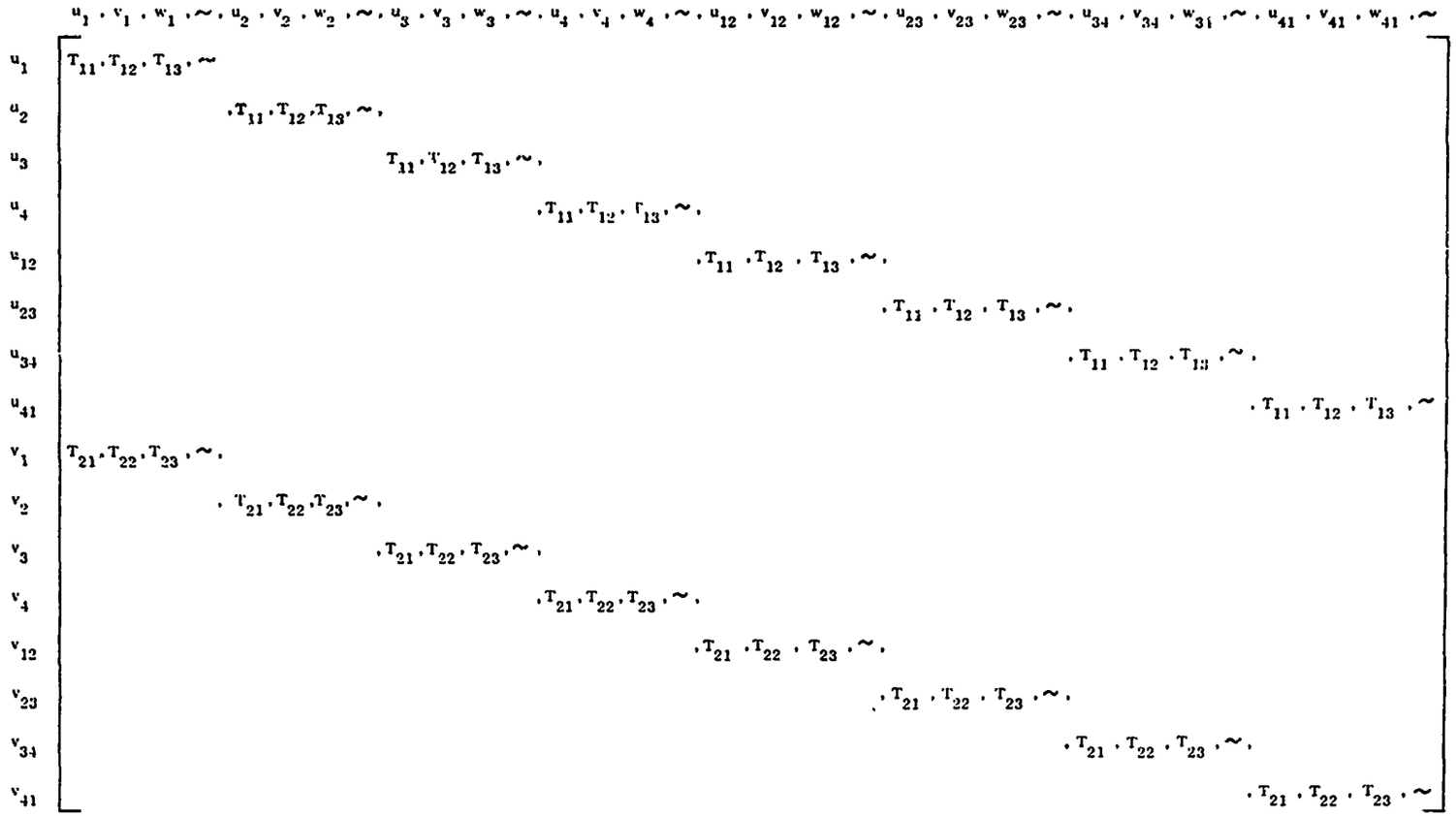

Figure 62. Membrane Coordinate Transformation $\left[\Gamma_{gs}^{(m)}\right]$

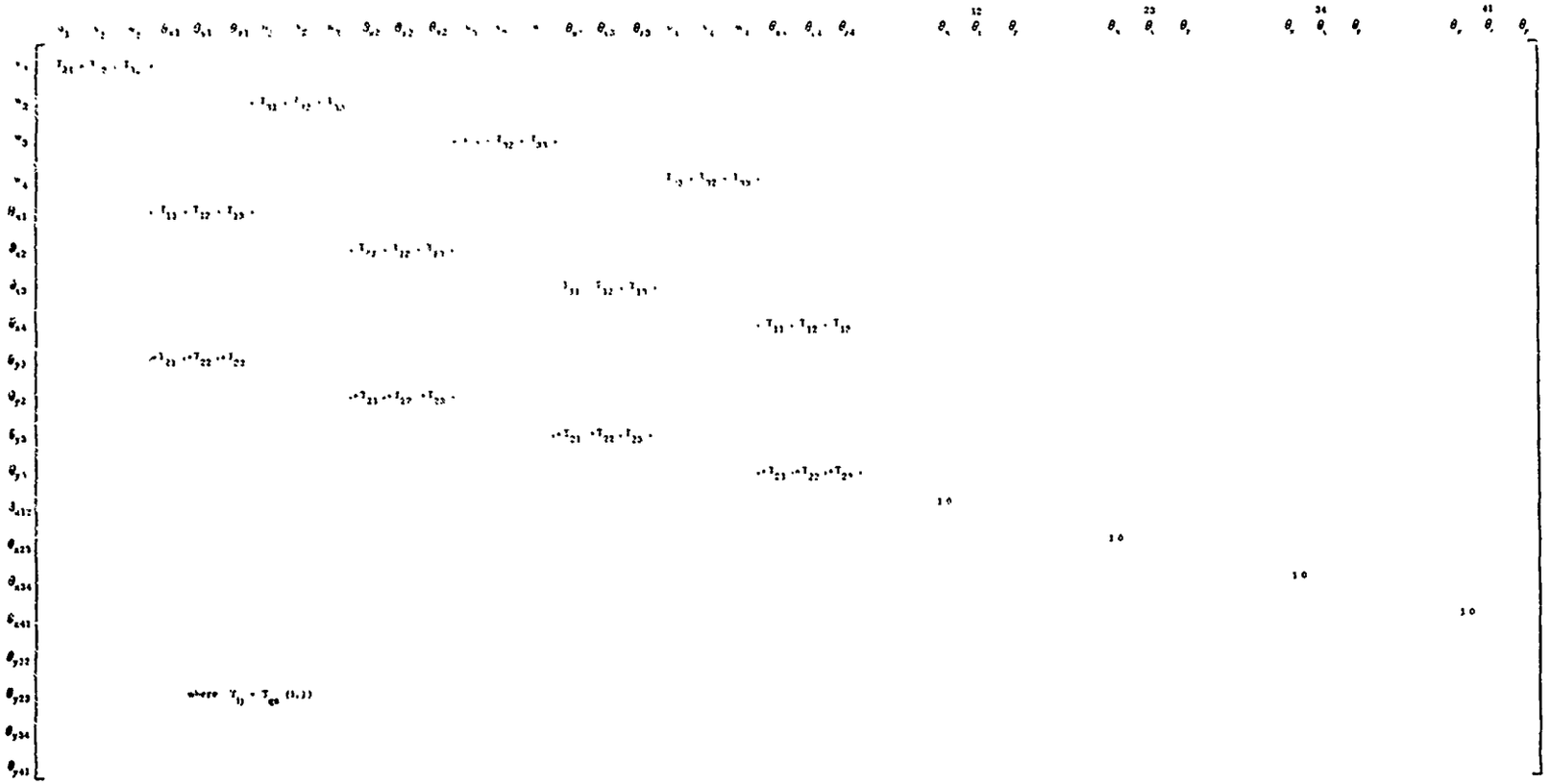

Figure 63. Flexure Displacement Coordinate Transformation $\left[\Gamma_{ge}^{(f)}\right]$

The matrix $\left[\Gamma_{sq}\right]$ is made up of the individual gridpoint axes direction cosine transformations from the relations

$$\left\{x_s\right\} = \left[T_{sq}\right]_j \left\{x_q\right\}_j \tag{267}$$

positioned along the major diagonal as shown in Figure 64.

The foregoing transformations may be collected symbolically to obtain a single transformation between the field coordinate displacement degrees-of-freedom $\left\{\beta\right\}$ and the final gridpoint displacement degrees-of-freedom $\left\{q\right\}$. The results are as follows:

$$\left\{\beta_m\right\} = \left[\Gamma_{\beta q}{}^{(m)}\right]\left\{q\right\} \tag{268}$$

$$\left\{\beta_f\right\} = \left[\Gamma_{\beta q}{}^{(f)}\right]\left\{q\right\} \tag{269}$$

where

$$\left[\Gamma_{\beta q}{}^{(m)}\right] = \left[\Gamma_{\beta o}{}^{(m)}\right]\left[\Gamma_{og}{}^{(m)}\right]\left[\Gamma_{sup}{}^{(m)}\right]\left[I \,\vdots\, \Gamma_e{}^{(m)}\right]\left[\begin{array}{c:c} \Gamma_{gs}{}^{(m)} & \\ \hdashline & \Gamma_{gs}{}^{(f)} \end{array}\right] \tag{270}$$

$$\left[\Gamma_{\beta q}{}^{(f)}\right] = \left[\Gamma_{\beta o}{}^{(f)}\right]\left[\Gamma_{og}{}^{(f)}\right]\left[\Gamma_{sup}{}^{(f)}\right]\left[\Gamma_{sgn}{}^{(f)}\right]\left[\Gamma_{gs}{}^{(f)}\right]\left[\Gamma_{sq}\right] \tag{271}$$

This completes the explicit statement of the displacement functions employed for the Mallett quadrilateral thin shell element.

2. Potential Energy

The strain energy density for a thin shell element of zero curvature is defined as

$$dU \equiv \int \left[d\epsilon\right]\left\{\sigma\right\} \tag{272}$$

where

$$\left\{\epsilon\right\}^T = \left[\epsilon_x,\ \epsilon_y,\ \epsilon_{xy}\right] \tag{273}$$

$$\left\{\sigma\right\}^T = \left[\sigma_x,\ \sigma_y,\ \sigma_{xy}\right] \tag{274}$$

Given:

$$\begin{Bmatrix} \sigma_x \\ \sigma_y \\ \sigma_z \end{Bmatrix} = \begin{bmatrix} S_{11}, S_{12}, S_{13} \\ S_{12}, S_{22}, S_{23} \\ S_{13}, S_{23}, S_{33} \end{bmatrix} \begin{Bmatrix} \epsilon_x \\ \epsilon_y \\ \epsilon_z \end{Bmatrix} \qquad \begin{Bmatrix} \epsilon_x \\ \epsilon_y \\ \epsilon_z \end{Bmatrix} = \begin{bmatrix} C_{11}, C_{12}, C_{13} \\ C_{12}, C_{22}, C_{23} \\ C_{13}, C_{23}, C_{33} \end{bmatrix} \begin{Bmatrix} \sigma_x \\ \sigma_y \\ \sigma_z \end{Bmatrix}$$

Known:

Plane Stress $\sigma_z \equiv 0$

Plane Strain $\epsilon_z \equiv 0$

} by definition

Observe:

For both plane stress and plane strain

$$dU = \int \left[d\epsilon_x, d\epsilon_y, d\epsilon_z, d\epsilon_{xy} \right] \begin{Bmatrix} \sigma_x \\ \sigma_y \\ \sigma_z \\ \sigma_{xy} \end{Bmatrix} \equiv \int \left[d\epsilon_x, d\epsilon_y, d\epsilon_{xy} \right] \begin{Bmatrix} \sigma_x \\ \sigma_y \\ \sigma_{xy} \end{Bmatrix}$$

Specialize:

For plane Stress

$$\begin{Bmatrix} \sigma_x \\ \sigma_y \end{Bmatrix} = \begin{bmatrix} S_{11}, S_{12}, S_{13} \\ S_{12}, S_{22}, S_{23} \end{bmatrix} \begin{bmatrix} 1, 0 \\ 0, 1 \\ -\frac{S_{13}}{S_{33}}, -\frac{S_{23}}{S_{33}} \end{bmatrix} \begin{Bmatrix} \epsilon_x \\ \epsilon_y \end{Bmatrix} = \begin{bmatrix} S_{11} - \frac{S_{13}^2}{S_{33}}, S_{12} - \frac{S_{13}S_{23}}{S_{33}} \\ S_{12} - \frac{S_{13}S_{23}}{S_{33}}, S_{22} - \frac{S_{23}^2}{S_{33}} \end{bmatrix} \begin{Bmatrix} \epsilon_x \\ \epsilon_y \end{Bmatrix}$$

For plane strain

$$\begin{Bmatrix} \epsilon_x \\ \epsilon_y \end{Bmatrix} = \begin{bmatrix} C_{11}, C_{12}, C_{13} \\ C_{12}, C_{22}, C_{23} \end{bmatrix} \begin{bmatrix} 1, 0 \\ 0, 1 \\ -\frac{C_{13}}{C_{33}}, -\frac{C_{23}}{C_{33}} \end{bmatrix} \begin{Bmatrix} \epsilon_x \\ \epsilon_y \end{Bmatrix} = \begin{bmatrix} C_{11} - \frac{C_{13}^2}{C_{33}}, C_{12} - \frac{C_{13}^2 C_{23}}{C_{33}} \\ C_{12} - \frac{C_{13}C_{23}}{C_{33}}, C_{22} - \frac{C_{23}^2}{C_{33}} \end{bmatrix} \begin{Bmatrix} \sigma_x \\ \sigma_y \end{Bmatrix}$$

Note:

$$\begin{bmatrix} C_{11}, C_{12}, C_{13} \\ C_{12}, C_{22}, C_{23} \\ C_{13}, C_{23}, C_{33} \end{bmatrix} = \begin{bmatrix} \frac{1}{Exx}, -\frac{Vxx}{Fy}, -\frac{Vzx}{Ez} \\ \frac{1}{Eyy}, -\frac{Vzy}{Ez} \\ \text{SYMM} \quad \frac{1}{Ezz} \end{bmatrix} \text{ and } \begin{bmatrix} S_{11}, S_{12}, S_{13} \\ S_{12}, S_{22}, S_{23} \\ S_{13}, S_{23}, S_{33} \end{bmatrix} = \begin{bmatrix} \frac{E_x}{(1 - \nu_{xy}\nu_{yx})}, \frac{\nu_{xy}E_y}{(1 - \nu_{xy}\nu_{yx})}, 0 \\ \frac{E_y}{(1 - \nu_{xy}\nu_{yx})}, 0 \\ G_{xy} \end{bmatrix}$$

Also

$$\{\alpha\}^T = \left[(\alpha_x + \nu_{yx}\alpha_y)dy, (\alpha_y + \nu_{xy}\alpha_x)dx, 0 \right]$$

Figure 64. Plane Stress/Strain Option

Linear elastic material behavior is assumed to take place from an initial state of strain $\{\epsilon_i\}$ to a final state of stress $\{\sigma\}$ and strain $\{\epsilon\}$,

$$\{\sigma^{(m)}\}^T = [E^{(m)}] \{\{\epsilon^{(m)}\} - \{\epsilon_i^{(m)}\}\} \tag{275}$$

The matrix of elastic constants $[E]$ is given explicit expression for the special case of orthotropy in Figure 64. The superscript m indicates the coordinate axes of reference.

Substitution of the assumed constituitive relation into the strain energy density definition yields, after integration, an expression for the strain energy of elastic deformation in terms of the strains.

$$dU = \frac{1}{2} \lfloor \epsilon^{(m)} \rfloor [E^{(m)}] \{\epsilon^{(m)}\} - \lfloor \epsilon^{(m)} \rfloor [E^{(m)}] \{\epsilon_i^{(m)}\} \tag{276}$$

If the material axes (m) are orientated at an angle with respect to the chosen element geometric axes (g) a transformation must be introduced.

$$\{\epsilon^{(m)}\} = [T_{\epsilon\sigma}] \{\epsilon^{(g)}\} \tag{277}$$

$$\{\sigma^{(g)}\} = [T_{\epsilon\sigma}]^T \{\sigma^{(m)}\} \tag{278}$$

The transformation $[T_{\epsilon\sigma}]$ is defined in Figure 65. Transforming the axes of reference of the strain energy density and the constituitive equation obtain

$$dU = \frac{1}{2} \lfloor \epsilon^{(g)} \rfloor [E^{(g)}] \{\epsilon^{(g)}\} - \lfloor \epsilon^{(g)} \rfloor \{\bar{\epsilon}_i^{(g)}\} \tag{279}$$

and

$$\{\sigma^{(g)}\} = [E^{(g)}] \{\epsilon^{(g)}\} - \{\bar{\epsilon}_i^{(g)}\} \tag{280}$$

where

$$[E^{(g)}] = [T_{\epsilon\sigma}]^T [E^{(m)}] [T_{\epsilon\sigma}] \tag{281}$$

$$\{\bar{\epsilon}_i^{(g)}\} = [T_{\epsilon\sigma}]^T [E^{(m)}] \{\epsilon_i^{(m)}\} = [E^{(g)}] \{\epsilon_i^{(g)}\} \tag{282}$$

$$\left[T_{\epsilon\sigma}\right] = \begin{array}{c} (m) \\ \epsilon_x \\ \epsilon_y \\ \epsilon_{xy} \end{array} \overset{(g)}{\begin{array}{c} \epsilon_x \\ \left[\begin{array}{ccc} +\cos^2\gamma, & +\sin^2\gamma, & +\sin\gamma\cos\gamma \\ +\sin^2\gamma, & +\cos^2\gamma, & -\sin\gamma\cos\gamma \\ -2\sin\gamma\cos\gamma, & +2\sin\gamma\cos\gamma, & +\cos^2\gamma - \sin^2\gamma \end{array}\right. \end{array}} \begin{array}{c} \epsilon_y \\ \epsilon_{xy} \\ \left.\begin{array}{c} \\ \\ \end{array}\right] \end{array}$$

Figure 65. Strain Transformation $\left[T_{\epsilon\sigma}\right]$

The well known strain-displacement relations for a thin shell element of zero curvature can be written as a sum of membrane $\{e\}$ and flexure $\{K\}$ contributions.

$$\left\{\epsilon^{(g)}\right\} = \left\{e^{(g)}\right\} + z\left\{K^{(g)}\right\} \tag{283}$$

It is convenient to separate the membrane strain into linear and nonlinear parts.

$$\left\{e^{(g)}\right\} = \left\{e_u^{(g)}\right\} + \left\{e_w^{(g)}\right\} \tag{284}$$

Explicit definition of the strain contributions in terms of the displacement is given by

$$\left\{e_u^{(g)}\right\}^T = \left\lfloor u_x \;,\; v_y \;,\; u_y + v_x \right\rfloor \tag{285}$$

$$\left\{e_w^{(g)}\right\}^T = \left\lfloor \frac{1}{2} w_x^2 \;,\; \frac{1}{2} w_y^2 \;,\; w_x w_y \right\rfloor \tag{286}$$

$$\left\{K^{(g)}\right\}^T = \left\lfloor -w_{xx} \;,\; -w_{yy} \;,\; -2w_{xy} \right\rfloor \tag{287}$$

It is convenient to carry forward the separation of membrane and flexure strains into the strain energy expression prior to introducing these strain-displacement relations. In so doing it is assumed that $\{\epsilon_i\}$ is a linear function of the z coordinate.

$$\left\{\epsilon_i\right\} = \left\{\epsilon_{mi}\right\} + z\left\{\epsilon_{fi}\right\} \tag{288}$$

The resulting expression for the strain energy is written as a sum of membrane Φ_m, flexure Φ_f, and coupling Φ_c contributions. Including an external work term Φ_p as well, the set of four energy contributions is written as,

$$\Phi_m = \int_A \left(\frac{t}{2} \left[e_u^{(g)} \right] \left[E^{(g)} \right] \left\{ e_u^{(g)} \right\} - t \left[e_u^{(g)} \right] \left\{ \bar{\epsilon}_{mi}^{(g)} \right\} \right) dA \tag{289}$$

$$\Phi_f = \int_A \left(\frac{t^3}{24} \left[K^{(g)} \right] \left[E^{(g)} \right] \left\{ K^{(g)} \right\} - \frac{t^3}{12} \left[K^{(g)} \right] \left\{ \bar{\epsilon}_{fi} \right\} \right) dA \tag{290}$$

$$\Phi_c = \int_A \left(t \left[e_u^{(g)} \right] \left[E^{(g)} \right] \left\{ e_w^{(g)} \right\} \right) dA \tag{291}$$

$$\Phi_p = \int_A \left(p_z w^{(g)} \right) dA \tag{292}$$

This set of energy functions is employed as the point of departure in deriving the companion triangular thin shell element representation in Section 9.

In order to realize the algebraic simplification afforded by oblique coordinates axes, it is necessary to transform the displacement functions of Equations 285, 286 and 287 before substituting into the strain energy. Given the transformation relation

$$\begin{Bmatrix} x_o \\ y_o \end{Bmatrix} = \begin{bmatrix} 1 & , & -\frac{\cos \alpha}{\sin \alpha} \\ 0 & , & \frac{1}{\sin \alpha} \end{bmatrix} \begin{Bmatrix} x_g \\ y_g \end{Bmatrix} \tag{293}$$

and using the chain rule for partial differentiation, the following transformation relations are derived.

$$f_{x_g} = f_{x_o} \tag{294}$$

$$f_{y_g} = -\frac{\cos \alpha}{\sin \alpha} f_{x_o} + \frac{1}{\sin \alpha} f_{y_o} \tag{295}$$

$$f_{x_g x_g} = f_{x_o x_o} \tag{296}$$

$$f_{y_g y_g} = \frac{\cos^2 \alpha}{\sin^2 \alpha} f_{x_o x_o} + \frac{1}{\sin^2 \alpha} f_{y_o y_o} - \frac{2 \cos \alpha}{\sin^2 \alpha} f_{x_o y_o} \tag{297}$$

$$f_{x_g y_g} = -\frac{\cos \alpha}{\sin \alpha} f_{x_o x_o} + \frac{1}{\sin \alpha} f_{x_o y_o} \tag{298}$$

Invoking these transformation relations, 285, obtain the strains expressed in terms of displacement functions defined with reference to the element oblique coordinate system:

$$\left\{ e_u^{(g)} \right\} = \left[T_u \right] \left\{ \Delta_{mu} \right\} \tag{299}$$

$$\left\{ e_w^{(g)} \right\} = \left[T_w \right] \left\{ \Delta_{mw} \right\} \tag{300}$$

$$\left\{ K^{(g)} \right\} = \left[T_w \right] \left\{ \Delta_{fw} \right\} \tag{301}$$

where

$$\left\{ \Delta_{mu} \right\}^T = \left\lfloor u_x, u_y, v_x, v_y \right\rfloor \tag{302}$$

$$\left\{ \Delta_{mw} \right\}^T = \left\lfloor \frac{1}{2} w_x^2, \frac{1}{2} w_y^2, w_x w_y \right\rfloor \tag{303}$$

$$\left\{ \Delta_{fw} \right\}^T = \left\lfloor - w_{xx}, -w_{yy}, -2w_{xy} \right\rfloor \tag{304}$$

The matrices $\left[T_u \right]$ and $\left[T_w \right]$ are given in Figure 66.

Introducing these strain-displacement relations obtain the energy functionals in terms of displacements referenced to the oblique coordinate system.

$$\Phi_m = \int_{xy} \left(\frac{1}{2} \left\lfloor \Delta_{mu} \right\rfloor \left[I_{mk} \right] \left\{ \Delta_{mu} \right\} - \left\lfloor \Delta_{mu} \right\rfloor \left\{ I_{m\epsilon} \right\} \right) dx\, dy \tag{305}$$

$$\Phi_f = \int_{xy} \left(\frac{1}{2} \left\lfloor \Delta_f \right\rfloor \left[I_{fk} \right] \left\{ \Delta_f \right\} - \left\lfloor \Delta_f \right\rfloor \left\{ I_{f\epsilon} \right\} \right) dx\, dy \tag{306}$$

$$\Phi_c = \int_{xy} \left(\left\lfloor \Delta_{mu} \right\rfloor \left[I_c \right] \left\{ \Delta_{mw} \right\} \right) dx\, dy \tag{307}$$

$$\Phi_p = \int_{xy} \left(p_z \; w \; \sin \alpha \right) dx\, dy \tag{308}$$

where

$$\left[I_{mk} \right] = t \sin \alpha \left[T_u \right]^T \left[E^{(g)} \right] \left[T_u \right] \tag{309}$$

$$
\left[T_u\right] = \begin{array}{c} (g) \\ u_x \\ v_y \\ (u_y + v_x) \end{array} \begin{array}{c} (0) \\ \begin{array}{cccc} u_x & u_y & v_x & v_y \end{array} \\ \left[\begin{array}{cccc} +1 & 0 & 0 & 0 \\ 0 & 0 & -\frac{\cos\alpha}{\sin\alpha} & +\frac{1}{\sin\alpha} \\ -\frac{\cos\alpha}{\sin\alpha} & +\frac{1}{\sin\alpha} & +1 & 0 \end{array}\right] \end{array}
$$

$$
\left[T_w\right] = \begin{array}{c} (g) \\ -w_{xx}, \frac{1}{2}w_x^2 \\ -w_{yy}, \frac{1}{2}w_y^2 \\ -2\,w_{xy}, w_x w_y \end{array} \begin{array}{c} (0) \\ \begin{array}{ccc} -w_{xx}, \frac{1}{2}w_x^2 & -w_{yy}, \frac{1}{2}w_y^2 & -2\,w_{xy}, w_x w_y \end{array} \\ \left[\begin{array}{ccc} +1 & 0 & 0 \\ \frac{\cos^2\alpha}{\sin^2\alpha} & +\frac{1}{\sin^2\alpha} & -\frac{2\cos\alpha}{\sin^2\alpha} \\ -\frac{\cos\alpha}{\sin\alpha} & 0 & \frac{1}{\sin\alpha} \end{array}\right] \end{array}
$$

Figure 66. Displacement Function Transformations

$$
\left\{I_{m\epsilon}\right\} = t \sin\alpha \left[T_u\right]^T \left\{\bar{\epsilon}_{mi}^{(g)}\right\} \tag{310}
$$

$$
\left[I_{fk}\right] = \frac{t^3 \sin\alpha}{12} \left[T_w\right]^T \left[E^{(g)}\right] \left[T_w\right] \tag{311}
$$

$$
\left\{I_{f\epsilon}\right\} = \frac{t^3 \sin\alpha}{12} \left[T_w\right]^T \left\{\bar{\epsilon}_{fi}^{(g)}\right\} \tag{312}
$$

$$
\left[I_c\right] = t \sin\alpha \left[T_u\right]^T \left[E^{(g)}\right] \left[T_w\right] \tag{313}
$$

Equations 303, 304, 305 and 306 are the desired form of the energy functional. It should be noted that, in expressing the nonlinear coupling energy, the second order terms in the prestrain have been assumed small relative to the corresponding first order terms in the total potential energy functional.

The next step in constructing the element representation is to effect the discretization by introducing the previously derived mode shapes into Equations 300, 303, and 304. This results in the relations.

$$\{\Delta_{mu}\} = [D_m^{(j)}] \{\beta_m\} \tag{314}$$

$$\{\Delta_{fw}\} = [D_f^{(j)}] \{\beta_f\} \tag{315}$$

The matrices $[D_m^{(j)}]$ and $[D_f^{(j)}]$ are presented in Figures 67 and 68, respectively. The vector $\{\Delta_{mw}\}$ is a quadratic function of the coordinates $\{\beta_f\}$ and symbolic representation is not attempted at this point.

Algebraic statement of the membrane energy contribution of Equation 305 is considered first. Examination of the component relations of Equation 314 leads to identification of a typical form for each element of the vector $\{\Delta_{mu}\}$, i.e.

$$(\Delta_{mu})_\ell^{(k)} = \lfloor d \rfloor \lceil c_m \rfloor_\ell^{(k)} \{\alpha_m\}_\ell^{(k)} \tag{316}$$

where

$$\{d\}^T = \lfloor 1, x, y \rfloor \tag{317}$$

For example, focusing on the first zone (k = 1), the first element (ℓ = 1) is given by

$$(\Delta_{mu})_1^{(1)} = u_x^{(1)} = \lfloor 1, x, y \rfloor \begin{bmatrix} 1, & & \\ & ,2, & \\ & & ,1 \end{bmatrix} \begin{Bmatrix} \beta_{m2} \\ \beta_{m4} \\ \beta_{m5} \end{Bmatrix} \tag{318}$$

Explicit statement of the $\lceil c_m \rfloor$ and $\{\alpha_m\}$ matrices for each of the four zones is given in Figures 69 through 72.

$$
\begin{array}{c}
 \\
\left[D_m^{(1)}\right] = \\
 \\
 \\
 \\
 \\
\left[D_m^{(2)}\right] = \\
 \\
 \\
 \\
 \\
\left[D_m^{(3)}\right] = \\
 \\
 \\
 \\
 \\
\left[D_m^{(4)}\right] = \\
 \\
 \\
 \\
 \\
\end{array}
\begin{array}{c}
\begin{array}{cccccccccccccccc}
1 & 2 & 3 & 4 & 5 & 6 & 7 & 8 & 9 & 10 & 11 & 12 & 13 & 14 & 15 & 16
\end{array} \\
\begin{array}{c}
u_x \\ u_y \\ v_x \\ v_y
\end{array}
\left[\begin{array}{cccccccc|cccccccc}
0, & 1, & 0, & 2x, & y, & 0, & 0, & 0, & & & & & & & & \\
0, & 0, & 1, & 0, & x, & 2y, & 0, & 0, & & & & & & & & \\
 & & & & & & & , & 0, & 1, & 0, & 2x, & y, & 0, & 0, & 0 \\
 & & & & & & & , & 0, & 0, & 1, & 0, & x, & 2y, & 0, & 0
\end{array}\right] \\
\begin{array}{c}
u_x \\ u_y \\ v_x \\ v_y
\end{array}
\left[\begin{array}{cccccccc|cccccccc}
0, & 1, & 0, & 0, & y, & 0, & 0, & 2x, & & & & & & & & \\
0, & 0, & 1, & 0, & x, & 2y, & 0, & 0, & & & & & & & & \\
 & & & & & & & , & 0, & 1, & 0, & 0, & y, & 0, & 0, & 2x \\
 & & & & & & & , & 0, & 0, & 1, & 0, & x, & 2y, & 0, & 0
\end{array}\right] \\
\begin{array}{c}
u_x \\ u_y \\ v_x \\ v_y
\end{array}
\left[\begin{array}{cccccccc|cccccccc}
0, & 1, & 0, & 0, & y, & 0, & 0, & 2x, & & & & & & & & \\
0, & 0, & 1, & 0, & x, & 0, & 2y, & 0, & & & & & & & & \\
 & & & & & & & , & 0, & 1, & 0, & 0, & y, & 0, & 0, & 2x \\
 & & & & & & & , & 0, & 0, & 1, & 0, & x, & 0, & 2y, & 0
\end{array}\right] \\
\begin{array}{c}
u_x \\ u_y \\ v_x \\ v_y
\end{array}
\left[\begin{array}{cccccccc|cccccccc}
0, & 1, & 0, & 2x, & y, & 0, & 0, & 0, & & & & & & & & \\
0, & 0, & 1, & 0, & x, & 0, & 2y, & 0, & & & & & & & & \\
 & & & & & & & , & 0, & 1, & 0, & 2x, & y, & 0, & 0, & 0 \\
 & & & & & & & , & 0, & 0, & 1, & 0, & x, & 0, & 2y, & 0
\end{array}\right]
\end{array}
$$

Figure 67. Membrane Displacement Derivative Matrices

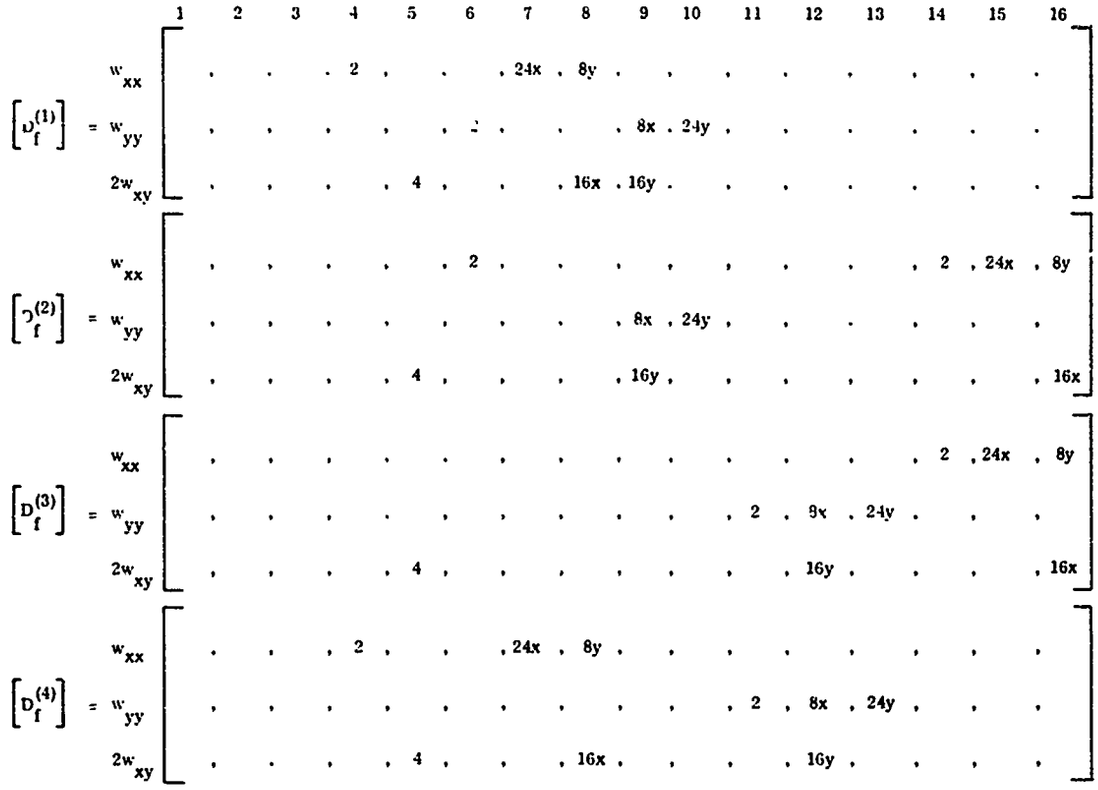

Figure 68. Flexure Displacement Derivative Matrices

$$(\Delta_{mu})_1 : [c_m] = [\,1\,,\,2\,,\,1\,]$$

$$\{\alpha_m\}^T = [\,\beta_{m2}\,,\beta_{m4}\,,\beta_{m5}\,]$$

$$(\Delta_{mu})_2 : [c_m] = [\,1\,,\,1\,,\,2\,]$$

$$\{\alpha_m\}^T = [\,\beta_{m3}\,,\beta_{m5}\,,\beta_{m6}\,]$$

$$(\Delta_{mu})_3 : [c_m] = [\,1\,,\,2\,,\,1\,]$$

$$\{\alpha_m\}^T = [\,\beta_{m10},\beta_{m12},\beta_{m13}]$$

$$(\Delta_{mu})_4 : [c_m] = [\,1\,,\,1\,,\,2\,]$$

$$\{\alpha_m\}^T = [\,\beta_{m11},\beta_{m13},\beta_{m14}]$$

Figure 69. Zone 1 Membrane Stiffness Parameters

$$(\Delta_{mu})_1 : \quad \lceil c_m \rfloor = \lceil\ 1 \quad , \quad 2 \quad , \quad 1\ \rfloor$$

$$\{\alpha_m\}^T = \lfloor \beta_{m2} \ , \beta_{m8} \ , \beta_{m5} \rfloor$$

$$(\Delta_{mu})_2 : \quad \lceil c_m \rfloor = \lceil\ 1 \quad , \quad 1 \quad , \quad 2\ \rfloor$$

$$\{\alpha_m\}^T = \lfloor \beta_{m3} \ , \beta_{m5} \ , \beta_{m6} \rfloor$$

$$(\Delta_{mu})_3 : \quad \lceil c_m \rfloor = \lceil\ 1 \quad , \quad 2 \quad , \quad 1\ \rfloor$$

$$\{\alpha_m\}^T = \lfloor \beta_{m10} \ , \beta_{m16} \ , \beta_{m13} \rfloor$$

$$(\Delta_{mu})_4 : \quad \lceil c_m \rfloor = \lceil\ 1 \quad , \quad 1 \quad , \quad 2\ \rfloor$$

$$\{\alpha_m\}^T = \lfloor \beta_{m11} \ , \beta_{m13} \ , \beta_{m14} \rfloor$$

Figure 70. Zone 2 Membrane Stiffness Parameters

$$(\Delta_{mu})_1 : \quad \lceil c_m \rfloor = \lceil\ 1 \quad , \quad 2 \quad , \quad 1\ \rfloor$$

$$\{\alpha_m\}^T = \lfloor \beta_{m2} \ , \beta_{m8} \ , \beta_{m5} \rfloor$$

$$(\Delta_{mu})_2 : \quad \lceil c_m \rfloor = \lceil\ 1 \quad , \quad 1 \quad , \quad 2\ \rfloor$$

$$\{\alpha_m\}^T = \lfloor \beta_{m3} \ , \beta_{m5} \ , \beta_{m7} \rfloor$$

$$(\Delta_{mu})_3 : \quad \lceil c_m \rfloor = \lceil\ 1 \quad , \quad 2 \quad , \quad 1\ \rfloor$$

$$\{\alpha_m\}^T = \lfloor \beta_{m10} \ , \beta_{m16} \ , \beta_{m13} \rfloor$$

$$(\Delta_{mu})_4 : \quad \lceil c_m \rfloor = \lceil\ 1 \quad , \quad 1 \quad , \quad 2\ \rfloor$$

$$\{\alpha_m\}^T = \lfloor \beta_{m11} \ , \beta_{m13} \ , \beta_{m15} \rfloor$$

Figure 71. Zone 3 Membrane Stiffness Parameters

$$(\Delta_{mu})_1 : \quad [c_m] = [\,1 \;,\; 2 \;,\; 1\,]$$
$$\{\alpha_m\}^T = [\beta_{m2} \;,\; \beta_{m4} \;,\; \beta_{m5}\,]$$

$$(\Delta_{mu})_2 : \quad [c_m] = [\,1 \;,\; 1 \;,\; 2\,]$$
$$\{\alpha_m\}^T = [\beta_{m3} \;,\; \beta_{m5} \;,\; \beta_{m7}\,]$$

$$(\Delta_{mu})_3 : \quad [c_m] = [\,1 \;,\; 2 \;,\; 1\,]$$
$$\{\alpha_m\}^T = [\beta_{m10} \;,\; \beta_{m12} \;,\; \beta_{m13}]$$

$$(\Delta_{mu})_4 : \quad [c_m] = [\,1 \;,\; 1 \;,\; 2\,]$$
$$\{\alpha_m\}^T = [\beta_{m11} \;,\; \beta_{m13} \;,\; \beta_{m15}]$$

Figure 72. Zone 4 Membrane Stiffness Parameters

$$\delta_{00}^{(j)} = +\frac{1}{2}\, x_j\, y_j \qquad \delta_{02}^{(j)} = +\frac{1}{12}\, x_j\, y_j^3$$

$$\delta_{10}^{(j)} = +\frac{1}{6}\, x_j^2\, y_j \qquad \delta_{12}^{(j)} = +\frac{1}{60}\, x_j^2\, y_j^3$$

$$\delta_{20}^{(j)} = +\frac{1}{12}\, x_j^3\, y_j \qquad \delta_{22}^{(j)} = +\frac{1}{180}\, x_j^3\, y_j^3$$

$$\delta_{30}^{(j)} = +\frac{1}{20}\, x_j^4\, y_j \qquad \delta_{03}^{(j)} = +\frac{1}{20}\, x_j\, y_j^4$$

$$\delta_{40}^{(j)} = +\frac{1}{30}\, x_j^5\, y_j \qquad \delta_{13}^{(j)} = +\frac{1}{120}\, x_j^2\, y_j^4$$

$$\delta_{01}^{(j)} = +\frac{1}{6}\, x_j\, y_j^2 \qquad \delta_{04}^{(j)} = +\frac{1}{30}\, x_j\, y_j^5$$

$$\delta_{11}^{(j)} = +\frac{1}{24}\, x_j^2\, y_j^2$$

$$\delta_{21}^{(j)} = +\frac{1}{60}\, x_j^3\, y_j^2$$

$$\delta_{31}^{(j)} = +\frac{1}{120}\, x_j^4\, y_j^2$$

Note: Make these expressions negative for Zones 2 & 4.

Figure 73. Definition of V $\delta_{pq}^{(j)}$ Notation

The general form identified with the elements of the vector $\{\Delta_{mu}\}$ leads naturally to a general form for the associated energy contributions. Firstly, the membrane energy is expressed in indicial notation.

$$\Phi_m = \sum_{k=1}^{4} \sum_{j=1}^{4} \sum_{i=1}^{4} (\Phi_m)_{ij}^{(k)} \tag{319}$$

where

$$(\Phi_m)_{ij}^{(k)} = \int_{\text{zone } k} \left(\frac{1}{2} (I_{mk})_{ij} (\Delta_{mu})_i^{(k)} (\Delta_{mu})_j^{(k)} \right.$$

$$\left. - (I_{me})_i (\Delta_{mu})_i^{(k)} \right) dx\, dy \tag{320}$$

The general contributing energy form now follows directly by introducing the general form for the elements defined in Equation 316, i.e.

$$(\Phi_m)_{ij}^{(k)} = \frac{1}{2} (I_{mk})_{ij} \lfloor \alpha_m \rfloor_i^{(k)} \lceil c_m \rfloor_i^{(k)} [C_k]^{(k)} \lceil c_m \rfloor_j^{(k)} \{\alpha_m\}_j^{(k)}$$

$$- (I_{m\epsilon})_i \lfloor \alpha_m \rfloor_i^{(k)} \lceil c_m \rfloor_i^{(k)} \{C_\epsilon\}^{(k)} \tag{321}$$

where

$$\lfloor C_k \rfloor^{(k)} = \int_{\text{zone } k} \{d\} \lfloor d \rfloor\, dx\, dy \tag{322}$$

$$\{C_\epsilon\}^{(k)} = \int_{\text{zone } k} \{d\}\, dx\, dy \tag{323}$$

Presentation of these matrices is prefaced by definition of notation in Figure 73. Then, $[C_k]$ and $\{C_\epsilon\}$ are given in Figure 74. The knowledge of these matrices together with that of the $\lceil c_m \rfloor$ and $\{\alpha_m\}$ matrices specified in Figures 69 through 72 enables explicit algebraic expression of each of the $(\Phi_m)_{ij}^{(k)}$. These individual energy contributions are summed to obtain the objective algebraic expression for the total membrane potential energy, i. e.

$$\Phi_m = \frac{1}{2} \lfloor \beta_m \rfloor [\tilde{K}_m] \{\beta_m\} - \lfloor \beta_m \rfloor \{\tilde{F}_\epsilon\} \tag{324}$$

$$\left[C_k\right]^{(k)} = \begin{bmatrix} \delta_{00} , \delta_{10} , \delta_{01} \\ \delta_{10} , \delta_{20} , \delta_{11} \\ \delta_{01} , \delta_{11} , \delta_{02} \end{bmatrix}^{(k)}$$

$$\left[C_\epsilon\right]^{(k)} = \left[\delta_{00} , \delta_{10} , \delta_{01} \right]^{(k)}$$

Figure 74. Stiffness Submatrices

As disclosed by the notation employed, $\left[\tilde{K}_m\right]$ and $\left\{\tilde{F}_\epsilon\right\}$ are the membrane stiffness and prestrain matrices referenced to field coordinate displacement degrees-of-freedom $\left\{\beta\right\}$. Explicit statement of these matrices is redundant since they are simply the assembled results of explicitly specified contributions.

It is convenient to have separate load vectors for prestrains due to temperature. The desired modification is available immediately from Equation 310.

$$\left\{I_\epsilon\right\} = \Delta T_m \; t \sin\alpha \left[T_u\right]^T \left[T_{\epsilon\sigma}\right]^T \left[E^{(m)}\right] \left\{\alpha^{(m)}\right\} \tag{325}$$

The objective algebraic statement of the flexural potential energy follows in analogy with the development for the membrane potential energy. Examination of the component relations of Equation 315 leads to identification of a typical form for each element of the vector $\left\{\Delta_f\right\}$, i.e.

$$\left\{\Delta_f\right\}_\ell^{(k)} = \left[d\right] \left[c_f\right]_\ell^{(k)} \left\{a_f\right\}_\ell^{(k)} \tag{326}$$

For example, focusing on the first zone (k = 1), the first element (ℓ = 1) is given by

$$\left(\Delta_f\right)_\ell^{(1)} = -w_{xx}^{(1)} = \left[1 , x , y\right] \begin{bmatrix} -2, & & \\ & , -24, & \\ & & , -8 \end{bmatrix} \begin{Bmatrix} \beta_{f4} \\ \beta_{f7} \\ \beta_{f8} \end{Bmatrix} \tag{327}$$

Explicit statement of the $\left[c_f\right]$ and $\left\{a_f\right\}$ matrice for each of the four zones is given in Figures 75 through 78.

$$(\Delta_f)_1 : \left[c_f\right] = \left[\, 2 \;,\; 24 \;,\; 8 \,\right]$$
$$\left\{\alpha_f\right\}^T = \left[\beta_{f4} \;,\; \beta_{f7} \;,\; \beta_{f8}\right]$$

$$(\Delta_f)_2 : \left[c_f\right] = \left[\, 2 \;,\; 8 \;,\; 24 \,\right]$$
$$\left\{\alpha_f\right\}^T = \left[\beta_{f6} \;,\; \beta_{f9} \;,\; \beta_{f10}\right]$$

$$(\Delta_f)_3 : \left[c_f\right] = \left[\, 4 \;,\; 16 \;,\; 16 \,\right]$$
$$\left\{\alpha_f\right\}^T = \left[\beta_{f5} \;,\; \beta_{f8} \;,\; \beta_{f9}\right]$$

Figure 75. Zone 1 Flexure Stiffness Parameters

$$(\Delta_f)_1 : \left[c_f\right] = \left[\, 2, \quad 24, \quad 8 \,\right]$$
$$\left\{\alpha_f\right\}^T = \left[\beta_{f14}, \; \beta_{f15}, \; \beta_{f16}\right]$$

$$(\Delta_f)_2 : \left[c_f\right] = \left[\, 2, \quad 8, \quad 24 \,\right]$$
$$\left\{\alpha_f\right\}^T = \left[\beta_{f6}, \; \beta_{f9}, \; \beta_{f10}\right]$$

$$(\Delta_f)_3 : \left[c_f\right] = \left[\, 4, \quad 16, \quad 16 \,\right]$$
$$\left\{\alpha_f\right\}^T = \left[\beta_{f5}, \; \beta_{f16}, \; \beta_{f9}\right]$$

Figure 76. Zone 2 Flexure Stiffness Parameters

$$(\Delta_f)_1 : \left[c_f \right] = \left[2 \quad , \quad 24 \quad , \quad 8 \right]$$
$$\left\{ \alpha_f \right\}^T = \left[\beta_{f14} , \beta_{f15} , \beta_{f16} \right]$$

$$(\Delta_f)_2 : \left[c_f \right] = \left[2 \quad , \quad 8 \quad , \quad 24 \right]$$
$$\left\{ \alpha_f \right\}^T = \left[\beta_{f11} , \beta_{f12} , \beta_{f13} \right]$$

$$(\Delta_f)_3 : \left[c_f \right] = \left[4 \quad , \quad 16 \quad , \quad 16 \right]$$
$$\left\{ \alpha_f \right\}^T = \left[\beta_{f5} , \beta_{f16} , \beta_{f12} \right]$$

Figure 77. Zone 3 Flexure Stiffness Parameters

$$(\Delta_f)_1 : \left[c_f \right] = \left[2 \quad , \quad 24 \quad , \quad 8 \right]$$
$$\left\{ \alpha_f \right\}^T = \left[\beta_{f4} , \beta_{f7} , \beta_{f8} \right]$$

$$(\Delta_f)_2 : \left[c_f \right] = \left[2 \quad , \quad 8 \quad , \quad 24 \right]$$
$$\left\{ \alpha_f \right\}^T = \left[\beta_{f11} , \beta_{f12} , \beta_{f13} \right]$$

$$(\Delta_f)_3 : \left[c_f \right] = \left[4 \quad , \quad 16 \quad , \quad 16 \right]$$
$$\left\{ \alpha_f \right\}^T = \left[\beta_{f5} , \beta_{f8} , \beta_{f12} \right]$$

Figure 78. Zone 4 Flexure Stiffness Parameters

The general form identified with the elements of the vector $\{\Delta_f\}$ leads to a general form for the associated energy contributions. As before, the energy function is expressed in indicial notation as

$$\Phi_f = \sum_{k=1}^{4} \sum_{j=1}^{3} \sum_{j=1}^{3} \left(\Phi_f\right)_{ij}^{(k)} \tag{328}$$

where

$$\left(\Phi_f\right)_{ij}^{(k)} = \int_{\text{zone } k} \left(\frac{1}{2} \left(I_{fk}\right)_{ij} \left(\Delta_f\right)_i^{(k)} \left(\Delta_f\right)_j^{(k)} - \left(I_{f\epsilon}\right)_i \left(\Delta_f\right)_i^{(k)} \right) dx\, dy \tag{329}$$

The general contributing energy form now follows directly by introducing the general form for the elements $\{\Delta_f\}$ defined in Equation 326, i.e.

$$\left(\Phi_f\right)_{ij}^{(k)} = \frac{1}{2} \left(I_{fk}\right)_{ij} \left\lfloor \alpha_f \right\rfloor_i^{(k)} \left\lceil c_f \right\rfloor_i^{(k)} \left[C_k\right]^{(k)} \left\lceil c_f \right\rfloor_j^{(k)} \left\{\alpha_f\right\}_j^{(k)} - \left(I_{f\epsilon}\right)_i \left\lfloor \alpha_f \right\rfloor_i^{(k)} \left\lceil c_f \right\rfloor_i^{(k)} \left\{C_\epsilon\right\}^{(k)} \tag{330}$$

Particularization of this general form to the individual $\left\lceil c_f \right\rfloor$ and $\{\alpha_f\}$ and summation yields the objective algebraic expression for the total flexural potential energy, i.e.

$$\Phi_f = \frac{1}{2} \left\lfloor \beta_f \right\rfloor \left[\tilde{K}_f\right] \{\beta_f\} - \left\lfloor \beta_f \right\rfloor \left\{\tilde{F}_\epsilon\right\} \tag{331}$$

As disclosed by the notation employed, $\left[\tilde{K}_f\right]$ and $\left\{\tilde{F}_\epsilon\right\}$ are the flexure stiffness and prestrain matrices referenced to field coordinate displacement degrees-of-freedom $\{\beta\}$. Explicit statement of these matrices is omitted since they are simply the assembled results of explicitly specified contributions.

As in the case of the membrane prestrain load vector, the flexure prestrain load vector is particularized to thermal loading. The desired modification follows immediately from Equation 309, i.e.

$$\left\{I_{f\epsilon}\right\} = \Delta T_f \frac{t^3 \sin\alpha}{12} \left[T_w\right]^T \left[T_{\epsilon\sigma}\right]^T \left[E^{(m)}\right] \left\{\alpha^{(m)}\right\} \tag{332}$$

Work equivalent gridpoint forces are provided for the case of a transverse load uniformly distributed over the quadrilateral thin shell element. The external work of this loading is defined by

$$\Phi_p = \int_{xy} p_z \; w \; \sin\alpha \; dx \, dy \tag{333}$$

The introduction of the assumed displacement modes into this expression yields

$$\Phi_p = \sum_{k=1}^{4} \int_{\text{zone } k} p_z \sin\alpha \quad \lfloor \beta_f \rfloor \left\{ B_w \right\}^{(k)} dx \, dy \tag{334}$$

Substitution from Equation 246 and integration then yields an algebraic expression for the external work, i.e.

$$\Phi_p = \lfloor \beta_f \rfloor \left\{ \tilde{F}_p \right\} \tag{335}$$

The matrix $\left\{ \tilde{F}_p \right\}$, referred to as the pressure load matrix referenced to field coordinate displacement degrees-of-freedom, is given in Figure 79.

3. Stress Matrices

The stress resultants for a thin shell of zero curvature are defined in the notation of Figure 80 as follows:

$$N_x = \int_z \sigma_x \, dz \quad ; \quad N_y = \int_z \sigma_y \, dz \; ; \; N_{xy} = \int_z \tau_{xy} \, dz \tag{336}$$

$$M_x = \int_z z \, \sigma_x \, dz \quad ; \quad M_y = \int_z z \, \sigma_y \, dz \; ; \; M_{xy} = -\int_z z \, \tau_{xy} \, dz \tag{337}$$

$$Q_x = \int_z z \left(\frac{\partial \sigma_x}{\partial x} \right) dz + \int_z z \left(\frac{\partial \tau_{xy}}{\partial y} \right) dz \tag{338}$$

$$Q_y = \int_z z \left(\frac{\partial \sigma_y}{\partial y} \right) dz + \int_z z \left(\frac{\partial \tau_{xy}}{\partial x} \right) dz \tag{339}$$

$$
P \sin \alpha \left\{ \begin{array}{llll}
\delta_{00}^{(1)} + & \delta_{00}^{(2)} + & \delta_{00}^{(3)} + & \delta_{00}^{(4)} \\
\delta_{10}^{(1)} + & \delta_{10}^{(2)} + & \delta_{10}^{(3)} + & \delta_{10}^{(4)} \\
\delta_{01}^{(1)} + & \delta_{01}^{(2)} + & \delta_{01}^{(3)} + & \delta_{01}^{(4)} \\
\delta_{20}^{(1)} + & \delta_{20}^{(4)} & & \\
2\,\delta_{11}^{(1)} + & 2\,\delta_{11}^{(2)} + & 2\,\delta_{11}^{(3)} + & 2\,\delta_{11}^{(4)} \\
\delta_{02}^{(1)} + & \delta_{02}^{(2)} & & \\
4\,\delta_{30}^{(1)} + & 4\,\delta_{30}^{(4)} & & \\
4\,\delta_{21}^{(1)} + & 4\,\delta_{21}^{(4)} & & \\
4\,\delta_{12}^{(1)} + & 4\,\delta_{12}^{(2)} & & \\
4\,\delta_{03}^{(1)} + & 4\,\delta_{03}^{(2)} & & \\
\delta_{02}^{(3)} + & \delta_{02}^{(4)} & & \\
4\,\delta_{12}^{(3)} + & 4\,\delta_{12}^{(4)} & & \\
4\,\delta_{03}^{(3)} + & 4\,\delta_{03}^{(4)} & & \\
\delta_{20}^{(2)} + & \delta_{20}^{(3)} & & \\
4\,\delta_{30}^{(2)} + & 4\,\delta_{30}^{(3)} & & \\
4\,\delta_{21}^{(2)} + & 4\,\delta_{21}^{(3)} & &
\end{array} \right\} \begin{array}{l}
\beta_1 \\ \beta_2 \\ \beta_3 \\ \beta_4 \\ \beta_5 \\ \beta_6 \\ \beta_7 \\ \beta_8 \\ \beta_9 \\ \beta_{10} \\ \beta_{11} \\ \beta_{12} \\ \beta_{13} \\ \beta_{14} \\ \beta_{15} \\ \beta_{16}
\end{array}
$$

Figure 79. Pressure Load Vector, $\left\{ \tilde{F}_p \right\}$

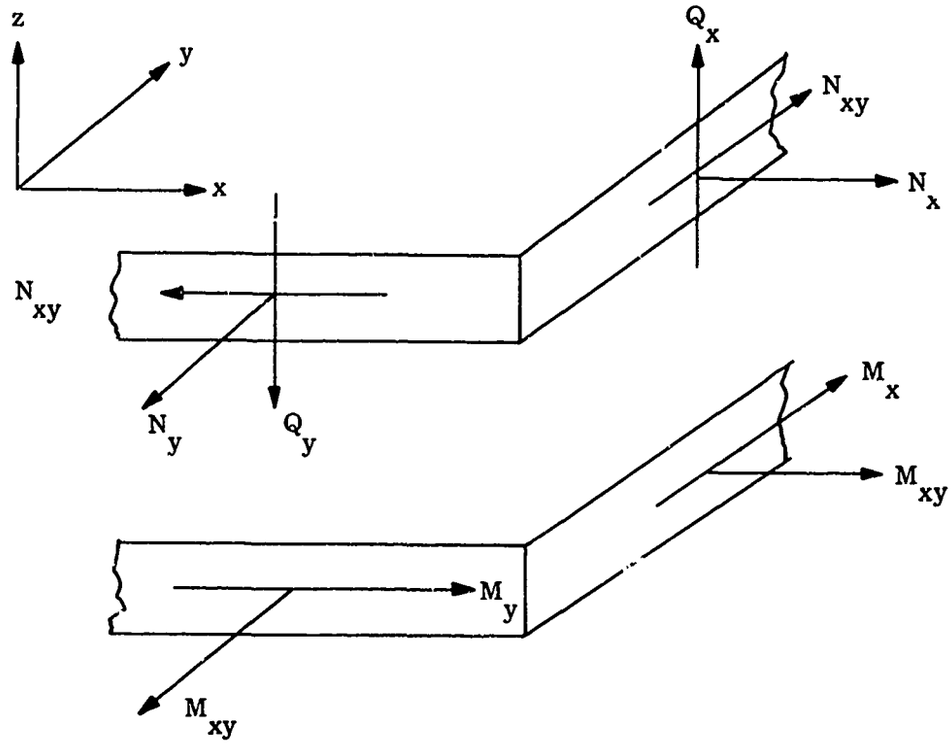

Figure 80. Stress Resultants

It was tacitly assumed in defining the stress resultants that nonlinear membrane flexure coupling contributions to the stress resultants are small relative to first order terms. This assumption is carried forward in writing the stress resultants in terms of the strains

$$\left\{N_f^{(g)}\right\} = t\left[E^{(g)}\right]\left[T_u\right]\left\{\Delta_{mu}^{(o)}\right\} - t\left\{\bar{\epsilon}_{mi}^{(g)}\right\} + t\left\{\bar{\sigma}_{mo}^{(g)}\right\} \quad (340)$$

$$\left\{M_f^{(g)}\right\} = \frac{t^3}{12}\left[E^{(g)}\right]\left\{K^{(g)}\right\} - \frac{t^3}{12}\left\{\bar{\epsilon}_{fi}^{(g)}\right\} + \frac{t^3}{12}\left\{\bar{\sigma}_{fo}^{(g)}\right\} \quad (341)$$

$$\left\{Q_f\right\} = \frac{t^3}{12}\left[Q1\right]\left[E^{(g)}\right]\left\{\frac{\partial}{\partial xg}K^{(g)}\right\} + \frac{t^3}{12}\left[G2\right]\left[E^{(g)}\right]\left\{\frac{\partial}{\partial yg}K^{(g)}\right\} \quad (342)$$

where $$\left[G1\right] = \begin{bmatrix}1, 0, 0\\ 0, 0, 1\end{bmatrix}, \quad \left[G2\right] = \begin{bmatrix}0, 0, 1\\ 0, 1, 0\end{bmatrix} \quad (343)$$

The stress resultants are expressed with reference to displacement functions defined in the oblique coordinate system of the element by substituting from Equations 299, 300, and 301.

$$\left\{N_f^{(g)}\right\} = t\left[E^{(g)}\right]\left[T_u\right]\left\{\Delta_{mw}^{(o)}\right\} - t\left\{\bar{\epsilon}_{mi}^{(g)}\right\} + t\left\{\bar{\sigma}_{mo}^{(g)}\right\} \quad (344)$$

$$\left\{M_f^{(g)}\right\} = \frac{t^3}{12}\left[E^{(g)}\right]\left[T_w\right]\left\{\Delta_{fw}^{(o)}\right\} - \frac{t^3}{12}\left\{\bar{\epsilon}_{fi}^{(g)}\right\} + \frac{t^3}{12}\left\{\bar{\sigma}_{fo}^{(g)}\right\} \quad (345)$$

$$\left\{Q_f^{(g)}\right\} = \frac{t^3}{12}\left[G1\right]\left[E^{(g)}\right]\left[T_w\right]\left\{\frac{\partial}{\partial x_o}\Delta_{fw}^{(o)}\right\} + \frac{t^3}{12}\left[G2\right]\left[E^{(g)}\right]\left[T_w\right]\left\{-\frac{\cos\alpha}{\sin\alpha}\left\{\frac{\partial}{\partial x_o}\Delta_{fw}^{(o)}\right\} + \frac{1}{\sin\alpha}\left\{\frac{\partial}{\partial y_o}\Delta_{fw}^{(o)}\right\}\right\} \quad (346)$$

Introducing the displacement mode shapes assumed over the four zones of the element, the stress resultants can be written collectively as

$$\begin{Bmatrix} N_f^{(g)} \\ M_f^{(g)} \\ Q_f^{(g)} \end{Bmatrix} = \begin{bmatrix} S_N \\ S_M \\ S_Q \end{bmatrix}\{q\} - \begin{Bmatrix} \Delta_N \\ \Delta_M \\ 0 \end{Bmatrix} \quad (347)$$

where

$$\left\{S_N^{(\ )}\right\} = t\left[E^{(g)}\right]\left[T_u\right]\left[D_m^{(j)}(\ )\right]\left[\Gamma_{ms}\right] \quad (348)$$

$$\left\{S_M^{(\ )}\right\} = \frac{t^3}{12}\left[E^{(g)}\right]\left[T_w\right]\left[D_f^{(j)}(\ )\right]\left[\Gamma_{fs}\right] \quad (349)$$

$$\left\{S_Q(\ )\right\} = \frac{t^3}{12}\left[G1\right]\left[E^{(g)}\right]\left[T_w\right]\left[\frac{\partial}{\partial x_o}D_f^{(j)}(\ )\right]\left[\Gamma_{fs}\right] + \frac{t^3}{12}\left[G2\right]\left[E^{(g)}\right]\left[T_w\right]\left[-\frac{\cos\alpha}{\sin\alpha}\left[\frac{\partial}{\partial x_o}D_f^{(j)}(\ )\right] + \frac{1}{\sin\alpha}\left[\frac{\partial}{\partial y_o}D_f^{(j)}(\ )\right]\right]\left[\Gamma_{fs}\right] \quad (350)$$

$$\left\{\Delta_N\right\} = -t\left\{\bar{\epsilon}_{mi}^{(g)}\right\} \quad (351)$$

$$\left\{\Delta_M\right\} = -\frac{t^3}{12}\left\{\bar{\epsilon}_{fi}^{(g)}\right\} \quad (352)$$

C. EVALUATION

1. Membrane Stress Analysis

The first illustration which uses the quadrilateral thin shell element in a structural evaluation will be the following. Consider a thin square isotropic plate loaded with a self equilibrating parabolic membrane load as shown in Figure 81. The material properties and pertinent geometric data are also shown in the figure.

The idealizations used for the finite element analyses are shown in Figure 82. Three different grid sizes were employed in this evaluation. One element, four element, and 16 element solutions were obtained in order to evaluate convergence characteristics. Due to conditions of symmetry it should be noted that only one quadrant of the plate was analyzed. For the finite element idealizations employed in this evaluation, the midside nodes which were loaded by the parabolic load were suppressed. This suppression invokes a linear edge displacement under the load.

The results obtained from this set of convergence studies are presented in Figures 83 and 84. Figure 83 is a plot of the membrane displacement, u_q, at the middle of the plate's edge versus degrees-of-freedom employed in the analyses. The reference solution (Reference 44) is designated by the solid line. Figure 84 presents a curve of the membrane displacement, u_x, and stress resultant, N_x, versus the edge span of the plate for the idealization shown in Figure 82 (16 element solution).

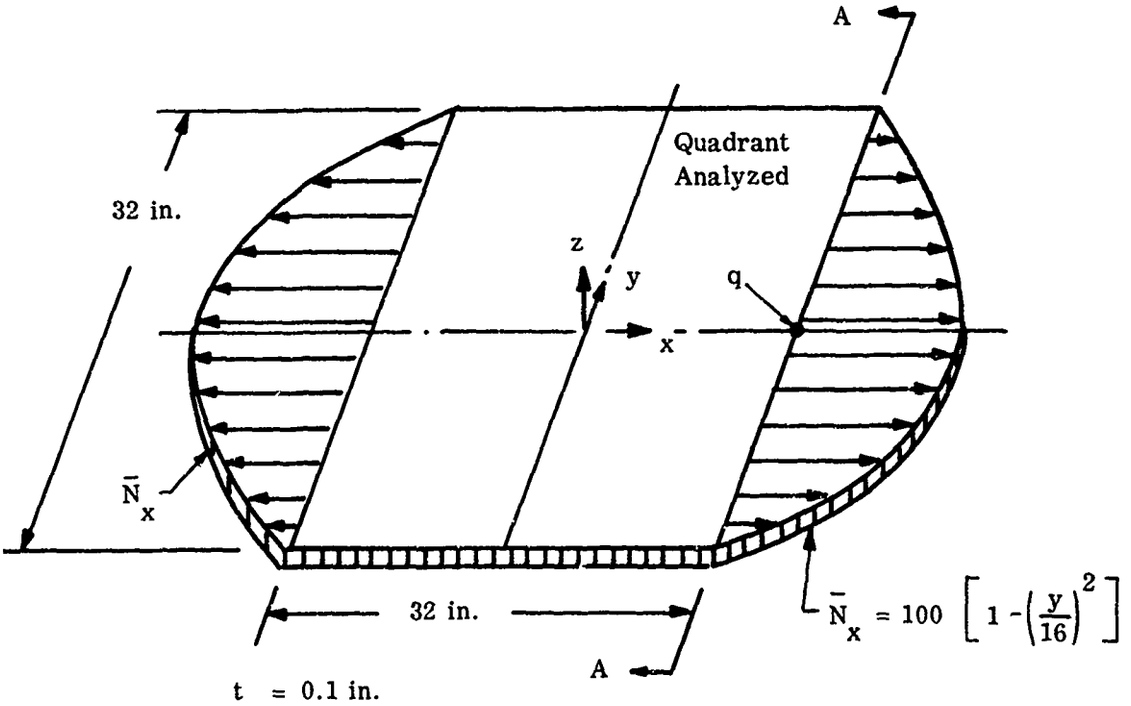

t = 0.1 in.

$E = 30 \times 10^6$ lb/in.^{2} $\quad \nu = 0.3$

Figure 81. Parabolically Loaded Membrane

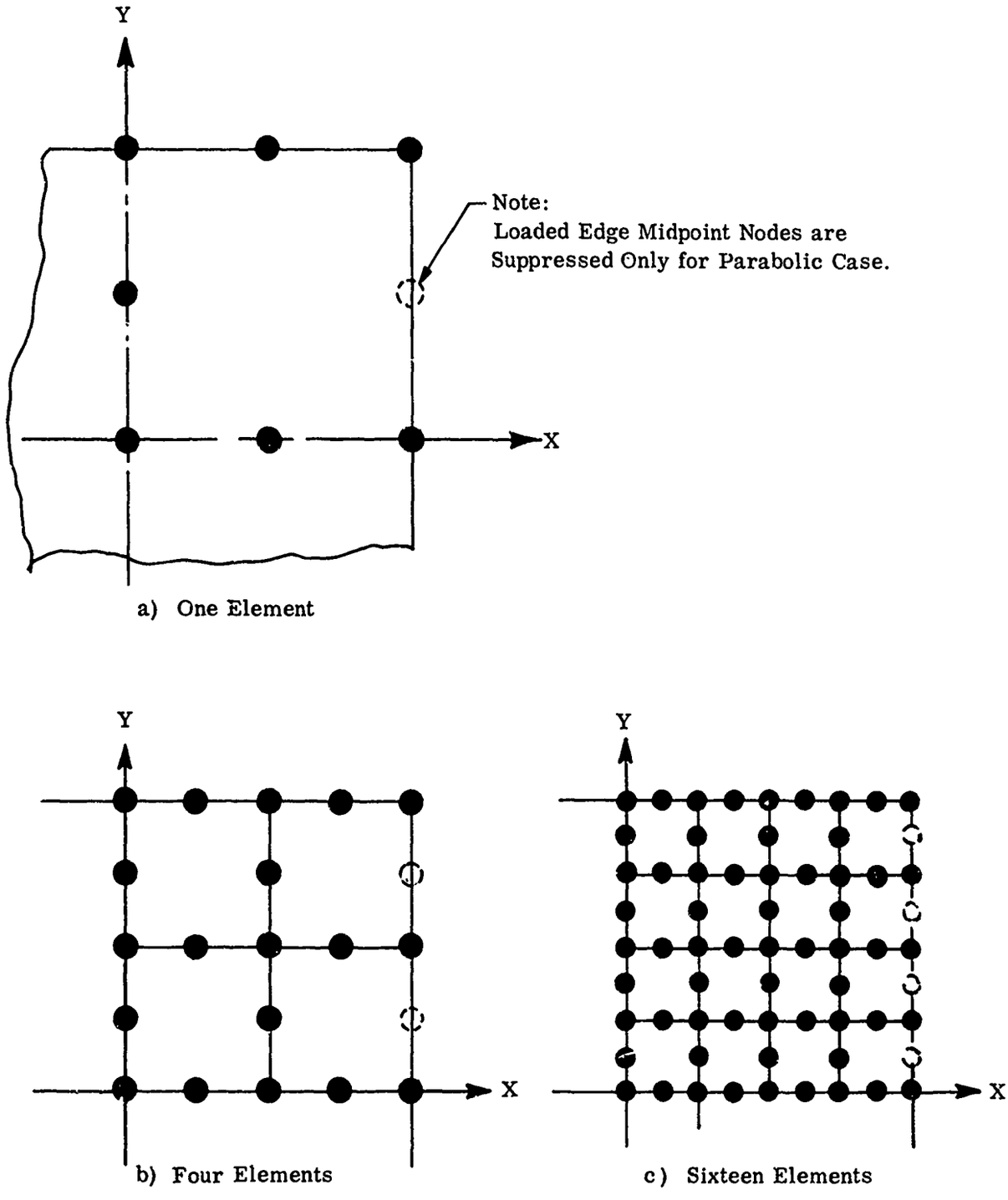

Figure 82. Idealization

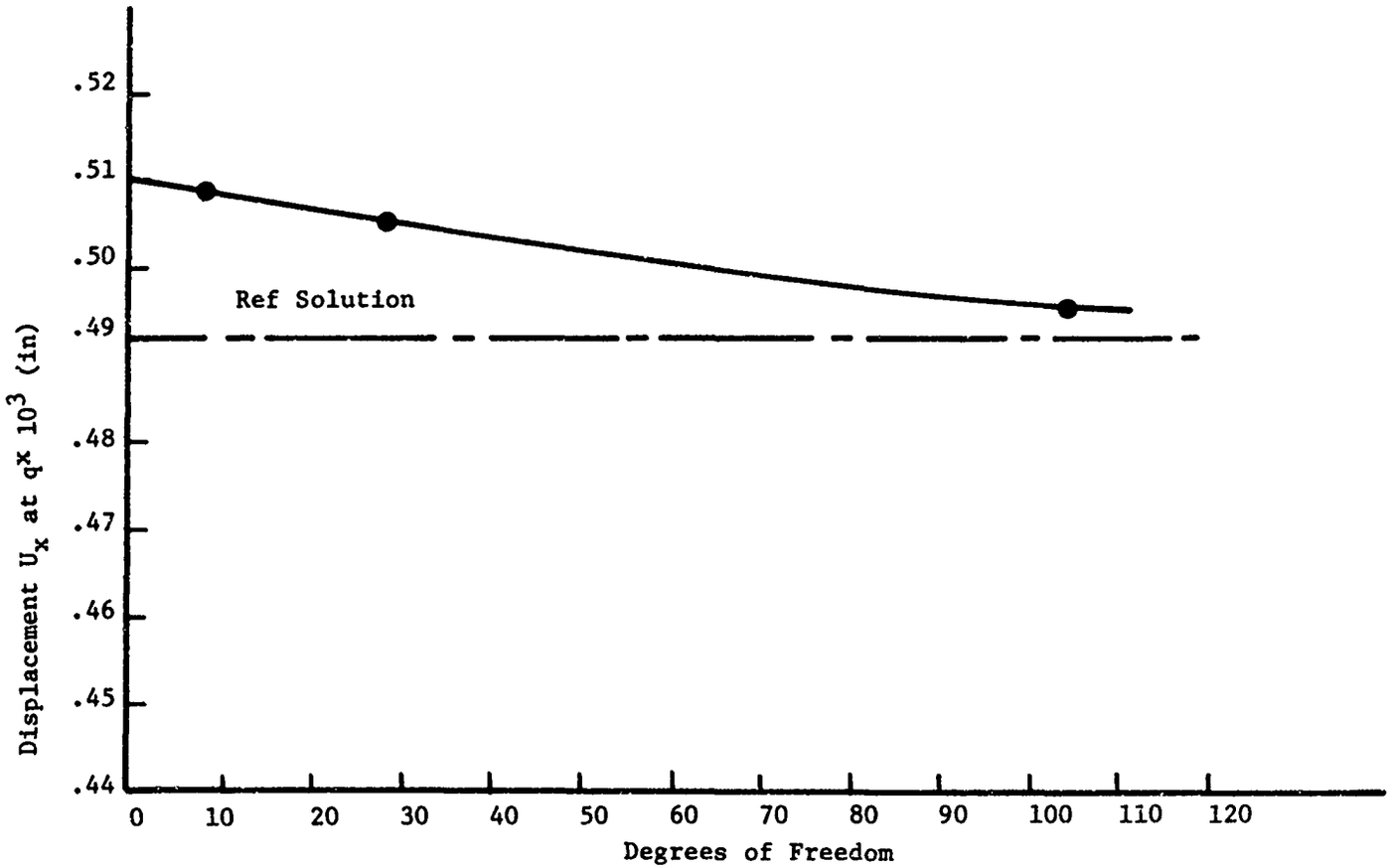

Figure 83 Membrane Displacement At Midside vs Degrees of Freedom

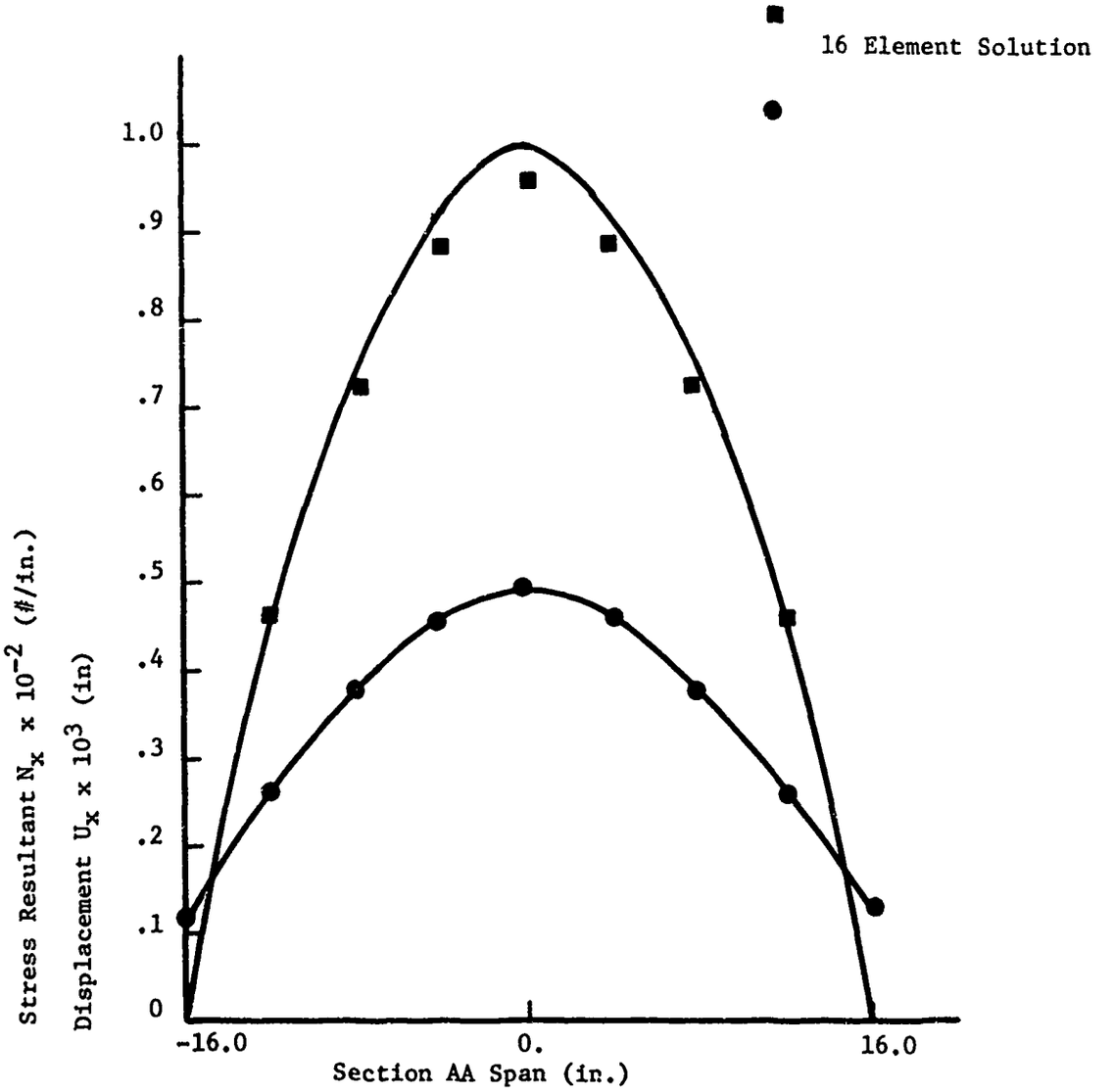

Figure 84 Membrane Displacement And Stress Behavior Versus Plate Edge Span

Again it should be noted that the reference solution is designated by the solid lines and no discernible difference between solutions can be detected.

2. Membrane Gridwork Influences

The second illustration which utilizes the quadrilateral thin shell element in a structural evaluation will be the following. Again, consider a thin square isotropic plate loaded with a self equilibrating parabolic membrane load as shown in Figure 81. This illustration will involve the effect that the shape of the elements used in the structural idealization has on the determination of the center edge displacement of the membrane.

The six idealizations used for the shape study are shown in Figure 85. It should be noted that due to symmetry only one quadrant of the plate was analyzed. The midside nodes which were loaded by the parabolic membrane load were suppressed in this solution.

The results obtained from the subject shape studies are shown in Figure 86. These solutions indicate that the displacement values, u_q, obtained for the middle of the plate's edge, are fairly insensitive to the shape of the element for this class of problem.

3. Plate Stress Analysis

The third illustration which utilizes the quadrilateral thin shell element in a structural evaluation will be the following. A simply supported isotropic square plate with a uniform normal pressure load of one psi is shown in Figure 87 along with its material properties and pertinent dimensions.

The idealizations used for the finite element analyses are shown in Figure 82. Note that no node points are suppressed in this analysis. Three different grid sizes were employed in this evaluation. One element, four element and 16 element solutions were obtained in order to evaluate convergence characteristics. Due to conditions of symmetry only one quadrant of the plate was analyzed.

Figure 88 is a plot of the transverse displacement at the center of the plate versus degrees-of-freedom employed in the analyses. The reference solution (Reference 45) is designated by the solid line. Figure 89 presents a curve of the transverse displacement, w_X, and bending moment, M_X, versus the center span of the plate for the idealization shown in Figure 82 (c) (16 element solution). Again, it should be noted that the reference solution is designated by the solid lines and no discernible difference between solutions can be detected.

4. Plate Gridwork Influences

The fourth illustration which utilizes the quadrilateral thin shell element in a structural evaluation will be the following. A simply supported isotropic plate with a

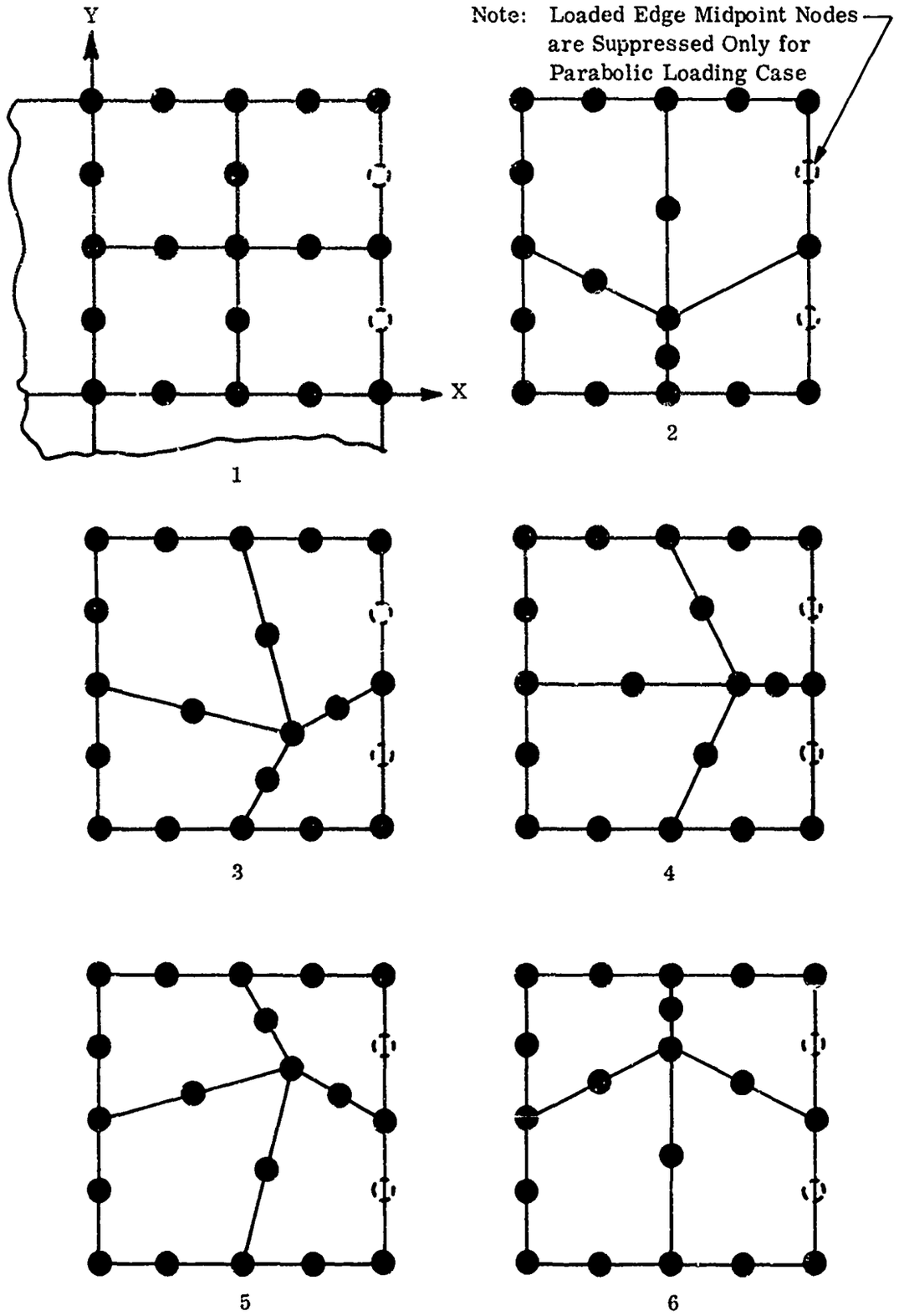

Figure 85. Shape Study Idealizations

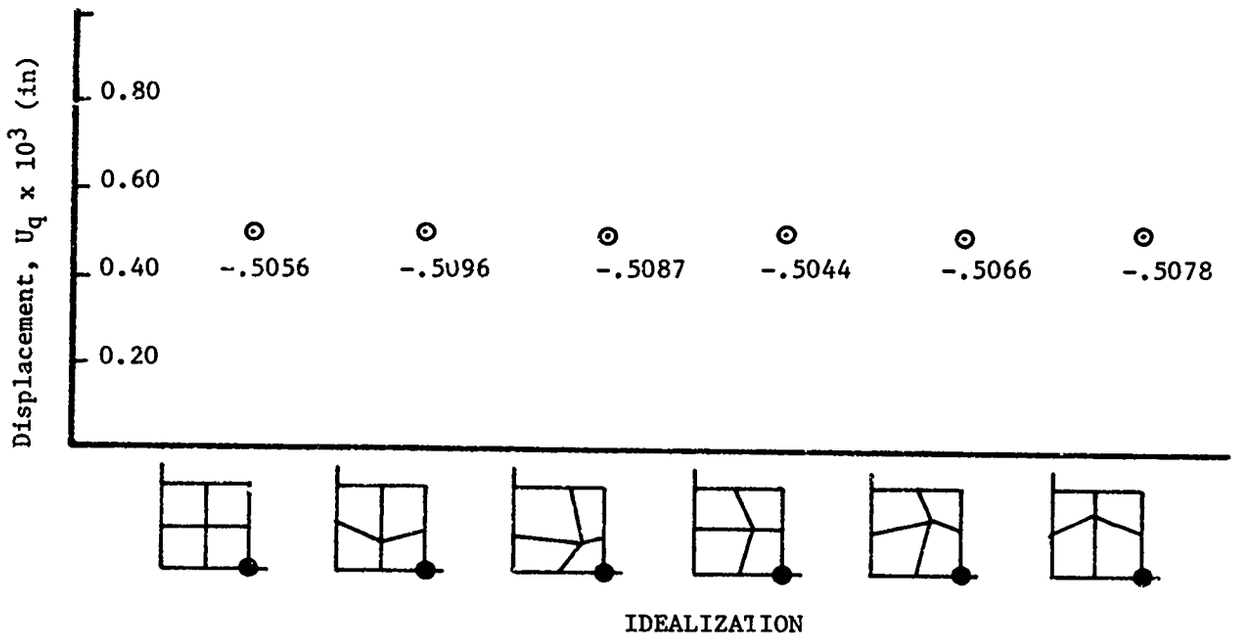

Figure 86 Shape Study/Quadrilateral Elements Membrane, Square, Isotropic, Self Equilibrating Parabolic Edge Loads

Plate Edges are Simply Supported

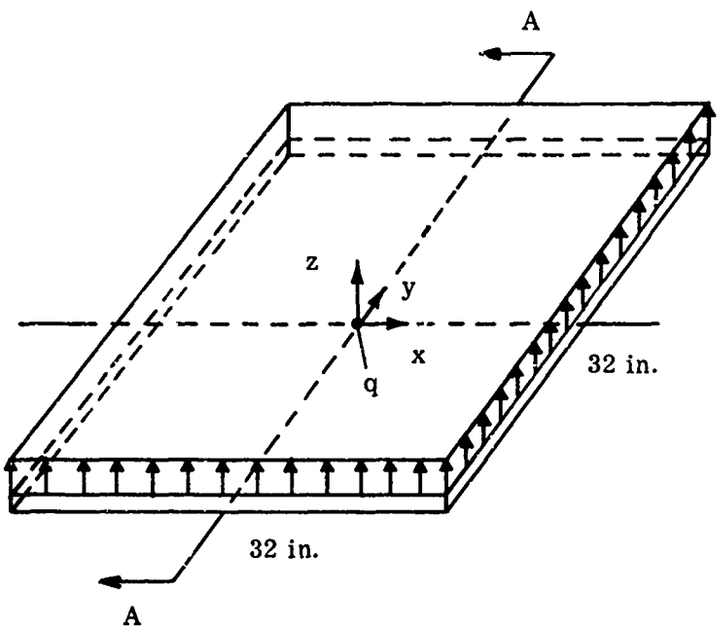

$t = 0.1$ in.

$E = 30 \times 10^6$ lb/in.^{2}

$\nu = 0.3$

$p_z = 1$ lb/in.^{2}

Figure 87. Simply Supported Square Plate with Uniform Normal Load

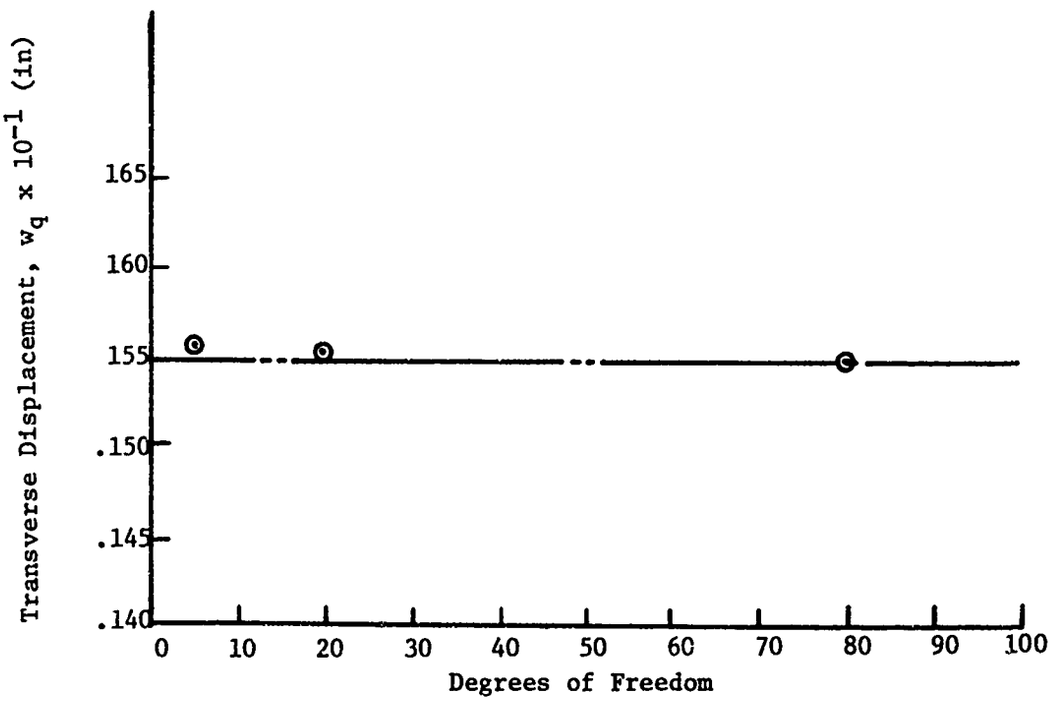

Legend:

O Magic Quadrilateral

—— Reference Alternate Solution

Figure 88 Convergence of Quadrilateral Element
Plate, Square, Isotropic, Simple Support, Uniform Pressure

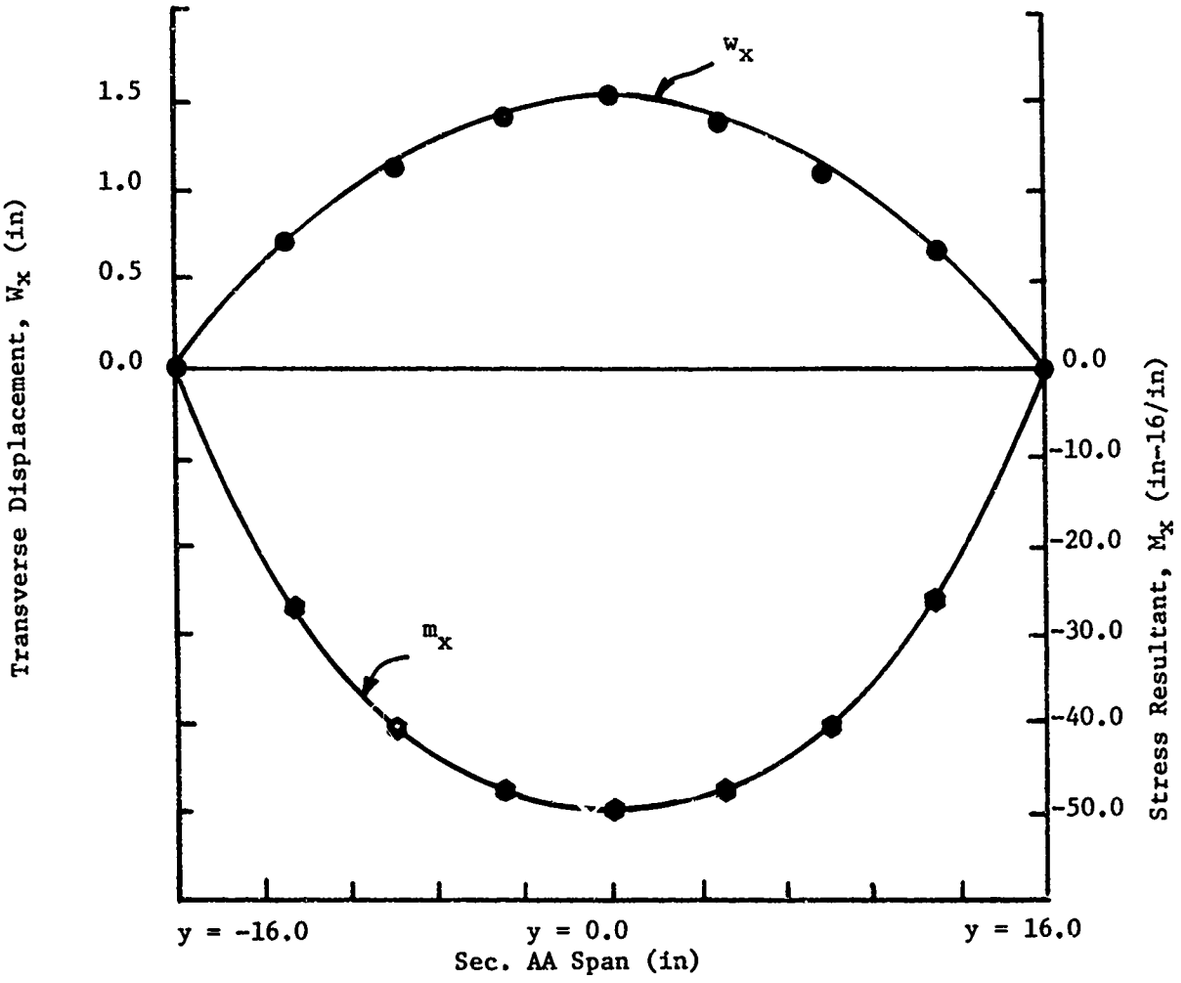

Legend:

● ● Bell Quadrilateral, Grid CQ
Reference Quadrilateral
——— Reference Alternate Solution

Figure 89 Behavior Of Quadrilateral Element Plate, Square, Isotropic, Simple Support Unit Uniform Load

a uniform normal pressure load of one psi is shown in Figure 87 along with its material properties and pertinent dimensions.

This illustration will involve the effect that the shape of the elements used in the structural idealization has on the determination of the maximum displacement of the plate.

The six idealizations used for the shape study are shown in Figure 85. Due to conditions of symmetry only one quadrant of the plate was analyzed.

The results obtained from the subject shape studies are shown in Figure 90. These solutions indicate that the determination of the plate's center transverse displacement is fairly insensitive to the shape of the element for this class of problem.

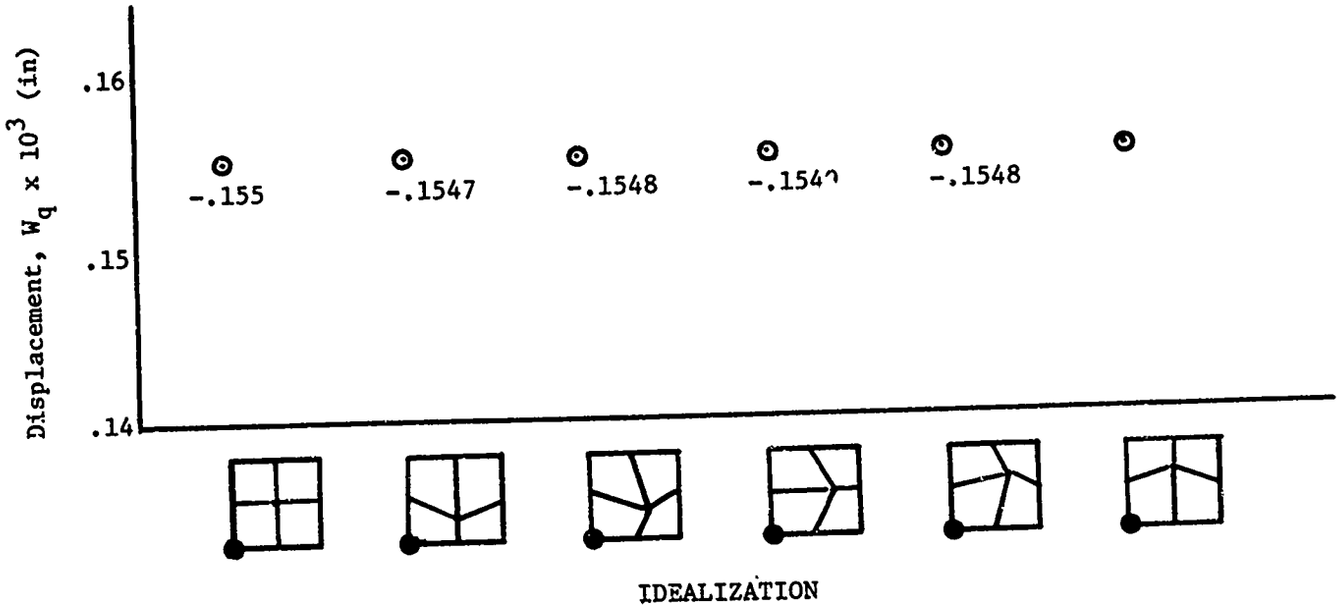

Figure 90 Shape Study Quadrilateral Element Plate, Square, Isotropic, Simple Supports Uniform Pressure Load

9. HELLE TRIANGULAR THIN SHELL ELEMENT

A. INTRODUCTION

A triangular thin shell element is incorporated in the discrete element library of the MAGIC System. This element, illustrated in Figure 91, is recommended for use as the basic building block for most doubly curved shells. Additionally, it is useful in combination with the Mallett quadrilateral thin shell element for dealing with irregular geometries of all membrane, plate, and shell structures. The Helle triangular thin shell element representation is developed in detail in Reference 46.

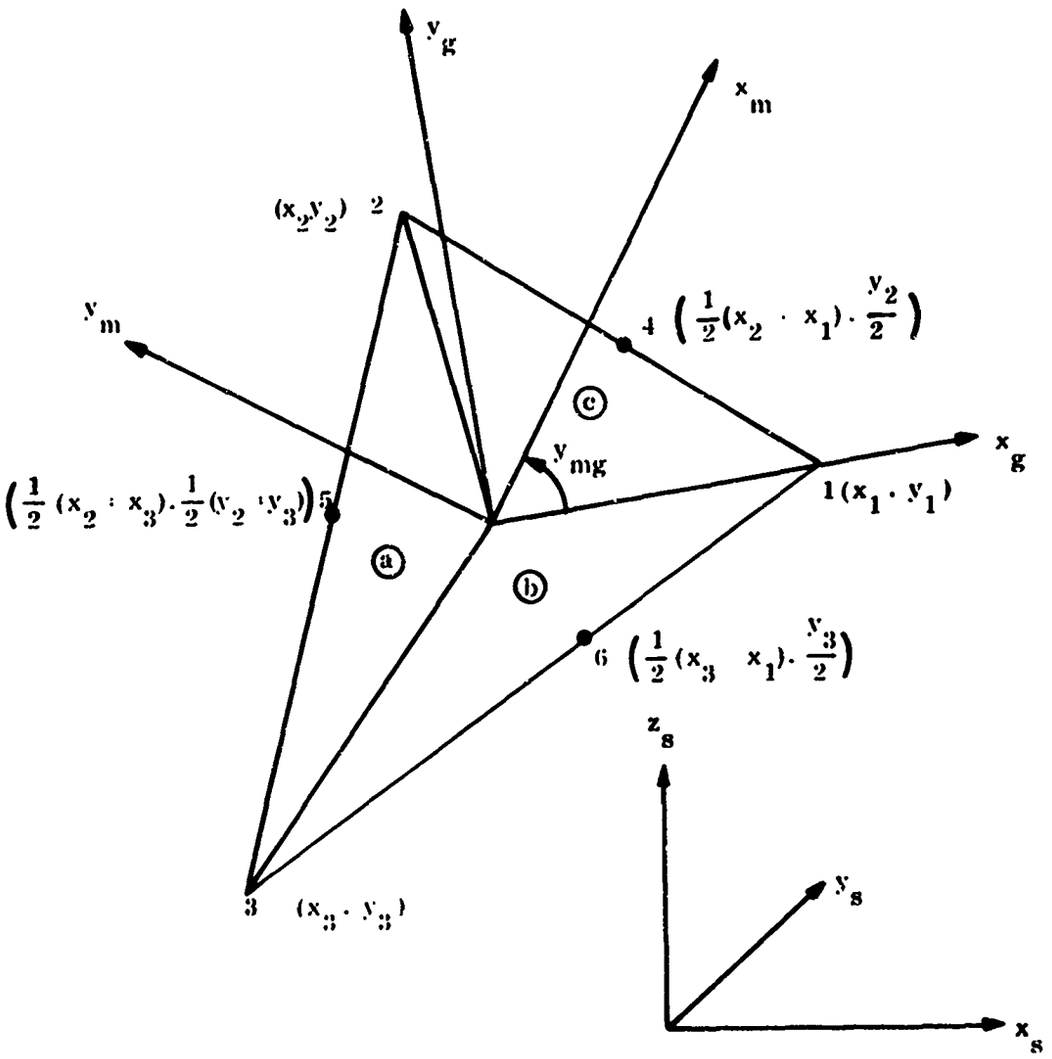

Figure 91. Triangular Thin Shell Element Representation

The shape of the general triangular element is defined by the coordinates of the three corner points. It is a zero curvature element. The plane of the element is determined by the three corner point coordinates.

The subject element is a thin shell element in that both membrane and flexure action are represented. Referenced to axes in the plane of the element, the membrane and flexure representations are uncoupled. Optional generation of either or both of the representations is controlled by the provision of associated effective thicknesses. The distinct membrane and flexure effective thicknesses are assumed constant over the plane of the element.

Under normal circumstances, three corner points and three midside points participate in establishing continuous connection of the Helle triangular thin shell element with adjacent elements. Used in this way input data volume is reduced and accuracy is enhanced. An option is provided to suppress the midside nodes individually if associated complexities arise in grid refinement or nonstandard connections with adjacent elements. Invoking this suppression option causes linear variation to be imposed on the specified midside variables.

The Helle thin shell element is written to accommodate anisotropy of mechanical and physical material properties. Orientation of material axes is data specified. Temperature referenced material properties, selected from the Materials Library, are assumed constant over the element.

A linear generalized Hooke's Law is employed for the equations of state. Three options are provided; namely, conventional plane stress, corrected plane stress, and restricted plane strain.

The element formulation is discretized by the construction of mode shapes. Membrane displacements within the subject element are approximated by quadratic polynomials. Transverse displacement is represented by cubic polynomials. A linear variation is provided for midplane and gradient variations in thermal loading. Other element loadings such as pressure are assumed constant over the element.

Deformation behavior of the Helle triangular thin shell element is taken to be described by the displacement degrees-of-freedom associated with the gridpoints which it connects.

The linear variation in strain within the element which is permitted by the assumed displacement functions leads to similar stress variation. Advantage is taken of this by exhibiting predicted stress resultants at the three corners as well as at the center of the element. Inplane and normal; direct, shear, and bending stress resultants are included. The display of stresses implies a set of axes of reference. These axes are data specified.

B. FORMULATION

1. Displacement Functions

The displacement functions for the triangular thin shell element are constructed with reference to the coordinate system (x_g, y_g) shown in Figure 91. The origin of this system is located at the centroid of the triangle. The orientation of the x_g axis is defined by corner gridpoint number 1. The y_g axis of this right-handed coordinate system is taken counterclockwise from the x_g axis in the plane of the element.

Polynomial mode shapes are employed to represent the displacement functions over the element. These mode shapes, for the membrane displacements, take the form

$$u = \left\lfloor B_u \right\rfloor \left\{ \beta_m \right\} \tag{353}$$

$$v = \left\lfloor B_v \right\rfloor \left\{ \beta_m \right\} \tag{354}$$

where

$$\left\{ \beta_m \right\} = \left\lfloor \beta_{m1}, \beta_{m2}, \cdots, \beta_{m12} \right\rfloor \tag{355}$$

The mode shape matrices $\left\lfloor B_u \right\rfloor$ and $\left\lfloor B_v \right\rfloor$ are exhibited in Figure 92. It should be noted that both of these represent complete quadratic polynominals.

The transverse displacement function is approximated by distinct polynomials over each of the three zones of the triangular element identified in Figure 91. The basic cubic polynomials may be written symbolically as

$$w^{(j)} = \left\lfloor B_w \right\rfloor \left\{ \gamma^{(j)} \right\} \qquad j = 1, 2, 3. \tag{356}$$

where the mode shape matrix $\left\lfloor B_w \right\rfloor$ is given in Figure 92 and the $\left\{ \gamma^{(j)} \right\}$ are simply the undetermined coefficients.

Interzone continuity requirements impose interdependencies among these undetermined coefficients, yielding

$$\left\{ \gamma^{(j)} \right\} = \left[\Gamma_{\gamma\beta}^{(j)} \right] \left\{ \beta_f \right\} \tag{357}$$

The resulting admissible displacement functions are given by

$$\left\{ w^{(j)} \right\} = \left\lfloor B_w \right\rfloor \left[\Gamma_{\gamma\beta}^{(j)} \right] \left\{ \beta_f \right\} \tag{358}$$

where

$$\left\{ \beta_f \right\}^T = \left\lfloor \beta_{f1}, \beta_{f2}, \cdots, \beta_{f12} \right\rfloor \tag{359}$$

The transformation $\left[\Gamma_{\gamma\beta}^{(j)} \right]$ to independent field coordinate displacement degrees-of-freedom for transverse displacement $\left\{ \beta_f \right\}$ are exhibited in Figures 93 through 95.

$$
\begin{array}{l}
\qquad\qquad \beta_1 \quad \beta_2 \quad \beta_3 \quad \beta_4 \quad \beta_5 \quad \beta_6 \quad \beta_7 \quad \beta_8 \quad \beta_9 \quad \beta_{10} \quad \beta_{11} \quad \beta_{12} \\
\left[B_u \right] = u \left[1 \;,\; x \;,\; y \;,\; x^2 \;,\; x \;,\; y^2 \;,\; \;,\; \;,\; \;,\; \;,\; \;,\; \; \right] \\
\left[B_v \right] = v \left[\;,\; \;,\; \;,\; \;,\; \;,\; \;,\; 1 \;,\; x \;,\; y \;,\; x^2 \;,\; xy \;,\; y^2 \right]
\end{array}
$$

$$
\begin{array}{l}
\qquad\qquad \gamma_1^{(j)} \quad \gamma_2^{(j)} \quad \gamma_3^{(j)} \quad \gamma_4^{(j)} \quad \gamma_5^{(j)} \quad \gamma_6^{(j)} \quad \gamma_7^{(j)} \quad \gamma_8^{(j)} \quad \gamma_9^{(j)} \quad \gamma_{10}^{(j)} \\
\left[B_w \right] = \left[1 \;,\; x \;,\; y \;,\; x^2 \;,\; xy \;,\; y^2 \;,\; x^3 \;,\; x^2y \;,\; xy^2 \;,\; y^3 \right]
\end{array}
$$

$$
\begin{array}{ll}
w_x & \left[1 \quad 2x \quad y \quad 3x^2 \quad 2xy \quad y^2 \right] \\
w_y & \left[1 \quad x \quad 2y \quad x^2 \quad 2xy \quad 3y^2 \right] \\
w_{xx} & \left[2 \quad 6x \quad 2y \right] \\
w_{yy} & \left[2 \quad 2x \quad 6y \right] \\
w_{xy} & \left[1 \quad 2x \quad 2y \right]
\end{array}
$$

Figure 92. Displacement Mode Shape Matrices

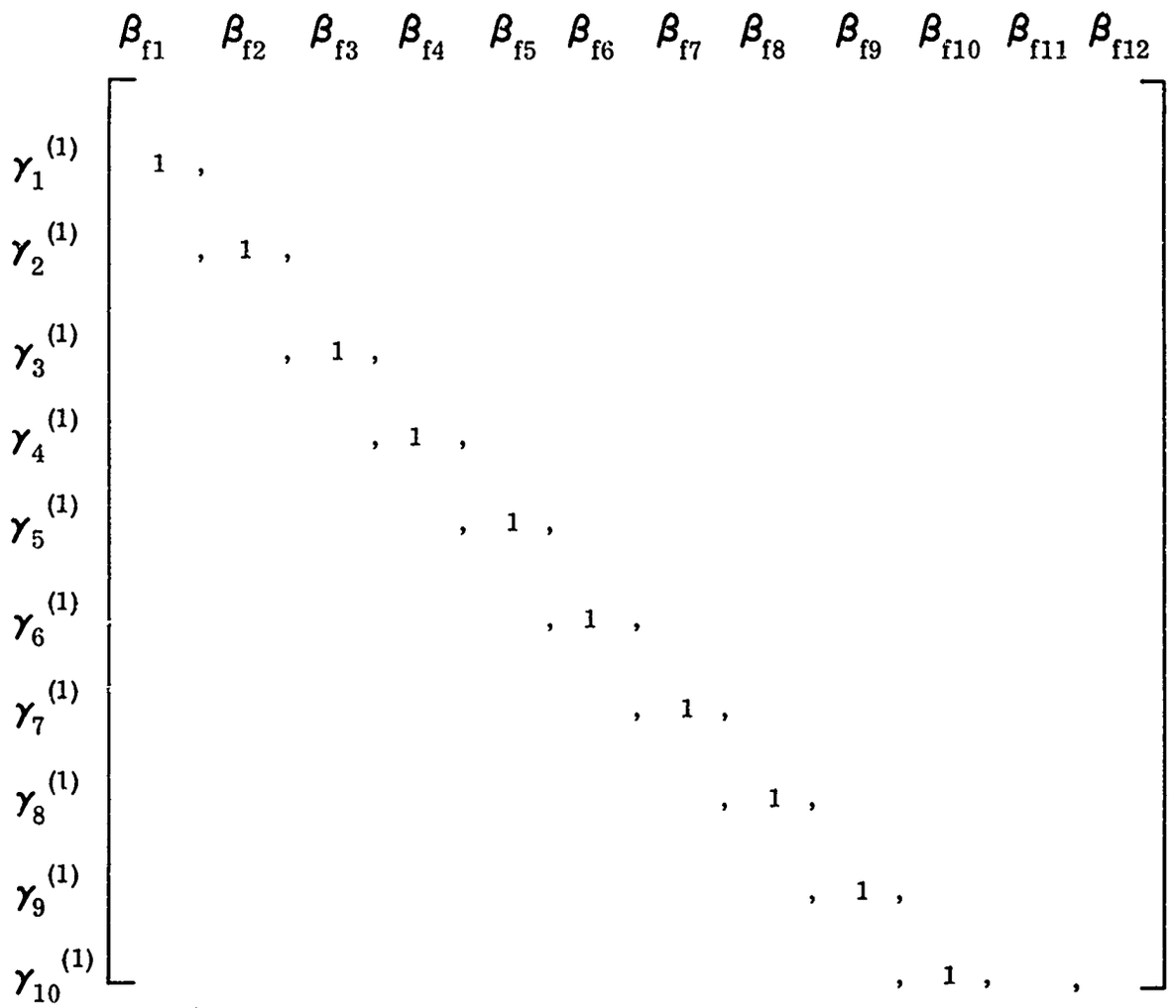

Figure 93. Flexure Displacement Interzone Transformation $\left[\Gamma_{\gamma\beta}^{(1)}\right]$

$$p_2 = \frac{x_2}{y_2} \; ; \; p_3 = \frac{x_3}{y_3}$$

$$\begin{array}{c} \\ \gamma_1^{(2)} \\ \gamma_2^{(2)} \\ \gamma_3^{(2)} \\ \gamma_4^{(2)} \\ \gamma_5^{(2)} \\ \gamma_6^{(2)} \\ \gamma_7^{(2)} \\ \gamma_8^{(2)} \\ \gamma_9^{(2)} \\ \gamma_{10}^{(2)} \end{array} \begin{array}{c} \begin{array}{cccccccccccc} \beta_{f1} & \beta_{f2} & \beta_{f3} & \beta_{f4} & \beta_{f5} & \beta_{f6} & \beta_{f7} & \beta_{f8} & \beta_{f9} & \beta_{f10} & \beta_{f11} & \beta_{f12} \end{array} \\ \left[\begin{array}{cccccccccccc} 1 & , & & & & & & & & & & \\ , & 1 & , & & & & & & & & & \\ & , & 1 & . & & & & & & & & \\ & & . & 1 & , & & & & & & & \\ & & & , & 1 & , & & & & & & \\ & & & & , & 1 & , & & & & & \\ & & & & & & , & . & . & , & . 1 & , \\ & & & & & & , & , & . & , & . & 1 \\ & & & & & & , 3p_3^2 & , 2p_3 & . 1 & , & . -3p_3^2 & , -2p_3 \\ & & & & & & , -2p_3^3 & . -p_3^2 & , & 1 & . 2p_3^3 & . p_3^2 \end{array}\right] \end{array}$$

Figure 94. Flexure Displacement Interzone Transformation $\left[\Gamma_{\gamma\beta}^{(2)}\right]$

Elementary interpolation theory is invoked to obtain transformations from field coordinate to gridpoint $\{\delta\}$ displacement degrees-of-freedom, i.e.

$$\{\beta_m\} = \left[\Gamma_{\beta g}^{(m)}\right] \{\delta_{gm}\} \tag{360}$$

$$\{\beta_f\} = \left[\Gamma_{\beta g}^{(f)}\right] \{\delta_{gf}\} \tag{361}$$

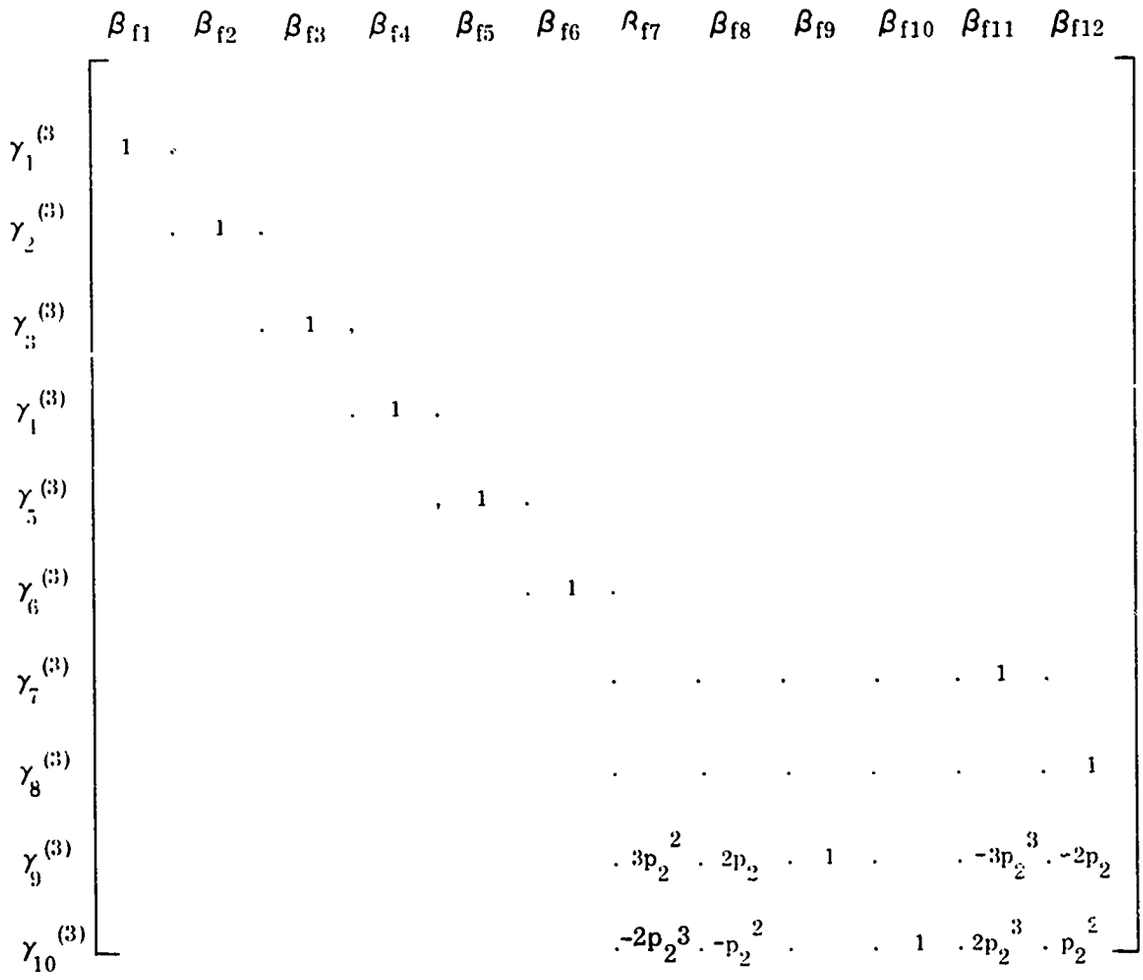

Figure 95. Flexure Displacement Interzone Transformation $\left[\Gamma_{\gamma\beta}^{(3)}\right]$

where

$$\left\{\delta_{gm}\right\}^T = \left[u_{q1}, u_{q2}, u_{q3}, u_{g4}, u_{g5}, u_{g6}, v_{g1}, v_{g2}, v_{g3}, v_{g4}, v_{g5}, v_{g6}\right] \quad (362)$$

$$\left\{\delta_{gf}\right\}^T = \left[w_{g1}, w_{gx1}, w_{gy1}, w_{g2}, w_{gx2}, w_{gy2}, w_{g3}, w_{gx3}, w_{gy3}, w_{n4}, w_{n5}, w_{n6}\right] \quad (363)$$

It is convenient to define the transformation matrices $\left[\Gamma_{\beta_g}{}^{m}\right]^{-1}$ and $\left[\Gamma_{\beta_g}{}^{(f)}\right]^{-1}$ in terms of submatrices by writing

$$\left[\Gamma_{\beta_g}{}^{(m)}\right]^{-1} = \begin{bmatrix} \left[\Gamma_m\right] & & \\ & \ddots & \\ & & \left[\Gamma_m\right] \end{bmatrix} \tag{364}$$

$$\left[\Gamma_{\beta_g}{}^{(f)}\right]^{-1} = \begin{bmatrix} 0 & 0 & \left[B_1\right] \\ \left[B_2\right] & 0 & 0 \\ 0 & \left[B_3\right] & 0 \\ 0 & 0 & \left[B_{12}\right] \\ \left[B_{23}\right] & 0 & 0 \\ 0 & \left[B_{31}\right] & 0 \end{bmatrix} \begin{bmatrix} \left[\Gamma_{\gamma\beta}{}^{(1)}\right] \\ \left[\Gamma_{\gamma\beta}{}^{(2)}\right] \\ \left[\Gamma_{\gamma\beta}{}^{(3)}\right] \end{bmatrix} \tag{365}$$

These submatrices are now given explicit definition in Figures 96 and 97.

At this point, optional transformations are introduced to enable suppression of the midside displacement degrees-of-freedom. This feature provides flexibility in idealization and facilitates consideration of eccentric connections. The transformations take the form

$$\left\{\delta_{gm}\right\} = \left[\Gamma_{sup}{}^{(m)}\right] \left\{\delta'_{gm}\right\} \tag{366}$$

$$\left\{\delta_{gm}\right\} = \left[\Gamma_{sup}{}^{(f)}\right] \left\{\delta'_{gf}\right\} \tag{367}$$

The degrees-of-freedom $\left\{\delta'_{gm}\right\}$ and $\left\{\delta'_{gf}\right\}$ may be interpreted according to Equations 362 and 363. The suppression transformations $\left[\Gamma_{sup}{}^{(m)}\right]$ and $\left[\Gamma_{sup}{}^{(f)}\right]$ are given in Figures 98 and 99.

A transformation related only to flexure is defined to establish a vectorial sign convention for the rotational degrees-of-freedom associated with the three corner gridpoints. In addition, the midside rotations are signed so as to be compatible with adjoining elements. Specifically, they are assigned vectorially positive in the direction from the corner gridpoint with the smaller gridpoint number toward the corner gridpoint with the larger number. This transformation relation is written symbolically as

$$\left\{\delta'_{gf}\right\} = \left[\Gamma_{sgn}{}^{(f)}\right] \left\{\delta''_{gf}\right\} \tag{368}$$

where

$$\left\{\delta''_{gf}\right\} = \left[w_{g1}, \theta_{gx1}, \theta_{gy1}, w_{g2}, \theta_{gx2}, \theta_{gy2}, w_{g3}, \theta_{gx3}, \theta_{gy3}, \theta_{n4}, \theta_{n5}, \theta_{n6} \right] \tag{369}$$

$$
\begin{array}{c|cccccc}
 & 1 & 2 & 3 & 4 & 5 & 6 \\
1 & 1 & x_1 & 0 & x_1^2 & 0 & 0 \\
2 & 1 & x_2 & y_2 & x_2^2 & x_2y_2 & y_2^2 \\
3 & 1 & x_3 & y_3 & x_3^2 & x_3y_3 & y_3^2 \\
4 & 1 & \frac{1}{2}(x_1+x_2) & \frac{1}{2}y_2 & \frac{1}{4}(x_1+x_2)^2 & \frac{1}{4}(x_1+x_2)y_2 & \frac{1}{4}y_2^2 \\
5 & 1 & \frac{1}{2}(x_2+x_3) & \frac{1}{2}(y_2+y_3) & \frac{1}{4}(x_2+x_3)^2 & \frac{1}{4}(x_2+x_3)(y_2+y_3) & \frac{1}{4}(y_2+y_3)^2 \\
6 & 1 & \frac{1}{2}(x_3+x_1) & \frac{1}{2}y_3 & \frac{1}{4}(x_3+x_1)^2 & \frac{1}{4}(x_3+x_1)y_3 & \frac{1}{4}y_3^2
\end{array}
$$

Figure 96. Membrane Displacement Coordinate Transformation $[\Gamma_m]$

$$\left[B_1\right] = \begin{bmatrix} 1 & x_1 & 0 & x_1^2 & 0 & 0 & x_1^3 & 0 & 0 & 0 \\ 0 & 1 & 0 & 2x_1 & 0 & 0 & 3x_1^2 & 0 & 0 & 0 \\ 0 & 0 & 1 & 0 & x_1 & 0 & 0 & x_1^2 & 0 & 0 \end{bmatrix}$$

$$\left[B_3\right] \begin{bmatrix} 1 & x_2 & y_2 & x_2^2 & x_2y_2 & y_2^2 & x_2^3 & x_2^2y_2 & x_2y_2^2 & y_2^3 \\ 0 & 1 & 0 & 2x_2 & y_2 & 0 & 3x_2^2 & 2x_{2y_2} & y_2^2 & 0 \\ 0 & 0 & 1 & 0 & x_2 & 2y_2 & 0 & x_2^2 & 2x_2y_2 & 3y_2^2 \end{bmatrix}$$

$$\left[B_3\right] = \begin{bmatrix} 1 & x_3 & y_3 & x_3^2 & x_3y_3 & y_3^2 & x_3^3 & x_3^2y_3 & x_3y_3^2 & y_3^3 \\ 0 & 1 & 0 & 2x_3 & y_3 & 0 & 3x_3^2 & 2x_3y_3 & y_3^2 & 0 \\ 0 & 0 & 1 & 0 & x_3 & 2y_3 & 0 & x_3^2 & 2x_3y_3 & 3y_3^2 \end{bmatrix}$$

$$\left[B_{12}\right] = \frac{1}{r_{12}} \left[0, -y_2, (x_2 - x_1), -(x_1 + x_2)\, y_2, \frac{1}{2}\left[(x_2^2 - x_1^2) - y_2\right], (x_2 - x_1)\, y_2, -\frac{3}{4}(x_1 + x_2)^2 y_2,\right.$$

$$\left.\left[\frac{1}{4}(x_1 + x_2)^2 (x_2 - x_1) - \frac{1}{2}(x_1 + x_2)\, y_2^2\right], \left[\frac{1}{2}(x_2^2 - x_1^2)\, y_2 - \frac{1}{4} y_2^3\right], \frac{3}{4}(x_2 - x_1)\, y_2^2\right]$$

$$\left[B_{23}\right] = \frac{1}{r_{23}} \left[0, (y_2 - y_3), (x_3 - x_2), (x_2 + x_3)(y_2 - y_3), \frac{1}{2}\left[(x_3^2 - x_2^2) - (y_3^2 - y_2^2)\right], (x_3 - x_2)(y_2 + y_3),\right.$$

$$\frac{3}{4}(x_2 + x_3)^2 (y_2 - y_3), \frac{1}{2}(x_2 + x_3)\left[\frac{1}{2}(x_3^2 - x_2^2) - (y_3^2 - y_2^2)\right], -\frac{1}{2}(y_2 + y_3)\left[(x_2^2 - x_1^2)\right.$$

$$\left.\left. -\frac{1}{2}(y_3^2 - y_2^2)\right], \frac{3}{4}(x_3 - x_2)(y_2 + y_3)^2\right]$$

$$\left[B_{31}\right] = \frac{1}{r_{31}} \left[0, y_3, (x_1 - x_3), (x_3 + x_1)\, y_3, \frac{1}{2}\left[(x_1^2 - x_3^2) + y_3\right], (x_1 - x_3)\, y_3, \frac{3}{4}(x_3 + x_1)^2 y_3,\right.$$

$$\left.\frac{1}{2}(x_3 + x_1)\left[\frac{1}{2}(x_1^2 - x_3^2) + y_3^2\right], \frac{1}{2}\left[(x_1^2 - x_3^2)\, y_3 + \frac{1}{2} y_3^3\right], \frac{3}{4}(x_1 - x_3)\, y_3^2\right]$$

Figure 97. Flexure Displacement Coordinate Transformation $\left[\Gamma_{\beta_g}^{(i)}\right]^{-1}$

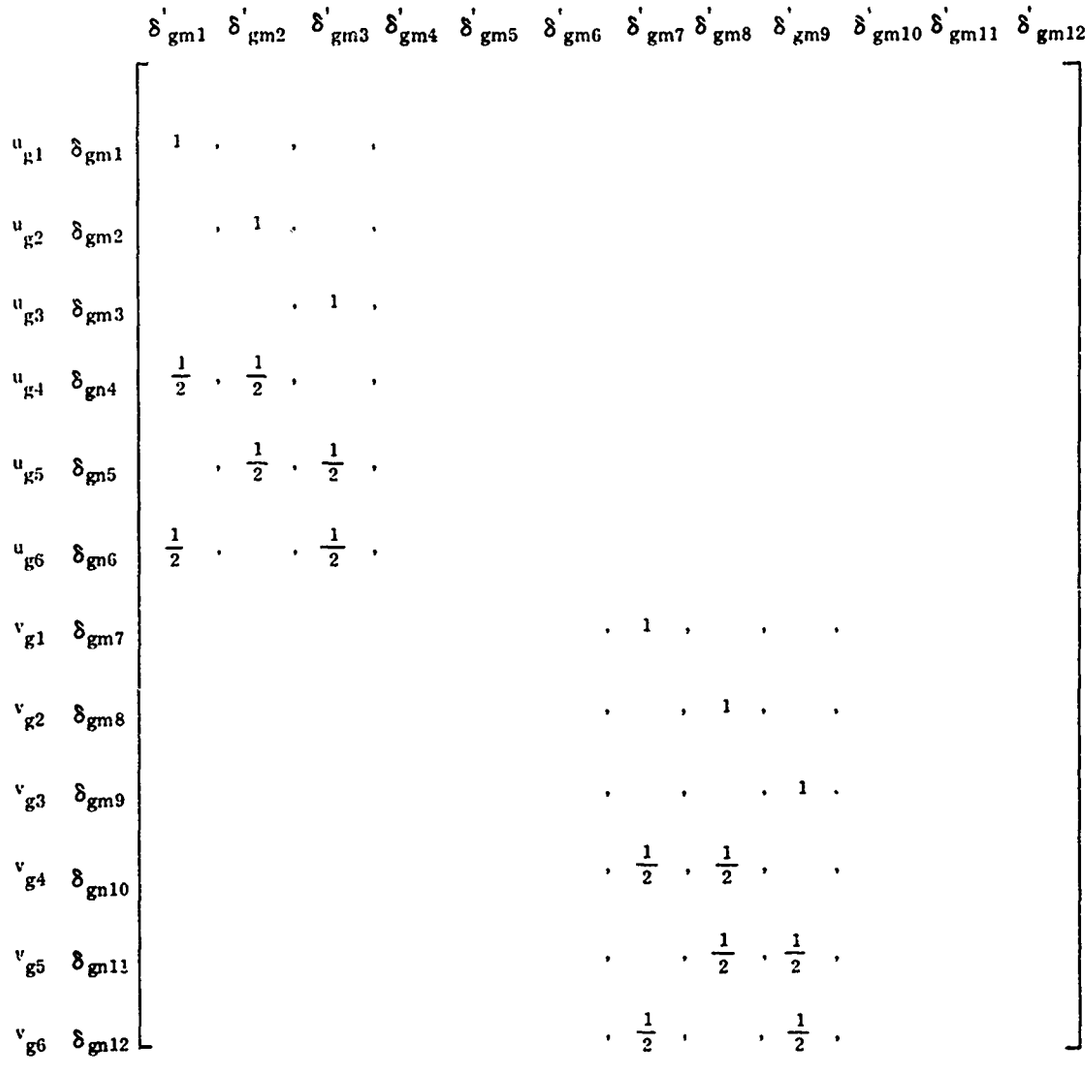

Figure 98. Flexure Displacement Coordinate Transformation $\left[\Gamma_{sup}^{(m)}\right]$

The transformation matrix $\left[\Gamma_{sgm}^{(f)}\right]$ is shown in Figure 100.

The transformation introduced next is designed to enable eccentric connection of the triangular thin shell element to a surface which is a distance e_z above the element. This transformation effects a coupling of the flexure degrees-of-freedom to the membrane displacements and is written as

$$\left\{\delta'_{gm}\right\} = \left[\left[I\right], \left[\Gamma_e\right]\right] \begin{Bmatrix} \left\{\delta''_{gm}\right\} \\ \left\{\delta''_{gf}\right\} \end{Bmatrix} \tag{370}$$

where: $a_j = \frac{x_j + 1 - x_j}{L}$

$b_j = \frac{y_j + 1 - y_j}{L}$

	w_{g1}	w_{gx1}	w_{gy1}	w_{g2}	w_{gx2}	w_{gy2}	w_{g3}	w_{gx3}	w_{gy3}	w_{n4}	w_{n5}	w_{n6}
w_{g1}	1											
w_{gx1}		1										
w_{gy1}			1									
w_{g2}				1								
w_{gx2}					1							
w_{gy2}						1						
w_{g3}							1					
w_{gx3}								1				
w_{gy3}									1			
w_{n4}	0	$+b_j$	$-a_j$	0	$+b_j$	$-a_j$	0	0	0	0	0	0
w_{n5}	0	0	0	0	b_j	$-a_j$	0	b_j	$-a_j$	0	0	0
w_{n6}	0	b_j	$-a_j$	0	0	0	0	b_j	$-a_j$	0	0	0

Figure 99. Flexure Displacement Coordinate Transformation $\left[\Gamma^{(f)}_{sup}\right]$

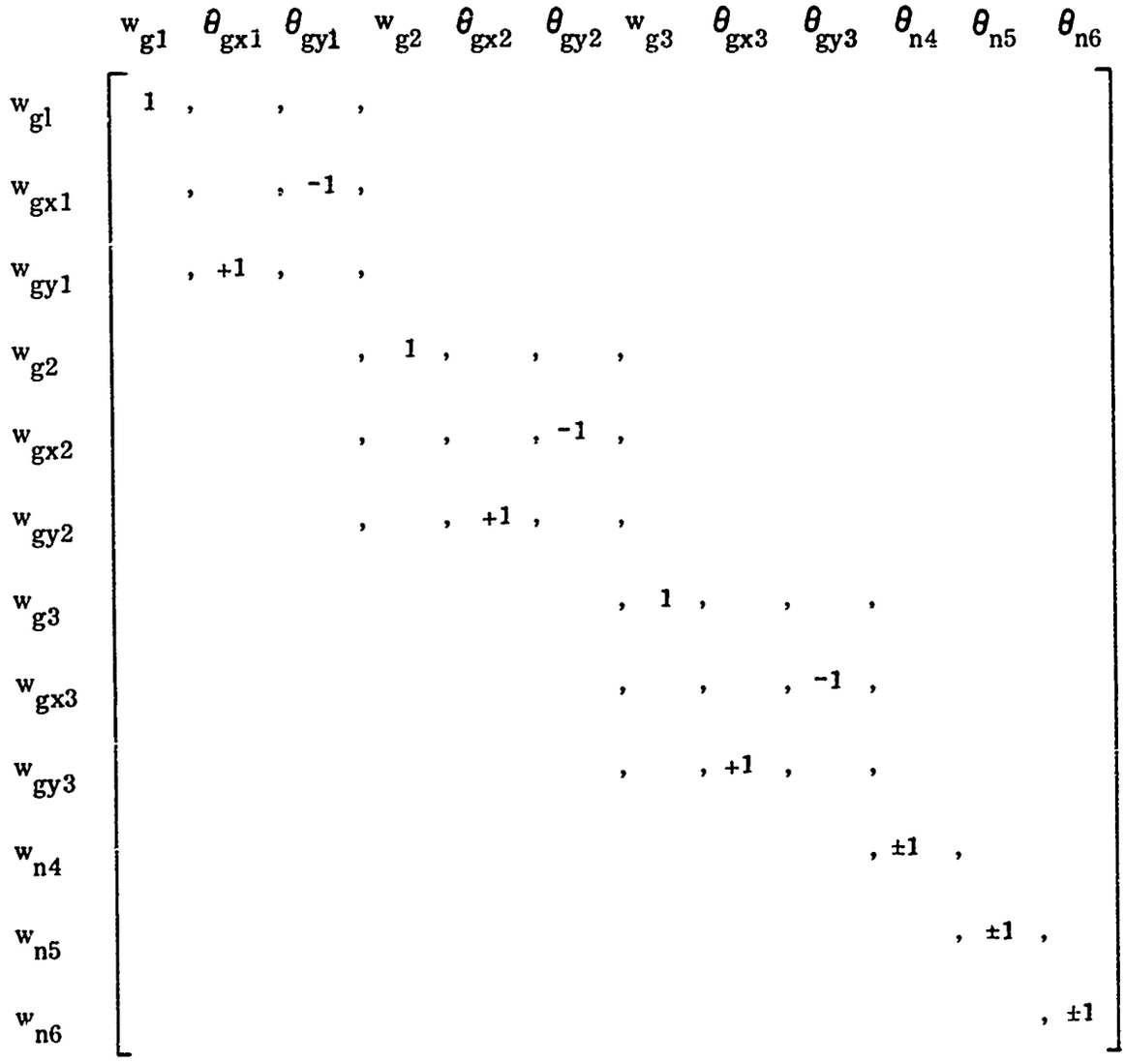

Figure 100. Flexure Displacement Coordinate Transformation $\left[\Gamma_{sgn}^{(f)}\right]$

The degrees-of-freedom $\left\{\delta''_{gm}\right\}$ and $\left\{\delta''_{gf}\right\}$ may be interpreted according to Equations 362 and 369 with the understanding that these quantities now refer to the eccentric gridpoints. The eccentric connection transformation $\left[\Gamma_e\right]$ is given in Figure 101. Note that utilization of this eccentric connection feature requires the presuppression of the midside gridpoint displacement degrees-of-freedom.

Global or "system" displacement degrees-of-freedom are introduced via a further set of transformation relations of the form

$$\left\{\delta''_{gm}\right\} = \left[\Gamma_{gs}^{(m)}\right] \left\{\delta_s\right\} \tag{371}$$

$$\left\{\delta''_{gf}\right\} = \left[\Gamma_{gs}^{(f)}\right] \left\{\delta_s\right\} \tag{372}$$

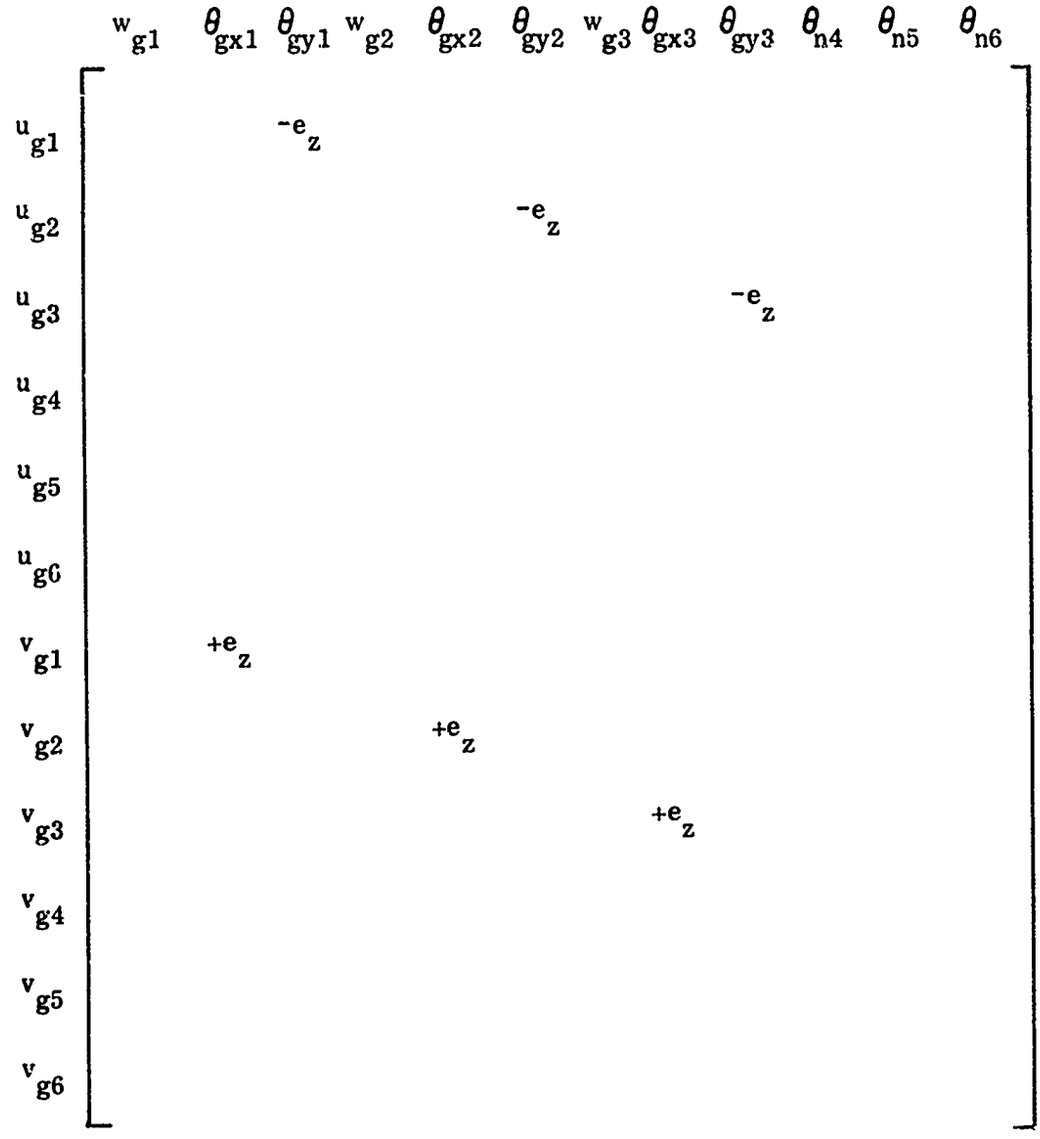

Figure 101. Eccentric Connection Transformation $\left[\Gamma_e \right]$

where

$$\left\{ \delta_s \right\} = \left\lfloor u_{s1}, v_{s1}, w_{s1}, \theta_{sx1}, \theta_{sy1}, \theta_{sz1}, \right. \tag{373}$$

$$u_{s2}, v_{s2}, w_{s2}, \theta_{sx2}, \theta_{sy2}, \theta_{sz2},$$

$$u_{s3}, v_{s3}, w_{s3}, \theta_{sx3}, \theta_{sy3}, \theta_{sz3},$$

$$u_{s4}, v_{s4}, w_{s4}, \theta_{sn4}, \quad 0 , \quad 0 ,$$

$$u_{s5}, v_{s5}, w_{s5}, \theta_{sn5}, \quad 0 , \quad 0 ,$$

$$\left. u_{s6}, v_{s6}, w_{s6}, \theta_{sn6}, \quad 0 , \quad 0 \right\rfloor$$

The matrices $\left[\Gamma_{gs}^{(m)}\right]$ and $\left[\Gamma_{gs}^{(f)}\right]$ which accomplish the transformation to system displacements are given in Figures 102 and 103. These system displacement degrees-of-freedom can be employed to assemble discrete elements; however, in many applications, it is convenient to employ special gridpoint coordinate axes. Accordingly, a final transformation relation is provided to reference the displacement degrees-of-freedom to gridpoint coordinate axes, i.e.

$$\left\{\delta_s\right\} = \left[\Gamma_{sq}\right] \left\{\delta_q\right\} \tag{374}$$

where

$$\begin{aligned}\left\{\delta_q\right\}^T = \Big[& u_{q1}, v_{q1}, w_{q1}, \theta_{qx1}, \theta_{qy1}, \theta_{qz1}, \\ & u_{q2}, v_{q2}, w_{q2}, \theta_{qx2}, \theta_{qy2}, \theta_{qz2}, \\ & u_{q3}, v_{q3}, w_{q3}, \theta_{qx3}, \theta_{qy3}, \theta_{qz3}, \\ & u_{q4}, v_{q4}, w_{q4}, \theta_{qn4}, 0, 0, \\ & u_{q5}, v_{q5}, w_{q5}, \theta_{qn5}, 0, 0, \\ & u_{q6}, v_{q6}, w_{q6}, \theta_{qn6}, 0, 0 \Big]\end{aligned} \tag{375}$$

The matrix $\left[\Gamma_{sg}\right]$ is made up of the individual gridpoint axes direction cosine transformations from the relation

$$\left\{x_s\right\} = \left[T_{sq}\right] \left\{x_q\right\}_j \tag{376}$$

positioned along the major diagonal as shown in Figure 104.

The foregoing transformations may be collected symbolically to obtain a single transformation between the field coordinate displacement degrees-of-freedom $\left\{\beta\right\}$ and the final gridpoint displacement degrees-of-freedom $\left\{\delta_q\right\}$. The results are as follows:

$$\left\{\beta_m\right\} = \left[\Gamma_{\beta q}^{(m)}\right] \left\{\delta_q\right\} \tag{377}$$

$$\left\{\beta_f\right\} = \left[\Gamma_{\beta q}^{(f)}\right] \left\{\delta_q\right\} \tag{378}$$

where

$$\left[\Gamma_{\beta q}^{(m)}\right] = \left[\Gamma_{\beta g}^{(m)}\right] \left[\Gamma_{sup}^{(m)}\right] \left[I\right], \left[\Gamma_e\right] \left[\begin{matrix}\left[\Gamma_{gs}^{(m)}\right], \\ , \left[\Gamma_{gs}^{(f)}\right]\end{matrix}\right] \left[\Gamma_{sq}\right] \tag{379}$$

$$\left[\Gamma_{\beta q}^{(f)}\right] = \left[\Gamma_{\beta g}^{(f)}\right] \left[\Gamma_{sup}^{(f)}\right] \left[\Gamma_{sgn}^{(f)}\right] \left[\Gamma_{gs}^{(f)}\right] \left[\Gamma_{sq}\right] \tag{380}$$

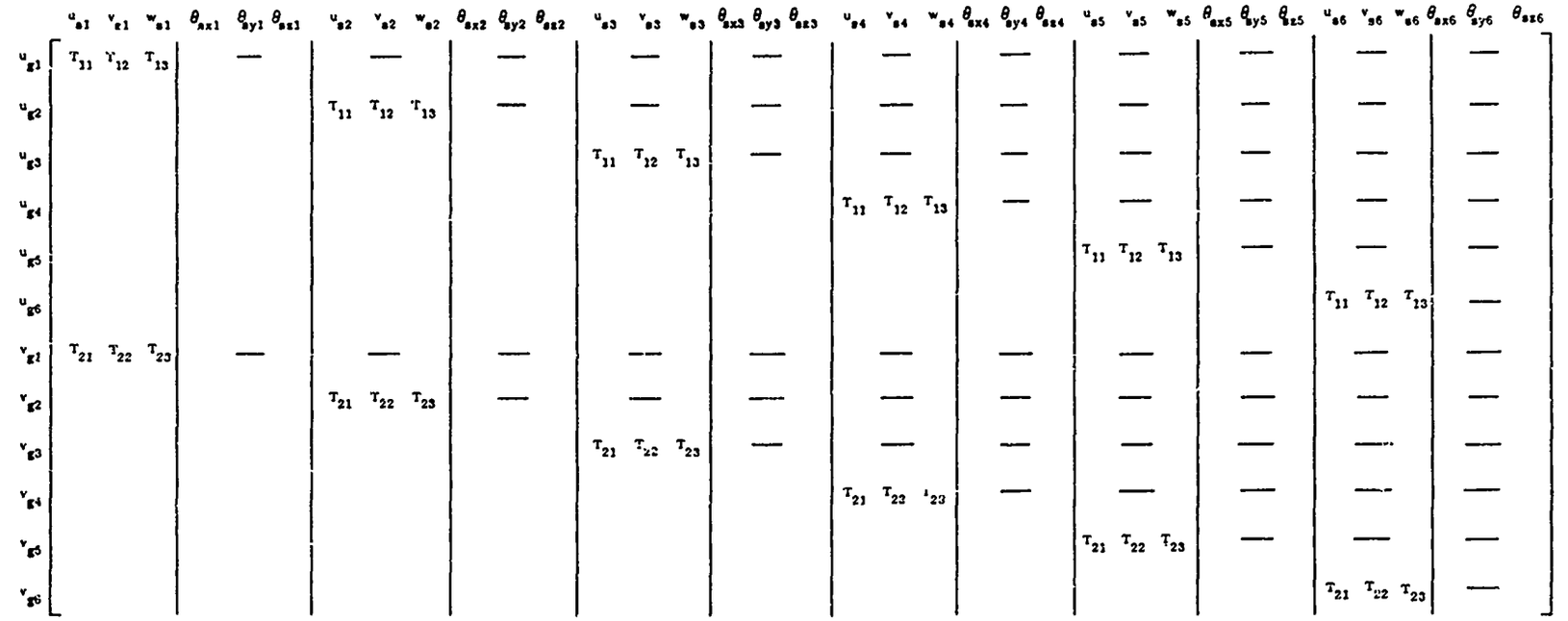

Figure 102. Membrane Displacement Coordinate Transformation $\left[\Gamma_{ge}^{(m)}\right]$

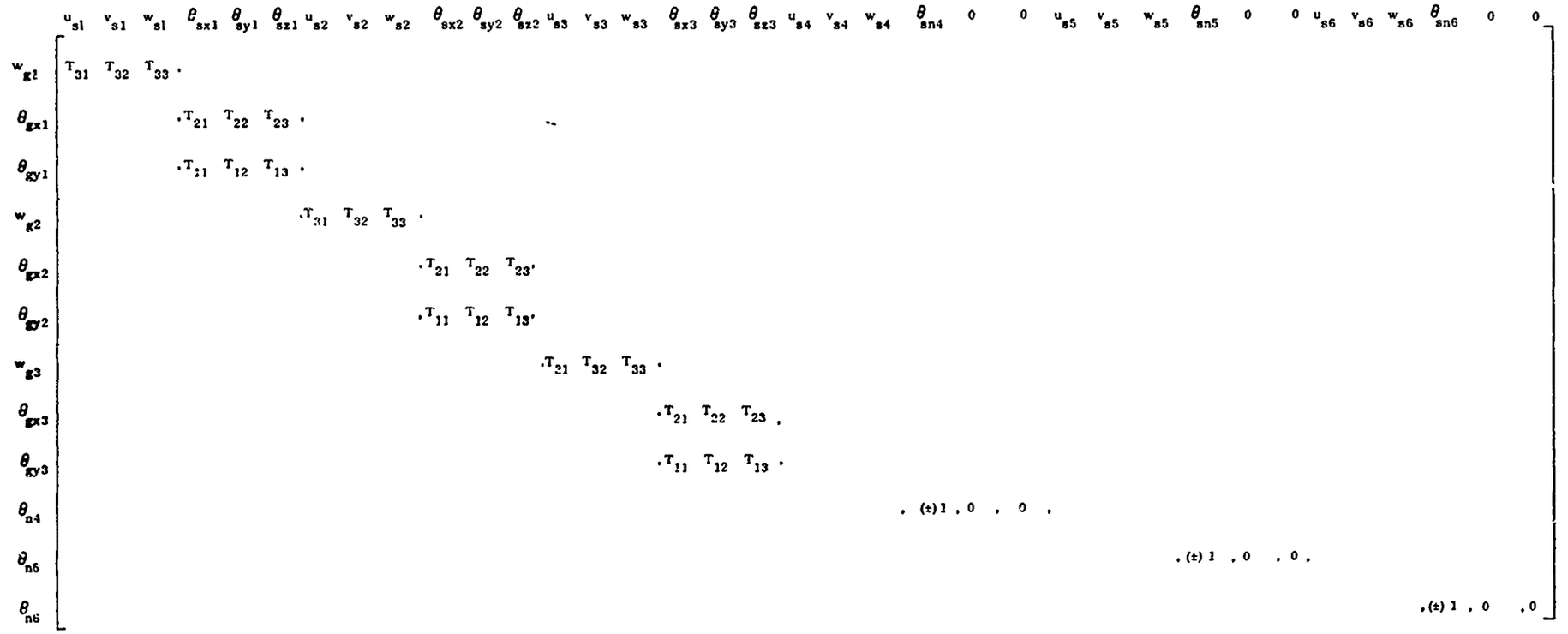

Figure 103. Flexure Displacement Coordinate Transformation $\left[\Gamma_{gs}^{(f)}\right]$

$$
\begin{bmatrix}
\left[T_{sq}\right]_1 & & & & & & & & & & & \\
& \left[T_{sq}\right]_1 & & & & & & & & & & \\
& & \left[T_{sq}\right]_2 & & & & & & & & & \\
& & & \left[T_{sq}\right]_2 & & & & & & & & \\
& & & & \left[T_{sq}\right]_3 & & & & & & & \\
& & & & & \left[T_{sq}\right]_3 & & & & & & \\
& & & & & & \left[T_{sq}\right]_4 & & & & & \\
& & & & & & & \left[I\right] & & & & \\
& & & & & & & & \left[T_{sq}\right]_5 & & & \\
& & & & & & & & & \left[I\right] & & \\
& & & & & & & & & & \left[T_{sq}\right]_6 & \\
& & & & & & & & & & & \left[I\right]
\end{bmatrix}
$$

Figure 104. Displacement Coordinate Transformation $\left[\Gamma_{sq}\right]$

This completes the explicit statement of the displacement functions constructed for the Helle triangular thin shell element.

2. Potential Energy

The total potential energy functional appropriate to thin shells of zero curvature was stated in Equations 289 through 292 in terms of four contributions, i.e.

$$\Phi_m = \int_A \left(\frac{t}{2} \left[e_u^{(g)}\right] \left[E^{(g)}\right] \left\{e_u^{(g)}\right\} - t \left[e_u^{(g)}\right] \left\{\epsilon_{mi}^{(g)}\right\} \right) dA \qquad (381)$$

$$\Phi_f = \int_A \left(\frac{1}{2} \left(\frac{t^3}{12}\right) \left[K^{(g)}\right] \left[E^{(g)}\right] \left\{K^{(g)}\right\} - \left(\frac{t^3}{12}\right) \left[K^{(g)}\right] \left\{\bar{\epsilon}_{fi}^{(g)}\right\} \right) dA \qquad (382)$$

$$\Phi_c = \int_A \left(t \left[e_u^{(g)} \right] \left[E^{(g)} \right] \left\{ e_w^{(g)} \right\} \right) dA \tag{383}$$

$$\Phi_p = \int_A \left(p_z w^{(g)} \right) dA \tag{384}$$

Accepting the foregoing statement of the total potential energy function as the point of departure, the first step is executed primarily for notational convenience. The strains are written in terms of the displacement functions via the relations

$$\left\{ e_u^{(g)} \right\}^T = \left\{ \Delta_{mu} \right\}^T \left[T_u \right]^T = \left[u_x, u_y, v_x, v_y \right] \begin{bmatrix} 1, & 0, & 0 \\ 0, & 0, & 1 \\ 0, & 0, & 1 \\ 0, & 1, & 0 \end{bmatrix} \tag{385}$$

$$\left\{ e_w^{(g)} \right\}^T = \left\{ \Delta_{mw} \right\}^T \equiv \left[\frac{1}{2} w_x^2, \frac{1}{2} w_y^2, w_x w_y \right] \tag{386}$$

$$\left\{ K^{(g)} \right\}^T = \left\{ \Delta_{fw} \right\}^T \equiv \left[-w_{xx}, -w_{yy}, -2w_{xy} \right] \tag{387}$$

The potential energy functional contributions for the triangular thin shell element are now written in analogy with those for the quadrilateral thin shell element as

$$\Phi_m = \int_A \left(\frac{1}{2} \left[\Delta_{mu} \right] \left[I_{mk} \right] \left\{ \Delta_{mu} \right\} - \left[\Delta_{mu} \right] \left\{ I_{m\epsilon} \right\} \right) dA \tag{388}$$

$$\Phi_f = \int_A \left(\frac{1}{2} \left[\Delta_{fw} \right] \left[I_{fk} \right] \left\{ \Delta_{fw} \right\} - \left[\Delta_{fw} \right] \left\{ I_{fw} \right\} \right) dA \tag{389}$$

$$\Phi_c = \int_A \left(\left[\Delta_{mw} \right] \left[I_n \right] \left\{ \Delta_{fw} \right\} \right) dA \tag{390}$$

$$\Phi_p = \int_A \left(p_z w \right) dA \tag{391}$$

where

$$\left[I_{mk} \right] = t \left[T_u \right]^T \left[T_{\epsilon\sigma} \right]^T \left[E^{(m)} \right] \left[T_{\epsilon\sigma} \right] \left[T_u \right] \tag{392}$$

$$\left\{ I_{m\epsilon} \right\} = t \left[T_u \right]^T \left[T_{\epsilon\sigma} \right]^T \left[E^{(m)} \right] \left\{ \epsilon_{mi}^{(m)} \right\} \tag{393}$$

$$\left[I_{fk} \right] = \frac{t^3}{12} \left[T_{\epsilon\sigma} \right]^T \left[E^{(m)} \right] \left[T_{\epsilon\sigma} \right] \tag{394}$$

$$\left[l_{f\epsilon} \right] = \frac{t^3}{12} \left[T_{\epsilon\sigma} \right]^T \left[E^{(m)} \right] \left\{ \epsilon_{fi}^{(m)} \right\} \tag{395}$$

$$\left[I_c \right] = t \left[T_u \right]^T \left[T_{\epsilon\sigma} \right]^T \left[E^{(m)} \right] \left[T_{\epsilon\sigma} \right] \tag{396}$$

The next step in constructing the element representation is to effect the discretization by introduction of the previously derived displacement mode shapes into Equations 385, 386, and 387. This substitution yields

$$\left\{ \Delta_{mu} \right\} = \left[D_m \right] \left\{ \beta_m \right\} \tag{397}$$

$$\left\{ \Delta_f \right\} = \left[D_f \right] \left\{ \gamma^{(k)} \right\} \tag{398}$$

The matrices $\left[D_m \right]$ and $\left[D_f \right]$ are presented in Figures 105 and 106. The vector $\left\{ \Delta_{mw} \right\}$ is a quadratic function of the coordinates $\left\{ \gamma \right\}$ and symbolic representation is not attempted at this point.

Algebraic statement of the membrane energy contribution of Equation 388 is considered first. Examination of the component relations of Equation 397 leads to identification of a typical form for each element of the vector $\left\{ \Delta_{mh} \right\}$, i.e.

$$\left(\Delta_{mu} \right)_\ell = \left\lfloor d \right\rfloor \left\lceil c_m \right\rfloor_\ell \left\{ \alpha_m \right\}_\ell \tag{399}$$

where

$$\left\{ d \right\}^T = \left\lfloor 1, x, y, \right\rfloor \tag{400}$$

For example, focusing upon the first term ($\ell = 1$) obtain,

$$\left(\Delta_{mu} \right)_\ell = u_x = \left\lfloor 1, x, y. \right\rfloor \begin{bmatrix} 1, & & \\ & , 2, & \\ & & , 1 \end{bmatrix} \begin{Bmatrix} \beta_{m2} \\ \beta_{m4} \\ \beta_{m5} \end{Bmatrix} \tag{401}$$

Explicit statement of all of these $\left\lceil c_m \right\rfloor$ and $\left\lceil \alpha_m \right\rfloor$ matrices is given in Figure 107.

The general form identified with the elements of the vector $\left\{ \Delta_{mu} \right\}$ leads naturally to a general form for the associated energy contributions. Firstly, the membrane energy functional is rewritten as

$$\Phi_m = \sum_{i=1}^{4} \sum_{j=1}^{4} \left(\phi_m \right)_{ij} \tag{402}$$

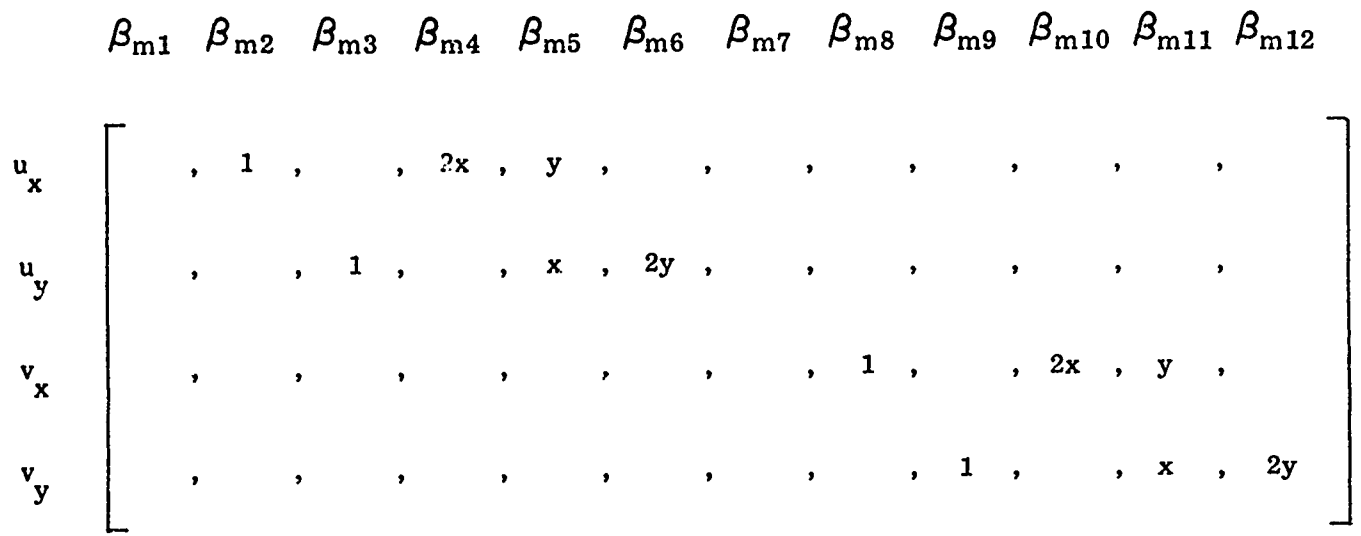

Figure 105. Membrane Displacement Derivatives Matrix $[D_m]$

$$
\begin{array}{c}
 \\
-w_{xx} \\
-w_{yy} \\
-2w_{xy}
\end{array}
\begin{array}{c}
\begin{array}{cccccccccc}
\gamma_1 & \gamma_2 & \gamma_3 & \gamma_4 & \gamma_5 & \gamma_6 & \gamma_7 & \gamma_8 & \gamma_9 & \gamma_{10}
\end{array} \\
\left[\begin{array}{cccccccccc}
, & , & , & -2 & , & , & -6x & -2y & , & , \\
, & , & , & , & , & -2 & , & , & -2x & -6y \\
, & , & , & , & -2 & , & , & -4x & -4y & ,
\end{array}\right]
\end{array}
$$

Figure 106. Flexure Displacement Derivatives Matrix $\left[D_f\right]$

$$
\left\{\alpha_m^{(1)}\right\}^T = \left[\beta_{m2}\ ,\ \beta_{m4}\ ,\ \beta_{m5}\right]
$$
$$
\left\{\alpha_m^{(2)}\right\}^T = \left[\beta_{m3}\ ,\ \beta_{m5}\ ,\ \beta_{m6}\right]
$$
$$
\left\{\alpha_m^{(3)}\right\}^T = \left[\beta_{m8}\ ,\ \beta_{m10},\ \beta_{m11}\right]
$$
$$
\left\{\alpha_m^{(4)}\right\}^T = \left[\beta_{m9}\ ,\ \beta_{m11},\ \beta_{m12}\right]
$$

$$
\left[c_m^{(1)}\right] = \left[1\ ,\ 2\ ,\ 1\right]
$$
$$
\left[c_m^{(2)}\right] = \left[1\ ,\ 1\ ,\ 2\right]
$$
$$
\left[c_m^{(3)}\right] = \left[1\ ,\ 2\ ,\ 1\right]
$$
$$
\left[c_m^{(4)}\right] = \left[1\ ,\ 1\ ,\ 2\right]
$$

Figure 107. Definition of Notation, $\left\{\alpha_m^{(\ell)}\right\}$ and $\left[c_m^{(\ell)}\right]$

$$\delta_{ij} = \sum_{\ell=1}^{3} \delta_{ij}^{(\ell)}$$

Zone $\ell = 1$:

$$\delta_{ij}^{(1)} = \int_{x_3}^{x_2} \int_{k_{30}x}^{k_{32}x + m_{32}} x^i y^j \, dy \, dx + \int_{x_2}^{0} \int_{k_{30}x}^{k_{20}x} x^i y^j \, dy \, dx$$

Zone $\ell = 2$:

$$\delta_{ij}^{(2)} = \int_{x_3}^{0} \int_{k_{31}x + m_{31}}^{k_{30}x} x^i y^j \, dy \, dx + \int_{0}^{x_1} \int_{k_{31}x + m_{13}}^{0} x^i y^j \, dy \, dx$$

Zone $\ell = 3$:

$$\delta_{ij}^{(3)} = \int_{0}^{x_2} \int_{0}^{k_{20}x} x^i y^j \, dy \, dx + \int_{x_2}^{x_1} \int_{k_{21}x + m_{21}}^{0} x^i y^j \, dy \, dx$$

where:

$$k_{21} = \frac{-y_2}{x_1 - x_2}, \quad k_{32} = \frac{y_2 - y_3}{x_2 - x_3}, \quad k_{20} = \frac{y_2}{x_2}, \quad k_{31} = \frac{-y_3}{x_1 - x_3}$$

$$m_{31} = \frac{x_1 y_3}{x_1 - x_3}, \quad m_{21} = \frac{x_1 y_2}{x_1 - x_2}, \quad m_{32} = \frac{x_2 y_3 - y_2 x_3}{x_2 - x_3}$$

Figure 108. Definition of Integral Notation, $\delta_{ij}^{(k)}$

where
$$\left(\phi_m\right)_{ij} = \int_A \left[\frac{1}{2}\left(I_{mk}\right)_{ij}\left(\Delta_{mu}\right)_i\left(\Delta_{mu}\right)_j - \left(I_{m\epsilon}\right)_i\left(\Delta_{mu}\right)_i\right] dx\, dy \tag{403}$$

The general contributing energy form now follows directly by introducing the general form for the elements defined in Equation 401, i.e.

$$\left(\phi_m\right)_{ij} = \frac{1}{3}\left(I_{mk}\right)_{ij}\left[\alpha_m\right]_i\left[c_m\right]_i\left[c_{mk}\right]\left[c_m\right]_j\left\{\alpha_m\right\}_j - \left(I_{m\epsilon}\right)_i\left[\alpha_m\right]_i\left[c_m\right]_i\left\{c_{m\epsilon}\right\} \tag{404}$$

where
$$\left[c_{mk}\right] = \int_A \left\{d\right\}\left[d\right] dx\, dy \tag{405}$$

$$\left[c_{m\epsilon}\right] = \int_A \left\{d\right\} dx\, dy \tag{406}$$

Presentation of these matrices is prefaced by definitions of notation in Figure 108. Then, $\left[c_{mk}\right]$ and $\left[c_{m\epsilon}\right]$ are given in Figure 109. The knowledge of these matrices, together with the statements of the $\left[c_{mk}\right]$ and $\left\{\alpha_m\right\}$ matrices, enables explicit expression of each of the $\left(\phi_m\right)_{ij}$. These individual contributions are summed to obtain the objective algebraic expression for the total membrane potential energy, i.e.

$$\Phi_m = \frac{1}{2}\left[\beta_m\right]\left[\tilde{K}_m\right]\left\{\beta_m\right\} - \left[\beta_m\right]\left\{\tilde{F}_{m\epsilon}\right\} \tag{407}$$

The matrix $\left[\tilde{K}_m\right]$ is the element membrane stiffness matrix and the vector $\left\{\tilde{F}_{m\epsilon}\right\}$ is the element membrane prestrain load representation. As disclosed by the notation, both of these are referenced to the field coordinate displacement degrees-of-freedom. Explicit statement of these matrices is considered redundant since they are simply the assembled results of known contributions.

It is convenient to define a special prestrain vector for thermal loading. This is easily accomplished by rewriting Equation 393 to read

$$\left\{I_{m\epsilon}\right\} = \Delta T_m\, t\left[T_u\right]^T\left[T_{\epsilon\sigma}\right]^T\left[E^{(m)}\right]\left[\alpha^{(m)}\right] \tag{408}$$

The objective algebraic statement of the element flexural potential energy follows in analogy with the development for the element membrane potential energy. Examination of the component relations of Equation 398 leads to identification of a typical form for each element of the vector $\left\{\Delta_f\right\}$, i.e.

$$\left[C_{mk}\right] = \begin{bmatrix} \delta_{00} , & \delta_{10} , & \delta_{01} \\ \delta_{10} , & \delta_{20} , & \delta_{11} \\ \delta_{01} , & \delta_{11} , & \delta_{02} \end{bmatrix}$$

$$\left\{C_{m\epsilon}\right\} = \left\lfloor \delta_{00} , \delta_{10} , \delta_{01} \right\rfloor$$

Figure 109. Definition of Notation, $\left[C_{mk}\right]$ and $\left\{C_{m\epsilon}\right\}$

$$\left(\Delta_f\right)_{\ell}^{(k)} = \left\lfloor d \right\rfloor \left[c_f\right]_{\ell}^{(k)} \left\{a_f\right\}_{\ell}^{(k)} \tag{409}$$

For example, focusing on the first zone (k = 1), the first element (ℓ = 1) is given by

$$\left(\Delta_f\right)_1^{(1)} = -w_{xx}^{(1)} = \left\lfloor 1, x, y \right\rfloor \begin{bmatrix} -2, & & \\ & -6, & \\ & & -2 \end{bmatrix} \begin{Bmatrix} \gamma_4 \\ \gamma_7 \\ \gamma_8 \end{Bmatrix} \tag{410}$$

Explicit statement of all these $\left[c_f\right]$ and $\left[a_f\right]$ matrices is given in Figure 110. It should be noted that these matrices are common to the three zones of the element.

Having defined the foregoing quantities, the flexure energy is accountably rewritten, i.e.

$$\Phi_f = \sum_{k=1}^{3} \sum_{i=1}^{3} \sum_{j=1}^{3} \left(\phi_f\right)_{ij}^{(k)} \tag{411}$$

where

$$\left(\phi_f\right)_{ij}^{(k)} = \int_{\text{zone k}} \frac{1}{2} \left(I_{fk}\right)_{ij}^{(k)} \left(\Delta_f\right)_i^{(k)} \left(\Delta_f\right)_j^{(k)} - \left(I_{f\epsilon}\right)_i \left(\Delta_f\right)_i^{(k)} \Big] \, dx \, dy \tag{412}$$

The general contributing energy form now follows directly by introducing the general form for the elements of $\left\{\Delta_f\right\}$ defined in Equation 410, i.e.

$$\left(\phi_c\right)_{ij}^{(k)} = \frac{1}{2} \left(I_{fk}\right)_{ij} \left\lfloor a_f \right\rfloor_i^{(k)} \left[c_f\right]_i \left[c_{fk}\right]^{(k)} \left[c_f\right]_j \left\{a_f\right\}_j^{(k)} - \left(I_{f\epsilon}\right)_i \left\lfloor a_f \right\rfloor_i^{(k)} \left[c_f\right]_i \left\{c_{f\epsilon}\right\}^{(k)} \tag{413}$$

$$\left\{ a_f^{(1)} \right\}^T = \left\lfloor \gamma_4 \ , \gamma_7 \ , \gamma_8 \right\rfloor$$

$$\left\{ a_f^{(2)} \right\}^T = \left\lfloor \gamma_6 \ , \gamma_9 \ , \gamma_{10} \right\rfloor$$

$$\left\{ a_f^{(3)} \right\}^T = \left\lfloor \gamma_5 \ , \gamma_8 \ , \gamma_9 \right\rfloor$$

$$\left\lceil c_f^{(1)} \right\rfloor = \left\lceil -2 \ , -6 \ , -2 \right\rfloor$$

$$\left\lceil c_f^{(2)} \right\rfloor = \left\lceil -2 \ , -2 \ , -6 \right\rfloor$$

$$\left\lceil c_f^{(3)} \right\rfloor = \left\lceil -2 \ , -4 \ , -4 \right\rfloor$$

Figure 110. Definition of Notation, $\left\lceil C_{fw}^{(\ell)} \right\rfloor$ and $\left\{ a_{fw}^{(\ell)} \right\}$

Particularization of this general form to the individual $\left\lceil c_f \right\rfloor$, $\left\{ a_c \right\}$, $\left[c_{fk} \right]$ and $\left\{ c_f \right\}$ matrices and summation yields an algebraic expression for the element flexural potential energy associated with the k^{th} zone, i.e.

$$\Phi_f^{(k)} = \frac{1}{2} \left\lfloor \gamma \right\rfloor^{(k)} \left[\hat{K}_f \right]^{(k)} \left\{ \gamma \right\}^{(k)} - \left\lfloor \gamma \right\rfloor^{(k)} \left\{ \hat{F}_{f\epsilon} \right\}^{(k)} \tag{414}$$

Substitution from Equation 357 brings in the field coordinate displacement degrees-of-freedom

$$\Phi_f^{(k)} = \frac{1}{2} \left\lfloor \beta_f \right\rfloor \left[\Gamma_{\gamma\beta}^{(k)} \right]^T \left[\hat{K}_f \right]^{(k)} \left[\Gamma_{\gamma\beta}^{(k)} \right] \left\{ \beta_f \right\} - \left\lfloor \beta_f \right\rfloor \left[\Gamma_{\gamma\beta}^{(k)} \right]^T \left\{ \hat{F}_{f\epsilon} \right\}^{(k)} \tag{415}$$

A final summation over the three zones yields the flexure stiffness $\left[\tilde{K}_f \right]$ and pre-strain load $\left\{ \tilde{F}_{f\epsilon} \right\}$ matrices referenced to field coordinate displacement degrees-of-freedom. This result is written

$$\Phi_f = \frac{1}{2} \left[\beta_f\right] \left[\tilde{K}_f\right] \left\{\beta_f\right\} - \left[\beta_f\right] \left\{\tilde{F}_{f\epsilon}\right\} \tag{416}$$

As in the case of the membrane prestrain load vector, the flexural prestrain load vector is particularized for thermal loading. The desired modification follows immediately from Equation 395, i.e.

$$\left\{I_{f\epsilon}\right\} = \Delta T_f \frac{t^3}{12} \left[T_{\epsilon\sigma}\right]^T \left[E^{(m)}\right] \left\{\alpha^{(m)}\right\} \tag{417}$$

The final element matrix which arises from the potential energy is the pressure load matrix. The external work term of Equation 389 is expanded in terms of the displacement mode shape for the ℓ^{th} zone to yield

$$W = p_z \int_{A_\ell} \left[\alpha^{(\ell)}\right] \left\{B_w\right\} dA_\ell \tag{418}$$

Integrating this expression obtain

$$W = \left[\gamma^{(\ell)}\right] \left\{\hat{F}_p^{(\ell)}\right\} \tag{419}$$

where $\left\{\hat{F}_p\right\}$ is given in Figure 111. Summation over the three zones is accomplished with the introduction of Equation 357. The result is an expression for the external work which contains the pressure load vector $\left\{\tilde{F}_p\right\}$ referenced to field coordinate displacement degrees-of-freedom

$$W = \left[\beta_f\right] \left\{\tilde{F}_p\right\} \tag{420}$$

$$\left\{F^{(l)}\right\}^T = \left[\delta_{00}^{(l)}, \delta_{10}^{(l)}, \delta_{01}^{(l)}, \delta_{20}^{(l)}, \delta_{11}^{(l)}, \delta_{02}^{(l)}, \delta_{30}^{(l)}, \delta_{21}^{(l)}, \delta_{12}^{(l)}, \delta_{03}^{(l)}\right]$$

Figure 111. Pressure Load Vector

3. Stress Matrices

The stress resultants for a thin shell of zero curvature are defined, in the notation of Figure 80, as follows:

$$N_x = \int_z \sigma_x \, dz \qquad N_y = \int_z \sigma_y \, dz \qquad N_{xy} = \int_z \tau_{xy} \, dz \tag{421}$$

$$M_x = \int_z z\sigma_x \, dz \qquad M_y = \int_z x\sigma_y \, dz \qquad M_{xy} = \int_z z\tau_{xy} \, dz \tag{422}$$

$$Q_x = \int_z z \left(\frac{\partial \sigma_x}{\partial x} + \frac{\partial \tau_{xy}}{\partial y} \right) dz \qquad Q_y = \int_z z \left(\frac{\partial \sigma_y}{\partial y} + \frac{\partial \tau_{xy}}{\partial x} \right) dz \tag{423}$$

It was tacitly assumed in defining the stress resultants that nonlinear membrane-flexure coupling contributions to the stress resultants are small relative to first order terms. This assumption is carried forward in writing the stress resultants in terms of the strains

$$\left\{ N_\sigma^{(g)} \right\} = t \left[E^{(g)} \right] \left\{ e_u^{(g)} \right\} - t \left\{ \bar{\epsilon}_{mi}^{(g)} \right\} \tag{424}$$

$$\left\{ M_\sigma^{(g)} \right\} = \frac{t^3}{12} \left[E^{(g)} \right] \left\{ K^{(g)} \right\} - \frac{t^3}{12} \left\{ \bar{\epsilon}_{fi}^{(g)} \right\} \tag{425}$$

$$\left\{ Q_\sigma^{(g)} \right\} = \frac{t^3}{12} \left[G1 \right] \left[E^{(g)} \right] \left\{ \frac{\partial}{\partial x_g} \left\{ K^{(g)} \right\} \right\} + \frac{t^3}{12} \left[G2 \right] \left[E^{(g)} \right] \left\{ \frac{\partial}{\partial y_g} \left\{ K^{(g)} \right\} \right\} \tag{426}$$

where

$$\left[G1 \right] = \begin{bmatrix} 1, & 0, & 0 \\ 0, & 0, & 1 \end{bmatrix} \tag{427}$$

$$\left[G2 \right] = \begin{bmatrix} 0, & 0, & 1 \\ 0, & 1, & 0 \end{bmatrix} \tag{428}$$

The stress resultants are expressed in terms of the displacement functions by substitution from Equations 383 and 384.

$$\left\{ N_\sigma^{(g)} \right\} = t \left[E^{(g)} \right] \left[T_u \right] \left\{ \Delta_{mu} \right\} - t \left\{ \bar{\epsilon}_{mi}^{(g)} \right\} \tag{429}$$

$$\left\{ M_\sigma^{(g)} \right\} = \frac{t^3}{12} \left[E^{(g)} \right] \left\{ \Delta_{fw} \right\} - \frac{t^3}{12} \left\{ \bar{\epsilon}_{fi}^{(g)} \right\} \tag{430}$$

$$\left\{ Q_\sigma^{(g)} \right\} = \frac{t^3}{12} \left[G1 \right] \left[E^{(g)} \right] \left\{ \frac{\partial}{\partial x_g} \left\{ \Delta_{fw} \right\} \right\} + \frac{t^3}{12} \left[G2 \right] \left[E^{(g)} \right] \left\{ \frac{\partial}{\partial y_g} \left\{ \Delta_{fw} \right\} \right\} \tag{431}$$

Introducing the displacement mode shapes assumed over the three zones of the triangular thin shell element, the stress resultants can be written collectively as

$$\left\{N_\sigma^{(g)}\right\} = \left[\tilde{S}_N\right] \left\{\beta_m\right\} - \left\{\delta_m\right\} \tag{432}$$

and

$$\begin{Bmatrix} M_\sigma \\ Q_\sigma \end{Bmatrix} = \begin{bmatrix} \tilde{S}_M \\ \tilde{S}_Q \end{bmatrix} \left\{\beta_f\right\} - \begin{Bmatrix} \delta_f \\ 0 \end{Bmatrix} \tag{433}$$

where

$$\left[\tilde{S}_N\right] = t \left[E^{(g)}\right] \left[T_u\right] \left[D_m\right] \tag{434}$$

$$\left[\tilde{S}_M^{(\ell)}\right] = \frac{t^3}{12} \left[E^{(g)}\right] \left[D_f\right] \left[\Gamma_{\sigma\beta}^{(\ell)}\right] \tag{435}$$

$$\left[\tilde{S}_Q^{(\ell)}\right] = \frac{t^3}{12} \left[G1\right] \left[E^{(g)}\right] \left[\frac{\partial}{\partial x_g}\left[D_f\right]\right] \left[\Gamma_{\sigma\beta}^{(\ell)}\right] + \frac{t^3}{12} \left[G2\right] \left[E^{(g)}\right] \left[\frac{\partial}{\partial y_g}\left[D_f\right]\right] \left[\Gamma_{\sigma\beta}^{(\ell)}\right] \tag{436}$$

$$\left\{\delta_N\right\} = - t \left\{\bar{\epsilon}_{mi}^{(g)}\right\} \tag{437}$$

$$\left\{\delta_M\right\} = - \frac{t^3}{12} \left\{\bar{\epsilon}_{fi}^{(g)}\right\} \tag{438}$$

This completes the statement of the matrices which comprise the Helle triangular thin shell element.

C. EVALUATION

1. Membrane Stress Analysis

The first illustration which utilizes the triangular thin shell element in a structural evaluation will be the following. A thin square isotropic plate loaded with a self equilibrating parabolic membrane load is shown in Figure 112 along with its material properties and pertinent geometric data.

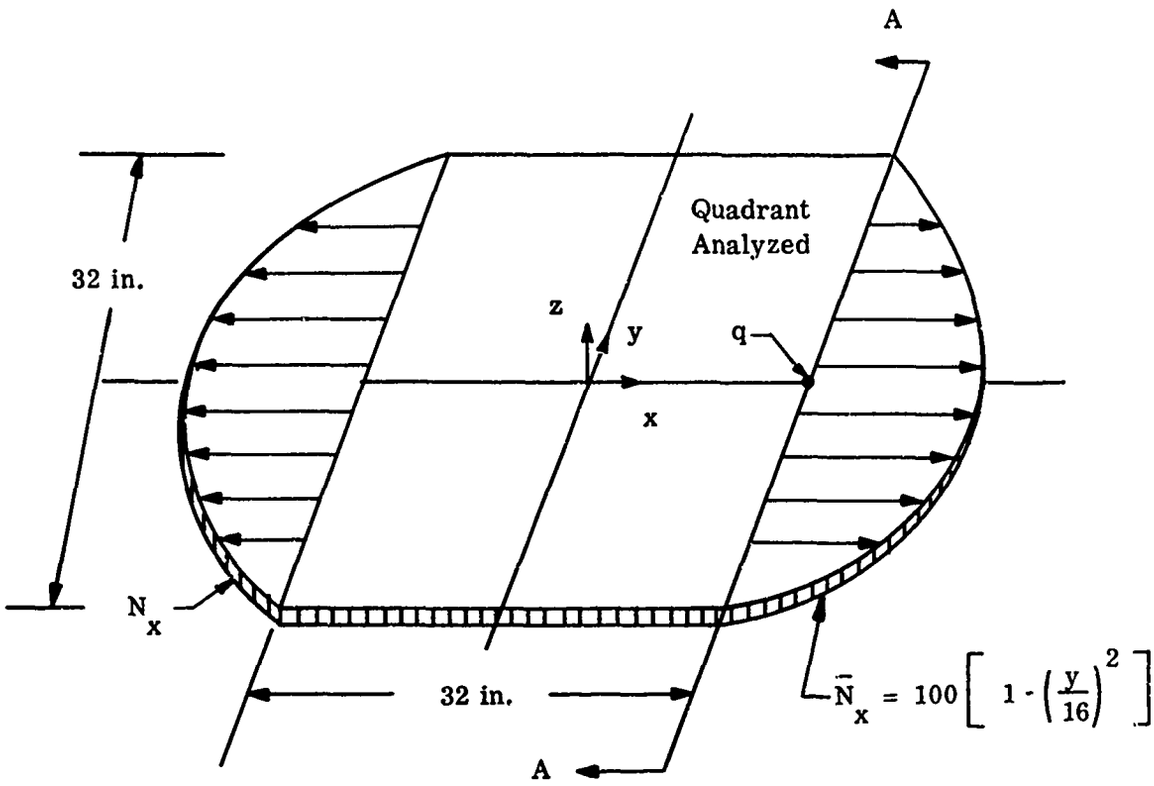

t = 0.1 in.

$\nu = 0.3$

$E = 30 \times 10^6$ lb/in.^{2}

Figure 112. Parabolically Loaded Membrane

The idealizations used for the finite element analyses are shown in Figure 113. Three different grid sizes were employed in this evaluation. Two element, eight element and 32 element solutions were obtained in order to evaluate convergence characteristics. Due to conditions of symmetry only one quadrant of the plate was analyzed. For the finite element idealizations employed in this evaluation, the mid-side nodes which were loaded by the parabolic load were suppressed. This suppression invokes a linear edge displacement under the load.

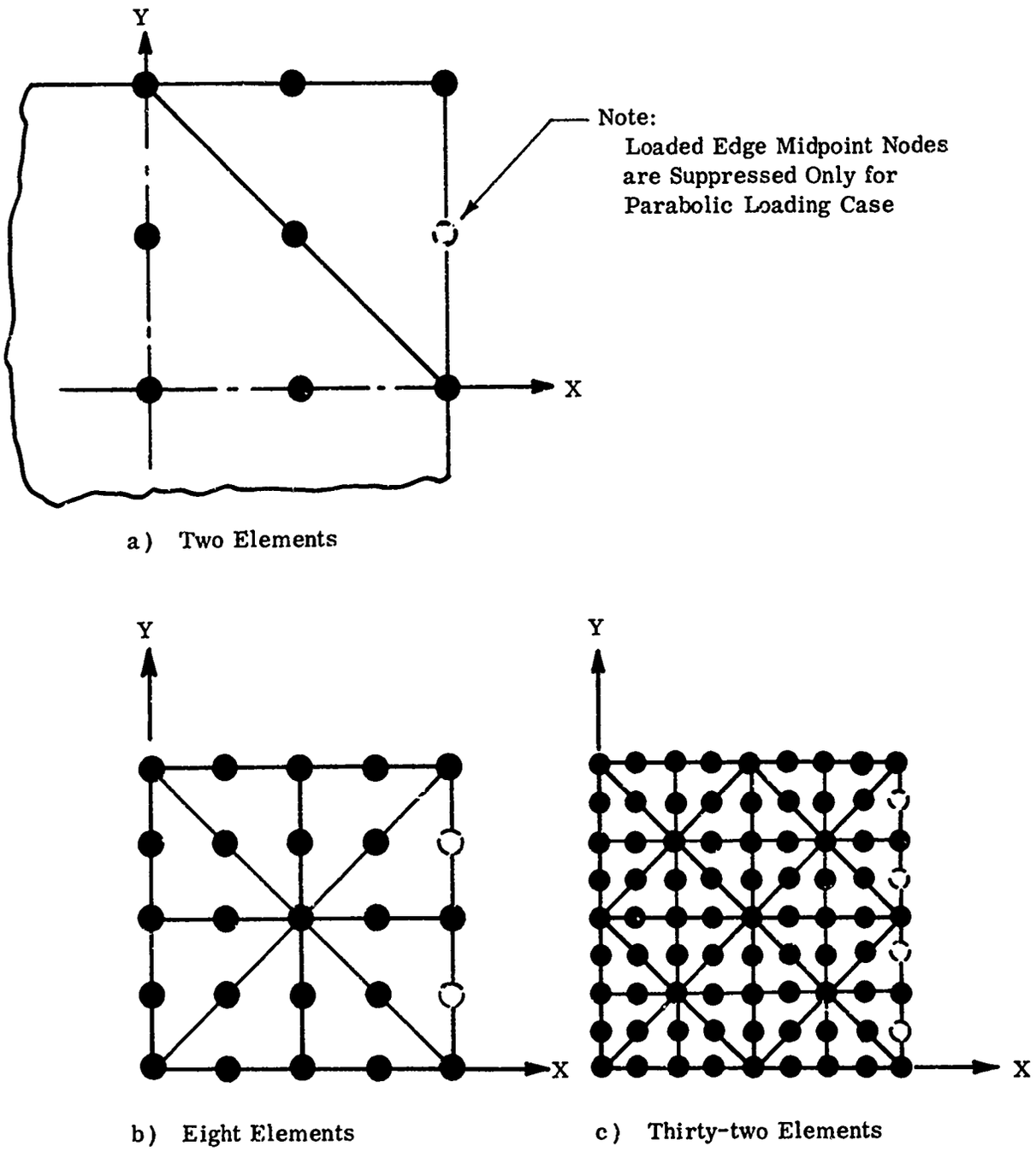

Figure 113. Idealization

The results obtained from this set of convergence studies are presented in Figures 114 and 115. Figure 114 is a plot of the membrane displacement, u_g at the middle of the plate's edge versus degrees-of-freedom employed in the analyses. The reference solution (Reference 44) is designated by the solid line. Figure 115 presents a curve of the membrane displacement, u_x and stress resultant, N_x, versus the edge span of the plate for the idealization shown in Figure 113 (c) (32 element solution). It should be noted that the reference solution is again designated by the solid lines and no discernible difference between solutions can be detected.

2. Membrane Gridwork Influences

The second illustration which utilizes the triangular thin shell element in a structural evaluation will be the following. Again, consider a thin isotropic square plate loaded with a self equilibrating parabolic membrane load as shown in Figure 112. This illustration will involve the effect that the shape of the elements used in the structural idealization has on the determination of center edge displacement of the membrane.

The six idealizations used for the shape study are shown in Figure 116. Due to conditions of symmetry only one quadrant of the plate was analyzed. The midside nodes which were loaded by the parabolic membrane load were suppressed in this solution.

The results obtained from the subject shape studies are shown in Figure 117. These solutions indicate that the displacement values, u_q, obtained for the middle of the plate's edge are fairly insensitive to the shape of the element for this class of problem.

3. Plate Stress Analysis

The third illustration which utilizes the triangular thin shell element in a structural evaluation will be the following. A simply supported square isotropic plate with a uniform normal pressure load of one psi is shown in Figure 118 along with its material properties and pertinent dimensions.

The idealizations used for the finite element analyses are shown in Figure 113. Note that no node points are suppressed in this analysis. Three different grid sizes were employed in this evaluation. Two element, 8 element, and 32 element solutions were obtained in order to evaluate convergence characteristics. Due to conditions of symmetry only one quadrant of the plate was analyzed.

Figure 119 is a plot of the center transverse displacement at the center of the plate versus the degrees-of-freedom employed in the analyses. The reference solution (Reference 45) is designated by the solid line. Figure 120 presents a curve of the transverse displacement, w_x and bending moment, M_x, versus the center span of the plate for the idealization shown in Figure 113 (c) (32 element solution). Again, it should be noted that the reference solution is designated by the solid lines and no discernible differences between solutions can be detected.

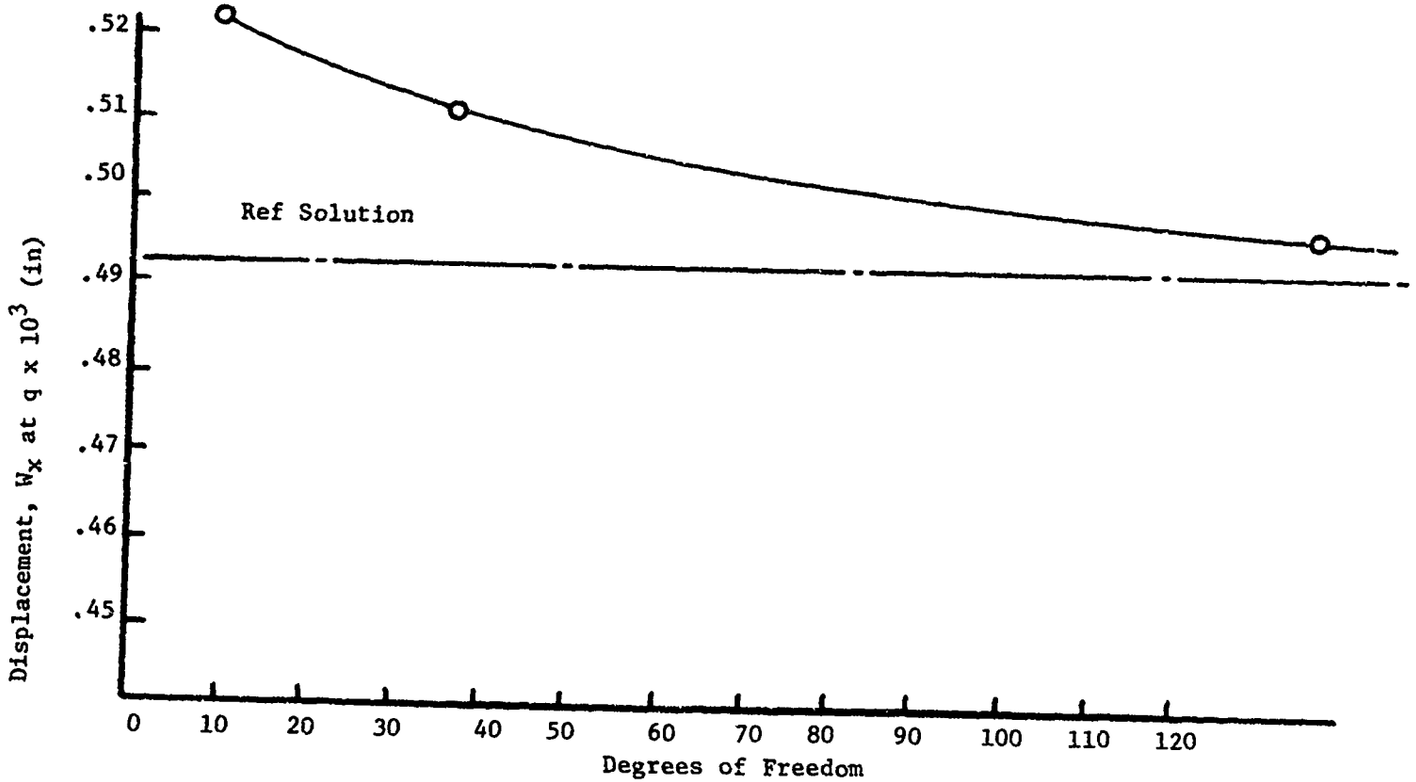

Figure 114 Membrane Displacement At Midside Versus Degrees of Freedom

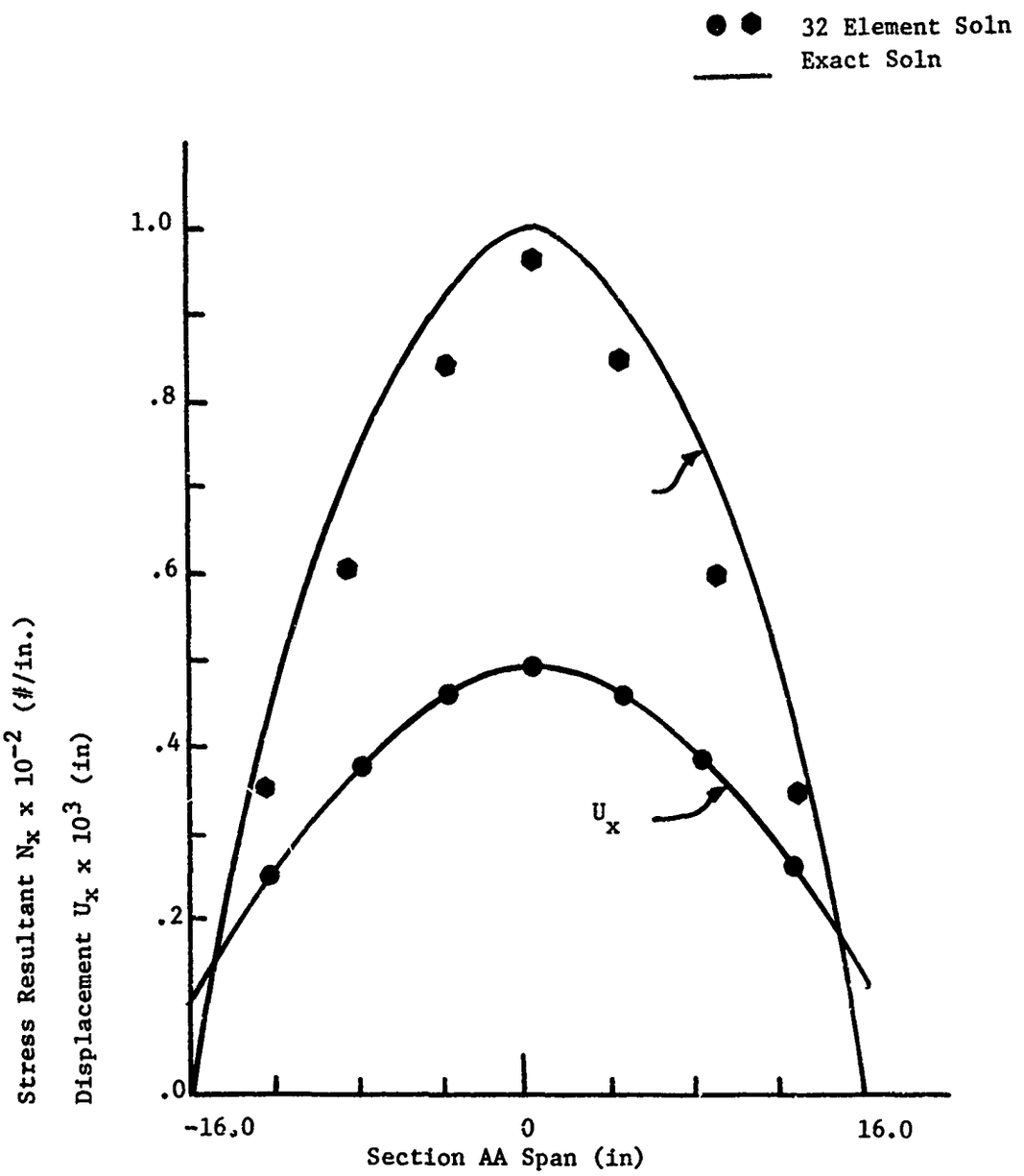

Figure 115 Membrane Displacement And Stress Behavior Versus Plate Edge Span

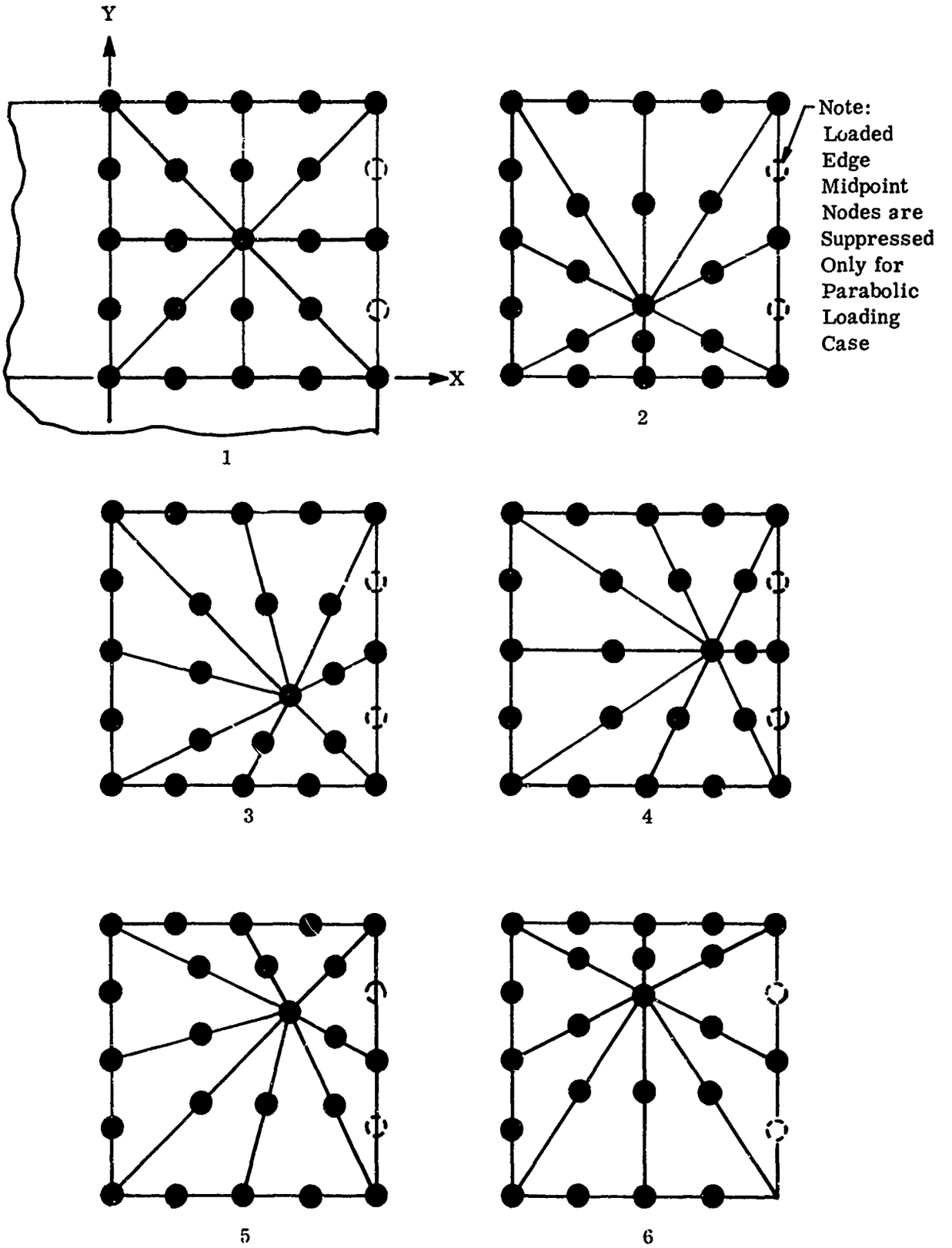

Figure 116. Shape Study Idealization

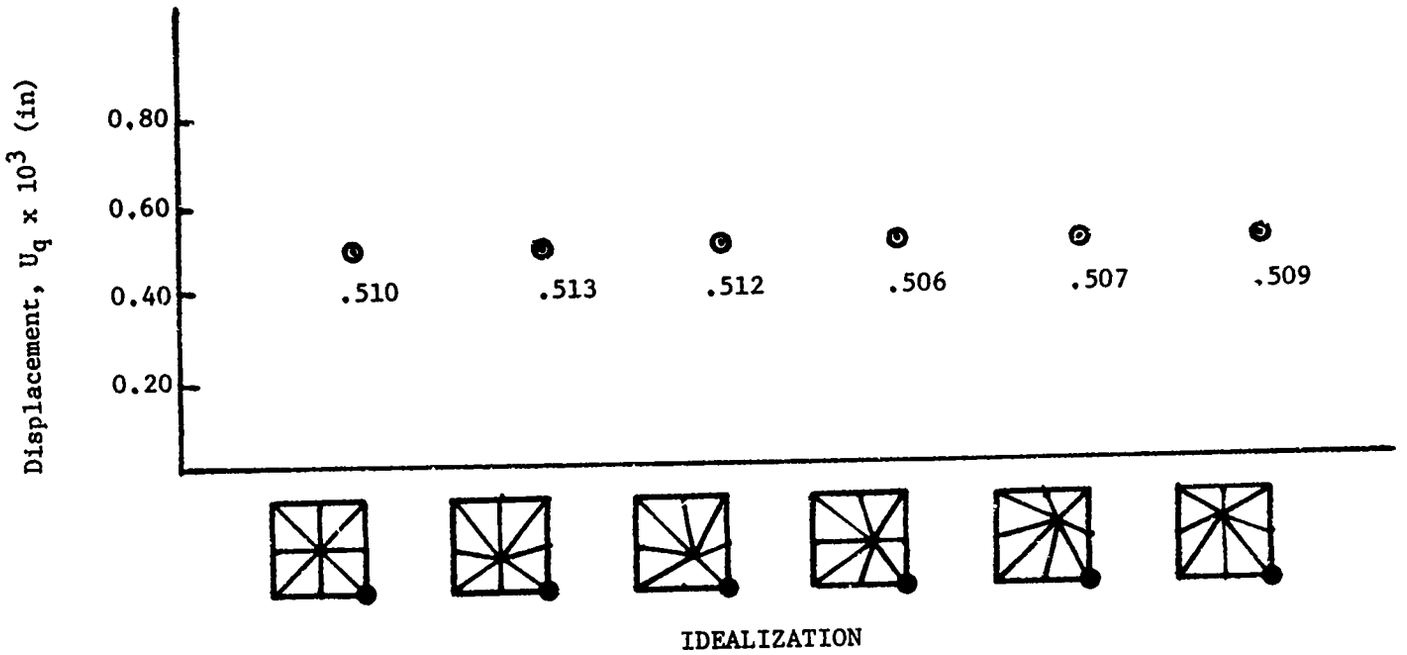

Figure 117 Shape Study Of Triangular Element Membrane, Square, Isotropic, Self Equilibrating Parabolic Edge Loads

Plate Edges are Simply Supported

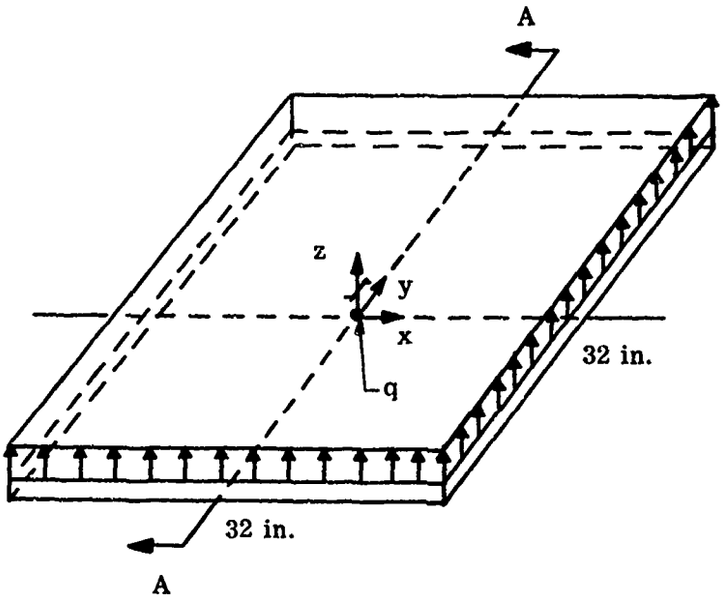

$t = 0.1$ in.

$E = 30 \times 10^6$ lb/in.^{2}

$\nu = 0.3$

$p_z = 1$ lb/in.^{2}

Figure 118. Simply Supported Square Plate with Uniform Normal Load

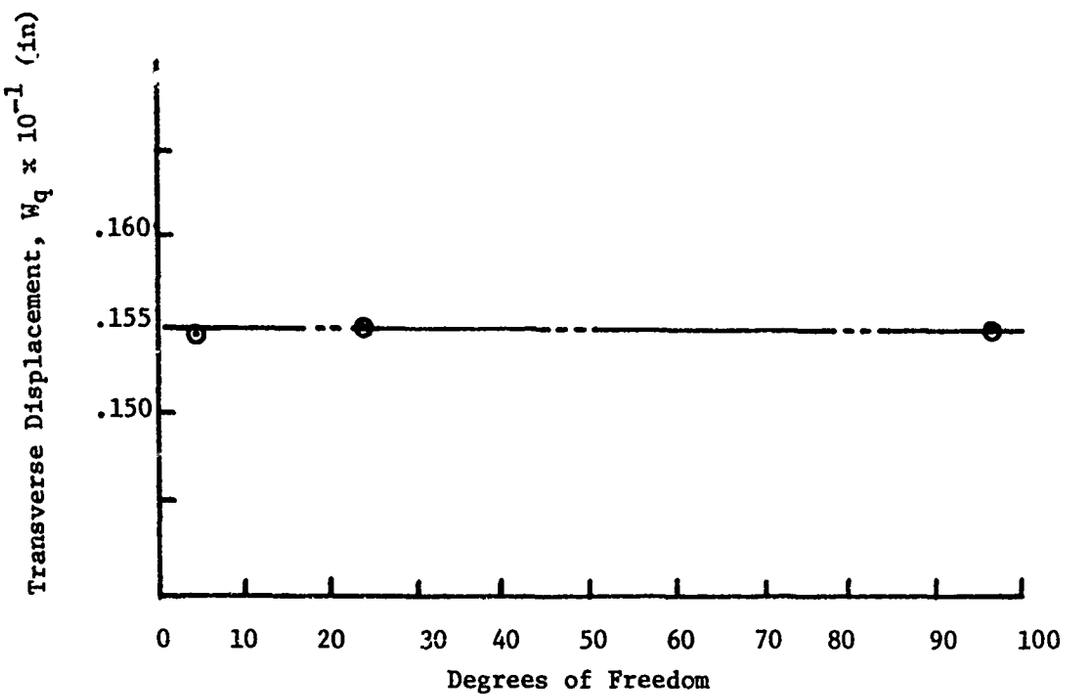

Figure 119 Convergence Of Triangular-Element Plate, Square, Isotropic, Simple Supports, Uniform Pressure

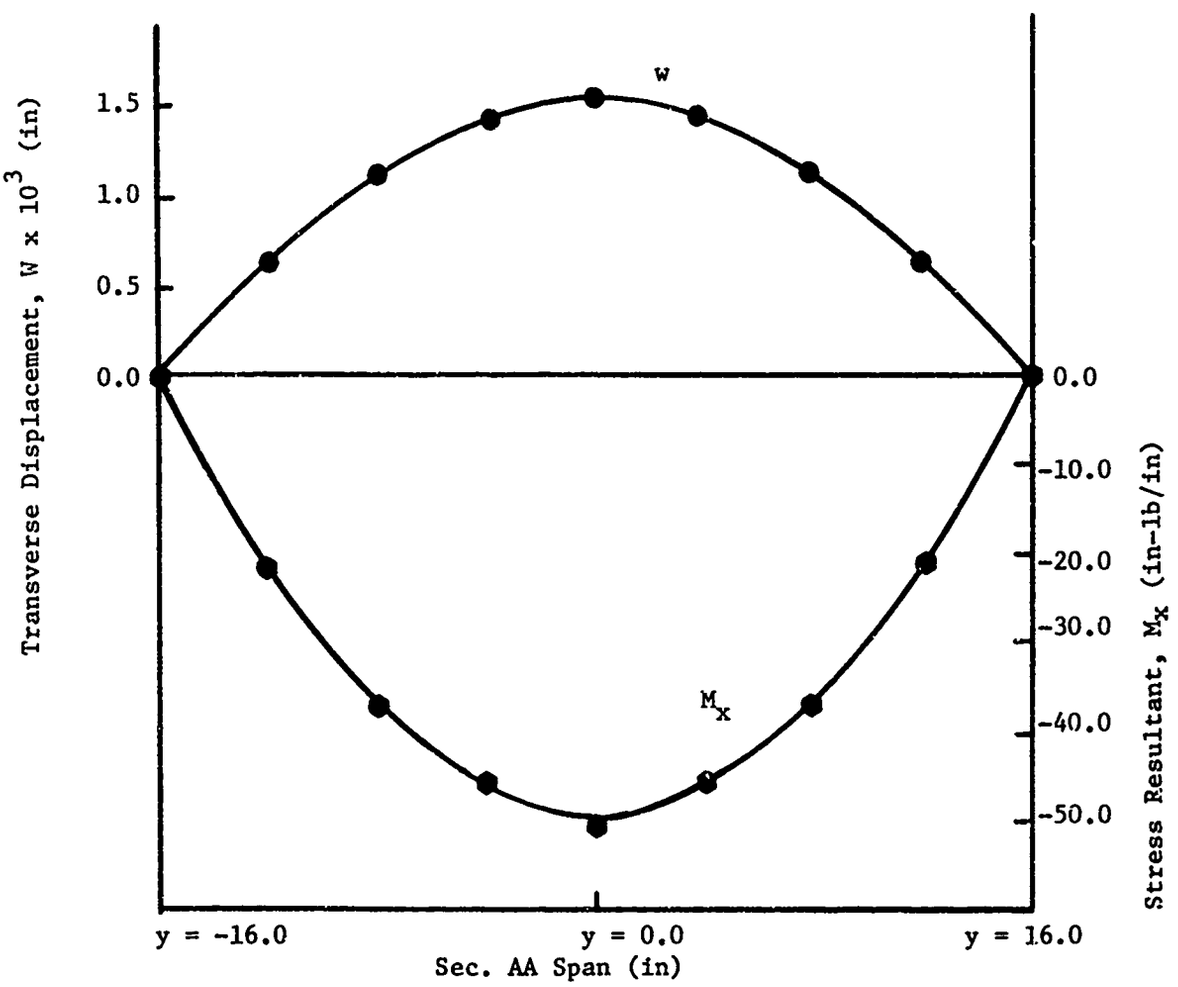

Legend:

●● Magic Triangle

—— Reference Alternate Solution

Figure 120 Behavior/Triangular Element Plate, Square, Isotropic, Simple Support Unit Uniform Load

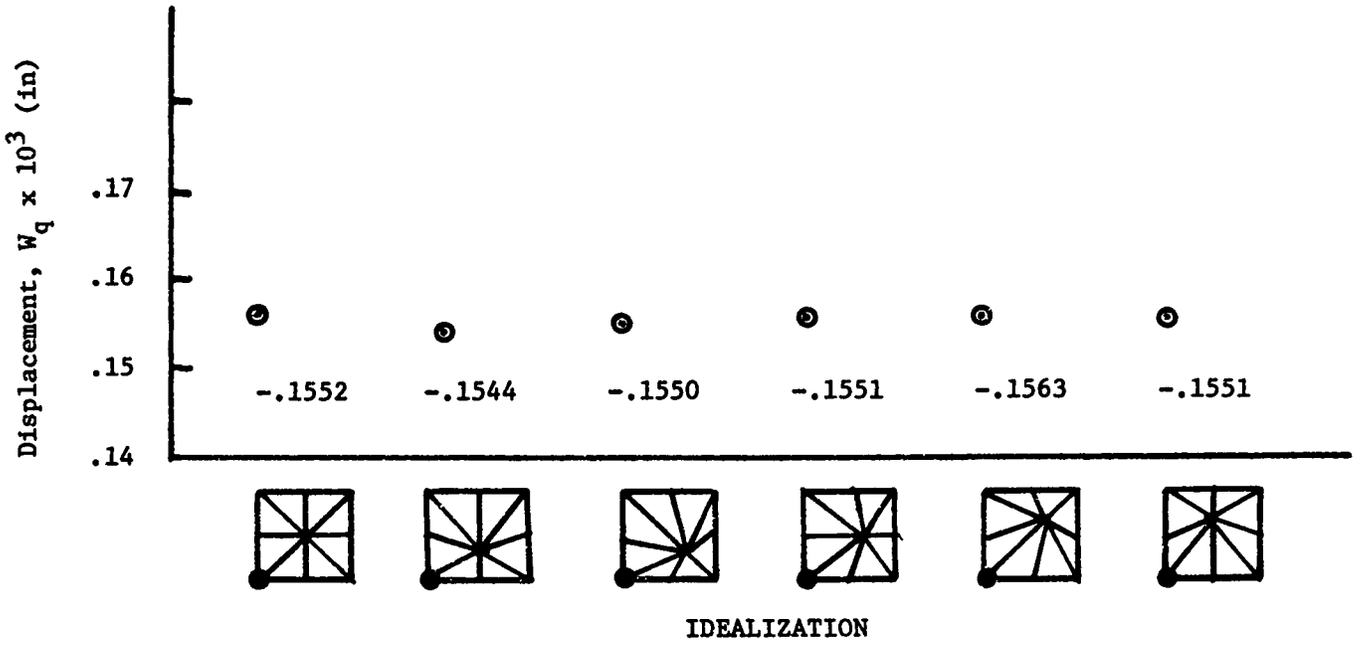

Figure 121 Shape Study Of Triangular Element Plate, Square, Isotropic, Simple Supports Uniform Pressure Load

4. Plate Gridwork Influences

The fourth illustration which utilizes the triangular thin shell element in a structural evaluation will be the following. A simply supported square isotropic plate with a uniform normal pressure load of one psi is shown in Figure 118 along with its material properties and pertinent dimensions.

This illustration will involve the effect that the shape of the elements used in the structural idealization has on the determination of the maximum displacement of the plate.

The six idealizations used for the shape study are shown in Figure.116. Due to conditions of symmetry only one quadrant of the plate was analyzed.

The results obtained from the subject shape studies are shown in Figure 121. These solutions indicate that the determination of the plate's center transverse displacement is fairly insensitive to the shape of the element for this class of problem.

10. DISCUSSION AND CONCLUSIONS

A. DISCUSSION

Integrated general purpose analysis capabilities of the MAGIC System class signal a major advance in the state-of-the-art of automated tools for analysis. The superior cost effectiveness of such systems over conventional multiple special purpose program capabilities is compelling.

This assertion of superior performance from large scale program systems may well contradict conclusions drawn from experience. Complexity and inefficiency have long been concomitant with large size and versatility in computer programs. Indeed, the elimination of these depreciating effects was prerequisite to realization of the favorable cost effectiveness of the MAGIC System.

Large size and versatility, without excessive complexity, are assumed intrinsic to the MAGIC System in subsequent paragraphs, as attention is focused upon the relative efficiencies of integrated general purpose analysis capabilities and multiple special purpose computer program analysis capabilities. This is to presume the prerequisite elimination of the greater hindrance; namely, the excessive complexity which choked off many early general purpose program developments. This problematical complexity was encountered when programs of simple organization grew to press upon the limits of computer software and hardware capabilities. Extensions beyond this point were accomplished by intricately coordinated multiple usage of valuable names and locations, special program versions with omitted features and other actions which accumulated to entangle the logic and data storage until further modification became impractical.

In the face of this situation increasingly powerful analytical models and solution methods were formulated and numerical implementation demanded. And, as is often the case, sufficient pressure was built up to bring about the technological advances needed in the computer technologies.

Advances were forthcoming in programming technology which established the technical feasibility of a truly general purpose computer program system. Advances in computer hardware insured the economic feasibility as the technical feasibility was established through a number of contributing developments. The collective result of these latter developments is, in a word, "organization." Among those organizational characteristics features considered essential are, the breakdown into single function modules, the program library concept, the matrix interpretive system, the SUBSYS routines, etc. In-depth discussion was given to these considerations in Section 2 and is not repeated here. Rather, attention is given to the benefits which accrue from their fulfillment in the MAGIC System.

It is appropriate to emphasize at this point, that the MAGIC System for structural analysis is more than a discrete element computer program. It is, in one sense, a Problem Oriented Language (POL) which enables various Analyst specified computational procedures. And, at the same time, it is designed with attendant structural analysis practices evolved from applications experience. These practices are discussed in detail in subsequent paragraphs. The point of interest here is that the efficiency of the MAGIC System is an overall efficiency governed more by men than machines.

The more comprehensive the comparison, the greater the advantage shown by the integrated general purpose analysis capabilities over multiple special purpose program capabilities. In nearly all cases an equitable comparison must include consideration of program development efforts since relevant technologies are continuously advanced. On this basis the integrated approach enjoys the greatest relative advantage. The integrated approach is also superior to the multiple program approach when considering only factors involved in utilization of operational capability. On the other hand, shorter execution times are conceded to special purpose programs without dispute, since execution efficiency is not essential to the case for the greater overall efficiency of integrated analysis capabilities.

Attention is focused now on the impact of the integrated general purpose computer program approach on the efficiency of the many processes involved in maintenance and application of responsive analysis tools in support of a broad structural design activity. Program maintenance efforts benefit from the highly modularized organizational structure to an even greater extent than the initial development effort.

In the initial development, functional modules are established against the requirements of the alternative analysis procedures taken collectively. And, since an extensive commonality exists, multiple repetitious coding is avoided. This same payoff is derived again as existing modules are retired in favor of new modules which offer improved performance. The introduction of a single improved module is reflected to advantage throughout all pertinent analysis procedures of the computer program system. The option exists to retain alternative modules for the same function without sacrifice. This provides useful operational flexibility and a convenient testbed for various candidate procedures. Alternative procedures can be evaluated within the system without disrupting its operational status.

The foregoing has dealt with maintenance of existing analysis capability. Maintenance is also interpretable as generalization of, and addition to, the overall analysis capability. Completely new analyses can be implemented with the addition of only those functional modules absent in the existing capability. For example, finite element heat conduction analyses are possible with relatively minor modifications to the MAGIC System.

The benefits derived from the organization of a general purpose computer program system in development, maintenance, generalization and extension are simultaneously important disadvantages associated with multiple computer program analysis capabilities. The extensive commonality among analyses leads in this latter case to the repeated development of coding to perform a given function. The preparation of special versions of new modules and the introduction of these into a multiplicity of computer programs is often not justified and the overall capability is depreciated.

Another particularly important handicap borne by the separate programs of a multiprogram capability is that these programs can not command, individually, the provision of many useful special features. For example, useful options and diagnostics are usually omitted from these special purpose program routines. Also, such programs frequently encounter obstacles such as machine storage capacity which must be avoided rather than surmounted in view of the limited applicability of the program. Advancements in computer software and hardware are further considerations of importance in the maintenance of an analysis capability. These advancements place multiple program capabilities in special peril. Those programs not being actively utilized at the time of transition in software or hardware are easily overlooked and in this way are lost from the overall analysis capability.

No single factor is more important in the provision of a responsive analysis capability than documentation. Engineering documentation must delineate analysis procedure, input data and output data. Programming documentation must provide for operation and modification of the program.

Consolidation of the analysis capability into a general purpose program results in a corresponding favorable consolidation of documentation. Not only is volume reduced but the total capability is described uniformly as a whole. Small programs tend to be the personal tool of the initiator. As a consequence, the documentation prepared is generally inadequate to enable general usage. This situation leads to extensive tutorial instruction to realize the benefits of the program development. At the very least, multiple program capabilities place the burden of assimilating the overall analysis capability from the individual manuals upon the user.

The foregoing has pointed out decisive advantages of general purpose program systems in the context of development and maintenance of analysis capability. The most compelling advantages, however, are found in operation. The greater efficiency of the MAGIC System relative to multiprogram capabilities for analysis stems in large measure from the extent of the analysis process which is covered. Time consuming, error prone, manual transfers of data between special purpose or single step computer programs are avoided. The integration of heat conduction and thermal stress analysis within a single system can circumvent the laborious preparation of temperature data. The integration of stiffness and vibration analyses can similarly circumvent the manual transfer of stiffness and mass data. These eliminations of manual effort yield reductions in calendar time which is often the paramount consideration for contribution of analysis to design. This is not to say that long continuous executions are desirable. Execution interruptions enter importantly into proper utilization of the MAGIC System.

The MAGIC System is designed to facilitate good structural analysis practices in support of the overall structural design process. Individual design organizations are best served by structural analysis practices and program versions which are, to some degree, distinct. On the other hand, the extensive commonality which does exist among design organizations provides strong motivation for reviewing the effective structural analysis practices and supplemented program version which have evolved at Bell Aerosystems.

The structural analysis process begins with the idealization of the structure into an assemblage of finite elements. This is a multistep operation if the structure is first separated into substructures. Generally, the separation into substructures is governed by the physical interconnections of the major structural components. The idealization into finite elements is governed by variations in geometry, dimensions, material, applied loading and boundary conditions.

Preprinted input data forms are employed to simplify and thereby improve the reliability of the input data specification. These preprinted input forms associated with the MAGIC System are an important improvement over card image forms for frequent as well as infrequent users since they incorporate automatic data generation features. These built-in data generation features are supplemented at Bell by auxiliary (not integrated into the MAGIC System) data generation programs. Some of these are employed routinely. Others are extremely simple programs written for a single, problem related calculation. Such auxiliary programs are frequently employed to advantage in the generation of gridpoint coordinates with reference to the global rectangular coordinate axes, since expression of these can require extensive tedious calculation. This gridpoint coordinate data set should be interpreted here to include points for specification of gridpoint axes transformations and stress and material angles as well as points associated with degrees-of-freedom.

The first MAGIC System execution undertaken is to confirm the assembled input data deck. This deck is read and the implied data is given explicit definition. For example, material properties are extracted from the Material Library and gridpoint axes transformations are generated from the coordinate table. The completed data set is examined in this preprocessing execution. All data items are stored for execution restart and printed for further checking by the analyst.

The preprocessing execution is supplemented at Bell to include the generation of a magnetic tape which, in turn, generates a plot of the structural model on an automatic plotting machine. This plot enables efficient and reliable confirmation of the two most problematical data items; namely, the gridpoint positions and the finite element connection arrangement. Beyond this point the structure plot is a useful identifying title sheet for the printed problem output.

The next phase of the analysis process proceeds via a restart through the generation of the structural matrices for stiffness, stress, loads, assembly, boundary conditions, etc. Built-in features control this matrix generation to selectively form only those matrices required for the current analysis. Completion of the matrix generation

phase signals exit from the Structural System Monitor. This is an interface point between matrix abstraction instruction statements, and, therefore, a point for optional interruption of the execution to examine the system level matrices. This interruption is used only infrequently at Bell.

Calculation proceeds under the FORMAT System to the governing matrix equation and thence to the solution for the displacement vectors for all load conditions. For some problems execution may be terminated at this point. For many other problems the validity of the analysis can be assessed against these displacement results and an execution interruption is justified by the computational investment required for the secondary results. Ideally, the deformed structure should be plotted to facilitate interpretation of the predicted displacement behavior.

The analysis proceeds from the displacement solution, with or without interruption, to calculation and print of the remainder of the output data items; namely, reactions, forces, stresses, etc. This is the conventional point of termination of finite element analyses. However, a number of relatively simple auxiliary programs are used to advantage at Bell to relieve the burden this output places on the stress engineers. As in the case of the input data generation auxiliary programs, some of the auxiliary output data reduction programs are employed repeatedly and others are special to a single problem. The functions of these programs include such things as principal stress calculations and margin of safety determinations. Auxiliary programs which do nothing but selectively print and label output data items are also helpful for large problems.

Several comments on the evaluation of output data are warranted in concluding discussion of good structural analysis practices. The examination of output by the Analyst should be initiated under the presumption that an error exists with confidence in the validity of the analysis accumulating as the examination proceeds. Given a complete set of output, attention should first be given to the gridpoint force balances and reactions. Assured that no unintended reactions exist and that residuals are negligibly small, the displacement states should be examined. If the general deformed configuration does not expose any inconsistencies, confirmation is completed by examination of the more extensive presentation of force and stress data.

The foregoing discussion has focused upon development, maintenance and utilization considerations important to the favorable cost effectiveness of the present MAGIC System for structural analysis. Further evolution of this system can be expected which will continue to improve its relative advantage. Updated versions of the MAGIC System will be compatible with all features developed in connection with prior versions.

B. CONCLUSIONS

It is concluded that the subject MAGIC System provides a capability for structural analysis equivalent to that of the predecessor programs delivered under Contract AF33(657)8963, taken collectively. The satisfactory achievement of this overall objective is given substantiation by a number of subsidiary conclusions. Specifically, it is concluded that:

(1) The finite element library enables effective idealization of most linear structures.

(2) Computational procedures attendant to the MAGIC System enable the conduct of linear displacement and stress analyses in the presence of general prestrain and thermal loading as well as distributed and concentrated mechanical loading.

(3) The stability analysis procedure provided in the MAGIC System enables the prediction of critical load levels for general framed structures.

(4) The preprinted input data forms facilitate the rapid and reliable specification of problem data.

(5) The computer program organization of the MAGIC System effectively utilizes the FORMAT System and is well suited to generalization.

11. REFERENCES

1. Gallagher, R. H., and Huff, R. D., "Thermal Stress Determination Techniques for Supersonic Transport Aircraft Structures: A Bibliography of Thermal Stress Analysis References 1955-1962," Part I, ASD-TDR-63-783, Part I, January, 1964.

2. Gellatly, R. A., and Gallagher, R. H., "Thermal Stress Determination Techniques for Supersonic Transport Aircraft Structures: Design Data for Sandwich Plates and Cylinders under Applied Loads and Thermal Gradients," Part II, ASD-TDR-63-783, January, 1964.

3. Gallagher, R. H., Padlog, J., and Huff, R. D., "Thermal Stress Determination Techniques for Supersonic Transport Aircraft Structures: Computer Programs for Beam Plate and Cylindrical Shell Analysis," Part III, ASD-TDR-63-783, January, 1964.

4. Gallagher, R. H., Padlog, J., and Huff, R., "Detailed Description - Computer Program for Beam Analysis," Report No. D2114-950006, AD No. 461 216, January, 1964.

5. Gallagher, R. H., and Huff, R., "Detailed Description - Computer Program for Plate Analysis," Report No. D2114-957007, AD No. 461 217, January, 1964.

6. Gallagher, R. H., Huff, R., and Dale, B. J., "Detailed Description - Computer Program for Stiffened Cylinder Analysis," Report No. D2114-950008, AD No. 461 218, January, 1964.

7. Jordan, S., Maddux, G. E., and Mallett, R. H., "MAGIC: An Automated General Purpose System for Structural Analysis: User's Manual," Volume II, AFFDL-TR-68-56, Air Force Flight Dynamics Laboratory, WPAFB, Ohio, March, 1968.

8. DeSantis, D., "MAGIC: An Automated General Purpose System for Structural Analysis: Programer's Manual," Volume III, AFFDL-TR-68-56, Air Force Flight Dynamics Laboratory, WPAFB, Ohio, March, 1968.

9. Pickard, J., "FORMAT II - Second Version of Fortran Matrix Abstraction Technique: Engineering User Report," Volume I, AFFDL-TR-66-207, Air Force Flight Dynamics Laboratory, WPAFB, Ohio, September, 1965.

10. Cogan, J. P., "FORMAT II - Second Version of Fortran Matrix Abstraction Technique: Description of Digital Computer Program," Volume II, AFFDL-TR-66-207, Air Force Flight Dynamics Laboratory, WPAFB, Ohio, December, 1966.

11. Morris, R. C., "FORMAT II - Second Version of Fortran Matrix Abstraction Technique: A User-Coded Matrix Generator for the Force Method," Volume III, AFFDL-TR-66-207, Air Force Flight Dynamics Laboratory, WPAFB, Ohio, December, 1966.

12. Serpanos, J., "FORMAT II - Second Version of Fortran Matrix Abstraction Technique: A User-Coded Matrix Generator for the Displacement Method," Volume IV, AFFD-TR-66-207, Air Force Flight Dynamics Laboratory, WPAFB, Ohio, December, 1966.

13. Mallett, R. H., "Mathematical Models for Structural Discrete Elements," Bell Aerosystems Report No. 8500-941002, June, 1966.

14. Gellatly, R. A., "Development of Procedures for Large Scale Automated Minimum Weight Structural Design," AFFDL-TR-66-180, Air Force Flight Dynamics Laboratory, WPAFB, Ohio, December, 1966.

15. Mallett, R. H., "Data Management Concepts for Automated Analysis and Design Tools," Air Force Report No. SAMSO-TR-67-108, Proceedings of the Nose Tip Stress Analysis Technical Interchange Meeting, November, 1967.

16. Frosberg, K. J., et al., "Development of Improved Structural Dynamic Analysis: Computer Graphics," Volume II, AFFDL-TR-66-187, Air Force Flight Dynamics Laboratory, WPAFB, Ohio, March, 1967.

17. Clough, R. W., and Rashid, Y., "Finite Element Analysis of Axisymmetric Solids," Journal of Engineering Mechanical Division, 91, 1965, pp. 71-85.

18. Grafton, P. E., and Strome, D. R., "Analysis of Axisymmetric Shells by the Direct Stiffness Method", AIAA Journal 1, 10, 1963, pp. 2342-2347.

19. Zienkiewicz, O. C., and Cheung, Y. K., "The Finite Element Method in Structural and Continuum Mechanics," McGraw-Hill Publishing Company, Britain, 1967.

20. Przemieniecki, J. S., "Theory of Matrix Structural Analysis," McGraw-Hill Book Company, New York, 1968.

21. Washizu, K., "Variational Principles in Continuum Mechanics," University of Washington Report No. 62-2, June, 1962.

22. Key, S. M., "A Convergence Investigation of the Direct Stiffness Method," Ph. D. Thesis, Department of Aeronautics and Astronautics, University of Washington, Seattle, Washington, 1966.

23. Bazeley, G. P., Cheung, Y. K., Irons, B. M., and Zienkiewicz, O. C., "Triangular Elements in Plate Bending - Conforming and Nonconforming Solutions," AFFDL-TR-66-80, December, 1965, pp. 547-546.

24. Gallagher, R. H., "The Development and Evaluation of Matrix Methods for Thin Shell Structural Analysis," a Thesis Submitted to the State University of New York at Buffalo, 1966.

25. Bogner, F. K., Mallett, R. H., Minich, M. D., and Schmit, L. A., "Development and Evaluation of Energy Search Methods of Nonlinear Structural Analysis," Technical Report No. AFDL-65-113, Air Force Systems Command, WPAFB, Ohio, October, 1965.

26. Bogner, F. K., Fox, R. L., and Schmit Jr., L. A., "The Generation of Interelement Compatible Stiffness and Mass Matrices by Use of Interpolation Formulas" (with Addendum), AFFDL-TR-66-80, December, 1965, pp. 397-444.

27. Mallett, R.H., and Marcal, P.V., "Consistent Matrices and Computational Procedures for Nonlinear Pre- and Post-Buckling Analyses," Bell Aerosystems Report No. 2500-941019, August, 1967.

28. Jordan, S., "Formulation and Evaluation of a Frame Discrete Element," Bell Aerosystems Report No. 9500-941010, September, 1967.

29. Martin, H. C., "Introduction to Matrix Methods of Structural Analysis," McGraw-Hill Book Company, New York, 1966.

30. Helle, E., "Formulation and Evaluation of a Triangular Ring Discrete Element," Bell Aerosystems Report No. 9500-941003, June, 1966.

31. Wilson, E. L., "Structural Analysis of Axisymmetric Solids," AIAA Journal 3, 12, December, 1965, pp. 2267-2274.

32. Wang, C. T., "Applied Elasticity," McGraw-Hill Book Company, 1963.

33. Meyers, R. R., and Hannon, M. B., "Conical Segment Method of Analyzing Open Crown Shells of Revolution for Edge Loading," AIAA Journal 1, 1963, pp. 886-891.

34. Popov, E. P., Penzien, J., and Lu, Z. A., "Finite Element Solution for Axisymmetric Shells," Journal of Engineering Mechanical Division, ASCE, October, 1964, pp. 119-145.

35. Percy, J. H., Pian, T. H. H., Klein, S., and Navaratna, D. R., "Application of Matrix Displacement Method to Linear Elastic Analysis of Shells of Revolution," AIAA Paper No. 65-142, January, 1965.

36. Jones, R. E., and Strome, D. R., "A Survey of the Analysis of Shells by the Displacement Method," Conference on Matrix Methods in Structural Mechanics, WPAFB, Ohio, 1965.

37. Klein, S., "Study of the Matrix Displacement Method as Applied to Shells of Revolution," Conference on Matrix Methods in Structural Mechanics, WPAFB, Ohio, October, 1965.

38. Stricklin, J. A., Navaratna, D. R., and Pian, T. H. H., "Improvements on the Analysis of Shells of Revolution by the Matrix Displacement Method", AIAA Journal Technical Note, Volume 4, 11, November, 1966, pp. 2069-2072.

39. Navaratna, D. R., Pian, T. H. H., and Witmer, E. A., "Analysis of Elastic Stability of Shells of Revolution by the Finite Element Method," Proceedings of the AIAA/ASME 8th Structures, Structural Dynamics, and Materials Conference, March, 1967.

40. Jones, R. E., and Strome, D. R., "Direct Stiffness Method Analysis of Shells of Revolution Utilizing Curved Elements," AIAA Journal, Volume 4, No. 9, September, 1966, pp. 1526-1530.

41. Mallett, R. H., and Helle, E., "Formulation and Evaluation of a Toroidal Ring Discrete Element," Bell Aerosystems Report No. 9500-941001, May, 1966.

42. Novozhilov, V., "The Theory of Thin Shells," P. Noordhoff, Ltd., Netherlands, 1959.

43. Mallett, R. H., "Formulation and Evaluation of a Quadriliateral Thin Shell Discrete Element," Bell Aerosystems Report No. 9500-941005, April, 1966.

44. Timoshenko, S., and Goodier, J. N., "Theory of Elasticity," 2nd Edition, McGraw-Hill Book Company, New York, 1951.

45. Timoshenko, S., Woinowsky-Krieger, S., "Theory of Plates and Shells," 2nd Edition, McGraw-Hill Book Company, 1959.

46. Helle, E., and Mallett, R. H., "Formulation and Evaluation of a Triangular Thin Shell Discrete Element," Bell Aerosystems Report No. 9500-941002, May, 1966.

47. Sander, G. and Fraeijs De Veubelce, B., "Upper and Lower Bounds to Structural Deformations by Dual Analysis in Finite Elements," AFFDL-TR-66-199 Air Force Flight Dynamics Laboratory, WPAFB, Ohio, January, 1967.

UNCLASSIFIED
Security Classification

DOCUMENT CONTROL DATA - R & D

(Security classification of title, body of abstract and indexing annotation must be entered when the overall report is classified)

1. ORIGINATING ACTIVITY (Corporate author)	2a. REPORT SECURITY CLASSIFICATION
Bell Aerosystems a Textron Company	Unclassified
	2b. GROUP N/A

3. REPORT TITLE

MAGIC - An Automated General Purpose System for Structural Analysis Volume I - Engineer's Manual

4. DESCRIPTIVE NOTES (Type of report and inclusive dates)

Final Report

5. AUTHOR(S) (First name, middle initial, last name)

Robert H. Mallett

6. REPORT DATE	7a. TOTAL NO. OF PAGES	7b. NO. OF REFS
January 1969	209	46

8a. CONTRACT OR GRANT NO.	9a. ORIGINATOR'S REPORT NUMBER(S)
AF33(615)-67-C-1505	AFFDL-TR-68-56, Vol. I
8. PROJECT NO. 1467	
c. Task No. 146702	9b. OTHER REPORT NO(S) (Any other numbers that may be assigned this report) None
d.	

10. DISTRIBUTION STATEMENT

This document has been approved for public release and sale. Its distribution is unlimited.

11. SUPPLEMENTARY NOTES	12. SPONSORING MILITARY ACTIVITY
None	Air Force Flight Dynamics Laboratory Research & Technology Division Wright-Patterson AF Base, Ohio

13. ABSTRACT

An automated general purpose system for analysis is presented. This system, identified by the aconym "MAGIC" for "Matrix Analysis via Generative and Interpretive Computations," provides a flexible framework for implementation of the finite element analysis technology. Powerful capabilities for displacement, stress and stability analyses are included in the subject MAGIC System for structural analysis.

The matrix displacement method of analysis based upon finite element idealization is employed throughout. Six versatile finite elements are incorporated in the finite element library. These are: frame, shear panel, triangular cross-section ring, toroidal thin shell ring, quadrilateral thin shell and triangular thin shell elements. These finite element representations include matrices for stiffness, incremental stiffness, perstrain load, thermal load, distributed mechanical load and stress.

Documentation of the MAGIC System is presented in three parts; namely, Volume I: Engineer's Manual, Volume II: User's Manual and Volume III: Programmer's Manual. The subject Volume, Volume III, is designed to facilitate implementation, operation, modification, and extension of the MAGIC System.

DD FORM 1 NOV 68 1473

UNCLASSIFIED
Security Classification

14. KEY WORDS	LINK A		LINK B		LINK C	
	ROLE	WT	ROLE	WT	ROLE	WT
1. Structural analysis 2. Matrix methods 3. Matrix abstraction 4. Digital computer methods						